

**THE EFFECT OF DUCT ARRANGEMENT ON BREAKOUT
OF INTERNAL POST-TENSIONING TENDONS IN
HORIZONTALLY CURVED CONCRETE
BOX GIRDER WEBS**

APPROVED:

Supervisor:

Dr. John E. Breen

Dr. Michael E. Kreger

**THE EFFECT OF DUCT ARRANGEMENT ON BREAKOUT
OF INTERNAL POST-TENSIONING TENDONS IN
HORIZONTALLY CURVED CONCRETE
BOX GIRDER WEBS**

by

DEAN WILLIAM VAN LANDUYT, B.S.

THESIS

**Presented to the Faculty of the Graduate School of
The University of Texas at Austin
in Partial Fulfillment
of the Requirements
for the Degree of
Master of Science in Engineering**

THE UNIVERSITY OF TEXAS AT AUSTIN

December, 1991

To those in the Texas Department of Transportation
who made this possible

ACKNOWLEDGEMENT

Succeeding in the structural engineering graduate program requires solitary perseverance and a single-minded sense of purpose. These qualities were instilled in me at a young age by my parents who, through example showed me the benefits of hard work. However no one gets out of here alone. There is too much to learn and do for anyone to rely entirely on their own resources.

I had the good fortune of working with Dr. John E. Breen who demands excellent work of himself and quietly inspires it in those around him. He allowed me the freedom to make my own decisions on the lab floor knowing that I would learn more from my mistakes than successes. Thanks also to Dr. Micheal E. Kreger for his helpful comments throughout the course of this project and his review of this thesis.

Deepak Ahuja assisted on all aspects of this investigation and his affable manner made unpleasant tasks bearable and the mundane lively. He worked tirelessly and without pay to gain lab experience and information for his report which is an excellent overview of the first two tests. The details of the test specimen which appear in Chapter 3 were drawn by Deepak.

I was woefully inexperienced with personal computers upon entering the program. Special thanks to Carin Roberts, Aziz Hindi and Jose Pincheira for their patience and ability to keep the snickering, if any, to themselves as they taught me the basics of the lab software.

Many other students volunteered their time to show me the tricks of getting a project built and tested in the lab. Others wandered too close to my project and got lassoed when an extra hand or strong back was needed. Thanks particularly to Bruce Russell, Jose Arrellaga, Rusty Barnhill, Ozgur Egilmez, Reed Freeman, Todd Helwig, Julio Jimenez, Karen Ryals, Raj Valluvan, Chris Tansil, Gregor Wollmann, Calvin Earvin and Leonard Joanes. Also thanks to my graduate assistant Santiago Lopez and undergraduate assistant David Vliet. Special thanks to Eric Solie whose ingenuity and intensity kept my project on schedule.

The staff of the Phil M. Ferguson Structural Engineering Laboratory was extremely helpful, especially Laurie Golding, Jean Gehrke, Sharon Cunningham, Wayne Fontenot, Wayne Little and C.R. Paul.

Also thanks to my family and friends for their continued interest and support.

The background research was made possible in large part because Mr. Ron Zimmerman of T.Y. Lin International and Mr. Donald Ornellas of the Hawaii DOT generously provided failure reports.

Finally thanks to the Texas Department of Transportation for supporting me financially and otherwise in this endeavor. I hope that my future contributions to the department are greater than the benefits that I received from the graduate program.

Dean Van Landuyt
November 25, 1991
Austin, Texas

TABLE OF CONTENTS

CHAPTER 1: INTRODUCTION	1
1.1 BACKGROUND	1
1.2 FAILURES	5
1.3 DUCT ARRANGEMENT	8
1.4 OBJECTIVES	17
1.5 SCOPE	18
CHAPTER 2: STATE OF THE ART	21
2.1 LATERAL PRESTRESSING FORCE ON THE BOX ...	21
2.2 LAS LOMAS FAILURE MODES ASSUMED BY TYLI .	26
2.2.1 Global Girder Action	27
2.2.2 Regional Beam Action	28
2.2.3 Local Beam Action	31
2.3 AUTHOR'S COMMENTS ON FAILURE THEORIES ..	33
2.3.1 Behavior	33
2.3.2 Global Girder Action	34
2.3.3 Regional Beam Action	34
2.3.4 Local Beam Action	35
2.3.5 Conclusions	36
2.4 KAPIOLANI	37

2.4.1	Global Girder Action	37
2.4.2	Regional Beam Action	38
2.4.3	Local Beam Action	38
2.5	DESIGN GUIDELINES	39
2.5.1	CALTRANS Details - 1973	39
2.5.2	CALTRANS Details - 1982	41
2.5.3	CALTRANS Details - 1985	43
2.5.4	AASHTO - 1989	43
2.5.5	NCHRP 12-33 (Draft) - 1991	44
CHAPTER 3:	MODEL DESIGN	46
3.1	MODEL SELECTION	46
3.2	SCALE FACTOR	47
3.3	BOX DIMENSIONS	47
3.4	CURVE LAYOUT	48
3.5	REINFORCEMENT	50
3.6	DUCT ARRANGEMENT	56
3.6.1	SPECIMEN BC	58
3.6.2	SPECIMEN 1.0DC	58
3.6.3	SPECIMEN 0.2DC	58
3.6.4	SPECIMEN BO	59
3.7	LONGITUDINAL DUCT LAYOUT	59
CHAPTER 4:	MATERIALS AND CONSTRUCTION	61
4.1	MATERIAL PROPERTIES	61
4.1.1	Concrete	61
4.1.2	Mortar Patch	64
4.1.3	Epoxy	64
4.1.4	Reinforcement	64

4.1.5	Ducts	65
4.1.6	Prestressing Strand	65
4.2	CONSTRUCTION	65
4.2.1	Formwork	66
4.2.1.1	Exterior Web Forms	66
4.2.1.2	Core Forms	67
4.2.2	Bottom Slab	70
4.2.3	Duct Positioning	71
4.2.4	Anchorage Plates	74
4.2.5	Casting Procedure	74
4.2.6	Honeycombs	80
4.2.7	Patching	84
4.2.8	Measured Dimensions	84
CHAPTER 5: LOADING AND INSTRUMENTATION		86
5.1	LOAD SYSTEM	86
5.1.1	Prestressing Strand	87
5.1.2	Load Beams	87
5.1.3	Rams	93
5.1.4	Bearing Plates	93
5.2	LOAD SYSTEM INSTRUMENTATION	94
5.2.1	Pressure Transducers	94
5.2.2	Switch and Balance	94
5.2.3	Data Acquisition System	96
5.2.4	Pressure Gauge	97
5.2.5	Strain Gages	97
5.3	SPECIMEN INSTRUMENTATION	97
5.3.1	Strain Gages	98

5.3.2	Web-Slab Potentiometers	98
5.3.3	Delamination Gages	103
5.3.4	Web-Web Potentiometers	105
5.3.5	Demec Gages	109
5.4	LOADING PROCEDURE	109
5.4.1	Friction Test	109
5.4.2	Load System Alignment	111
5.4.3	Monostrand Stressing	112
5.4.4	Loading Procedure	113
CHAPTER 6:	TEST RESULTS	117
6.1	VISUAL OBSERVATIONS	118
6.1.1	Specimen 1.0DC	118
6.1.2	Specimen BC	127
6.1.3	Specimen 0.2DC	133
6.1.4	Specimen BO	139
6.2	DELAMINATION GAGES	142
6.2.1	Comparisons of Web Delaminations	143
6.2.2	Web Delamination Profiles	144
6.2.2.1	Specimen 1.0DC	145
6.2.2.2	Specimen BC	146
6.2.2.3	Specimen 0.2DC	147
6.2.2.4	Specimen BO	148
6.2.3	Delaminations Outside Duct Groups	148
6.3	STRAIN GAGES	152
6.3.1	Comparison of Stresses at IM and IU	153
6.3.2	Stirrup Stresses on the Inside of the Duct Groups (IL, IM, IU)	157

6.3.2.1 Specimen 1.0DC	157
6.3.2.2 Specimen BC	159
6.3.2.3 Specimen 0.2DC	161
6.3.2.4 Specimen BO	163
6.3.3 Outside Leg Stirrup Stresses	164
6.4 WEB DEFLECTION POTENTIOMETERS	167
6.4.1 Web-Slab Deflections	167
6.4.2 Web-Web Potentiometers	170
6.4.3 Comparison of Web-Slab and Web-Web Potentiometers	172
6.5 DEMEC GAGES	173
CHAPTER 7: FAILURE THEORIES AND DESIGN	
RECOMMENDATIONS	175
7.1 REGIONAL BEAM ACTION	175
7.1.1 Frame Analysis	177
7.1.2 CALTRANS Analysis	180
7.1.3 Specimen 1.0DC Test Results	180
7.1.4 Comparison of Analysis and Test Results	182
7.1.5 Longitudinal Arching Action	184
7.2 LOCAL BEAM ACTION	188
7.2.1 Bending	188
7.2.2 Shear	190
7.2.2.1 Diagonal Tension	192
7.2.2.2 Shear Capacity	193
7.3 DESIGN RECOMMENDATIONS	196
7.3.1 Regional Beam Failure	197
7.3.2 Local Beam Failure	198

7.3.2.1 Bending	198
7.3.2.2 Shear	198
7.3.3 Detailing	204
CHAPTER 8: SUMMARY AND CONCLUSIONS	206
8.1 SUMMARY	206
8.2 CONCLUSIONS	208
8.3 DESIGN RECOMMENDATIONS	209
8.3.1 Shear	209
8.3.2 Flexure	209
8.3.3 Detailing	210
8.4 FUTURE RESEARCH	210
APPENDIX A: ADDITIONAL GRAPHS	212
REFERENCES	217

LIST OF TABLES

<u>Table</u>	<u>Page</u>
1.1 Bottom Stresses from PT for Las Lomas Example Arrangements	15
1.2 Effective Nominal Moments for Las Lomas Example Arrangements	16
2.1 Regional Beam Ultimate and Nominal Moments.	35
2.2 Local Beam Ultimate and Nominal Moments.	35
2.3 Local Beam Ultimate and Nominal Shears.	36
4.1 Girder Batch Weights and Slumps	62
4.2 Concrete Strengths at Testing Dates	62
4.3 Mortar Patch Batch Weights	64
5.1 Girder #1 Strain Gage Inventory	100
5.2 Girder #2 Strain Gage Inventory	101
5.3 Friction Loss Test Results	111
6.1 Delaminations at Ultimate	152
7.1 Regional Beam Analysis and Measured Loads	183
7.2 Calculated Coefficient for $\sqrt{f_c}$	195
7.3 Factor of Safety Provided by Shear Design Equation	202

LIST OF FIGURES

<u>Figure</u>	<u>Page</u>
1.1 San Antonio "Y" Concrete Box Girder.	2
1.2 Box Girder Segment with Internal Ducts in Webs.	3
1.3 Box Girder Bridge with External Tendons (from Ref. 7).	3
1.4 Las Lomas Cross Section with Bundled Ducts (based on Ref. 6).	6
1.5 Breakout of Tendons at Las Lomas (from Ref. 7).	7
1.6 Locations of Tendon Breakout at Las Lomas (from Ref. 7).	7
1.7 Kapiolani Cross-Section with Bundled Ducts (Based on Ref. 8).	9
1.8 Kapiolani Overview During Repair (from Ref. 8).	10
1.9 Kapiolani Close-up View During Repair (from Ref. 8).	11
1.10 Various Duct Arrangements.	12
1.11 Example Tendon Layouts at Las Lomas for Two Arrange- ments.	14
1.12 Cracking in Curved Bottom Slab from PT (from Ref. 7).	19
1.13 Failure of Bottom Slab at Schottwein (from Ref. 11).	20
2.1 Global Girder, Regional Beam and Local Beam Actions.	22
2.2 Curvature-Generated Forces on Tendon and Concrete.	23

2.3	Arch Action Force (C_{arch}).	24
2.4	Arch Action Forces on Compact and Box Cross-Sections	25
2.5	Shear and Moment in Web due to Lateral Prestress Force.	25
2.6	Arch Action Force Distribution from Unsymmetrical PT.	26
2.7	Direction of Unrestrained Girder Movement at Las Lomas (from Ref. 6).	27
2.8	Transverse Force at Bearing from Longitudinal Girder Move- ment at Las Lomas (from Ref. 6).	27
2.9	Global Girder Action at Las Lomas (Based on Ref. 6).	29
2.10	Regional Beam Moments as Calculated in Ref. [6].	30
2.11	Local Beam Moments as Calculated by Ref. [6].	32
2.12	Duct Arrangement at Kapiolani (from Ref. 6).	38
2.13	CALTRANS Standard Duct Arrangements-1973 (from Ref. 6).	40
2.14	CALTRANS Design Chart with #5 Stirrups (from Ref. 7).	41
2.15	CALTRANS Design Chart with #6 Stirrups (from Ref. 7).	42
2.16	CALTRANS Detail "A"-1982 (from Ref. 7).	43
2.17	CALTRANS Detail "A"-1985 (from Ref. 19).	44
3.1	End View of Girder.	48
3.2	Plan View of Girder.	49
3.3	Stirrup Layout.	51
3.4	Girder #1 Cross-Section in Curve (BC & 1.0DC).	52
3.5	Girder #2 Cross-Section in Curve (BO & 0.2DC).	53
3.6	Reinforcement Details of Bottom Slab.	54
3.7	Reinforcement Details of Top Slab.	54
3.8	Web Cross-Section at End of Girder.	55

3.9	Centered Duct.	57
3.10	Offset Duct.	57
3.11	Duct Profile.	60
4.1	Girder #1 Concrete Strength Gain.	63
4.2	Girder #2 Concrete Strength Gain.	63
4.3	Metal Duct Cross-Section.	65
4.4	Exterior Web Form.	68
4.5	Core and Exterior Web Forms.	68
4.6	Section of Core Form and Bracing.	69
4.7	Articulated Top Slab Soffits.	69
4.8	Stirrup Alignment System.	71
4.9	Stirrups and Jig Before Casting Bottom Slab.	72
4.10	Stirrups and Jig After Casting Bottom Slab.	72
4.11	Plastic Spacers.	73
4.12	BC Duct Arrangement (Overall View).	75
4.13	BC Duct Arrangement (Close-Up).	75
4.14	1.0DC Duct Arrangement (Overall View).	76
4.15	1.0DC Duct Arrangement (Close-Up).	76
4.16	0.2DC Duct Arrangement (Overall View).	77
4.17	0.2DC Duct Arrangement (Close-Up).	77
4.18	BO Duct Arrangement (Overall View).	78
4.19	BO Duct Arrangement (Close-Up).	78
4.20	Anchorage Plates (Not in Final Position).	79
4.21	Rodding, Internally Vibrating, Placing and Externally Vibrating.	79
4.22	Internal Vibrator.	81

4.23	Casting of Top Slab.	81
4.24	Web 0.2DC Voids.	82
4.25	Web BO Void.	83
4.26	Specimen BO Exterior Patch Form.	85
5.1	Strand Positions in Curve.	88
5.2	Live End Load System.	89
5.3	Live End Strand Anchorages.	89
5.4	Dead End Load Beam.	91
5.5	Dead End Screw Chuck Anchorages.	91
5.6	Dead End Chairs and Bearing Plates.	92
5.7	Live End Bearing Plates.	93
5.8	Load System Schematic.	95
5.9	Ram Calibration Curve.	96
5.10	Strain Gage Nomenclature.	99
5.11	Web-Slab Potentiometer.	102
5.12	Web-Slab Potentiometer Nomenclature.	102
5.13	Delamination Gage Schematic.	104
5.14	Typical Delamination Gage Installation.	104
5.15	Delamination Gage.	105
5.16	Delamination Gage Nomenclature.	106
5.17	Web-Web Potentiometers.	107
5.18	Web-Web Potentiometer Nomenclature.	107
5.19	Abundant Instrumentation for Specimen BC.	108
5.20	Reduced Instrumentation for Specimen BO.	108
5.21	Monostrand Stressing.	112
5.22	Grid Identifying Stirrups and Duct Centerlines.	115

6.1	Specimen Ultimate Capacities and Visible First Crack.	119
6.2	Typical First Crack (Flexural) for All Specimens.	119
6.3	1.0DC Elevation View of Failure.	121
6.4	1.0DC Concrete Fragments.	121
6.5	1.0DC Plan View of Failure.	122
6.6	1.0DC View of Interior Surface of Concrete Panel.	122
6.7	1.0DC Panel Top-Forward Tilt.	123
6.8	1.0DC Pullout of Stirrups.	123
6.9	1.0DC Failure Plane After Removing Concrete Panel.	124
6.10	Specimen Failure Planes.	125
6.11	Shear Diagram for Specimen 1.0DC.	126
6.12	1.0DC Top Slab Crack (Enhanced with a Felt-Tip Marker). . .	127
6.13	BC at Ultimate (Shear Cracks Barely Visible in Shadow). . . .	129
6.14	BC Cracking at One Stage After Ultimate.	129
6.15	BC at Two Load Stages After Ultimate.	130
6.16	BC at Snap-Through.	130
6.17	BC Flexural Cracking After Completion of Test.	131
6.18	BC After Removing Concrete Panel.	131
6.19	BC View of Surface Behind Ducts.	132
6.20	Overview of 1.0DC and BC.	132
6.21	0.2DC Start of Visible Delamination Cracks at Ultimate.	135
6.22	0.2DC at Load Stage after Ultimate.	135
6.23	0.2DC at Snap-Through.	136
6.24	0.2DC Elevation View of Failure.	136
6.25	0.2DC Plan View of Failure.	137
6.26	0.2DC View of Surface Behind Ducts.	137
6.27	0.2DC After Removing Concrete Panel.	138

6.28	0.2DC Flexural Cracking After Completion of Test.	138
6.29	BO at Snap-Through.	140
6.30	BO Cracking at Patch.	140
6.31	BO View of Surface Behind Ducts.	141
6.32	BO Top-Forward Tilt.	141
6.33	Comparison of Web Delaminations at D61.	143
6.34	Comparison of Web Delaminations at D64.	144
6.35	1.0 DC Web Delamination Profile at Stirrups #4 &6.	145
6.36	BC Web Delamination Profile at Stirrup #6.	146
6.37	0.2DC Web Delamination Profile at Stirrup #6.	147
6.38	BO Web Delamination Profile at Stirrup #6.	148
6.39	1.0DC Extrapolated Web Delamination Profile.	150
6.40	BC Extrapolated Web Delamination Profile.	150
6.41	BO Extrapolated Web Delamination Profile.	151
6.42	Comparison of Stirrup Stresses at 6IM.	154
6.43	Specimen Ultimate Capacities, Visible and Microcracking.	155
6.44	Comparison of Stirrup Stresses at 6IU.	156
6.45	1.0DC Stresses at Stirrup #6 (IL, IM, IU)	158
6.46	1.0DC Web Delamination and Stirrup Stresses.	159
6.47	BC Stresses at Stirrup #6 (IL, IM, IU).	160
6.48	Web Delamination and Stirrup Stresses.	161
6.49	0.2DC Stresses at Stirrup #6 (IL, IM, IU).	162
6.50	0.2DC Web Delamination and Stirrup Stresses.	163
6.51	BO Stresses at Stirrup #6 (IL, IM, IU).	164
6.52	BO Web Delamination and Stirrup Stresses.	165
6.53	1.0DC Stresses at Stirrup #4 (IL, IM, IU, OUU).	166

6.54	0.2DC Stresses at Stirrup #6 (ILL, IM, IUU, OLL, OM, OLL).	167
6.55	Comparison of Web Deflections at Stirrup #6.	168
6.56	Web Deflections After First Crack.	169
6.57	BC Web Deflections in Curve Relative to Web PC & PT.	171
6.58	Comparison of BC Web-Web and Web-Slab Deflections.	172
6.59	BC Longitudinal Concrete Strains.	174
7.1	Regional Beam and Local Beam Actions.	176
7.2	1.0DC Compression Arch Forces on Web at Microcracking Load.	178
7.3	1.0DC Frame Analysis at Microcracking.	179
7.4	1.0DC Moments (Measured) at Mid-Height of Web.	181
7.5	Web Cross-Section For Calculating Moments After Cracking.	181
7.6	1.0DC Moments (Analysis & Measured) at Mid-Height of Web.	183
7.7	Longitudinal and Vertical Strain Relationship at Mid-Height of Web.	185
7.8	Compression Arch Force Distribution on Cracked and Un-cracked Web.	186
7.9	BC Effective Shear Plane Depth.	190
7.10	1.0DC Effective Shear Plane Depth.	191
7.11	Shear Design Recommendation.	199
7.12	Possible Failure Planes When Vertical Clear Spacing is Greater Than or Equal to One Duct Diameter.	200
7.13	Design and Actual Ultimate Shear Capacities as a Function of Vertical Clear Spacing.	203

A.1	Comparison of Web Delaminations at D62.	213
A.2	Comparison of Delaminations at D63.	213
A.3	BC Web Delamination Profile at Stirrup #4.	214
A.4	1.0DC Stresses at Stirrup #6 (IL, IM, IU)-Complete Load History	214
A.5	BC Stresses at Stirrup #6 (IL, IM, IU)-Complete Load Histo- ry.	215
A.6	Comparison of Web Deflections Relative to Slabs at Stirrup #4.	215
A.7	Comparison of Web Deflections Relative to Slabs at Stirrup #4- Complete Load History.	216

CHAPTER 1: INTRODUCTION

1.1 BACKGROUND

Favorable economics, construction methods and aesthetics are responsible for the increased use of post-tensioned concrete box girder bridges. They are often less expensive to build and maintain than arches, steel plate girders and trusses in the 150' to 800' main span range. Not as widespread but becoming increasingly popular are 80' to 150' spans which can be built using the span-by-span construction method. This system of erecting the prefabricated superstructure from previously constructed spans has great appeal for long, multi-span urban bridges with limited right-of-way. Aesthetically, box girders have a smooth, continuous profile and when built with a sloped web or cantilevered wing, create a light and almost floating appearance [Figure 1.1].

Sometimes bridges must be built on horizontal curves as mandated by the roadway alignment. Nearly all urban double-deck bridges will be curved for some distance because of existing city streets, railways, utilities and buildings. Elevated entrance and exit ramps are likely to be curved and usually on a smaller radius than the mainlanes. Geographical features and alignments of other roadways force curvatures in bridges of all types and span lengths.

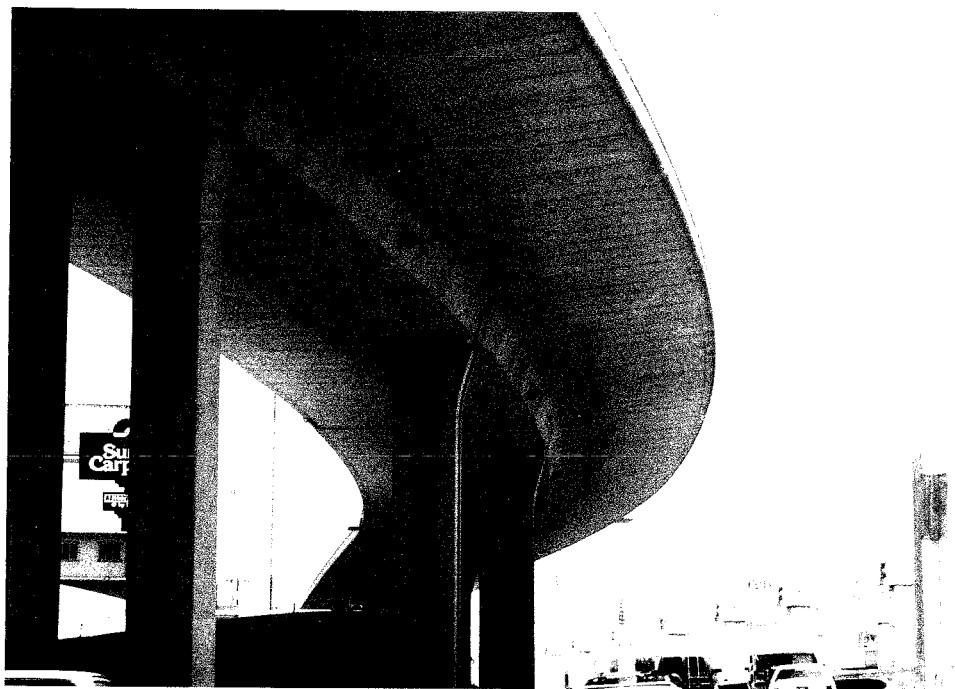


Figure 1.1 San Antonio "Y" Concrete Box Girder.

Tensioning of a concrete box girder is achieved with either internal or external tendons as defined relative to their position with the concrete section. Internal tendons are embedded in the concrete cross-section and external tendons are encased in the concrete only at the anchorages and deviation points [Figures 1.2 & 1.3]. Each type has its inherent advantages and disadvantages. Internal tendons have long been favored because they provide high ultimate flexural capacity. When grouted, they become fully bonded with the cross-section creating strain compatibility between the steel and concrete. Experimental tests have shown that bonded prestressing steel can develop stresses at ultimate nearly equal to that of the tendon ultimate strength. External tendons are not bonded to the concrete for much of their length and allow elongations created by a single crack or joint opening in the concrete to be dispersed over a long length of the tendon. In completely unbonded

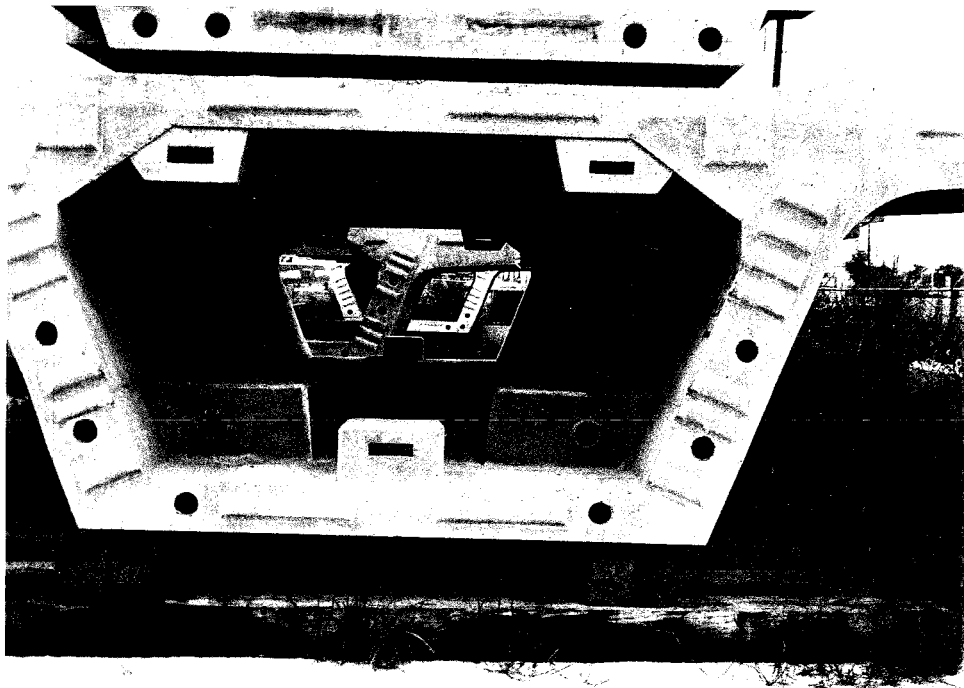


Figure 1.2 Box Girder Segment with Internal Ducts in Webs.

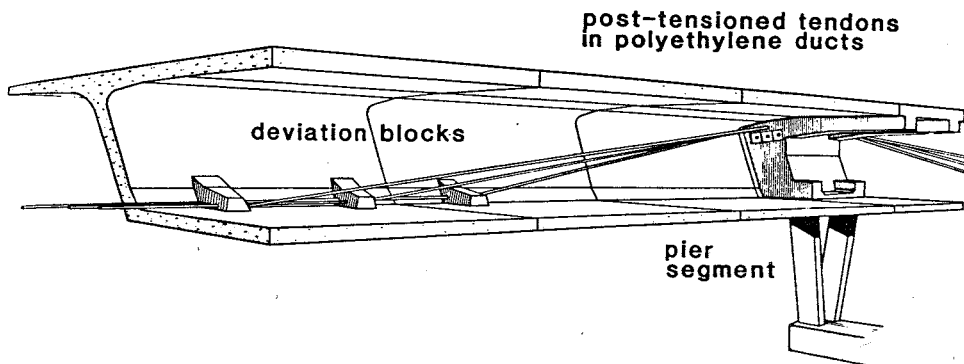


Figure 1.3 Box Girder Bridge with External Tendons (from Ref. 7).

tendon girders, crushing of the concrete will occur at ultimate before the stress in the tendon can increase much above the stress existing in the tendon prior to the addition of external loads. Tests have shown that unbonded girders are much weaker in ultimate capacity than bonded girders [1]. However recent research has shown that local bonding of external tendons at the deviators and a few well-positioned attachment points along the girder can greatly offset this strength loss [2]. At present, AASHTO does not recognize this new research and continues to severely limit the nominal design stress in the external tendons [3].

The force in a bonded internal tendon is also well distributed along the girder and not just at the anchorages and deviation points as with an external tendon. This reduces the high concentrated forces at deviation points and anchorages. The more numerous but smaller cracks that develop from overloads are not as conducive to water penetration thus giving more protection to the reinforcing steel. As for corrosion protection of the prestressing steel itself, there is a shift in favor of external tendons. Previously, many preferred the completely surrounded, bonded tendon but recent discoveries have shown that the internal tendon may be subject to water intrusion at mortar and dry joints in segmental bridges [4]. Furthermore the strands may not be fully encased as grouts are not prestressed and are prone to cracking. External tendons are usually placed in the open cell of the box and are sealed in plastic or metal ducts. They are only subject to water at locations continuous with the concrete or in case of flooding or high humidity. External tendon girders are usually easier to construct because the ducts are essentially independent of much of the cross-section allowing for less interference with the reinforcing cage and concreting operations [5].

Tendons are utilized most efficiently when they change elevation along the length of the bridge. Their eccentricities produce bending moments that counter those from gravity loads. Draping of internal tendons from top flange to bottom flange occurs by depressing the ducts along the web axes. When multiple tendons are used in a single web, maximum eccentricity is achieved by bundling the tendons. The bundle is generally maintained along the length of the bridge including low-moment regions where the tendons are near the neutral axis. However the tendons are usually then splayed near the girder end to accommodate anchorages and stressing equipment.

1.2 FAILURES

Two serious web failures have occurred during the construction of curved post-tensioned concrete box girders. Las Lomas Bridge in California was a cast-in-place, 3-span (176'-234'-176'), 2-celled box girder with the final approximately 100' built on a 250' radius [Figure 1.4] [6, 7]. Diaphragms were located at the quarter points of the curved span. The structure was post-tensioned with twelve draped tendons. Each tendon consisted of 27 or 28 one-half inch diameter strands. Four tendons were placed in each of the three webs. The tendons ran the entire length of the bridge and were located high in the cross-section over the interior piers and low in the web at the midspans. Stressing was done from both abutments at which time the concrete compressive strength was 3450 psi. The webs were 12" thick and reinforced with #5 GR40 bars spaced at 15". The length and location of the stirrup splices are not given in the report by T.Y. Lin International (TYLI), but they were adjacent to the tendons in some areas.

On October 4, 1978, while stressing the last of the twelve tendons, the web with the smallest radius failed with an explosive breakout allowing the

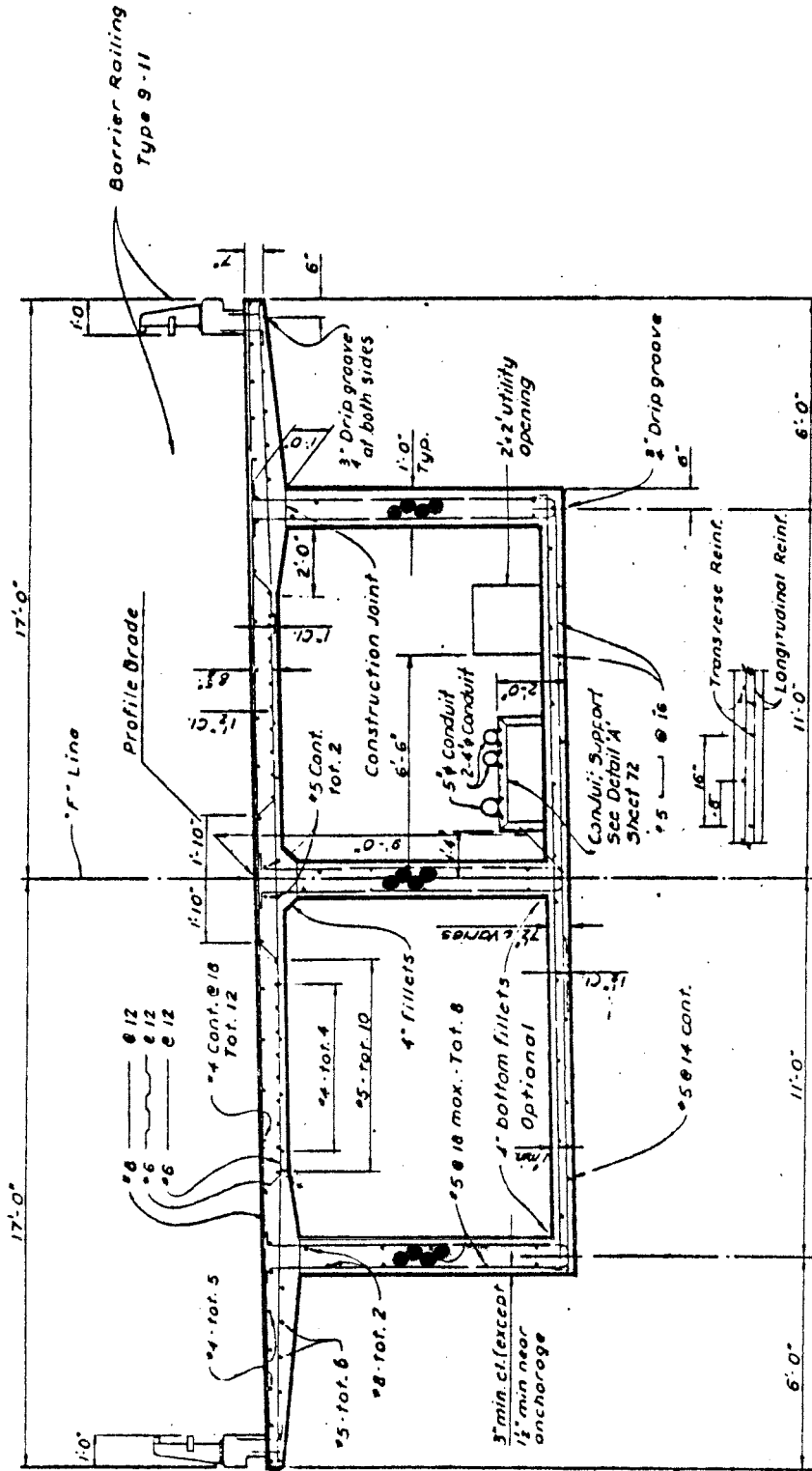


Figure 1.4 Las Lomas Cross Section with Bundled Ducts (based on Ref. 6).

tendons to form a straight line between the abutment and the first interior pier [Figure 1.5]. Two days later, the other outside web also ruptured but the failure length was limited to the distance between the abutment and first diaphragm [Figure 1.6].

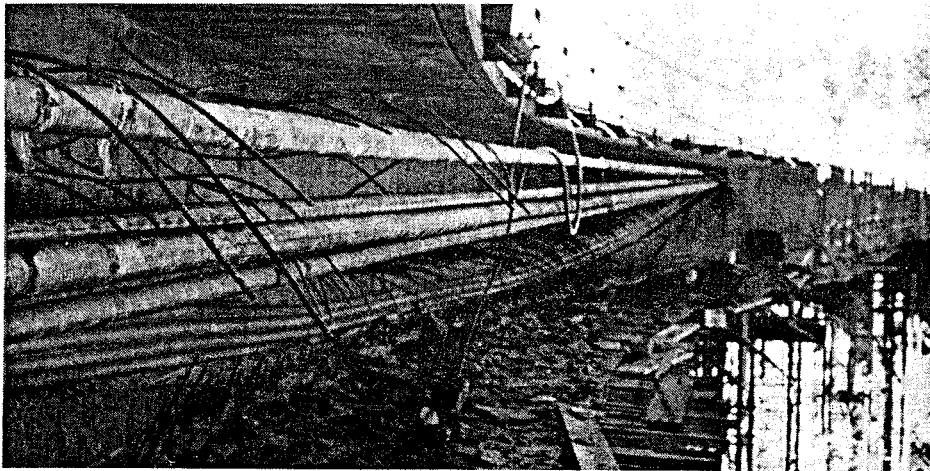
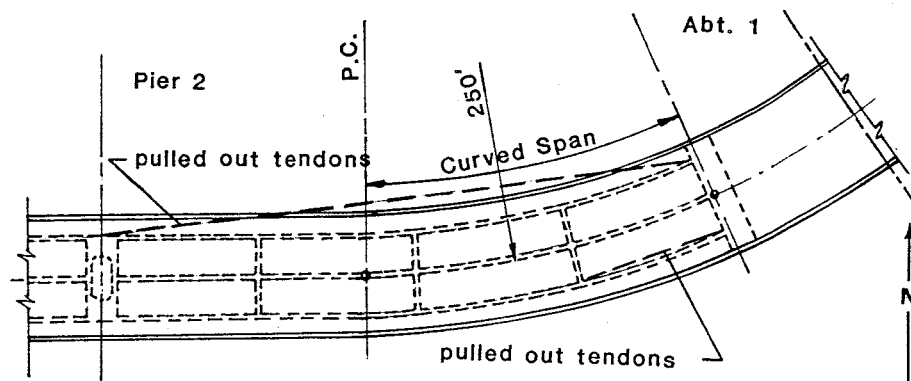
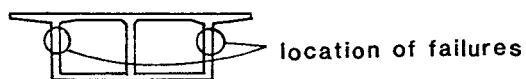


Figure 1.5 Breakout of Tendons at Las Lomas (from Ref. 7).



Partial Plan



section

Figure 1.6 Locations of Tendon Breakout at Las Lomas (from Ref. 7).

In 1981, the Kapiolani Interchange Ramp in Hawaii experienced web cracking and spalling adjacent to the tendons but no actual breakout [7, 8]. This also was a continuous, cast-in-place, 2-celled box girder [Figure 1.7]. The author is unaware of span lengths or box dimensions, but it is known that the bridge was constructed such that the inside web had a 540' radius. The failure occurred over the two spans of the central unit of a three unit bridge [Figure 1.8 & 1.9]. There were six ducts located in each web and failure occurred in the web with the smallest radius after the fourth tendon was stressed.

Failures of this type can be very costly in terms of repair, lost time and injuries. Fortunately, no workers were injured in either of these incidents. On urban construction projects there is also the additional threat of concrete debris being launched into traffic lanes. Both of these bridges were eventually repaired. The Kapiolani bridge was retrofitted with tie-back dowels and a thickened web at a cost of \$4 million. This nearly equaled the bid price in the original contract. The author is unaware of the cost to repair the more heavily damaged Las Lomas structure.

1.3 DUCT ARRANGEMENT

Perhaps the single variable that contributed most to these failures was the arrangement of post-tensioning ducts. Both of the failed bridges had bundled tendons. Kapiolani had six ducts stacked vertically and Las Lomas had its bundled tendons in a zig-zag arrangement with even more eccentricity. Bundled ducts create a large discontinuity in the web that appears to be the origin of the failures. Since the time of these failures, designers have used a number of different cross-sectional tendon positions to strengthen this region [Figure 1.10]. Ducts have been separated to create several small discontinuities rather than one large one. Another common arrangement is

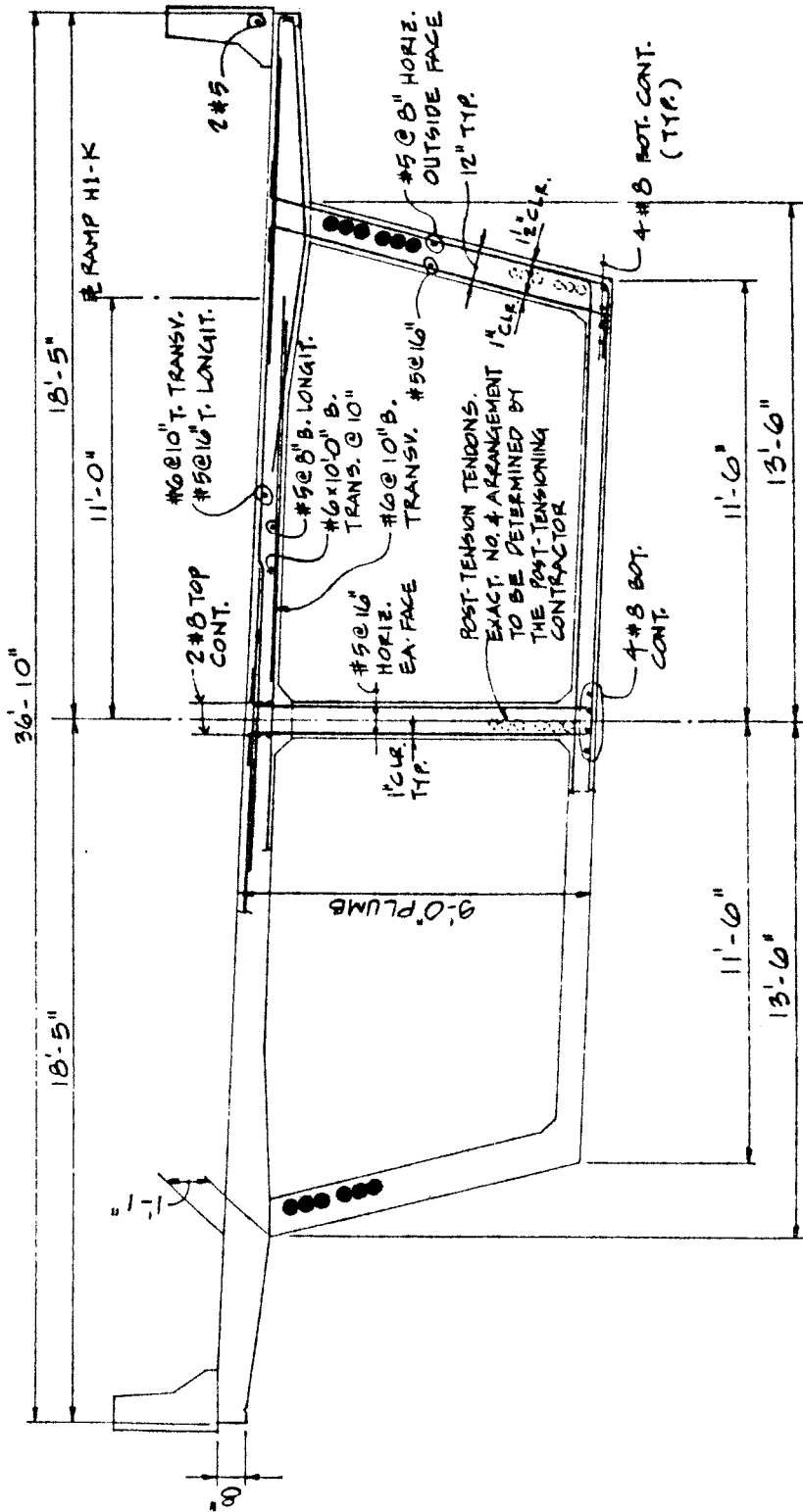


Figure 1.7 Kapiolani Cross-Section with Bundled Ducts (Based on Ref. 8).

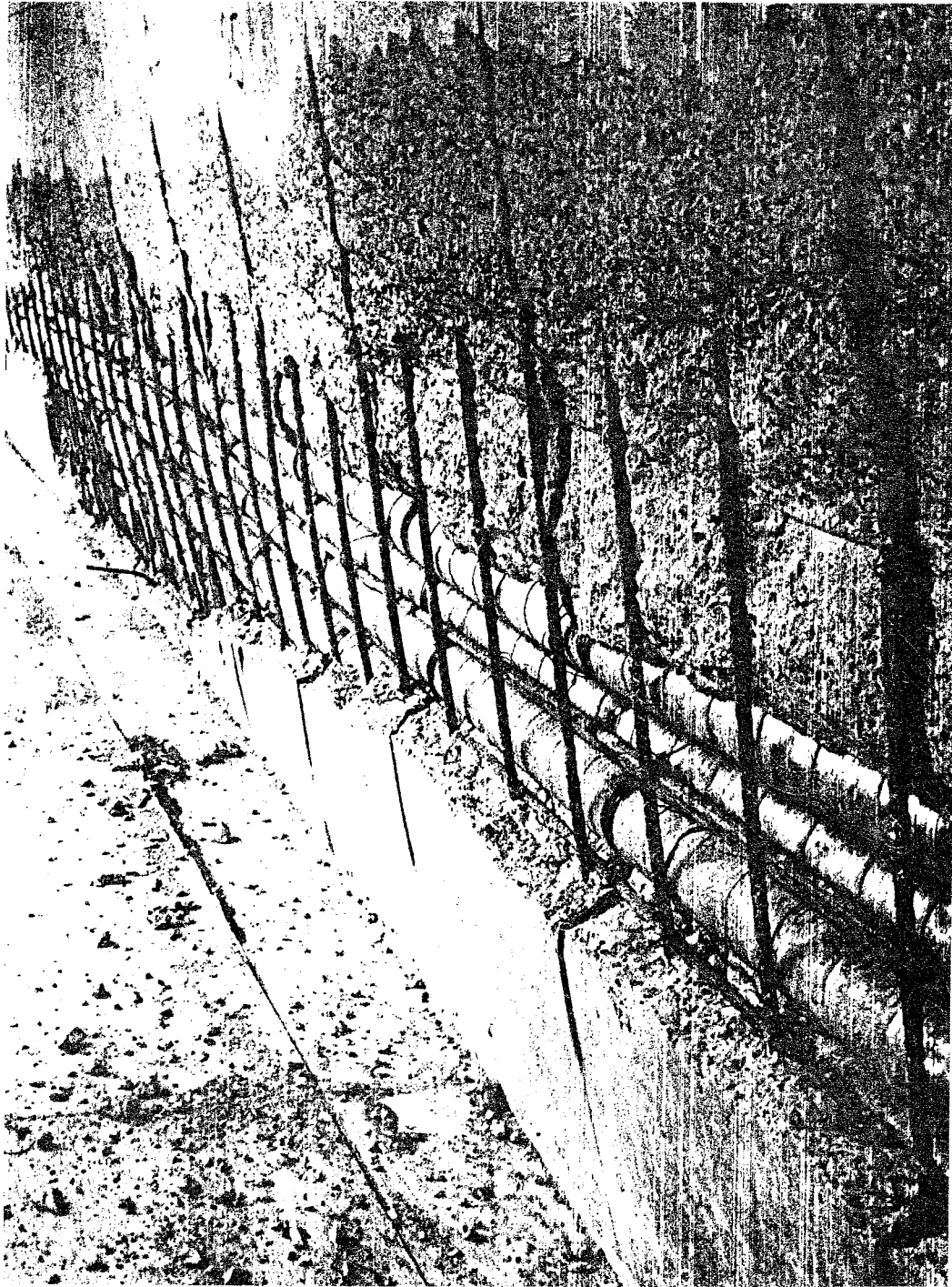


Figure 1.8 Kapiolani Overview During Repair (from Ref. 8).



Figure 1.9 Kapiolani Close-up View During Repair (from Ref. 8).

to offset the tendons from the web axis thereby creating more duct cover. In this arrangement, the ducts are usually tied against the stirrup leg furthest from the center of the curve.

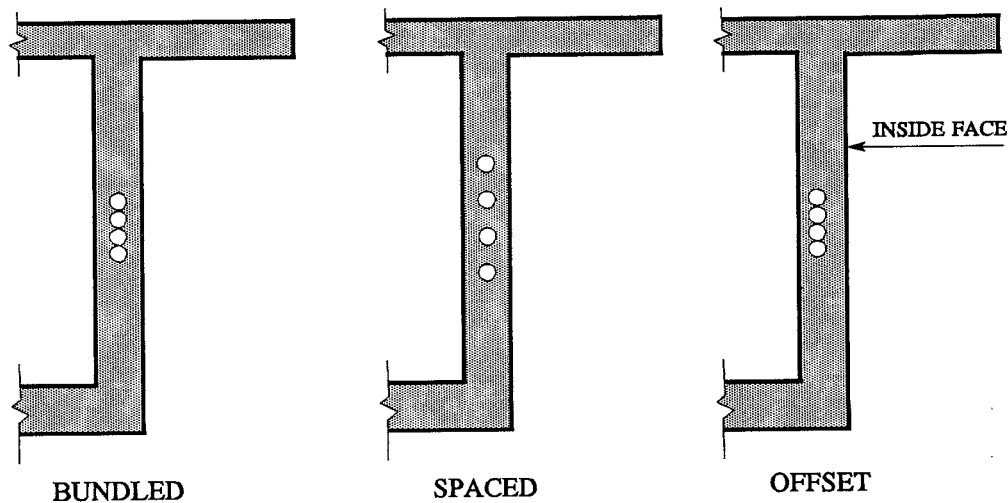


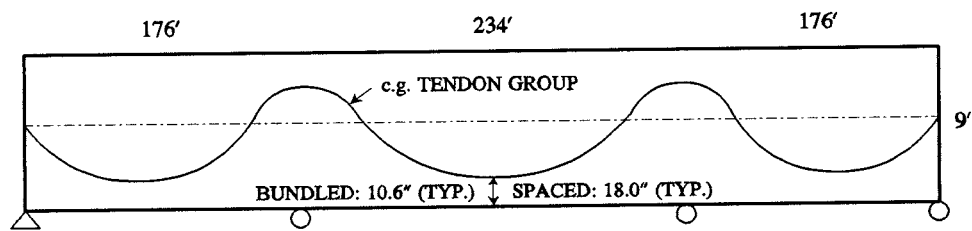
Figure 1.10 Various Duct Arrangements.

Designers are reluctant to use a spaced tendon arrangement because of the reduction in the internal moment arm. An investigation into the design of Las Lomas with its bundled ducts and an alternative design with a full duct diameter clear spacing between ducts illustrates this point. A complete redesign of the bridge is beyond the scope of this project, and is not necessary for this comparative study. While the critical regions are not known, stress at the bottom fiber at the midspan of span 2 is assumed to control the allowable stress design, likewise the ultimate moment at this same region is assumed to control the flexural strength design. It is recognized that every continuous girder will respond differently to changes in tendon eccentricity. However this example can be useful to illustrate what the designers of this particular bridge were saving in materials by choosing a bundled arrangement.

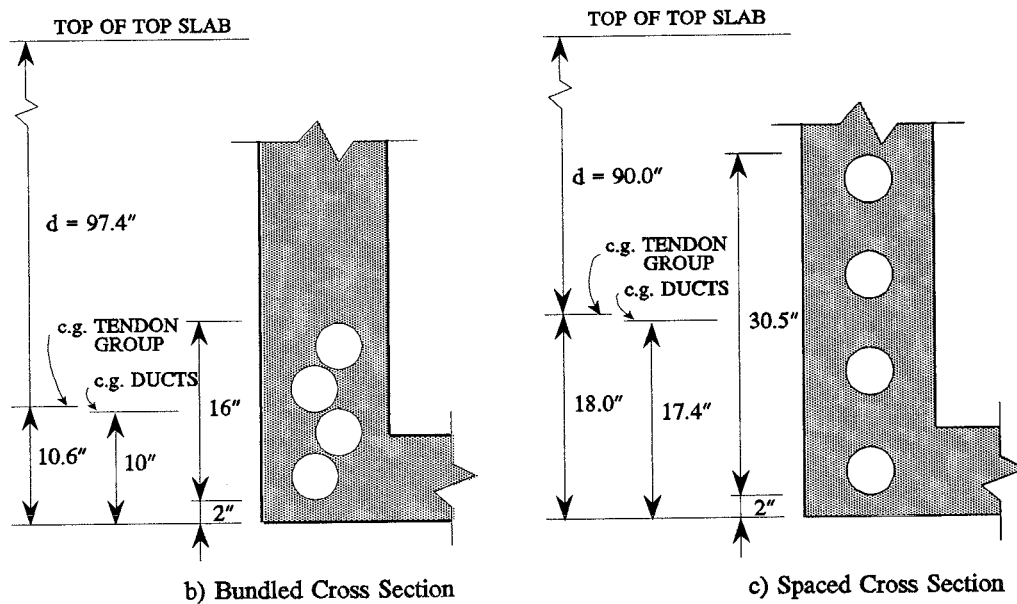
An elastic analysis of the continuous girder was performed to examine the girder effects from the twelve tendons. No self weight, additional dead, live or thermal loads were applied. Neither were long term post-tensioning losses considered. However coefficients of friction and wobble of 0.25 and 0.0015 respectively were used for friction losses. For simplicity, a constant bottom slab thickness of 7.5" was used over the length of the bridge. Cross-sectional properties were: Area = 9040 in², Moment of Inertia = 15,900,000 in⁴, $y_t = 45.7$ in. and $y_b = 62.3$ in.

Two computer runs were made using a post-tensioned beam program that computes tendon stressing losses and applies corresponding longitudinal forces and primary moments along the girder. Each run had a single, unique tendon path representing the centroid of the tendon group. The first run was the girder as designed with zig-zag bundled tendons assumed to approach within 2" of the bottom and top fibers [Figure 1.11b]. A value of $z = 0.55$ " was used to account for the offset of the tendons from the centers of the ducts in curved regions. The centroid of the tendon group was located 10.6" from both the top fibers over the interior piers and the bottom fibers at midspan. The tendon group was anchored at the neutral axis at both ends [Figure 1.11a]. Twelve, 28 strand (0.5" diameter) tendons were assumed.

The second run was made with the ducts aligned vertically with a one-duct diameter clear spacing (4.39") between them [Figure 1.11c]. One difference from the bundled example is that the centroid of the tendon group was 18.0" from the top or bottom fibers. The other is that trials were made with additional strands until the bottom fiber stresses at the midspan of span 2 were nearly equal to that of the bundled arrangement. This difference indicates the amount of additional post-tensioning steel which would be required of the spaced arrangement to meet the serviceability requirements



a) Tendon Profile



b) Bundled Cross Section

c) Spaced Cross Section

Figure 1.11 Example Tendon Layouts at Las Lomas for Two Arrangements.

in this region attained by the original design.

Table 1.1 shows that if serviceability requirements control this design, there is a small penalty in using the spaced arrangement. An increase of only two strands per duct (7.1%) is required because the axial stress component is more dominant than the effect of tendon eccentricity. The stress from the resultant external moment (M/S_b) is tempered by the fact that for continuous girders, greater eccentricities are accompanied by larger secondary moments.

Table 1.1 Bottom Stresses from PT for Las Lomas Example Arrangements

POST-TENSIONING STRESSES					
ARRANGEMENT	STRANDS PER DUCT	g	$\frac{P}{A}$ psi	$\frac{M}{S_b}$ psi	$f_{b_{PT}}$ psi
BUNDLED	28	10.6"	-627	-539	-1166
SPACED	30	18.0"	-689	-493	-1182

Nominal moment capacity was calculated for positive moment at midspan of span 2 assuming a 9" compression flange 34' wide. The sum of all web widths is 3' and the design concrete compressive strength is 3000 psi. For the bundled arrangement, $d=97.5"$ and for the spaced arrangement, $d=90.0"$. A ϕ factor of 0.9 was used.

Maximum percentage of steel controls the nominal moment calculation for the bundled arrangement. Therefore unlike the allowable stress

requirements, additional prestressing steel cannot be added to the spaced tendons to give a comparable capacity. By virtue of location of the neutral axis, the compression block is flanged rather than rectangular.

The ultimate moment generated at a section of a continuous girder is affected by the post-tensioning layout because of the secondary moments generated. AASHTO 9.7.1 requires that the secondary moments be added to the M_u calculation with a load factor of unity [3]. This has the same effect as lessening the nominal moment, so for comparative purposes, the secondary moments were subtracted from the nominal moment to get a so-called effective nominal moment ($\phi M_n - M_{sec}$).

Table 1.2 shows that the bundled tendon arrangement is preferable to the spaced arrangement should flexural strength govern the design process as it has 12.7% more capacity. Since no more prestressing steel can be added to the section designed, the spaced arrangement would require that the box dimensions or possibly the concrete strength would need to be increased.

Table 1.2 Effective Nominal Moments for Las Lomas Example Arrangements

EFFECTIVE NOMINAL MOMENTS					
ARRANGEMENT	STRANDS PER DUCT	d	ϕM_n k-ft	M_{sec} k-ft	$\phi M_n - M_{sec}$ k-ft
BUNDLED	28	97.4"	83,200	12,600	70,600
SPACED	28	90.0"	75,100	12,500	62,600

1.4 OBJECTIVES

In a fairly thorough literature search, no experimental research was located which reported tests that explored the phenomenon of tendon breakout. Several failure theories have been proposed and design procedures developed by various design agencies but they have not been validated by testing. The 1989 AASHTO Guide Specification for the Design and Construction of Segmental Concrete Bridges has a general, cursory equation which mandates the addition of reinforcing steel whenever concrete stresses from curved tendons become excessive [9]. An NCHRP research project to develop a new bridge specification is currently being written and contains slightly more comprehensive design guidelines [10]. All of these recommendations are discussed in detail in Chapter 2.

The specific objectives of this study were developed based on the premise that a series of physical tests were necessary to understand the actual behavior of tendon breakout. The detailed objectives were:

1. **Determine Which Tendon Arrangement is Most Resistant to Breakout-** Four of the most common tendon arrangements will be tested to determine first cracking and ultimate loads.
2. **Develop a Failure Model-** Instrumenting and stressing to failure curved box girder models are to be performed to provide a basis to determine which of the current theories best explains the actual failure mechanism. If none are satisfactory, a new one can be developed. Four different tendon arrangements are to be tested, so multiple failure modes may result.

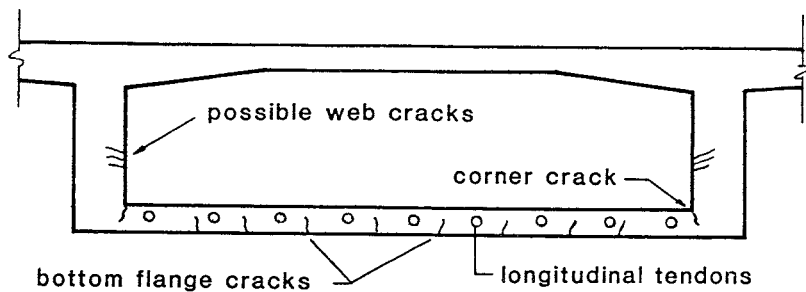
3. **Develop Design Recommendations-** A design guideline for determining the capacity of various duct arrangements will be developed.

1.5 SCOPE

Duct positioning is but one of many variables that can influence web breakout capacity. Thicker webs, stronger concrete, smaller stirrup spacing and additional hoop ties may likely improve the girder behavior. This pilot program is the first series of hopefully a continuing series of tests to examine this problem. Available resources limited the breadth of this particular study to an investigation of duct arrangements.

The research presented here is applicable for girders built with a continuous curvature. Segmental bridges are typically fabricated as individual straight elements with the curve made by small angle changes at the joints. Segment length will determine how closely the condition simulates a constant curvature. Long segments on small radius curvatures may have large, discrete lateral forces at the joints resulting in behavior different from that exhibited in these experiments.

A related problem that is not specifically addressed by this study is the failure of internal tendons from vertically curved bottom slabs. Long span, haunched girders often employ bottom soffit tendons in the midspan region to resist positive moments. Podolny reports that longitudinal cracks can develop both on the top and bottom of the bottom slab indicating high transverse flexural stresses [Figure 1.12]. In 1989, Schottwein Bridge in Austria suffered a separation of the middle section of the bottom soffit which contained 40 tendons made of 19 half-inch diameter strands [Figure 1.13].



Cracking from curved soffit tendons.

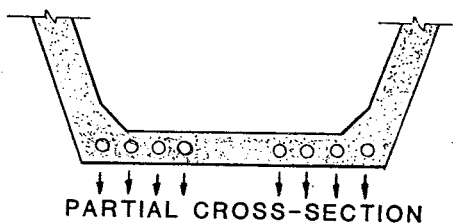
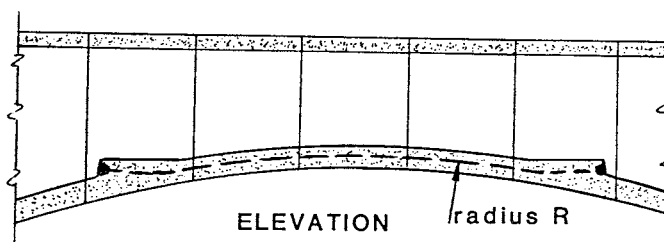


Figure 1.12 Cracking in Curved Bottom Slab from PT (from Ref. 7).

This failure is quite similar to the web failures in that a member of a box girder is supported at each end and is subjected to lateral loads generated from within the member via the stressing of post-tensioning tendons. Results from the test of the spaced duct arrangement may be useful in understanding the failure of these structures.

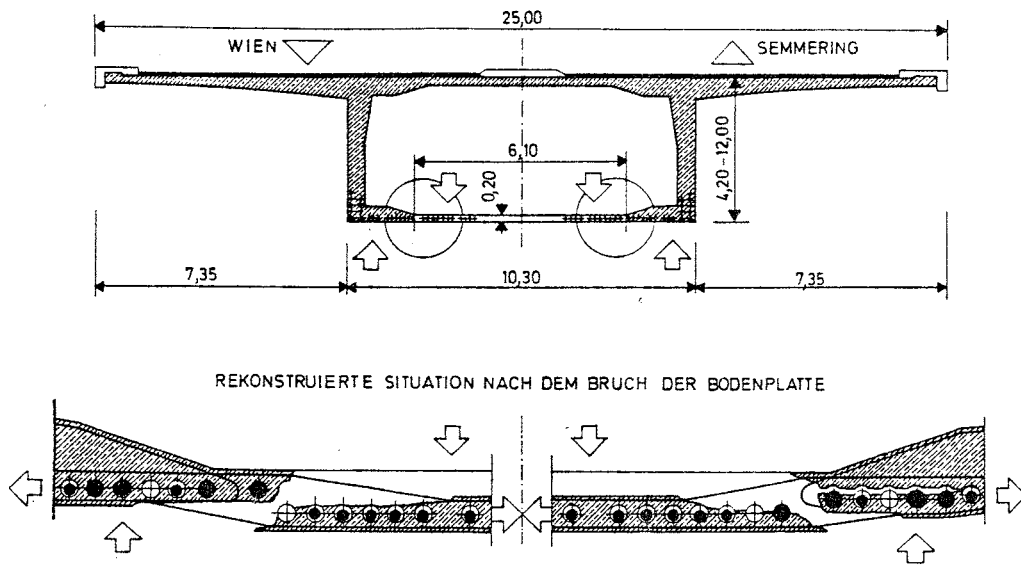


Figure 1.13 Failure of Bottom Slab at Schottwein (from Ref. 11).

CHAPTER 2: STATE OF THE ART

TYLI analyzed curved box girders subject to longitudinal prestressing according to three different actions [Figure 2.1] [6, 8]. The curved girder responds globally if the direction of free movement of uni-axial bearings at the piers is misaligned with the unrestricted direction of movement caused by the prestressing and volume change stresses. The behavior can also be envisioned as a regional action. The box acts as a frame with a lateral load where the webs containing ducts act as vertical flexural members. On a local scale, complex behavior develops in the region of the web directly adjacent to the duct group. These failure modes are discussed in greater detail in Section 2.2.

2.1 LATERAL PRESTRESSING FORCE ON THE BOX

A theory of transverse stresses developed in curved, box girder cross-sections due to the effects of post-tensioning was proposed by TYLI in the wake of the failure at Las Lomas [6]. Much of that report was summarized by Podolny [7]. When a horizontally curved girder is post-tensioned longitudinally with a tensile force, T_j , outwardly directed, distributed, lateral forces (F_r) are set up along the curved length of the tendon by the prestressing forces [Figure 2.2a]. Compressive reaction forces ($C_j = T_j$) tangent to the curve are developed in the concrete and the lateral forces from the tendon are directed inward [Figure 2.2b]. The subscript j is used in these

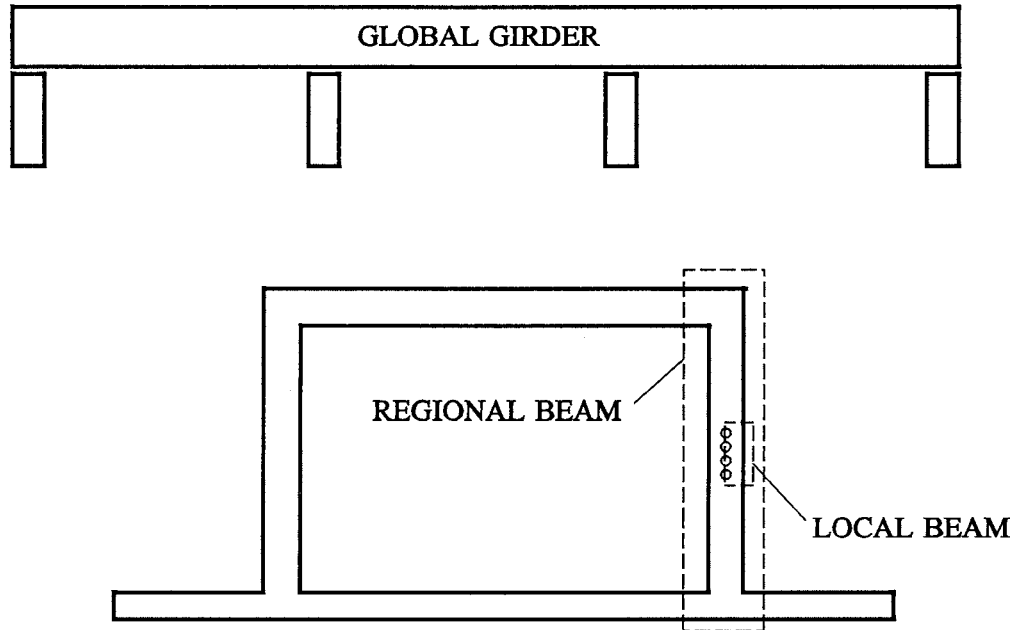


Figure 2.1 Global Girder, Regional Beam and Local Beam Actions.

terms because the maximum tendon force occurs during jacking. If friction and curvature losses are assumed to be non-existent and the curvature is constant, the lateral force is constant and the anchorage forces are equal.

A 1 foot long concrete segment anywhere along the curve has the force F_r acting along a radial line and the compression forces, C_j , acting perpendicular to the radial planes at the ends of the element [Figure 2.3]. The curvature causes the opposing compression forces to be misaligned. The normal components of these opposing compressive forces are additive and produce the force C_{arch} . Equilibrium is established by F_r which is equal to the component of the compression forces acting in the direction of F_r . As a result, no net lateral shear force due to post-tensioning exists on any radial plane. The compression force component is referred to by TYLI and Podolny as "distributed radial force arch action" or simply "arch action".

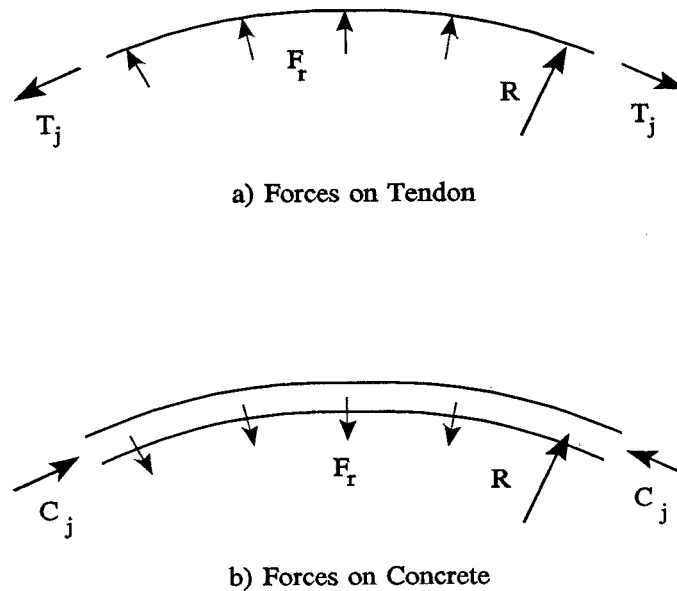
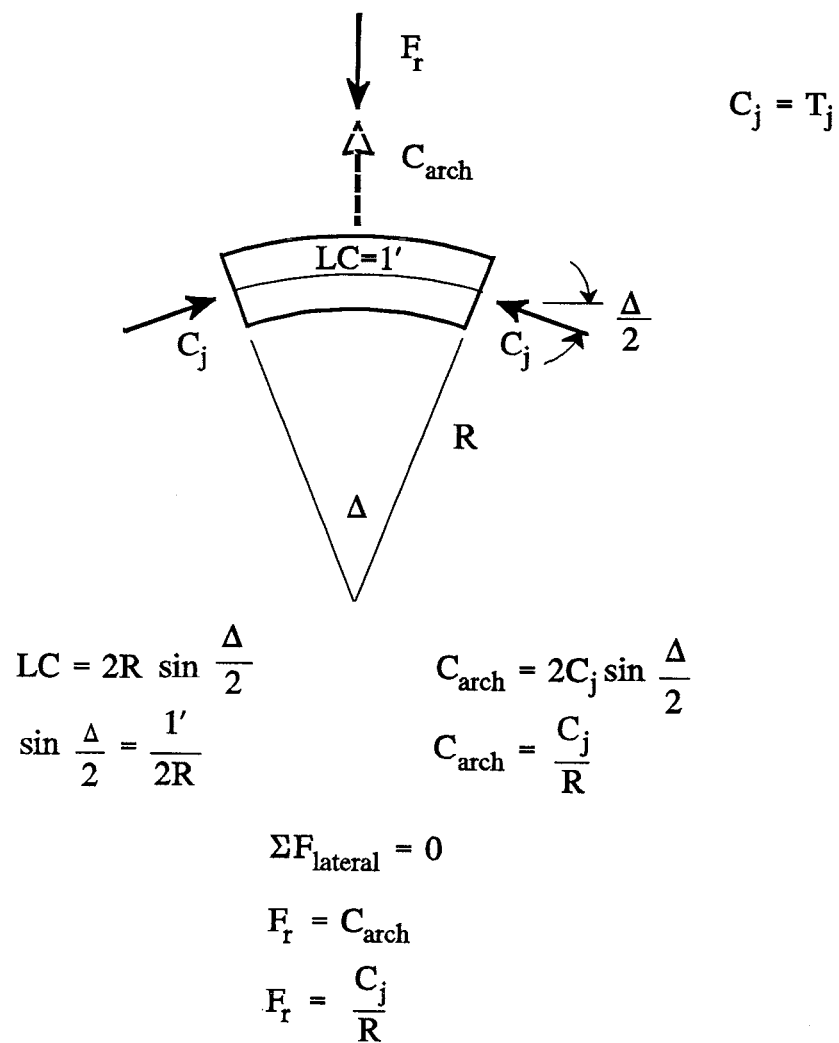
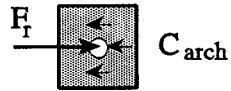


Figure 2.2 Curvature-Generated Forces on Tendon and Concrete.

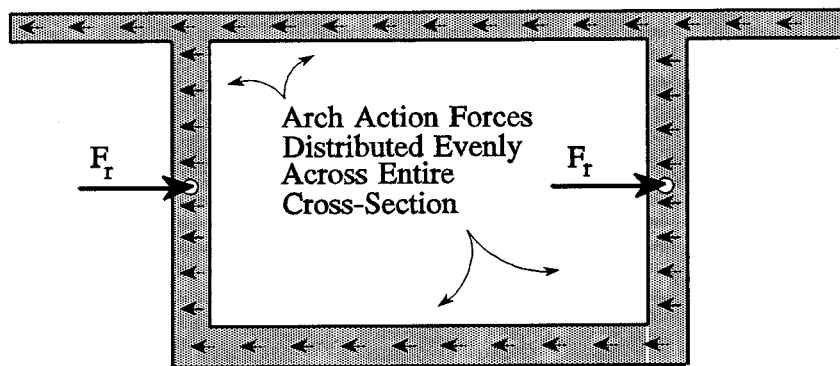
While the net lateral shear force on the radial plane is zero, the geometry of the cross-section and the point of application of F_r may produce high, local shear stresses. If post-tensioning is applied to a curved, compact cross-section, the aggregate of the arch action forces will be concentrated near F_r [Figure 2.4a]. As a result the shear stresses will be low and bending will be virtually non-existent. However for a curved box cross-section with a tendon located in the web, the situation is quite different. F_r is assumed to act locally at the tendon location, while the opposing uniform distribution of arch action forces is developed over the entire cross-section [Figure 2.4b]. In this case, high shear and bending stresses are present in the web [Figure 2.5].

TYLI and Podolny assume constant arch action forces over the entire cross-section. Implicit in their argument is that the arch action force is distributed across the cross-section by an axial post-tensioning force

Figure 2.3 Arch Action Force (C_{arch}).



a) Arch Action Forces on Compact Section



b) Arch Action Forces on Box Cross-Section

Figure 2.4 Arch Action Forces on Compact and Box Cross-Sections

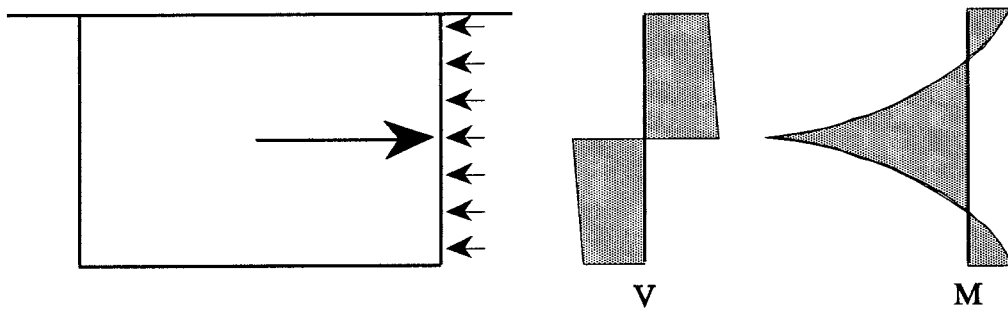


Figure 2.5 Shear and Moment in Web due to Lateral Prestress Force.

distribution. A uniform distribution of axial force only occurs when all prestress is applied symmetrically and at cross-sections at a sufficient distance from the anchorages so that the prestress is well distributed over the entire cross-section. This is not always the case. Box cross-sections are not always symmetrical and individual tendons are usually stressed in a slightly non-symmetrical manner. Care should be taken to set up the proper arch action forces in such an instance [Figure 2.6].

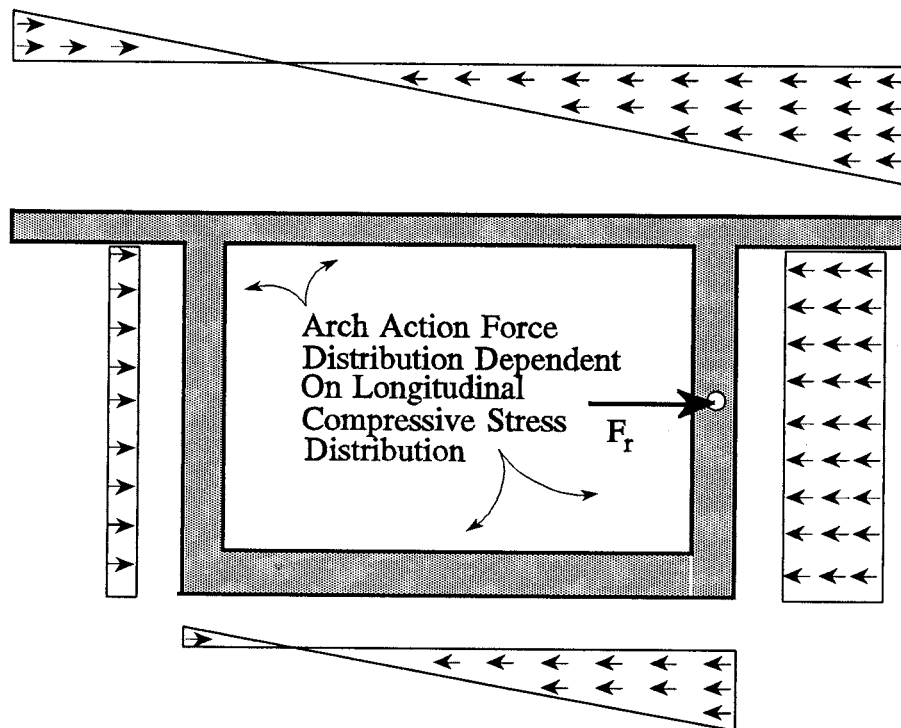


Figure 2.6 Arch Action Force Distribution from Unsymmetrical PT.

2.2 LAS LOMAS FAILURE MODES ASSUMED BY TYLI

Previous to this study, no known physical testing had been conducted on lateral breakout to substantiate TYLI failure theories. Three failure modes were advanced by TYLI and are discussed here [6]. Effects of the

girder self-weight are neglected in all calculations because the bridge was supported on falsework at the time of failure.

2.2.1 Global Girder Action

At Los Lomas, the non-alignment of abutment bearings and direction of longitudinal movement of a curved bridge produced transverse restraint forces [Figure 2.7]. Creep, shrinkage, elastic shortening and temperature change caused movement of the bridge on a line between the center of rigidity of the piers and the abutment bearings. The uni-directional abutment bearings were placed to give movement tangential to the alignment at the abutment. Therefore, when longitudinal movements occurred, the non-alignment caused a transverse component of force to develop at the bearing [Figure 2.8].

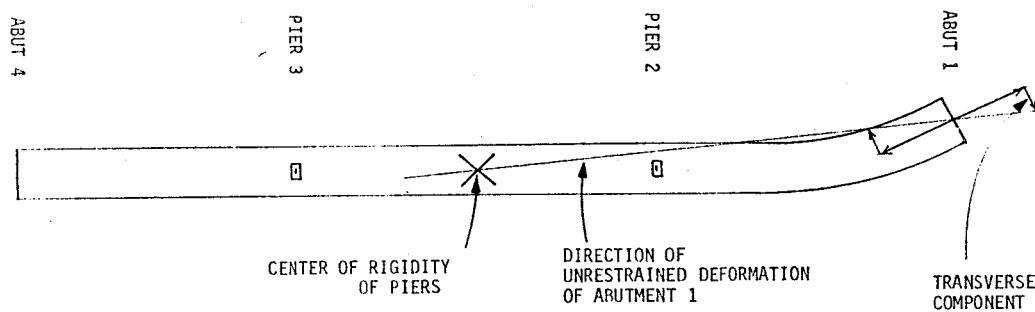


Figure 2.7 Direction of Unrestrained Girder Movement at Las Lomas (from Ref. 6).

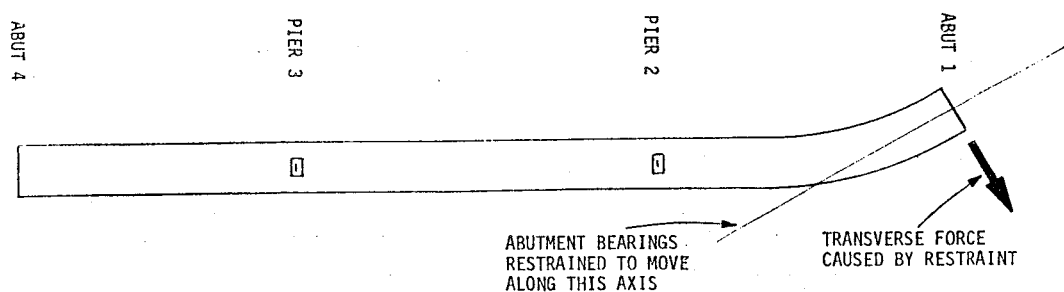


Figure 2.8 Transverse Force at Bearing from Longitudinal Girder Movement at Las Lomas (from Ref. 6).

This phenomenon was investigated by TYLI using a plane frame analysis. Post-tensioning forces were applied to a model of the last (curved) span [Figure 2.9]. A total post-tensioning force of 10,300 kips was applied. This assumed a stress of $0.75f_{pu}$ on all twelve tendons. A distributed lateral force of 41.2 k/ft resulted from dividing the post-tensioning force by the 250' radius. Fixity at the first interior pier and rotational and transverse restraint at the abutment were assumed. A constant shear force and reverse curvature moment diagram were developed. TYLI also applied a 100 degree Fahrenheit temperature drop to the model. The report does not show program output or results for creep or shrinkage.

TYLI did not carry out this analysis to show how transverse bending and shear actually contributed to failure. However it summarized, "The restraint of steel roller bearings at the abutment influences stresses in the concrete stems by about ten to twenty percent, but certainly not enough to produce failure".

It is important to recognize that this potential failure phenomenon only exists when uni-directional bearings are used and positioned such that they are not aligned with the girder's unrestrained direction of longitudinal travel.

2.2.2 Regional Beam Action

This failure mode assumed that the webs act like beams in a frame and span vertically between the top and bottom slabs. The webs are loaded by the concentrated lateral force from the tendon and the portion of the arch action forces acting on the webs [Figure 2.10]. Since a portion of the arch action forces is active over the flanges, the summation of arch action forces on any web is less than the concentrated lateral force on that web. This net force imbalance on the vertical span combines with the pattern of loading and causes shears and moments to develop. The relative stiffness of the webs and

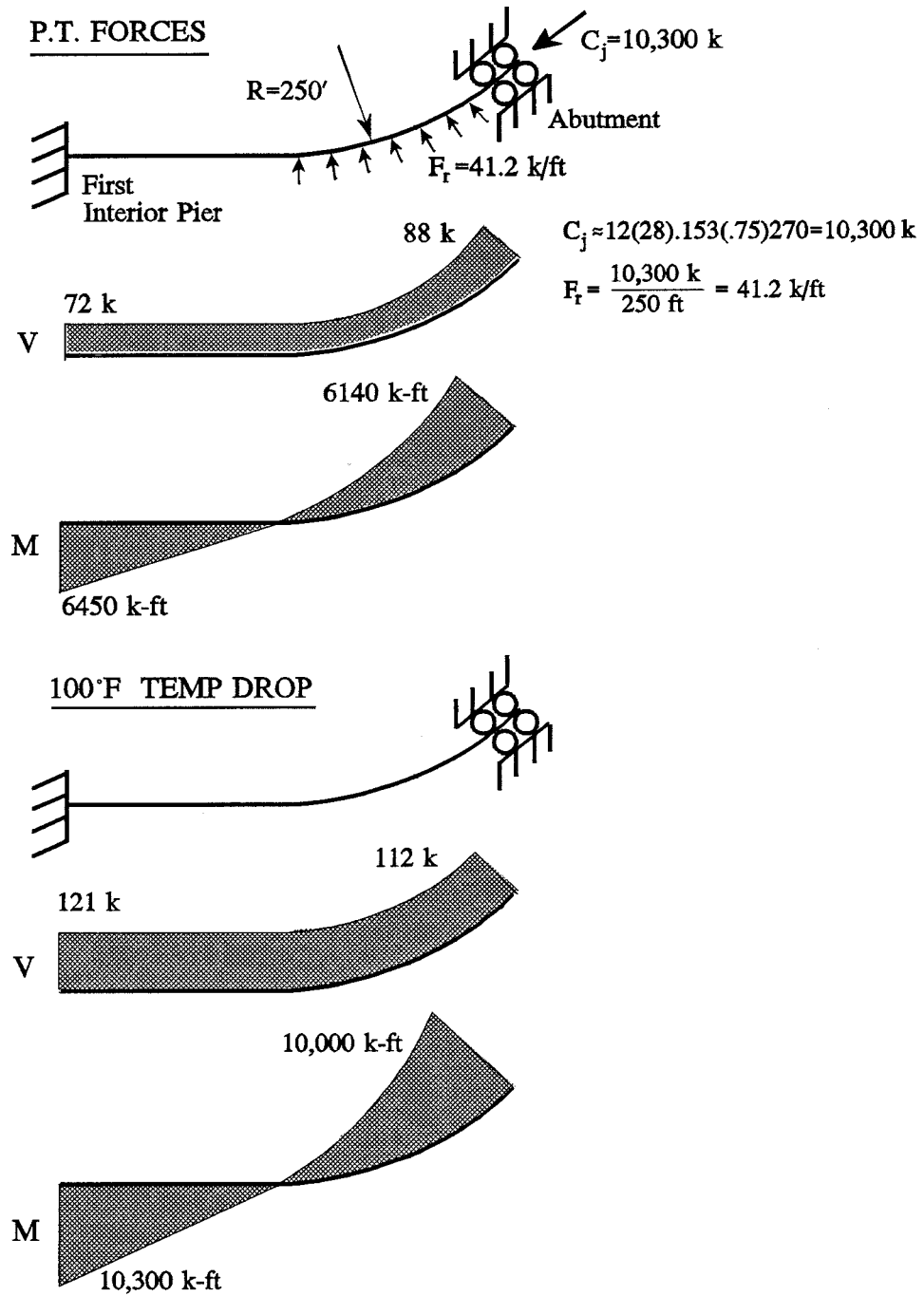


Figure 2.9 Global Girder Action at Las Lomas (Based on Ref. 6).

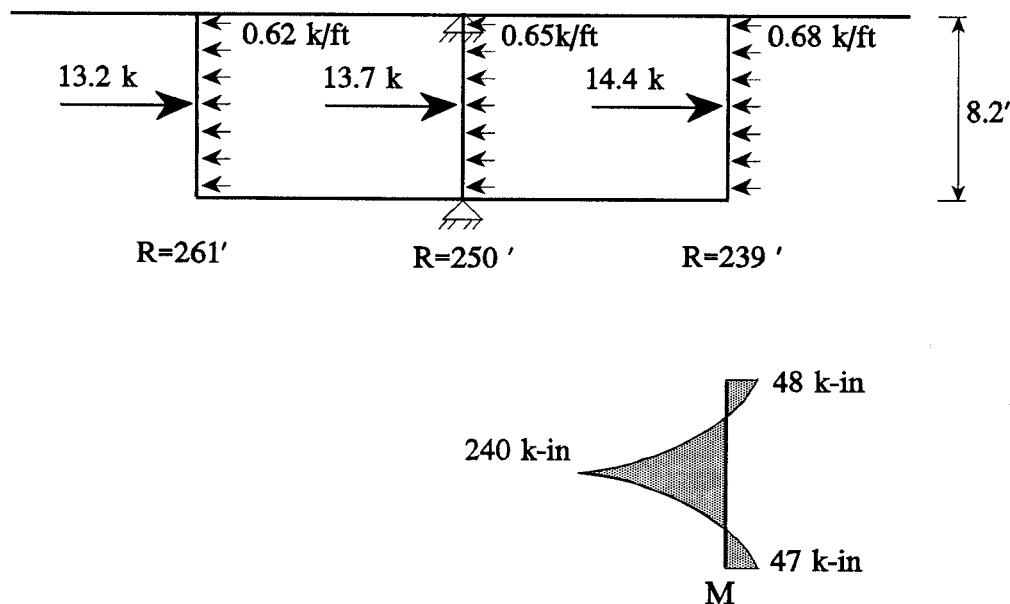


Figure 2.10 Regional Beam Moments as Calculated in Ref. [6].

flanges determines the rotational restraint provided to the webs.

TYLI analyzed Las Lomas as a frame supported vertically and horizontally at the top and bottom of the middle web. Although the actual tendon placement varied over the length of the span, lateral tendon forces were applied at mid-height of the web as this was the location that produces maximum flexural stresses. Each web had a different lateral tendon force because each had a unique radius. The arching action stresses were 1.13 ksi everywhere on the cross-section. This stress was multiplied by the thickness (12") and divided by the radius of each web to give the arching action distributed force. The member properties ignored the duct discontinuities and therefore were constant for the full height.

A maximum moment of 240 k-in occurred in the smallest radius web (239'). By comparison, the negative moment in the member ends was small (48 k-in). The maximum flexural stress on an assumed elastic, homogeneous

12" x 12" section was 830 psi. The cracking stress for 3450 psi concrete based on $7.5\sqrt{f'_c}$ was 440 psi. An ultimate strength analysis by TYLI showed a computed stress of 112 ksi required in the GR40 stirrups acting as flexural reinforcement. This indicates that the web was substantially inadequate for flexure.

In an investigation into stirrup splices, TYLI indicates that they were satisfactory. Actual splice lengths are not given in the report. TYLI suggests that perhaps the splices could have been made longer when located adjacent to the tendon or moved away from the maximum moment zone.

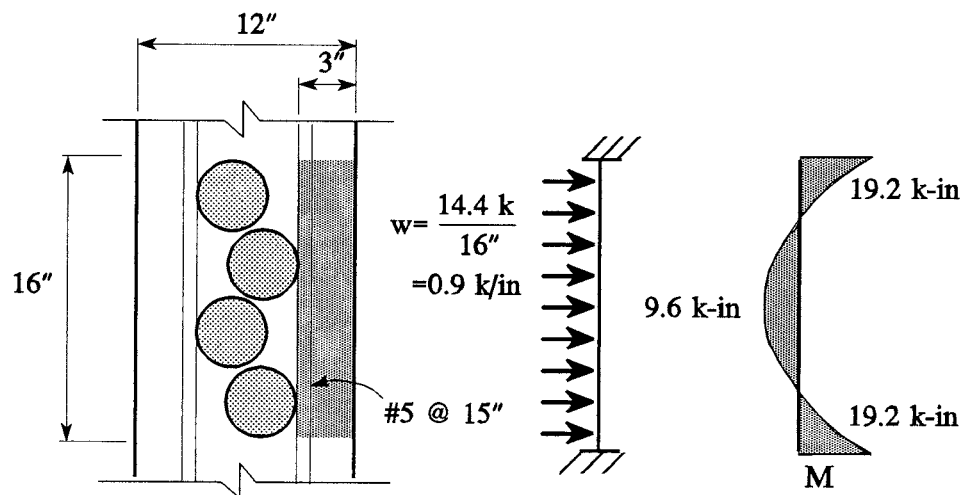
Shear capacity is not checked in the regional beam because it is controlled by the lower, local beam capacity.

2.2.3 Local Beam Action

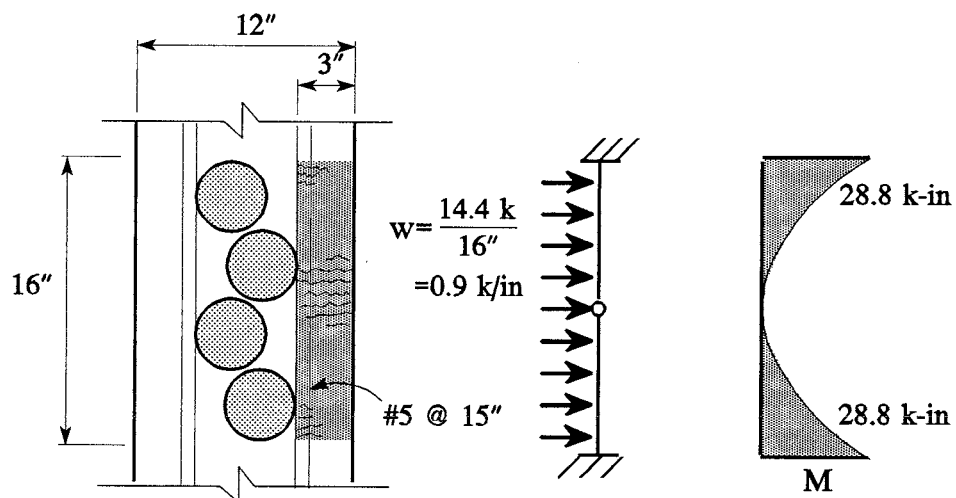
The region of the web adjacent to the ducts is subjected to high local forces from the lateral post-tensioning force. Assuming that the materials on the outside of the curve are ineffective, the concrete and stirrups along the side of the ducts can be thought of as acting as a local beam spanning the vertical height of the bundle [Figure 2.11a].

TYLI analyzed Las Lomas in this region as an homogeneous, elastic, 1 foot wide, fixed end beam. The maximum lateral prestress force on any web, 14.4 k/ft, was distributed evenly along the 16" span ($w = 0.9$ k/in). The maximum moment ($wl^2/12 = 19.2$ k-in) occurred in the negative moment regions which were considered adjacent to the top and bottom of the bundle. The tensile stress on this assumed uncracked member was 1100 psi. This greatly exceeded the modulus of rupture of 440 psi.

For further analysis, TYLI assumed that cracking at the effectively unreinforced for positive moment beam section at mid-height would immediately follow [Figure 2.11b]. (At mid-height, the steel was located only



a) Moments on Uncracked Section



b) Moments on Cracked Section

Figure 2.11 Local Beam Moments as Calculated by Ref. [6].

immediately adjacent to the ducts. This region would act like a plain concrete section for the type of moment indicated and once cracking was initiated, the section would rupture. In effect, a complete hinge would form and the moment would be shed to the beam supports.) The negative moment then increases to 28.8 k-in ($wl^2/8$). TYLI calculated the stress in the stirrups based on the factored moment ($1.3wl^2/\phi 8=41.6$ k-in). The use of load factors seems questionable since the report concluded that the prestress load was well controlled and the construction quite acceptable. Using an internal moment arm of 2.45", a stress of 68 ksi was calculated as required of the GR40 bars.

TYLI indicated that flexural failure could have occurred in either the negative or positive regions of the local beam. While addressing the regional beam theory, the report states "The local bending of the concrete protection and reinforcement just outside the tendons was much more serious (than regional beam action), although the overall bending capacity was also insufficient according to Code requirements."

Shear stresses on the concrete cover were also investigated. A shear force of 7.2 kips produced a stress of 200 psi on the 3" x 12" section. This exceeded the AASHTO allowable shear stress of 55 psi based on $0.95\sqrt{f'_c}$. TYLI acknowledges that this could have lead to failure [9].

2.3 AUTHOR'S COMMENTS ON FAILURE THEORIES

The author would like to discuss some of the assumptions regarding the behavior and clarify results of the failure theories.

2.3.1 Behavior

If post-tensioning is applied unsymmetrically with respect to the vertical axis of the box girder cross-section, the arch action force distribution is

changed. However at Las Lomas, the post-tensioning forces were nearly symmetrical at failure as the 12th and final tendon was being stressed.

2.3.2 Global Girder Action

It is unclear why TYLI used a 100 degree Fahrenheit temperature drop. AASHTO requires only a 40 degree Fahrenheit drop. Perhaps the large temperature change value accounts for creep and shrinkage effects which were not calculated.

TYLI concluded that there was relatively little effect of the global transverse shears and moments on the actual girder distress. The author analyzed the case of combined post-tensioning forces and temperature drop to give a maximum shear of 200 kips and moment of 16,750 k-ft. The transverse shear stress on the section (assuming it distributes to the webs and flanges uniformly) is 22 psi. Dividing the transverse moment by the transverse section modulus ($S=283 \text{ ft}^3$) yields a maximum tensile or compressive stress of 411 psi on the exterior webs. The author would agree with TYLI that the low stresses from global girder action had little effect on the failure of Los Lomas.

2.3.3 Regional Beam Action

TYLI does not report the ultimate moment capacity of the web. Using a singularly reinforced 12" square section with #5 GR40 bars at 15", the author calculated a nominal moment capacity of 91 k-in. This is less than the calculated cracking moment of 127 k-in. The ultimate moment due to post-tensioning calculated in Section 2.2.2 (240 k-in) is 1.88 times larger than the cracking moment [Table 2.1].

Table 2.1 Regional Beam Ultimate and Nominal Moments.

REGIONAL BEAM ULTIMATE AND NOMINAL MOMENTS					
BRIDGE	F_r k/ft	M_u k-in	M_{cr} k-in	M_n k-in	$\frac{M_u}{M_{capacity}}$
LAS LOMAS	14.4	240	127	91	1.88
KAPIOLANI	6.77	116	118	184	0.63

$M_{capacity}$ is the larger of M_{cr} and M_n

2.3.4 Local Beam Action

TYLI calculated the *factored* ultimate local beam moment (41.6 k-in) using load and resistance factors. The unfactored ultimate moment (28.8 k-in) is calculated without these factors and is shown in Table 2.2. TYLI also neglected to calculate the nominal moment capacity. The author assumes $b = 12"$ and $d = 2.69"$ to calculate a nominal moment of 25.3 k-in. The ultimate moment is only 1.14 times larger than the nominal moment.

Table 2.2 Local Beam Ultimate and Nominal Moments.

LOCAL BEAM ULTIMATE AND NOMINAL MOMENTS				
BRIDGE	F_r k/ft	M_u k-in	M_n k-in	$\frac{M_u}{M_n}$
LAS LOMAS	14.4	28.8	25.3	1.14
KAPIOLANI	6.77	28.0	24.0	1.17

The ultimate shear (7.2 kips) is 1.90 times larger than the author's calculated nominal shear capacity [Table 2.3].

$$V_n = 2\sqrt{3450}(12'')2.69'' = 3.79 \text{ kips}$$

The report also claims that stresses in the steel due to flexure were compounded by the shear force. A principal stress of 50 ksi was calculated from the combination of these effects. However Moe shows that longitudinal bars fail to develop significant stresses from transverse shear because the surrounding concrete is unable to provide the lateral restraint necessary to develop high steel shear stresses [12].

Table 2.3 Local Beam Ultimate and Nominal Shears.

LOCAL BEAM ULTIMATE AND NOMINAL SHEARS				
BRIDGE	F_r k/ft	V_u kips	V_n kips	$\frac{V_u}{V_n}$
LAS LOMAS	14.4	7.20	3.79	1.90
KAPIOLANI	6.77	3.38	2.38	1.42

2.3.5 Conclusions

Podolny made the following comment on the relative effects of each of the failure modes:

The order of magnitude of the stress produced by the three causes discussed, when compared to the allowable stresses in concrete or its reinforcement is approximately as follows:

1. For global secondary horizontal stress 1 to 10%
2. For regional bending stress 5 to 50%
3. For local beam bending stress 10 to 300%

These conflict with the calculations made by the author for Las Lomas. The ratio of forces to ultimate capacities indicate that regional bending or shear in the local beam are more likely causes of failure. Both of these failure modes would agree with the observed, explosive failure at Las Lomas; shear failure is typically sudden and flexural failure is brittle when the web cracking moment is greater than the nominal flexural moment.

TYLI summarized its report by stating that the combination of sharp curvature and bundling of tendons "aggravated the transfer of this force into the bridge deck system." The author would like to add that a large post-tensioning force is also a requirement. Failure would perhaps not have occurred in the case of shorter span lengths where less longitudinal prestressing force would have been necessary.

2.4 KAPIOLANI

TYLI applied the same failure theories to Kapiolani that were used for Las Lomas [8]. At Kapiolani, four 31 half-inch strand tendons were stressed to $0.75f_{pu}$ when failure occurred [Figure 2.12]. This resulted in a post-tensioning force of 3643 kips and a lateral prestress force of 6.77 k/ft on the 539' radius web. TYLI does not indicate which of the six tendons were stressed. It also does not give the actual concrete compressive strength but the author assumes 3000 psi for all calculations.

2.4.1 Global Girder Action

As at Las Lomas, TYLI concluded that global girder action had little effect on the failure.

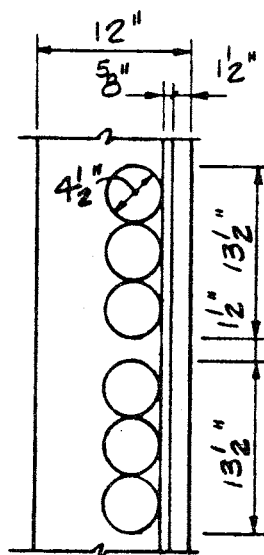


Figure 2.12 Duct Arrangement at Kapiolani (from Ref. 6).

2.4.2 Regional Beam Action

TYLI reports that the stirrups were overstressed in regional beam action and could have been a contributory cause of failure. A TYLI frame analysis similar to the one performed for Las Lomas produced an unfactored moment of 116 k-in at the web mid-height. The author calculated a nominal moment capacity of 184 k-in which is in excess of the applied moment [Table 2.1]. This was based on a 12" square section singularly reinforced with one #5 GR60 bar. Based on a M_u/M_n ratio of 0.63, it is the author's belief that regional beam action alone did not cause failure at Kapiolani.

2.4.3 Local Beam Action

TYLI states "the major cause of failure is very likely the inability of local slab (beam) action, both in shear and flexure, to resist the tendon radial force." TYLI assumed that the 1 1/2" of plain concrete separating the six tendons into two groups cracked due to shrinkage and provided no support to

the concrete cover. It also assumed that the force from the four stressed tendons was evenly distributed along the 28½" vertical span.

The author calculated an unfactored negative moment in the cover region of 28.0 k-in based on $wl^2/8$. A nominal moment capacity of 24 k-in was calculated using a 2.125" by 12" section singularly reinforced with one #5 GR60 bar. A M_u/M_n ratio of 1.14 suggests that local beam flexure may have caused failure [Table 2.2].

A nominal shear capacity of 2.38 kips was calculated by the author [Table 2.3]. The actual depth of the shear plane is uncertain, but the author used the minimum clear cover over the ducts ($d=1.81"$). This was substantially less than the shear present (3.38 kips) and a V_u/V_n of 1.42 indicates that shear may have been most responsible for failure. Recall that this analysis assumes that the force from the four stressed tendons was evenly distributed to all six ducts. The shear would have been greater and the moment smaller if the c.g. of the four stressed tendons was higher or lower in the bundle.

2.5 DESIGN GUIDELINES

The California Department of Transportation has been a leader in the design of post-tensioned box girder bridges. The history of their design guidelines for duct and web details is presented here via internal memos to designers. AASHTO has only recently addressed this problem and includes provisions in the Guide Specification for Segmental Concrete Bridges [9].

2.5.1 CALTRANS Details - 1973

The 1973 CALTRANS memo is included in TYLI [8]. Details for multiple tendon webs were based on tendon size [Figure 2.13].

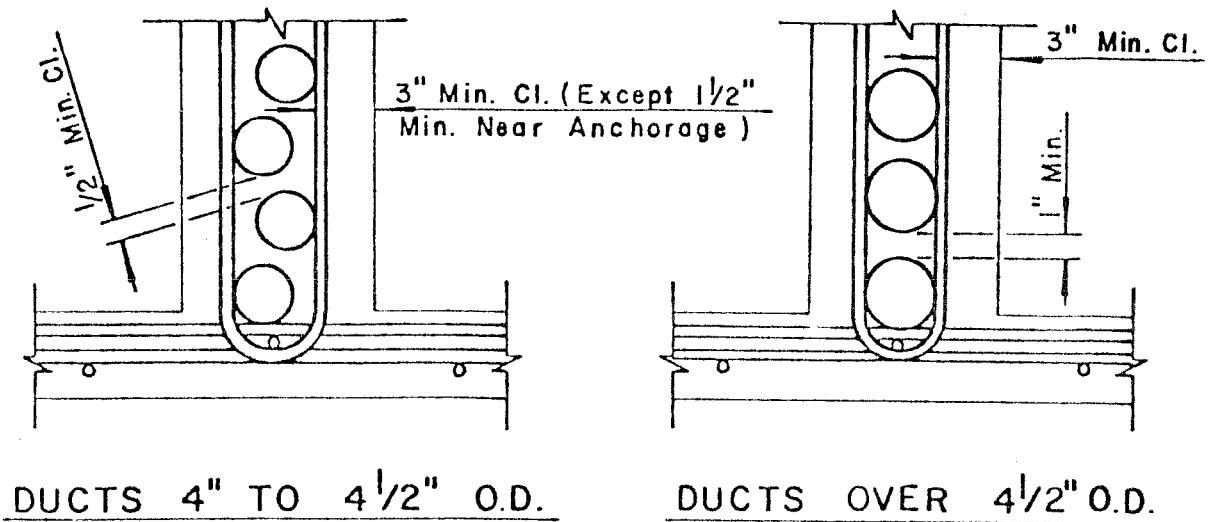
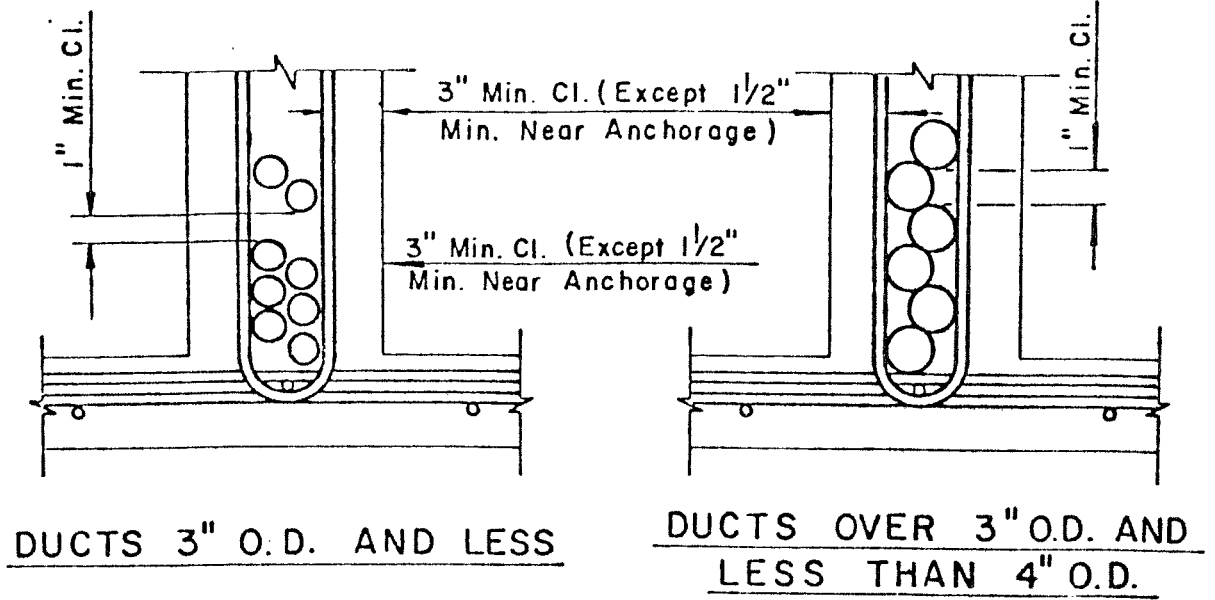


Figure 2.13 CALTRANS Standard Duct Arrangements-1973 (from Ref. 6).

2.5.2 CALTRANS Details - 1982

After the failures at Las Lomas and Kapiolani, CALTRANS issued a memo with complete design and detail requirements as reported by Podolny. The design requirements address the concern over regional beam bending. One design curve was developed for #5 stirrups [Figure 2.14] and a second for #6 stirrups [Figure 2.15]. The curves are based on a design moment of $PL/5$ with the assumptions that the force of all the tendons is concentrated at mid-height of the web and L is the clear span between flanges. The design moment assumes that enough rotational restraint is provided by the flanges to reduce the simple span moment ($PL/4$) by 20%. The shear on the stirrups

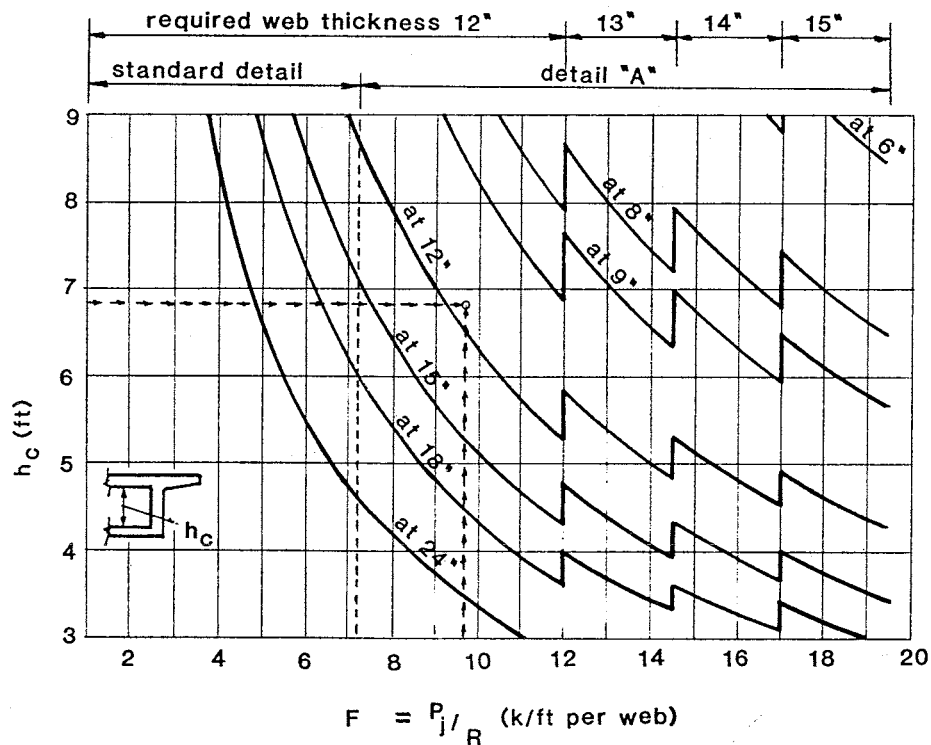


Figure 2.14 CALTRANS Design Chart with #5 Stirrups (from Ref. 7).

from gravity loads is neglected for two reasons: (1) the design assumption of mid-height loading of the web only occurs at two points along a span and (2) at the time of maximum tendon force (jacking), the girder is supported by falsework. The curves and titles were transposed in the reference by Podolny [7] but are shown in their corrected form here.

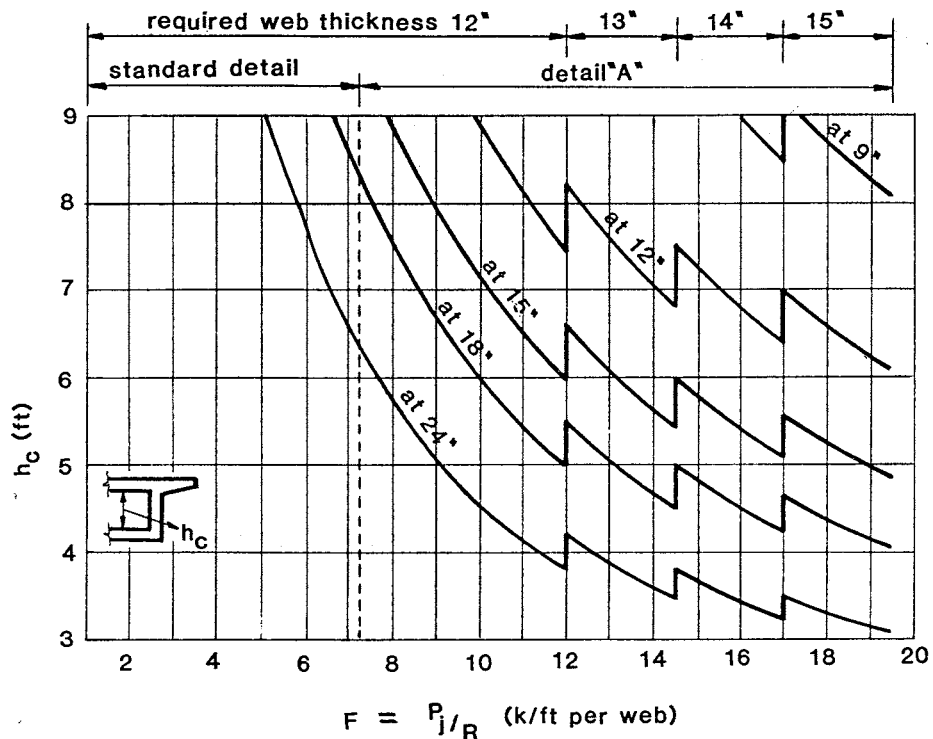


Figure 2.15 CALTRANS Design Chart with #6 Stirrups (from Ref. 7).

Whenever the lateral post-tensioning force is less than or equal to 7.2 k/ft, a standard bundle detail such as the one shown in Figure 2.8 may be used. For larger F_r values, Detail "A" must be used [Figure 2.16]. The author has calculated that the cut-off value is based on a shear force of $2\sqrt{f'_c} bd$ for 3000 psi concrete where $b=12$ " and $d=2.69$ ". Detail "A" locates the bundle against the inside face of the outside stirrup to create maximum cover. It also requires the use of two types of transverse hook ties.

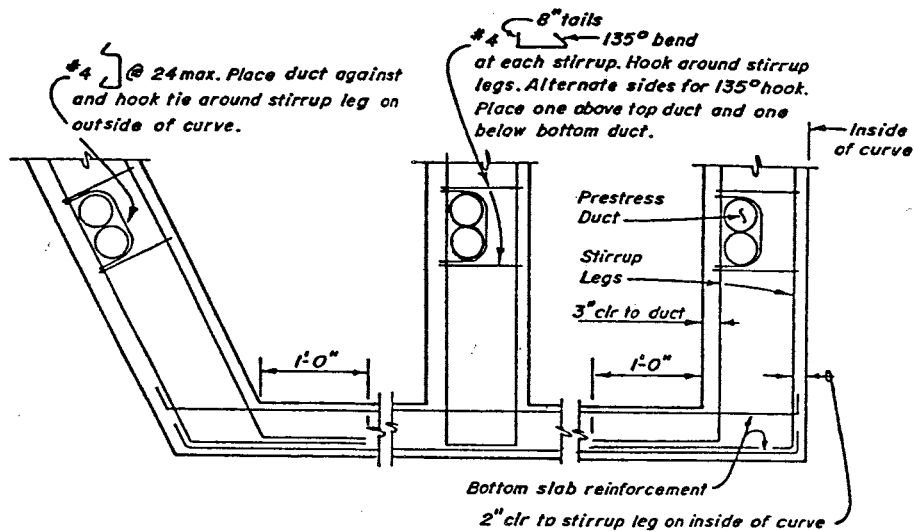


Figure 2.16 CALTRANS Detail "A"-1982 (from Ref. 7).

2.5.3 CALTRANS Details - 1985

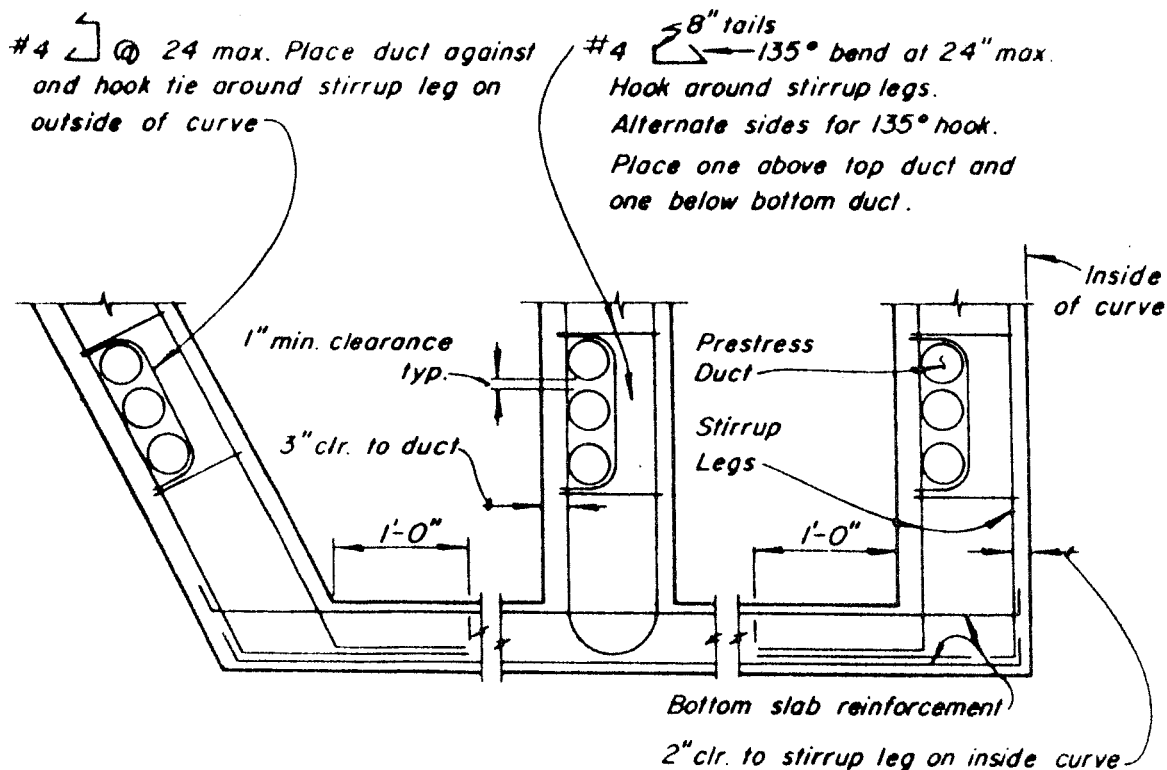
In an updated memo to designers, CALTRANS requires Detail "A" to be used whenever F_r is greater than 7.0 k/ft. It also includes a new Detail "A" for a three-duct bundle [Figure 2.17]. A 1" minimum clear spacing is required between ducts.

2.5.4 AASHTO - 1989

Section 16.6.1 of the AASHTO Guide Specification for Segmental Concrete Bridges requires reinforcing to prevent tendon breakout whenever the shear stress in the concrete cover beside the tendon exceeds $2\sqrt{f'_c}$ [9]. The area of steel required is dependent on the lateral prestress force and yield strength of the non-prestressed reinforcement.

$$A_s = \frac{P}{R \cdot 0.6f_{sy}}$$

The orientation of the reinforcement is not specified.



Note: Details shown are for a curve to the right with the section taken looking ahead on station. These details supersede duct patterns shown in



PART GIRDER SECTION

Figure 2.17 CALTRANS Detail "A"-1985 (from Ref. 19).

2.5.5 NCHRP 12-33 (Draft) - 1991

A draft copy of NCHRP 12-33 Development of a Comprehensive Bridge Specification and Commentary indicates that a more comprehensive requirement may be included in the next AASHTO edition [10]. A load factor of 1.2 is applied to the tendon force when calculating F_r . If equation 5.11.4-2 is satisfied, no additional reinforcement is required.

$$F_r \leq 2\phi\sqrt{f'_{ci}} 2d_c \quad (\text{eq. 5.11.4-2})$$

where:

- F_r is the in-plane deviation force in pounds per inch;
- ϕ is 0.75;
- f'_{ci} is the concrete compressive strength at the time of stressing, in psi;
- d_c is the minimum concrete cover over the tendon duct plus one half of the duct diameter, in inches.

If equation 5.11.4-2 is not satisfied, additional tie-back reinforcement shall be used. The limiting stress on this steel is $0.6f_y$ and shall be spaced not greater than $3d_c$ nor 24 inches. The draft also requires that both local bending capacity in the cover and the bending capacity of the web between flanges be adequate.

CHAPTER 3: MODEL DESIGN

3.1 MODEL SELECTION

A decision was made to build and test models based on the general Las Lomas details. Las Lomas was chosen for three reasons: (1) it was the most catastrophic tendon breakout failure, (2) failure models and stress calculations had been developed to explain its failure and (3) it would give a point of reference to gauge the results. As discussed later, conflicts with scaling and material availability, changes to non-critical details for construction simplicity and higher-than-planned model concrete strength resulted in a less than perfect scale model. However this investigation was not to be a forensic study of the Las Lomas failure, so exact scaling was not required.

Time and money constraints permitted only two models to be built. Construction could be greatly simplified if a single cell box was used with a different duct arrangement in each web. If the stressing of a single web during the first test on a specimen did not adversely affect the condition of the other web, then two details could be tested with the construction of just one girder. A computer frame analysis of a model cross-section loaded similarly to the regional beam model developed by TYLI was performed. It showed that on the non-loaded web, the shear force was only 7% of that on the loaded web. The maximum moment on the non-loaded web was only 14% of that on the loaded web. These low values indicated that two duct

arrangements could be used per girder with each one being tested separately to failure.

A single-cell box would be much easier to construct than the double cell actually used at Las Lomas. Since the frame analysis showed that there is little interaction between the webs, a 2-web box should perform similarly to a 3-web box.

3.2 SCALE FACTOR

A $\frac{1}{3}$ scale factor was chosen because it yielded the smallest possible model that was easily constructed. A small model is easier, cheaper and faster to build. However a model that is too small presents problems with construction tolerances and material availability.

3.3 BOX DIMENSIONS

The box cross-section was a scaled version of Las Lomas with changes made for simplifying construction [Figure 3.1]. To avoid having to build cantilever forms, the girder was built and tested in an inverted position. This did not significantly effect results since gravity loads are unimportant to breakout as noted by CALTRANS [7]. The model top slab therefore represents the bottom slab at Las Lomas. Likewise, the model bottom slab represents the top slab at Las Lomas. The top slab thickness at Las Lomas varied transversely and the bottom varied longitudinally. Average thicknesses were calculated, scaled and rounded off to an integral number of inches.

At Las Lomas, the centerline distance between interior and exterior webs was 11'. This scaled to 3'-8". The model was constructed with a centerline web to web distance of 4' so that the radius of each web was a whole number. To save on materials and labor, the cantilevers were

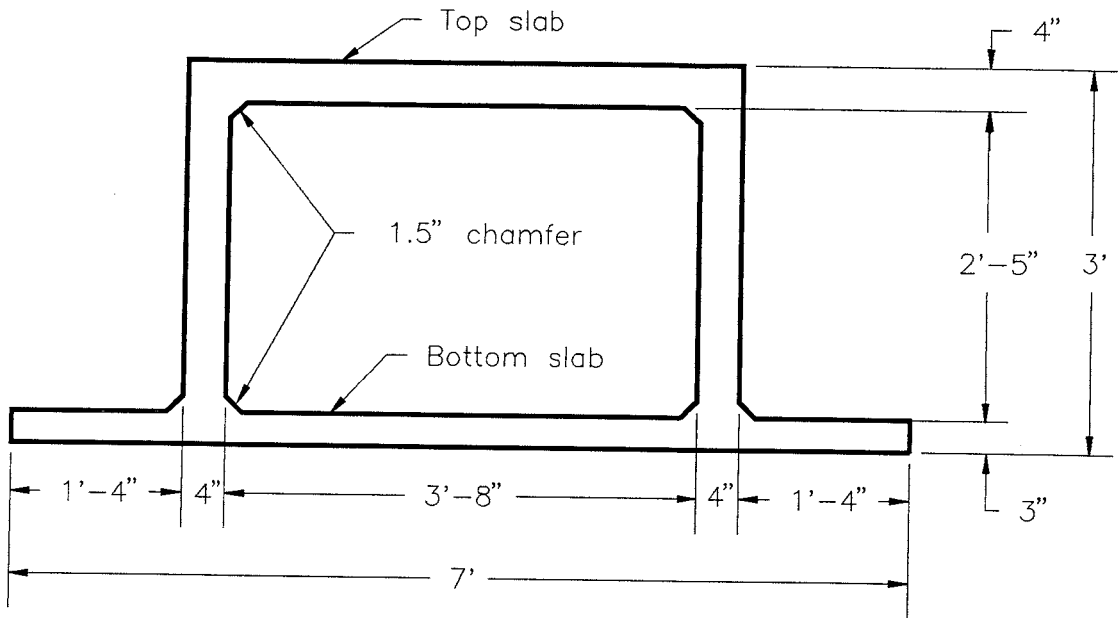


Figure 3.1 End View of Girder.

shortened slightly from a scaled value of 1-10" to 1'-4". The actual cantilever length has little effect on web behavior. The dimensions of the web were considered important. The exact scaled values of 4" for the thickness and 3' for the overall height were maintained.

3.4 CURVE LAYOUT

The web radii were chosen to be small enough so that the tendon breakout in the web would occur before failure of any other part of the girder or testing apparatus. If the curve was not sharp enough, anchorage zone failure may have resulted or the strands would have been loaded to an unsafe level.

Duct arrangement controlled the design of the curve radius. The capacity to resist shear failure was calculated for each tendon assuming two

failure planes would form and that the maximum concrete strength would be 5000 psi (see Figure 3.9 for value of $d=1.125''$).

$$F_{r_{reqd}} = 2\sqrt{5000}(2)12''(1.125'') = 3.8 \text{ k/ft}$$

Therefore a total F_r of 15.2 k/ft was required for all four tendons. A jacking force of 372 kips could be delivered from the loading apparatus as discussed in Section 5.1.1. An 18' radius for the inside web was decided on as it would permit a total F_r of 20.6 k/ft; this was more than a third larger than the anticipated failure load [Figure 3.2]. The previously determined cell width mandated that the companion web radius be 22'.

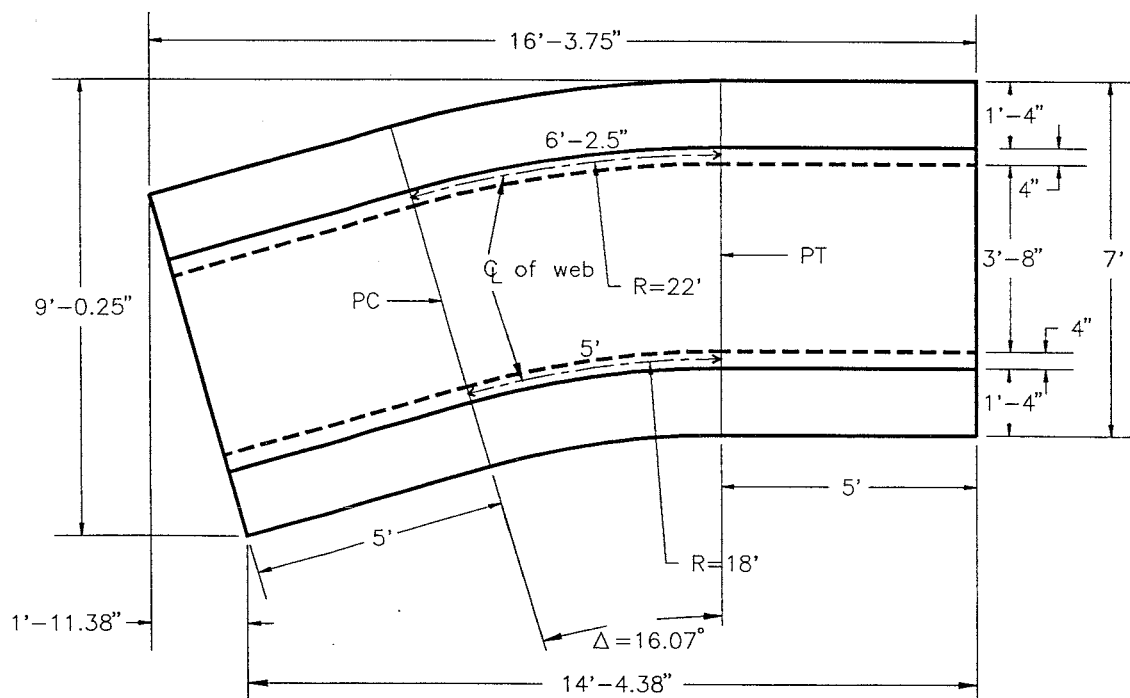


Figure 3.2 Plan View of Girder.

The curve length of 5' was chosen for the 18' radius. The curved region was the most difficult part of the model to construct and was kept as short as possible. Too small a length of curve would allow too much of the load to flow transversely through flexural action in the web and negate the possibility of a regional beam failure. This assumed that the PC and PT act as boundary elements. A 5' curve was more than twice the clear height of the web and was thought to be sufficient to allow regional bending. A 5' straight transition zone on each end insulated the curve from the complex stress region at the anchorages.

3.5 REINFORCEMENT

Las Lomas was reinforced with GR40 #5 stirrups spaced at 15". No standard bars match this on a 1/8 scale. The closest match was 6mm, 75 ksi bars from Sweden already available in the lab [13]. This was nearly equivalent to a #2 bar. The stirrup spacing needed to be adjusted to reflect the imprecise scaling of stirrup sizes. The first step was to find the equivalent spacing at Las Lomas if #6's were used in lieu of #5's.

$$s_6 = s_5 \frac{A_6}{A_5} = 15'' \frac{0.44}{0.31} = 21.3''$$

This spacing of #6's at 21.3 inches was scaled to 6mm bars at 7". The spacing was not increased to account for the greater yield strength of the Swedish bar. If the prototype spacing of 21.3" was increased by the ratio of 75/40, an equivalent reinforcement pattern of #6's at 40" would have resulted. This spacing was considered excessive and 7" was maintained in the model [Figure 3.3]. Stirrup spacing was reduced in the anchorage zones to 5½".

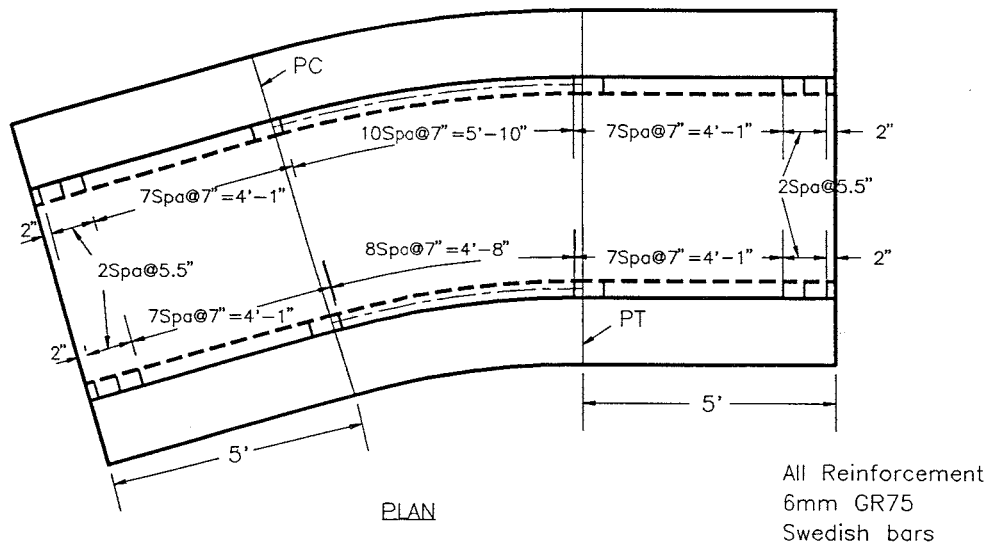


Figure 3.3 Stirrup Layout.

All stirrups were lapped at the top of the stirrup [Figures 3.4 & 3.5]. The lap was positioned on the inside face of the curve as this would locate it in the compression zone for regional beam bending of the web. A development length of 1.92" was calculated using AASHTO equation 8.25.1 [3]. Since no tension would exist in the splice, a reasonable lap length of 4" was used.

The top and bottom slabs were reinforced with double mats at Las Lomas. The top slab was heavily reinforced for live loads. The bottom slab was reinforced with #5's at 16" which was nearly equal to the web reinforcing. To simplify construction, single mats with transverse bars located at mid-height were used in the model slabs. To avoid premature slab failure, reinforcing was sized such that the slab ultimate nominal moments were not less than the web nominal moment. As a result, 6mm bars were spaced at 3" in the model bottom slab (Las Lomas top slab) and 4" in the top slab (Las Lomas bottom slab) [Figures 3.6 & 3.7]. Spacings were increased in the non-critical transition zones.

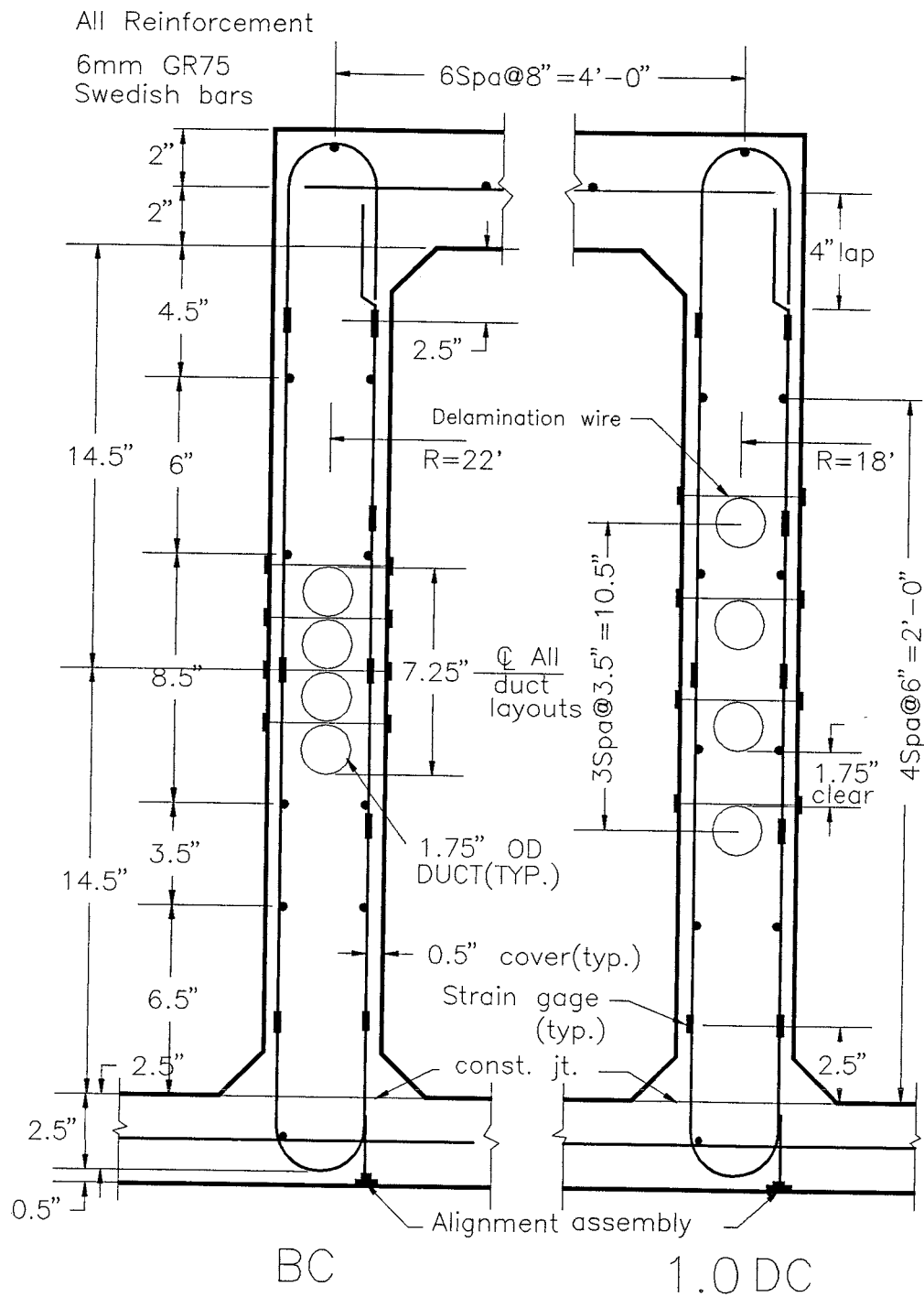


Figure 3.4 Girder #1 Cross-Section in Curve (BC & 1.0DC).

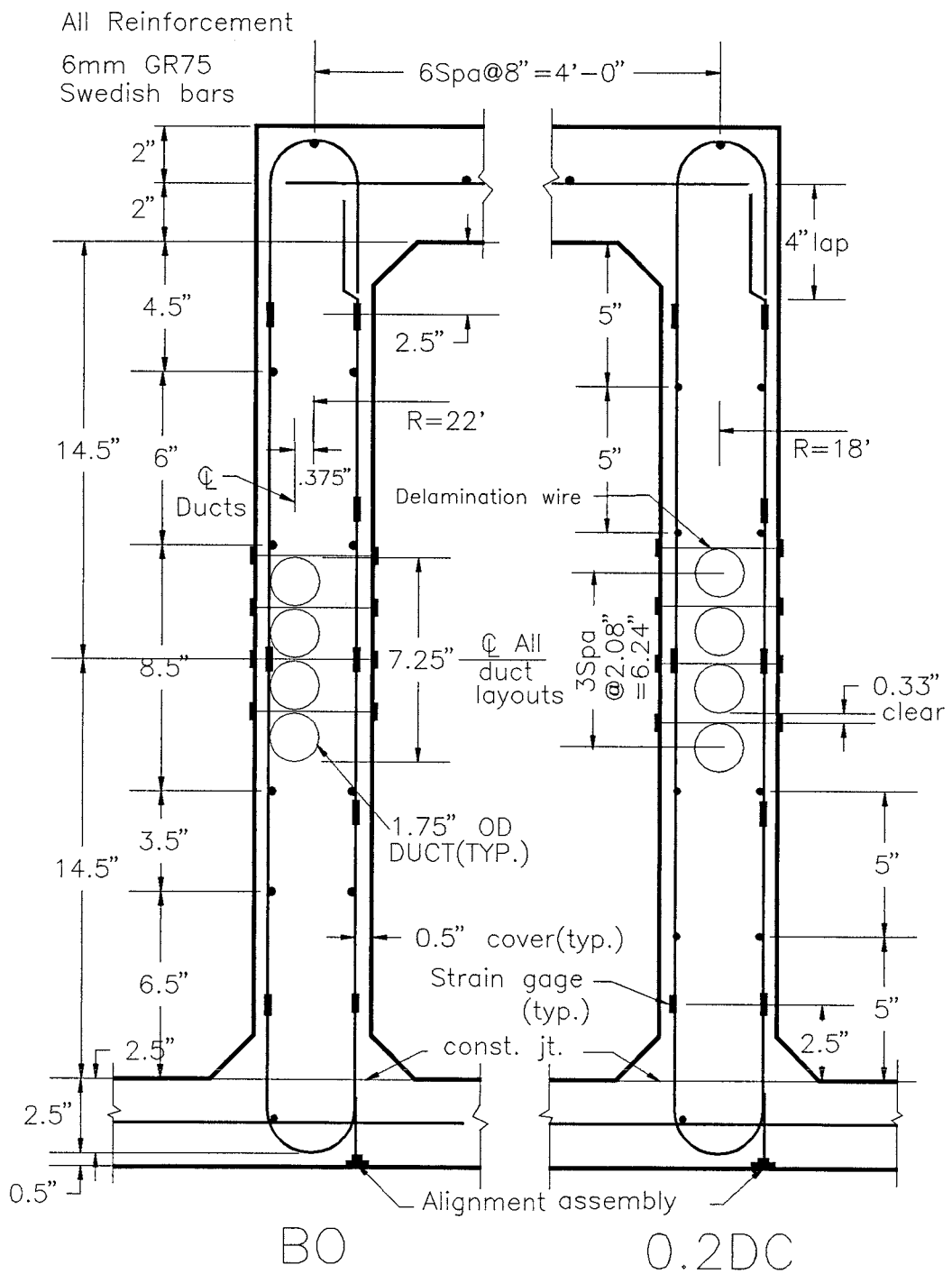


Figure 3.5 Girder #2 Cross-Section in Curve (BO & 0.2DC).

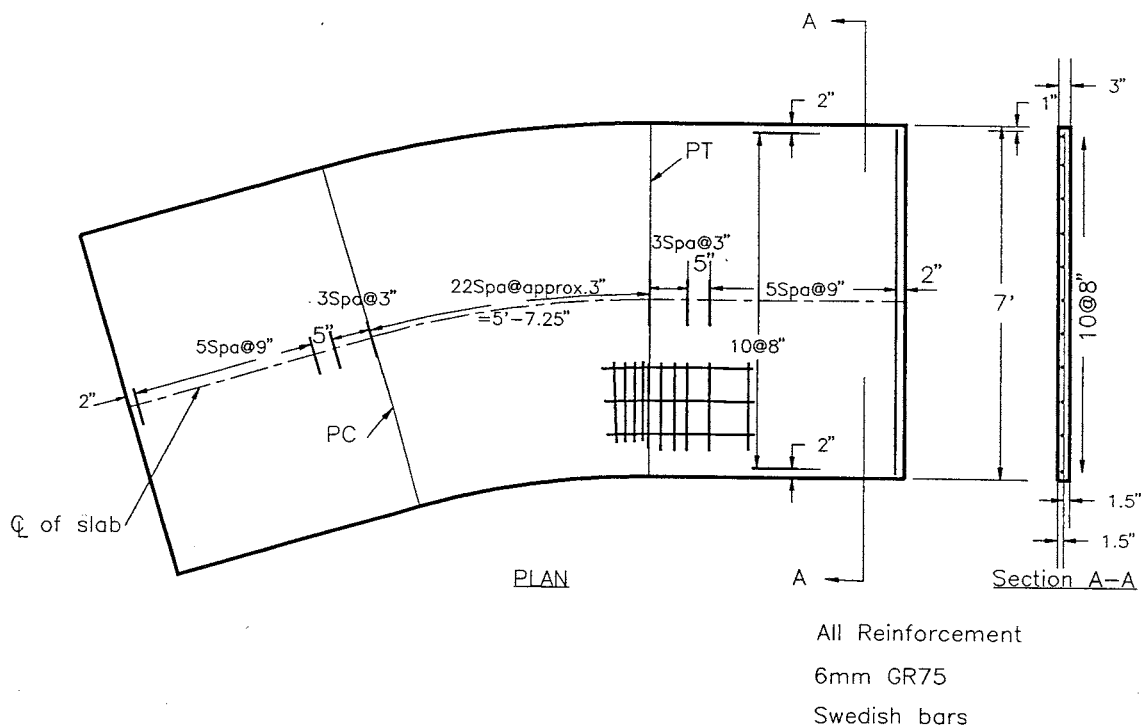


Figure 3.6 Reinforcement Details of Bottom Slab.

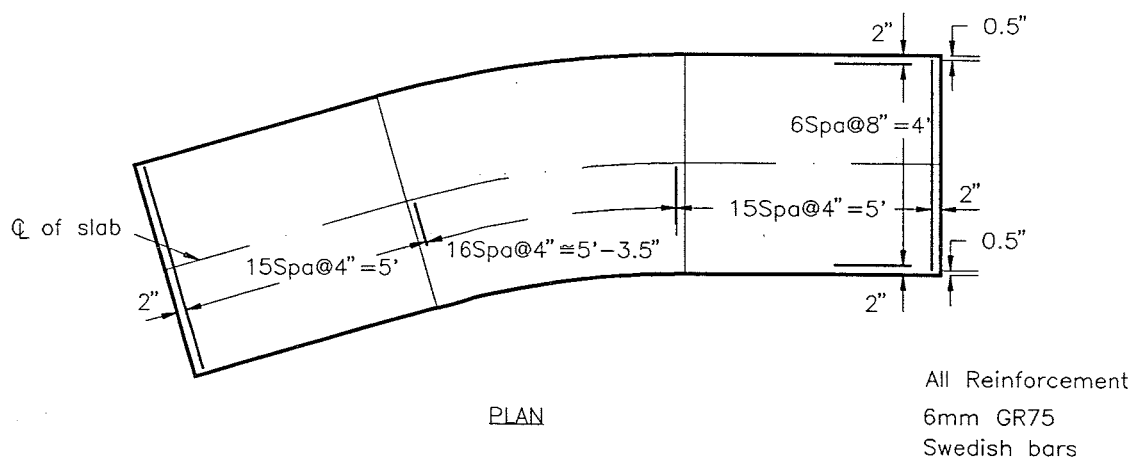


Figure 3.7 Reinforcement Details of Top Slab.

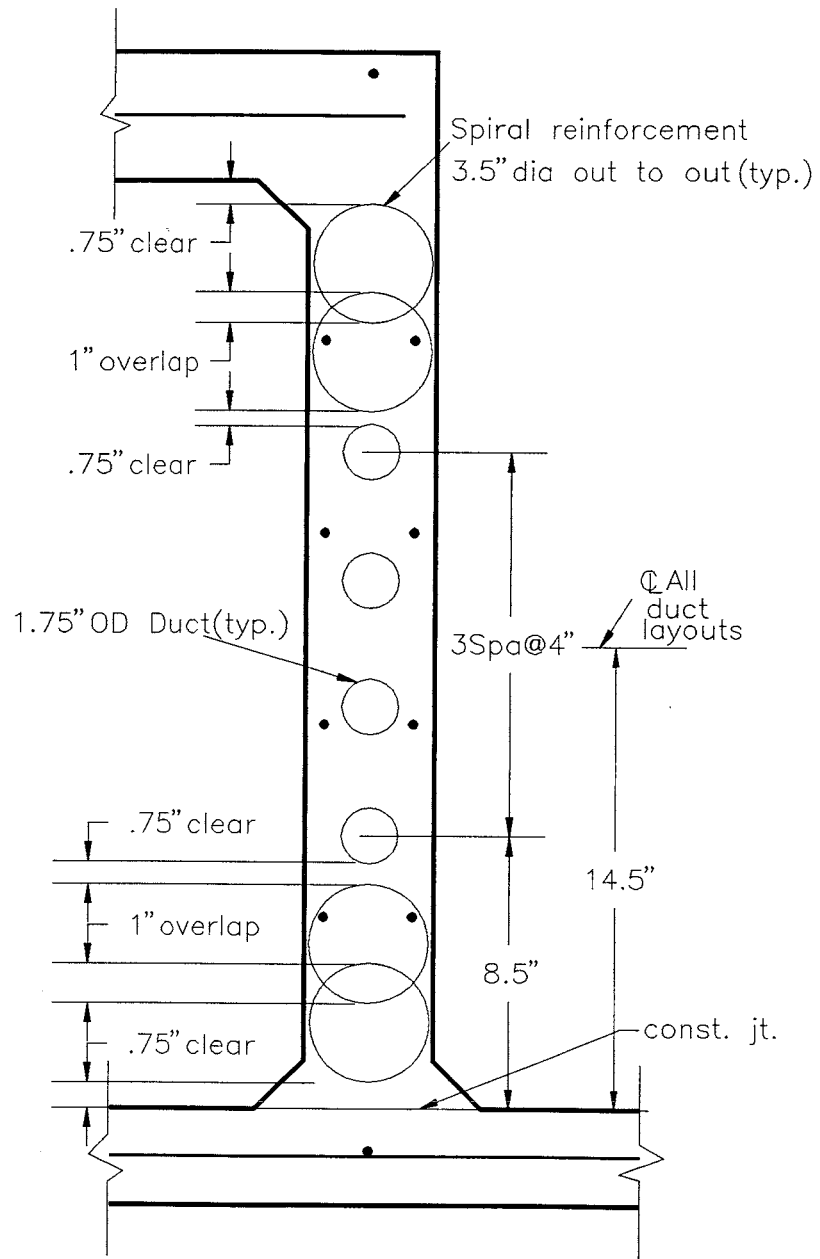


Figure 3.8 Web Cross-Section at End of Girder.

All longitudinal bars are for temperature and shrinkage and were spaced as shown in Figures 3.4 through 3.7. A set of two 4½" long and 3½" diameter (out-to-out) spirals made from 6mm bars were placed above and below the duct group at the anchorage zones [Figure 3.8].

3.6 DUCT ARRANGEMENT

TYLI states that tendon bundling and sharp curvature can be an unsafe combination in box girders [6]. A four-tendon bundle and three other promising arrangements were tested. Only duct positioning varied from web to web; all other details remained the same.

The identification system for labeling the various duct arrangements is as follows:

-The first number (if used) and letter refer to the vertical separation of ducts. The letter B indicates that the ducts are bundled vertically, one on top of the other. The letter D indicates that the ducts are separated. The number preceding the letter D is the ratio of the clear spacing between the ducts to the outside duct diameter (1.75").

-The second letter refers to the horizontal position of the duct group. The letter C indicates that all of the ducts are symmetrical about the centerline of the web [Figure 3.9]. The letter O indicates that the ducts are offset against the stirrup leg on the outside of the curve [Figure 3.10].

Duct size at Las Lomas was not given although based on the maximum number of strands (28), ducts of approximately 4½" O.D. should have been used. Scaling required 1½" ducts for the model, but this size is apparently not made by the major manufacturers of post-tensioning duct. The nearest available duct size (1.75") was used.

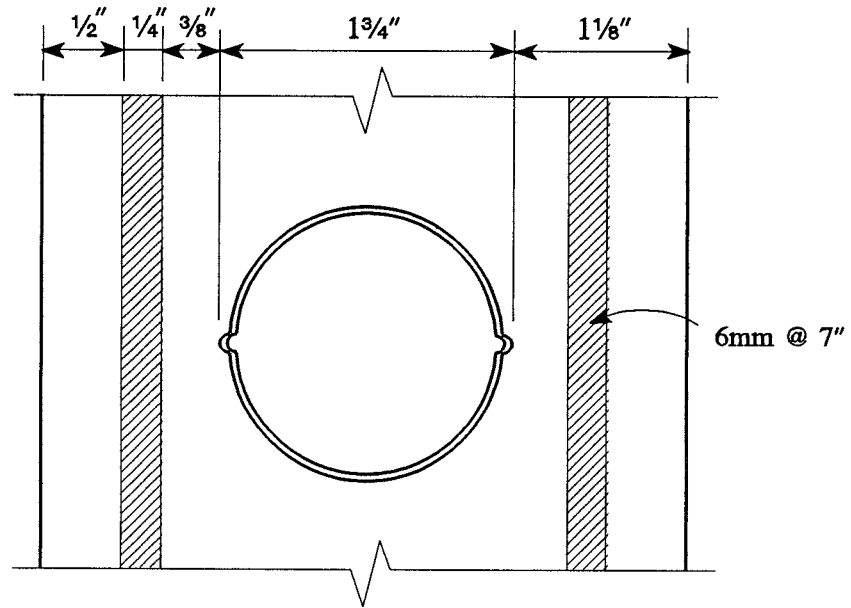


Figure 3.9 Centered Duct.

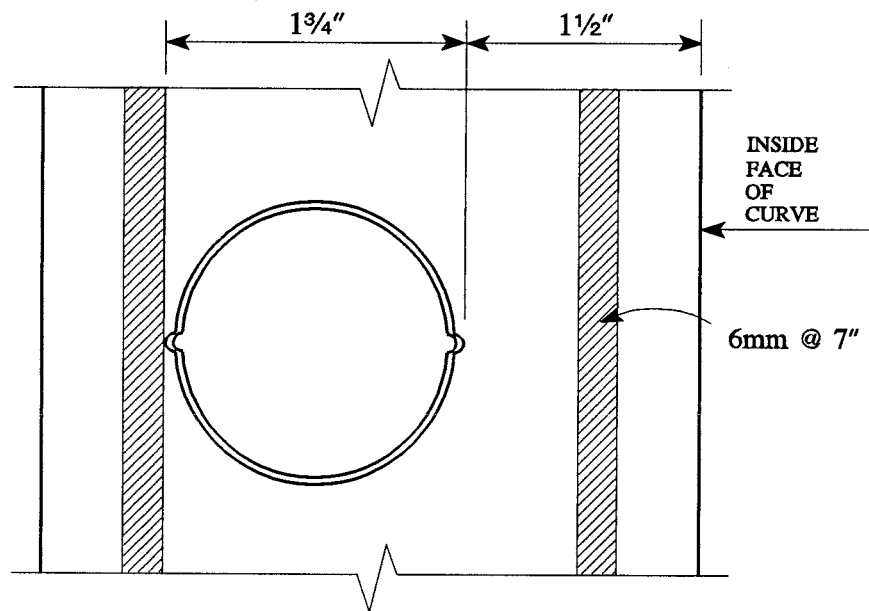


Figure 3.10 Offset Duct.

3.6.1 SPECIMEN BC

This is the duct arrangement similar to the one at Las Lomas. A slight modification was made for the model [Figure 3.4]. A straight vertical formation was used in lieu of the zig-zag because it was considered more universal. The relative horizontal offsets between ducts in a zig-zag pattern can change from bridge to bridge depending on the clear distance between the stirrup legs and the diameter of the ducts. No large difference in behavior between the two arrangements was anticipated. The vertical bundle height at Las Lomas was approximately 16"; a vertical stacked bundle would have been 17½". All ducts are centered on the web vertical axis.

3.6.2 SPECIMEN 1.0DC

The Texas State Department of Highways and Public Transportation design of the San Antonio "Y" project used an arrangement that maintained a clear spacing between ducts equal to the diameter of the duct. It is believed that this allowed for better consolidation and more importantly eliminated the single large discontinuity found at Las Lomas [Figure 3.4]. This arrangement is very conservative and would be considered an upper limit beyond which further spacing of ducts would provide no benefit. The scaled vertical spacing was 1.75". All ducts were centered on the web vertical axis.

3.6.3 SPECIMEN 0.2DC

The CALTRANS Detail "A" issued in 1985 mandates a 1" minimum vertical clearance between ducts in three-tendon webs [7]. Each 1" strip of concrete behaving in direct tension can theoretically provide sufficient tensile restraint to tie the front and back cover regions together. At Los Lomas, each 1" deep concrete tie may have been able to provide as much tensile capacity as 5.3 k/ft.

$$P_{\text{tie}} = 7.5\sqrt{3450(12'')^3} = 5.3k/ft$$

If concrete tensile ties are indeed capable of developing this magnitude of force, the local beam failure problem would be eliminated. However there is a strong possibility as noted by TYLI that the concrete tie may be pre-cracked due to shrinkage [8]. For the model, the scaled vertical clearance was 0.33" [Figure 3.5]. All ducts were centered on the web vertical axis.

0.2DC was not a complete test of Detail "A" which contains an offset and hook ties. This test with only the spacing varied was intended to test the theory that concrete ties alone can add to the strength of the detail. It also would add to the knowledge of transition in strength between the extreme cases of BC and 1.0DC

3.6.4 SPECIMEN BO

Both Detail "A" issued in 1982 and 1985 require the ducts to be offset against the outside stirrup leg [7]. This test provides more concrete cover adjacent to the ducts. The most indicative test of the offset arrangement would be with bundled tendons [Figure 3.5]. If the concrete surrounding the ducts in 0.2DC and 1.0DC provided the strength anticipated, offsetting could not further increase the capacity. Offsetting increased the minimum cover of the ducts to the inside face from 1.125" to 1.5".

3.7 LONGITUDINAL DUCT LAYOUT

The duct arrangements described above were maintained throughout the curve and continued 1' into both transition zones [Figure 3.11]. The tendons then flared in double-curvature through the next 3' before leveling out in the final 1' of the transition zone. The c.g. of the duct group was at the mid-height of the web along the entire specimen. The flaring of the ducts was

necessary to accommodate the stressing system. In the case of BO, the ducts moved toward the center of the web in the 3' flaring region.

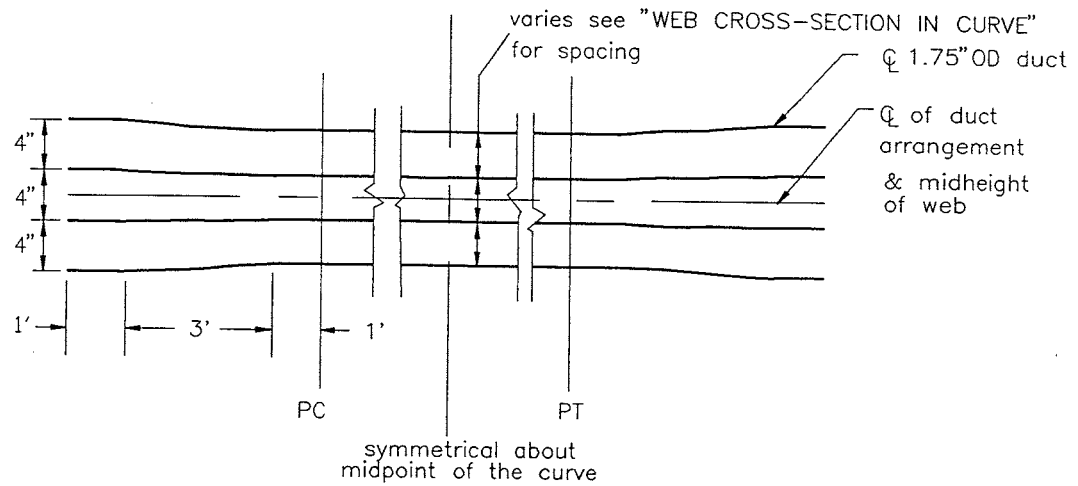


Figure 3.11 Duct Profile.

CHAPTER 4: MATERIALS AND CONSTRUCTION

4.1 MATERIAL PROPERTIES

4.1.1 Concrete

The concrete compressive strength at Las Lomas was 3450 psi. A design mix for a 28-day compressive strength of 3500 psi was used. The actual batch weights and slumps for 1 yd³ are shown in Table 4.1. Three yards of concrete were delivered for every cast. The web and top slab casts used Relcrete 150 superplasticizer to improve the workability. Coarse aggregate consisted of 3/8" maximum size pea gravel.

All exposed surfaces were covered with wet burlap and plastic approximately four hours after casting. They remained covered for a minimum of 24 hours and then were air-cured thereafter. Cylinders (6" x 12") were made for each cast and were cured under the same conditions as the girders. Cylinders were tested in uniaxial compression and the strengths recorded. Compressive strengths were measured on the testing days [Table 4.2]. Strengths were also measured at times prior to testing the specimen so strength gain curves could be developed [Figure 4.1 & 4.2].

All test concrete strengths were much greater than the 28-day design strength of 3500 psi. The slab and web concrete had higher overall strengths and faster strength gains as is typical of concrete containing superplasticizers.

Table 4.1 Girder Batch Weights and Slumps.

BATCH WEIGHTS AND SLUMPS				
all weights for 1 yd ³	GIRDER #1 BC & 1.0DC		GIRDER #2 0.2DC & BO	
	BOTTOM	TOP & WEBS	BOTTOM	TOP & WEBS
DATE CAST	10-3-90	2-5-91	3-27-91	4-16-91
CEMENT (TYPE I)	536#	513#	510#	517#
SAND	1573#	1692#	1620#	1633#
COARSE AGG.	1795#	1621#	1737#	1747#
WATER	96#	173#	133#	103#
DELIVERED SLUMP	3½"	2"	5½"	2"
SUPERPLASTICIZER	-	4.95#	-	4.89#
SLUMP W/ SUPERP.	-	7"	-	8"

Table 4.2 Concrete Strengths at Testing Dates.

CONCRETE STRENGTHS AT TESTING DATES					
		GIRDER #1		GIRDER #2	
		1.0DC	BC	0.2DC	BO
TESTING DATE		2-20-91	2-26-91	5-2-91	5-15-91
BOTTOM SLAB	STRENGTH (psi)	5400	5400	4400	4600
	AGE (days)	140	146	35	48
TOP & WEBS	STRENGTH (psi)	5900	6000	5000	5300
	AGE (days)	15	21	16	29

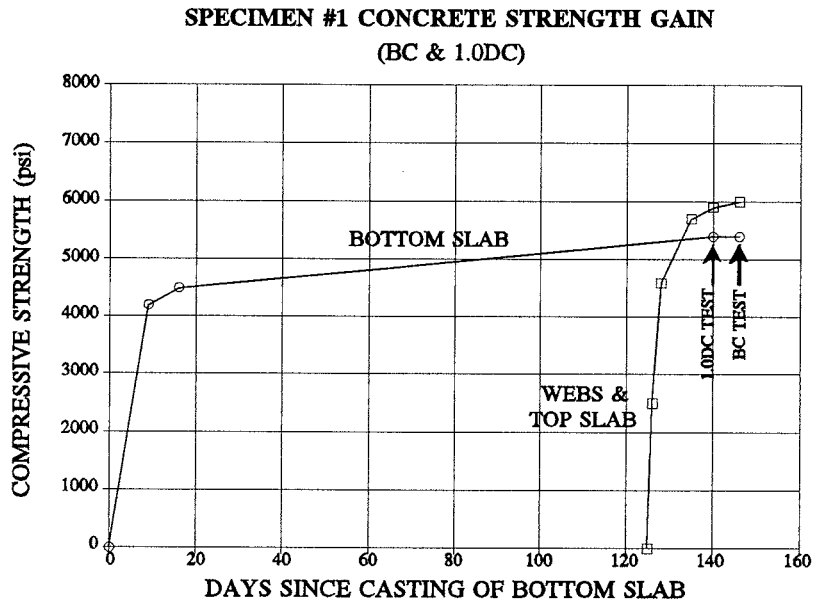


Figure 4.1 Girder #1 Concrete Strength Gain.

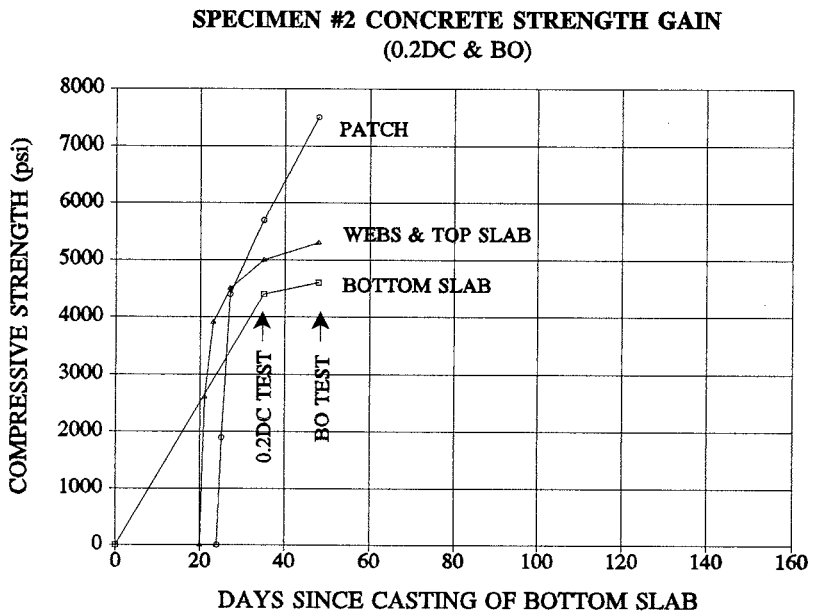


Figure 4.2 Girder #2 Concrete Strength Gain.

4.1.2 Mortar Patch

Mortar was used locally to patch girder #2 (see Section 4.2.6). The mortar was mixed in the lab and 2 inch square test cubes were made. The batch weights are shown in Table 4.3. The strength of the patch at the test date for web 0.2DC was 5700 psi. The web concrete strength was 5000 psi. Thirteen days later, web BO was tested and the patch strength was 7500 psi. The web concrete strength was 5300 psi.

Table 4.3 Mortar Patch Batch Weights.

BATCH WEIGHTS	
DATE CAST	4-20-91
CEMENT (TYPE I)	6.16#
SAND	22.44#
WATER	2.52#
SUPERPLASTICIZER	0.60#

4.1.3 Epoxy

Epoxy was used as a bonding agent between the cast concrete and mortar used for patching. The actual epoxy applied was an unused portion remaining from a test sample from the Materials and Test Division at the Texas State Department of Highways and Public Transportation. This epoxy met their specifications for epoxy type A103 [15].

4.1.4 Reinforcement

6mm diameter hot rolled bars were used for all reinforcement. Tensile tests on bars conducted at the lab showed an average yield strength of 75 ksi [13].

4.1.5 Ducts

Galvanized, corrugated, folded metal ducts were used in all instances. All dimensions were measured with a dial caliper in the lab. The outside ridge-to-outside ridge dimension was 1.75" [Figure 4.3]. The inside diameter was 1.60" and the gauge was 0.035".

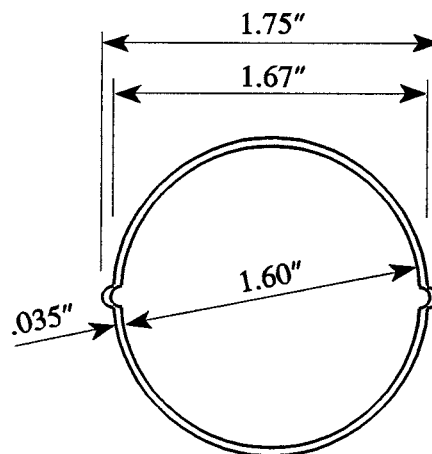


Figure 4.3 Metal Duct Cross-Section.

4.1.6 Prestressing Strand

Post-tensioning was applied to the specimens with 7-wire, $\frac{1}{2}$ " ϕ , 270 ksi, low relaxation strands. Test data provided with the strand showed an actual yield stress of 276 ksi and ultimate stress of 289.5 ksi.

4.2 CONSTRUCTION

Construction of a $\frac{1}{3}$ -scale model demanded careful planning and execution. Self-imposed tolerances were much tighter than those for general construction as the effects of typical construction misalignments would be magnified by the scale factor. The greatest care was taken in the construction

of the curved region. Particular attention was paid to constructing webs on the precise radius, maintaining proper lateral dimensions in the web cross-sections and locating duct arrangements accurately.

The simplest construction method was to cast the bottom slab separately from the webs and top slab. This was used in lieu of a single, continuous cast. A continuous cast requires a normal or stiff mix to prevent concrete from spilling out the bottom of the webs and into the bottom slab. Congestion in the webs required a high-slump mix that would have made construction of this type difficult. As was discussed in Section 3.3, the box was cast upside-down with respect to the actual Las Lomas structure.

4.2.1 Formwork

Construction began by building a soffit for the bottom flange. A transit was used to lay out horizontal curves on the soffit using the ordinate method. Offsets were made every three inches along the tangent. Curves were laid out for both slab edges and web exterior faces.

4.2.1.1 Exterior Web Forms. 4' x 8' x $\frac{3}{4}$ " plywood sheets were positioned lengthwise along the web curves such that the entire length of curve and equal lengths of each tangent were covered. They were temporarily nailed and the web curves were again laid out on the new sheets. The sheets were removed and cut with a jig saw using a 45 degree cut. These served as bottom sole plates for the external web forms with the requisite 45 degree chamfer. Three duplicates of each sole plate were made. Top and bottom plates were $1\frac{1}{2}$ " thick so each was made by gluing and screwing two pieces together. 2 x 4 studs 2'-6" long were glued and screwed to the top and bottom sole plates on 6" centers to complete the exterior web frames. Three-eighths inch deep kerfs were cut into two 2'-6" x 8' x $\frac{3}{4}$ " plywood sheets on 4" centers so that one could be bent, glued and screwed onto each frame [Figure 4.4].

Straight forms of similar construction were placed on either end of these 8' long center pieces to complete the external web forms.

4.2.1.2 Core Forms. The core formwork was comprised of inside web forms and top slab soffits. The design of the core formwork was governed by the need for easy removal and reusability. Internal formwork, particularly on small boxes such as this, can be extremely laborious to remove and may result in the destruction of forms. The solution to the problem was to use many small pieces with gaps between the wood so that no one form actually touched another [Figure 4.5]. Holes were drilled in the studs of the individual panels which were connected with $\frac{1}{2}$ " ϕ bolts.

A section of core formwork consisted of an internal web panel, two top slab soffits and another internal web panel on the opposite web [Figure 4.6]. Seven sections made up the core. Two sections were used in each tangent region and three were used in the core. Two top slab soffits were used in a single section because two small ones could be removed more easily than one large one [Figure 4.7].

The internal web forms in the curved region were themselves curved. The top and bottom sole plates were cut on a curve to match the external web form. As with construction of the external web forms, studs connected the top and bottom plates and kerfs were cut into plywood which was glued and screwed into the frame.

The individual sections essentially formed a frame with hinges at the corners. Stability and load carrying for the top slab soffit were achieved with an internal bracing system made of 2 x 4's [Figure 4.6]. Gaps of approximately $\frac{1}{2}$ " separated all panels. These gaps were spanned with 4" wide roof flashing duct-taped to the panels.

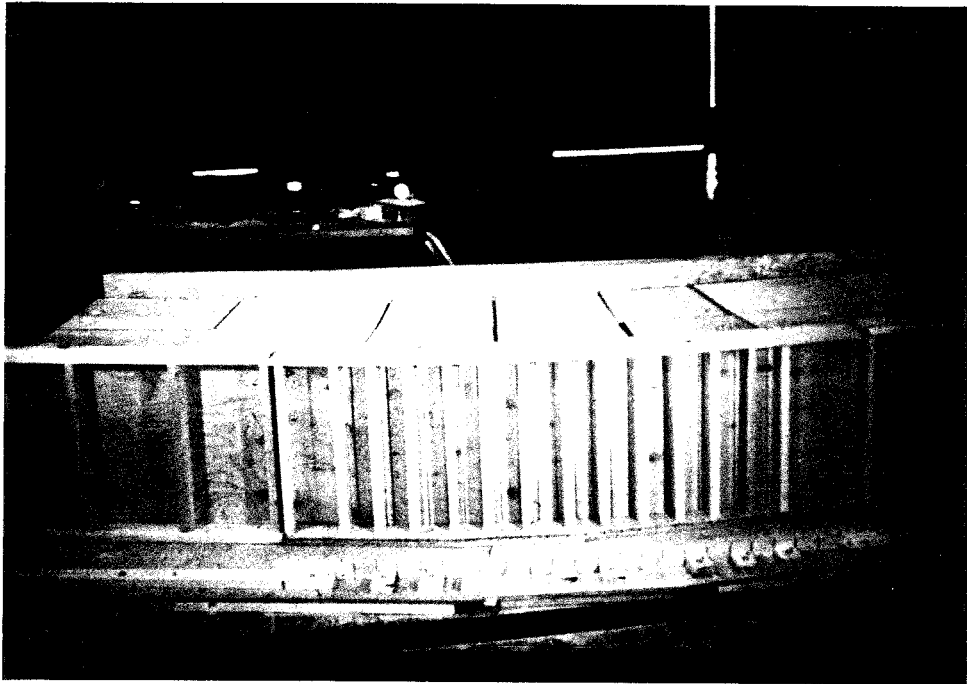


Figure 4.4 Exterior Web Form.

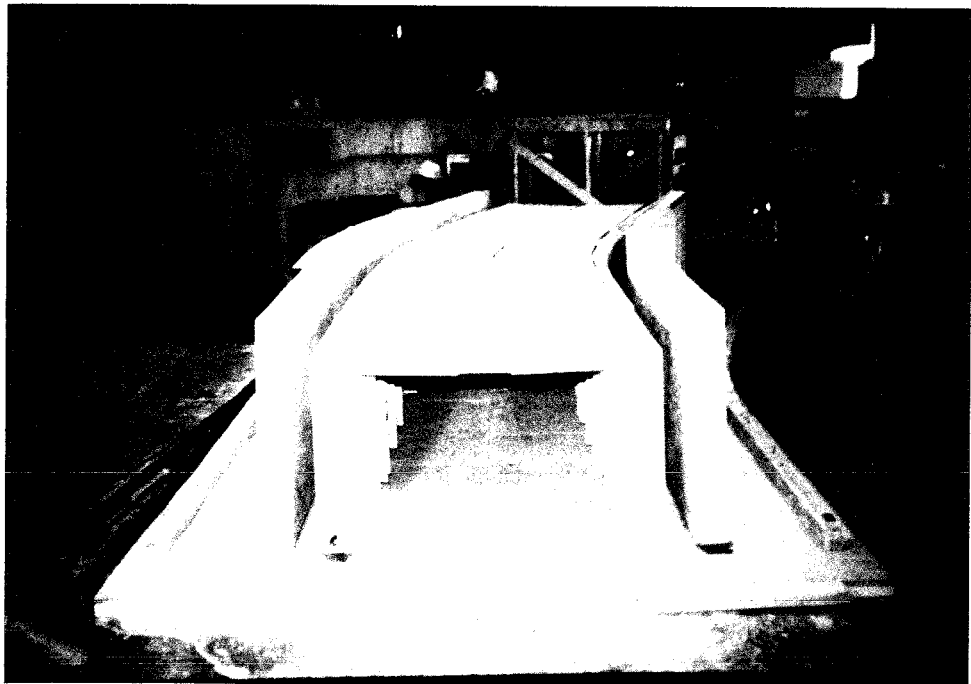


Figure 4.5 Core and Exterior Web Forms.

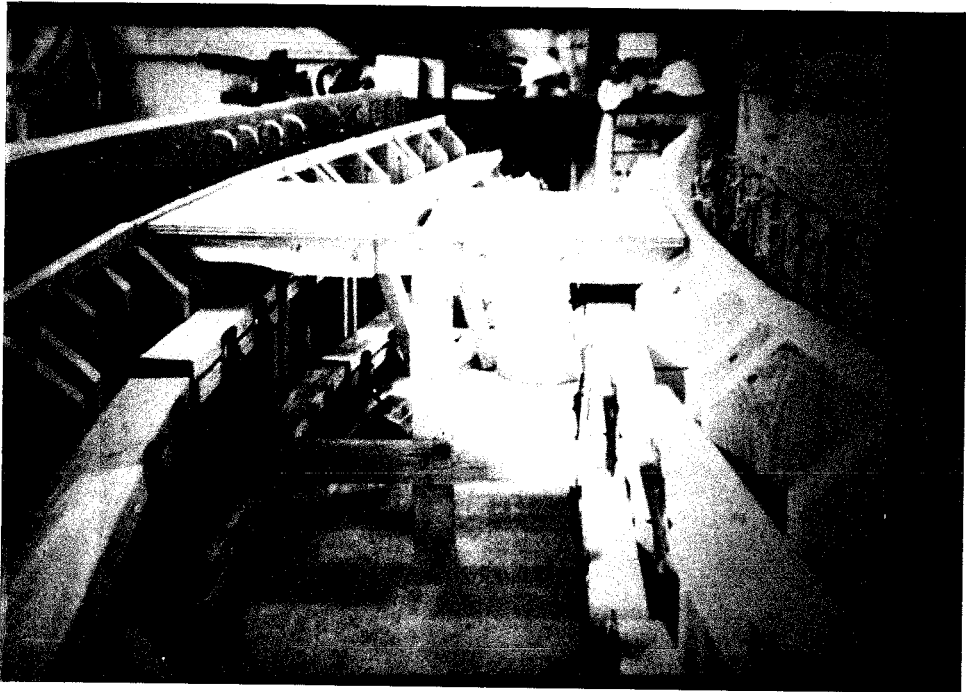


Figure 4.6 Section of Core Form and Bracing.

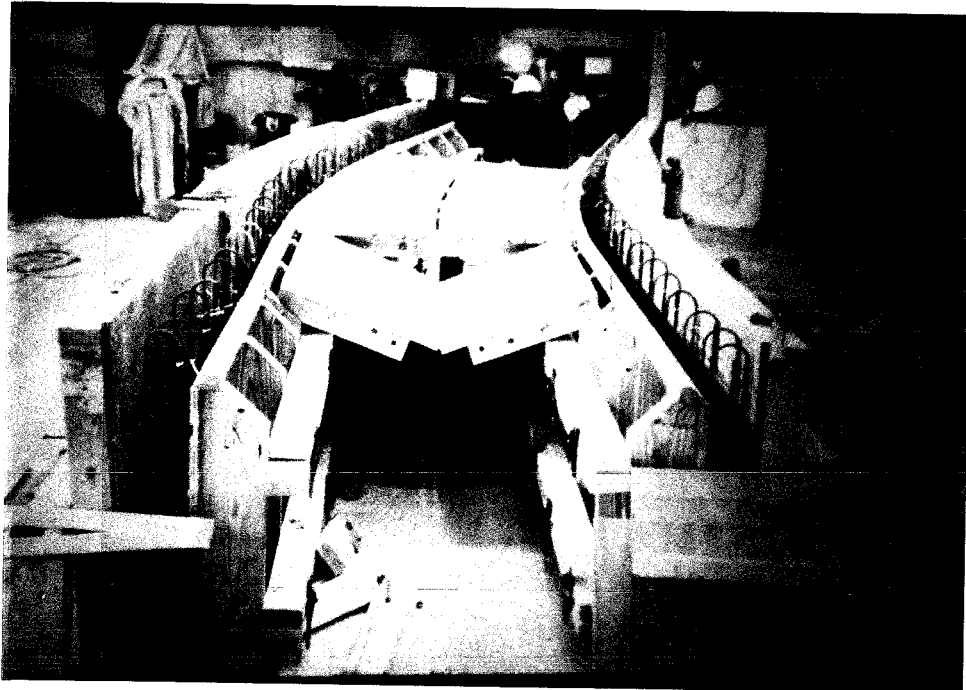


Figure 4.7 Articulated Top Slab Soffits.

Standard 4" wide wall ties connected the inside and outside wall forms. Web forms were bolted to pre-cast inserts located in the bottom concrete slab to keep the forms from floating. One-half inch thick compressible material was nailed to the bottom of the bottom sole plates prior to bolting to prevent mortar leakage between the web forms and bottom slab.

The internal forming system was very successful. The entire core formwork was stripped by one man in five hours with no damage to the forms. Forms were removed after 24 hours of curing at which time the top slab was strong enough to support itself ($f'_c = 2500$ psi for both girders) but before much shrinkage had taken place.

4.2.2 Bottom Slab

Construction of the bottom slab was straightforward aside from maintaining correct locations for the stirrups. It was essential that the stirrups be correctly positioned during this cast so that when the web forms were assembled, the correct cover of $\frac{1}{2}$ " was maintained.

This was accomplished by securing alignment assemblies to the bottom slab soffit along the tangents and the curve [Figure 4.8]. The assemblies consisted of a $\frac{3}{8}$ " nut tack welded to a large washer with pre-drilled holes. The assemblies were carefully aligned and fastened with screws through these holes. Stirrups were outfitted with an aligning bar tack welded to the vertical leg on the inside of the curve. This 6mm, 4" long bar was inserted into the assembly which kept the stirrup from moving in the horizontal plane. The bar was welded to the stirrup such that it extended $\frac{1}{2}$ " below the hooked portion of the stirrup. When this bar rested on the bottom slab soffit, it maintained a $\frac{1}{2}$ " bottom clear cover for the stirrup. Welding to reinforcing steel is not good construction practice. However this part of the stirrup was in compression when the web is analyzed as a regional beam. It was also



Figure 4.8 Stirrup Alignment System.

believed that proper alignment of the bar was much more crucial than reduction of bar strength in this low stress area.

The bottom assemblies alone could not support the free-standing stirrups. A jig was constructed to which the top of the stirrups were tied in their final position [Figures 4.9 & 4.10]. This system worked extremely well. The distance between the stirrups and the forms in the critical curve region were within $\frac{1}{8}$ " of the required clear cover.

4.2.3 Duct Positioning

After the bottom slab was cast and the core formwork assembled, post-tensioning ducts were threaded between the stirrup legs. Small plastic $\frac{3}{8}$ " thick spacers were used to connect the ducts to the stirrups [Figure 4.11].

It was important not to tie the ducts to the leg of the stirrup on the outside of the curve. The scale factor was $\frac{1}{3}$ but the tie wire was standard construction gauge wire. A simple load test in the lab indicated that the tie

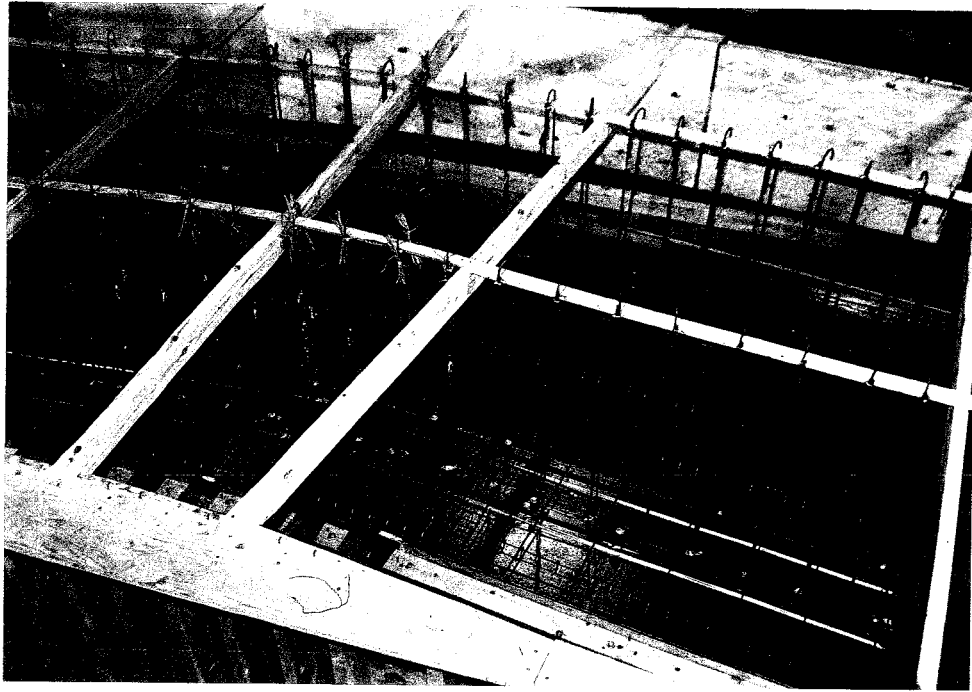


Figure 4.9 Stirrups and Jig Before Casting Bottom Slab.

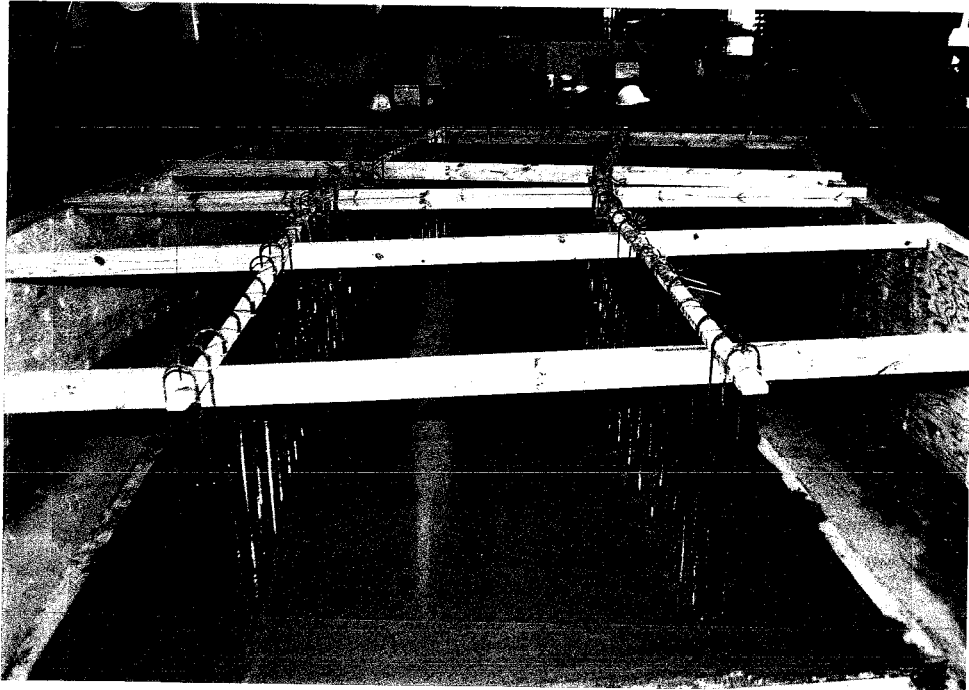


Figure 4.10 Stirrups and Jig After Casting Bottom Slab.

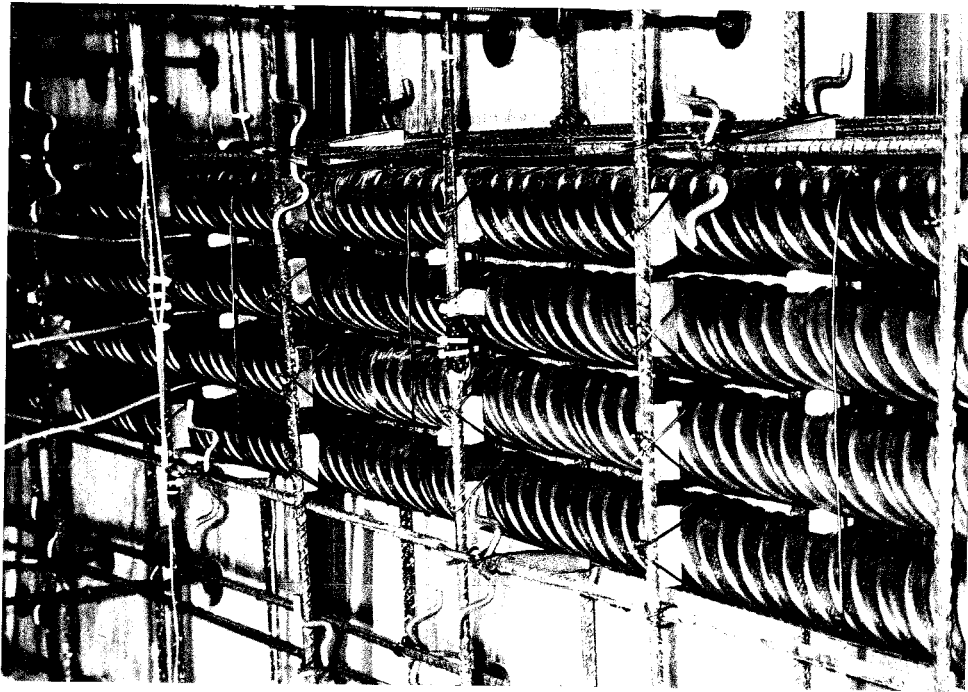


Figure 4.11 Plastic Spacers.

wire had a tensile strength of approximately 200 lbs. Ducts were secured at every stirrup in the curve with two ties tied in hoop formations. This meant that in every linear foot of curve, approximately four hoop ties were present per duct. For four ducts, this means that 32 tie legs were available to act as tension ties connecting the ducts to the back face. This could have supplied 6 k/ft of tension tie force to restrain the ducts to the back face. Since the tests were investigating the effect of duct arrangements without hook tie reinforcement, this could have seriously effected those results.

In the case of BO (the offset arrangement), two of the $\frac{3}{8}$ " plastic spacers were used to tie the duct to the front face stirrup leg. They were touching but not tied to, the outside stirrup leg.

Longitudinal bars were tied to the inside of the stirrup legs. Individual chairs ($\frac{3}{4}$ " high) were tied to the longitudinal bars. This created $\frac{1}{2}$ " of clear cover for the stirrups. To give rigidity and prevent the two mats of steel from

collapsing inward, two inch-long plastic spacers were tied between longitudinal bars on opposite mats [Figure 4.11].

Figures 4.12 through 4.19 show duct positions for each of the four details.

4.2.4 Anchorage Plates

High reaction forces from the loading system were applied to the ends of the specimen above and below the ducts. One-half inch steel plates doubled as bearing plates and end forms. Two in. diameter holes were drilled in the plates to allow the ducts to pass. Twelve $\frac{3}{8}$ " bolts 1" long were tack welded at the inside face of the plates to act as anchorage studs [Figure 4.20].

4.2.5 Casting Procedure

The casting of the bottom slab was routine. Concrete was bucketed, placed and vibrated. Screeding was done longitudinally because the stirrups prevented transverse screeding.

When the concrete truck arrived for the web and top slab casts, slumps were taken. Superplasticizer was added and the drum was spun for five minutes and a new slump was measured. The slumps and superplasticizer weights are recorded in Table 4.1.

The actual casting of the webs was labor intensive because of the thin webs and congestion. Bucketing of concrete was not used because rapid dumping could cause extensive bridging of concrete between the ducts, longitudinal bars and forms. Instead concrete was moved from the truck to the webs in wheelbarrows and hand-scooped into the forms. Concrete was placed starting at one end and working toward the other in three separate lifts. Each placer was trailed by a rodman who used a 6mm bar to clear any bridging that may occur [Figure 4.21].



Figure 4.12 BC Duct Arrangement (Overall View).



Figure 4.13 BC Duct Arrangement (Close-Up).

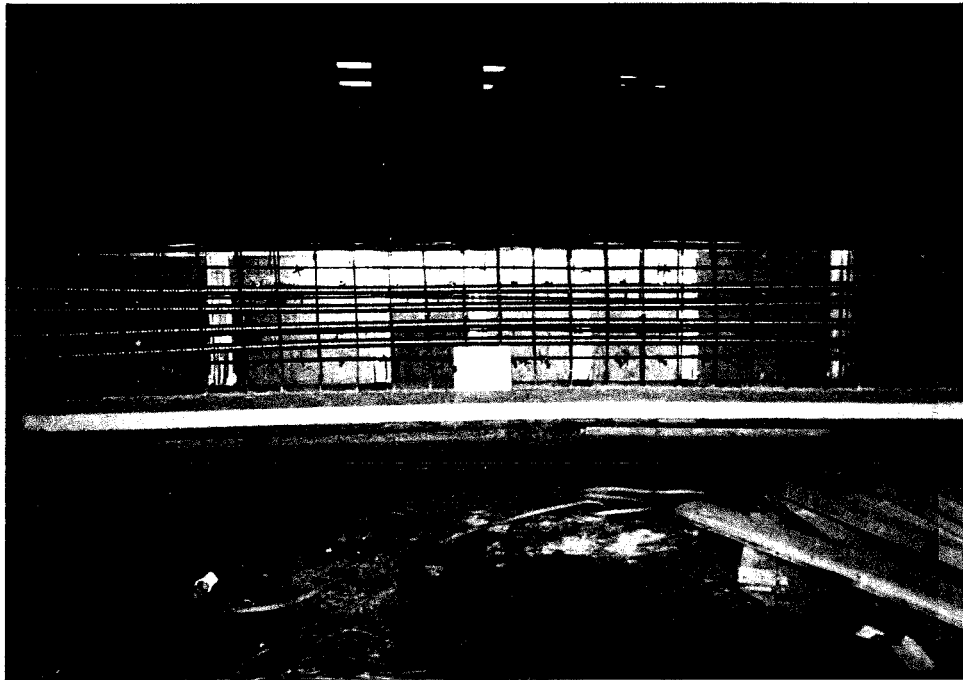


Figure 4.14 1.0DC Duct Arrangement (Overall View).



Figure 4.15 1.0DC Duct Arrangement (Close-Up).

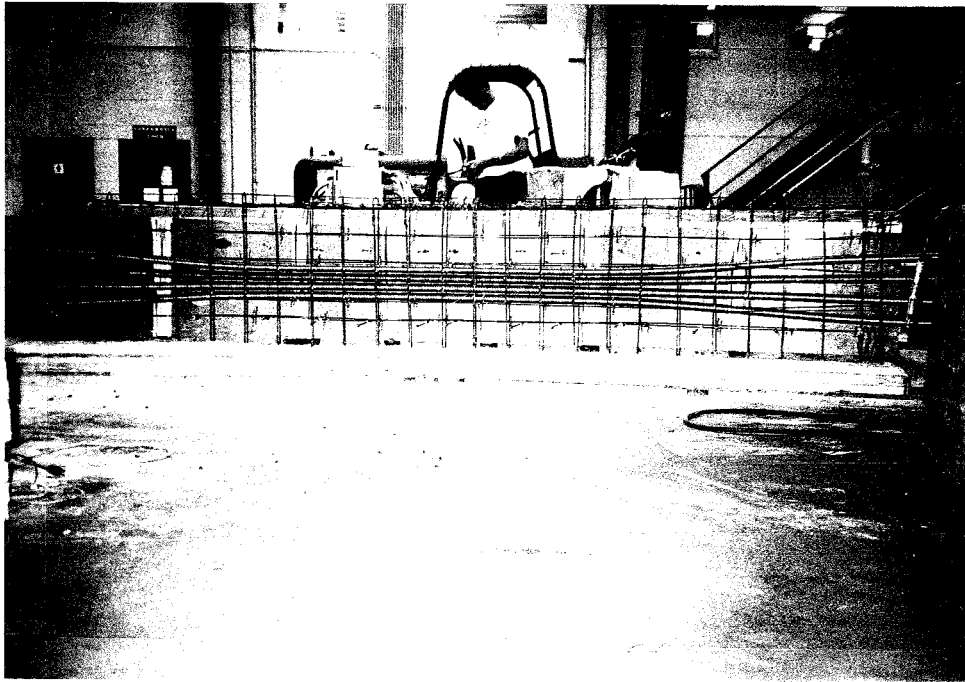


Figure 4.16 0.2DC Duct Arrangement (Overall View).

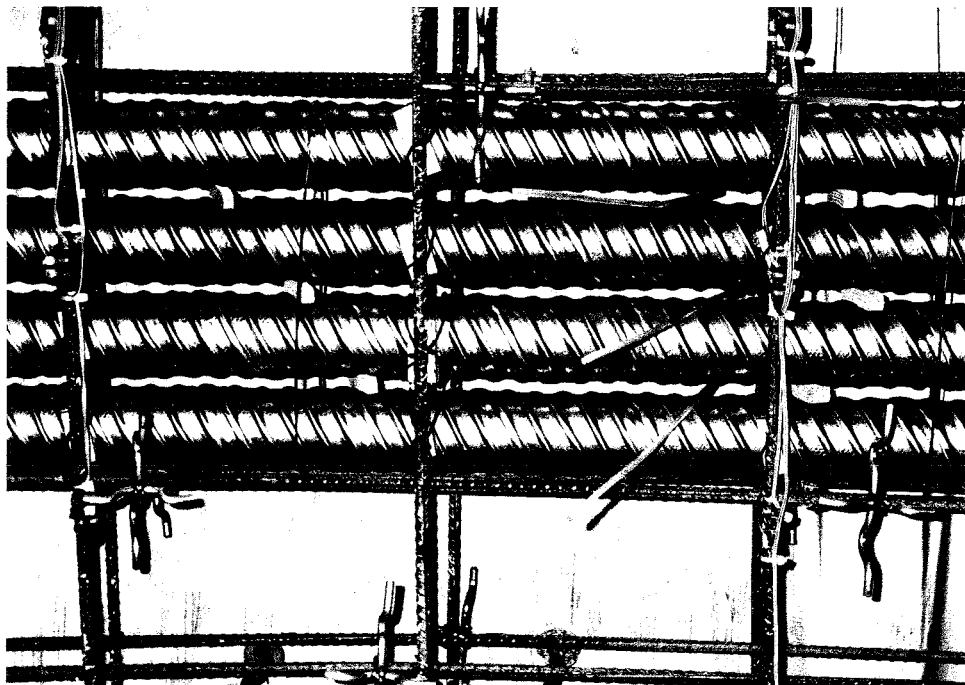


Figure 4.17 0.2DC Duct Arrangement (Close-Up).

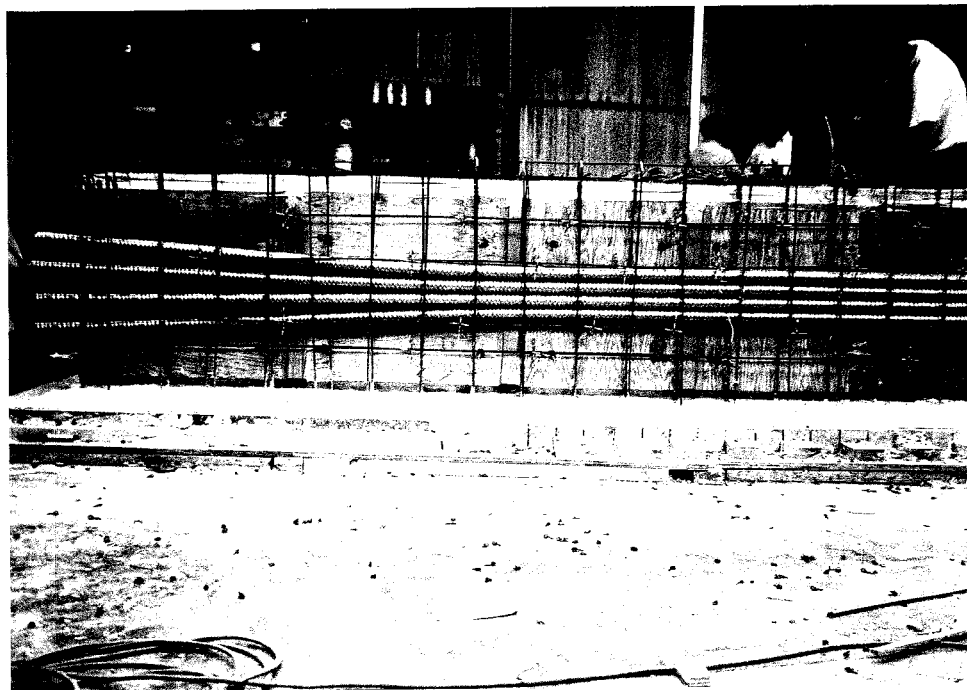


Figure 4.18 BO Duct Arrangement (Overall View).

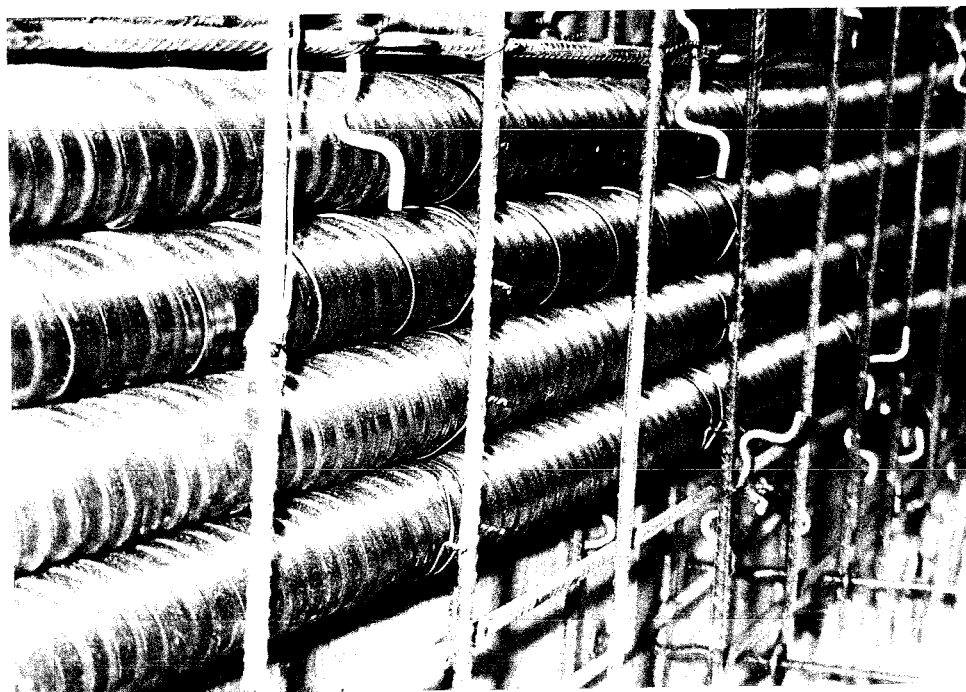


Figure 4.19 BO Duct Arrangement (Close-Up).

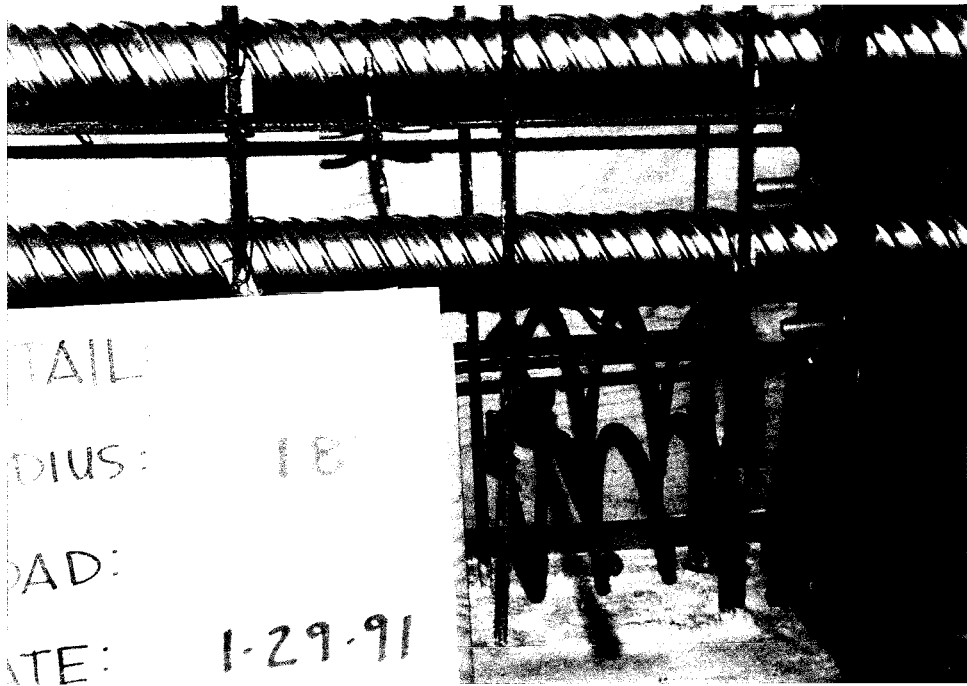


Figure 4.20 Anchorage Plates (Not in Final Position).

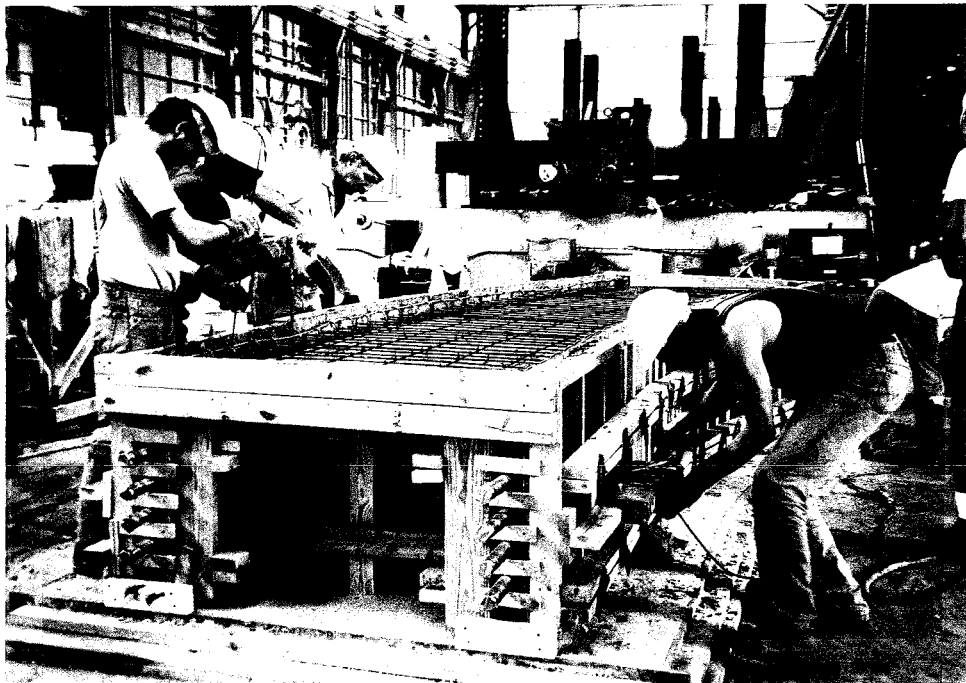


Figure 4.21 Rodding, Internally Vibrating, Placing and Externally Vibrating.

Each lift was vibrated internally. No vibrators were small enough to reach into the narrow openings within the web, so 3' x 2" x ¼" steel plates were fastened to vibrators with hose clamps [Figure 4.22]. These could reach to the bottom of the web but they could not provide as much vibratory action as an unadorned vibrator. Many clamps (6-10) were put on the vibrators because with use, the clamps at the tip would fracture and vibratory action was decreased with each clamp lost.

Teams of wheelbarrower, placer, rodman and vibration man attended each web. Each team made three passes until the webs were filled. An external form vibrator was attached to the web forms. Only one form vibrator was available and the attachment process was time-consuming. Therefore application of external vibration was more random as it was moved along and across both webs while teams were at work. The top slab casting was quick and easy in comparison to the web cast. Here concrete was bucketed, vibrated with a 1½" vibrator and screeded [Figure 4.23].

4.2.6 Honeycombs

In spite of the careful concrete placing procedures that were undertaken, voids were discovered in the webs of girder #2. The problem was compounded by the fact that not only were the voids located near the ducts, they were near anticipated failure planes.

In web 0.2DC, a 22" length of honeycomb ran longitudinally on the inside face at an elevation coincident with the top of the top duct. The void began at stirrup #3 and ended at stirrup #6 (see Figure 5.10 for stirrup identification). The honeycomb varied in depth from 0" to 1½" and averaged ¾" [Figure 4.24].

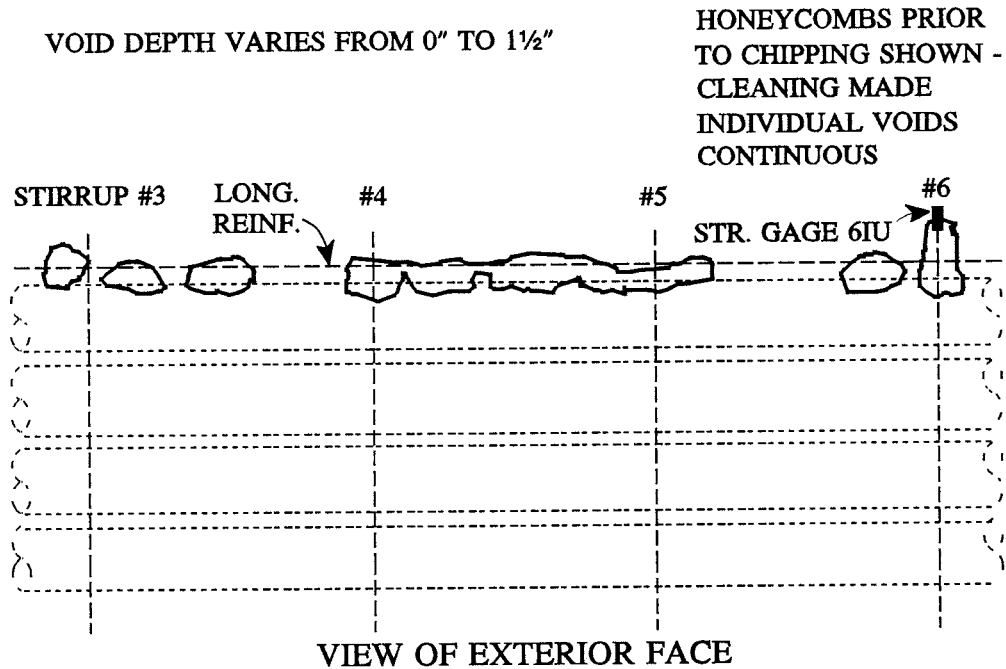


Figure 4.24 Web 0.2DC Voids.

Two voids were created on both faces of web BO. The voids were directly opposite one another and of similar shape. They could have been thought of as a single void extending entirely through the web except they were almost completely separated from one another by the ducts [Figure 4.25]. Both voids extended longitudinally from stirrup #6 to stirrup #7 and vertically from the bottom of the bottom duct to slightly above the top of the top duct.

The top of voids in both webs were bounded by longitudinal bars. There were many reasons for the voids. Although the slump was 8" (and greater than the 7" slump in girder #1), it had a stiff consistency. A few gallons of water would have improved the workability. Water was not added because similar concrete strengths were desired for both girders and water would have changed the w/c ratio. Also because of the placement success

with girder #1, there was no particular concern about this stiffer mix. Fourteen people worked on the casting of girder #1. Only 8 were available for the casting of girder #2. This slowed the concrete placing operation and the workability of the mix deteriorated with time. It also pressed the foreman into service and inspection suffered. Some of the plastic tubes that created voids for the delamination wires as described in section 5.3.4 shifted when casting girder #1. As a result their locations were noted in girder #2 and internal vibrators were kept away. The large void in web BO surrounded the four plastic tubes for that web. Lastly, the transverse studs that were glued and screwed to the web forms had somehow loosened between the two castings. Therefore the external vibrators that clamped to these studs had a marked loss of effectiveness as the attachments did more shaking than the forms.

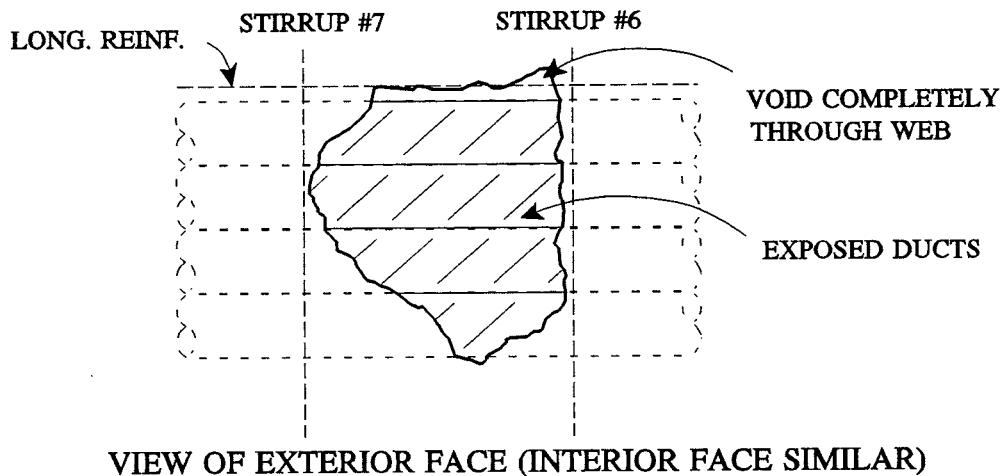


Figure 4.25 Web BO Void.

4.2.7 Patching

A hammer and chisel were used to remove loose rock and mortar and slightly bevel the edges of the voids. This provided a solid, roughened surface to hold the patch.

It was considered essential that the mortar patch be approximately the same strength as the concrete web. The 24 hour concrete strength for girder #2 was 2600 psi. Two days after casting the girder, nine trial mortar batches were mixed and cast into 2" cubes. These mixes varied in w/c and sand/mortar ratios so that one mix with the desired strength and workability would be found. Twenty-four hour cube breaks were made and a suitable mix was chosen.

Four days after casting girder #2, epoxy was brushed onto the prepared concrete surfaces. As per the specifications, the epoxy was cured for five hours and became tacky. The mortar was then mixed and hand troweled into web 0.2DC. Forms had been built and compressed against both faces of web BO [Figure 4.26]. Small openings were made in the sheet metal form faces to pass the plastic instrumentation tubes. Mortar was placed into the openings left above the forms. A 6mm bar was rodded into the patch through this opening to consolidate the mortar.

4.2.8 Measured Dimensions

Web transverse dimensions were considered critical. After all tests were completed, four holes were drilled through each of the webs. Two holes were made at each $\frac{1}{3}$ point of the curve. One of these holes was above the duct arrangement and the other below. Web widths were measured and the results were quite satisfactory. Of the sixteen holes drilled, the largest web width recorded was $4\frac{1}{8}$ " and the smallest was $3\text{-}15/16$ ". The average web width for each web was between 4" and $4\text{-}1/16$ ".

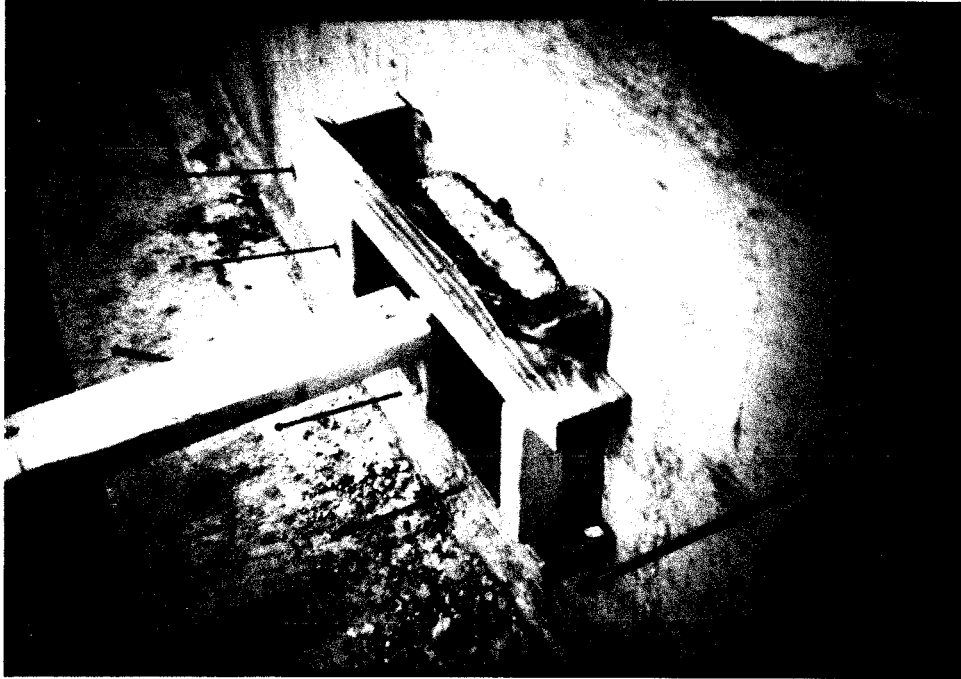


Figure 4.26 Specimen BO Exterior Patch Form.

A chipping hammer and acetylene torch were used to remove concrete and steel and expose the duct arrangements. All the ducts appeared to have remained securely in their tied positions. Clear covers of the stirrups were measured in these areas. The average cover for each of the webs was $7/16$ ". The maximum cover measured was $5/8$ ". The minimum cover was at stirrup #3 in web BO which had a cover of only $1/4$ ".

CHAPTER 5: LOADING AND INSTRUMENTATION

5.1 LOAD SYSTEM

Longitudinal prestressing creates external forces on a concrete box girder similar to other forces that bridges typically experience (dead load, live load, wind load, etc.). The benefit of prestressing is that it can apply forces in controlled, predetermined amounts and directions that usually oppose these other forces. In the case of Las Lomas and Kapiolani, the girders were not able to withstand the radial component effects of this particular type of external force. Since the experiments conducted here were not to be tests of girders in which the post-tensioning was provided to resist other types of forces, the post-tensioning forces were applied much as one would typically apply external loads to test specimens. That is to say the specimen was loaded to failure by applying small increments of post-tensioning force.

Typical stressing procedures were not deemed appropriate for applying load to the specimens because of tendon seating losses and the myriad of possible stressing sequences. During construction, an individual tendon is usually jacked to a maximum allowable stress and then seated which causes the tendon stress to decrease slightly. Previously seated tendons can lose stress as subsequent tendons are stressed and the girder shortens. Therefore the total prestressing force on a girder does not steadily increase, but increases with a series of small drop-offs as each tendon is seated. A large

number of stressing sequences are possible for a multi-tendon girder. The stressing order is dependent on a number of construction and design variables and can vary from bridge to bridge. Behavior and ultimate load capacity may change depending on the distribution of stressed and unstressed tendons in a tendon group. A series of tests dependent on stressing sequence was thought to be undesirable.

A loading system was developed to apply gradually increasing load simultaneously to all tendons with an equal force in each tendon. While this would not be a practical way to apply post-tensioning forces in the field, it was considered the most practical for laboratory tests in which the specimen capacity was unknown. Results could be more easily extrapolated to various tendon stressing operations if all tendons carried equal amounts of force. It also simplified the actual testing if not the overall test set-up. Tendons would not have to be individually stressed and seated and then possibly restressed to achieve failure of the specimen.

5.1.1 Prestressing Strand

It was necessary to consider how the strand or strands that would constitute a tendon would bear on a duct. The ducts at Las Lomas were nearly filled to capacity with strands. This meant that almost the entire 180 degrees of the duct on the inside of the curve was in contact with the strands. That same type of load distribution could be approximated with a minimum of three ½" diameter strands per duct [Figure 5.1]. Since there were four ducts, a total of twelve strands could be safely stressed to $0.75f_{pu}$ to develop a maximum force of 372 kips.

5.1.2 Load Beams

Twelve strands separated into four ducts and stressed simultaneously would have required four prestressing rams. These were not available in the

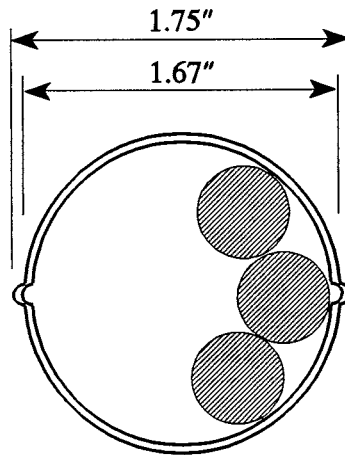


Figure 5.1 Strand Positions in Curve.

lab. The strands were instead stressed by connecting them to a stiff beam which was pushed away from the specimen by a pair of hydraulic rams [Figure 5.2].

The design of the load beam was highly dependent on the geometry of the girder and loading system. It was essential to use a deep beam to minimize deflections. Design calculations were made and a W24x76 which was available in the lab was used. Holes were drilled in each flange for the strands to pass through. The strands form a pattern in the curve as shown in actual size in Figure 5.1. The strands were attached to the beam with standard, commercially available $1\frac{3}{4}$ " diameter monostrand chucks. The chucks required a center-to-center spacing of $2\frac{1}{8}$ " for installation clearance [Figure 5.3]. Therefore slight flaring of the strands was required. Holes were drilled in both flanges in such a pattern as to minimize the strand angle change and ensure balanced loading on the beam. Holes were drilled as close as possible to the web. The holes in the flange nearest the specimen were drilled through the web-flange weld. Holes in the other flange were separated by $2\frac{1}{8}$ ". For each tendon, one strand passed on one side of the web and two

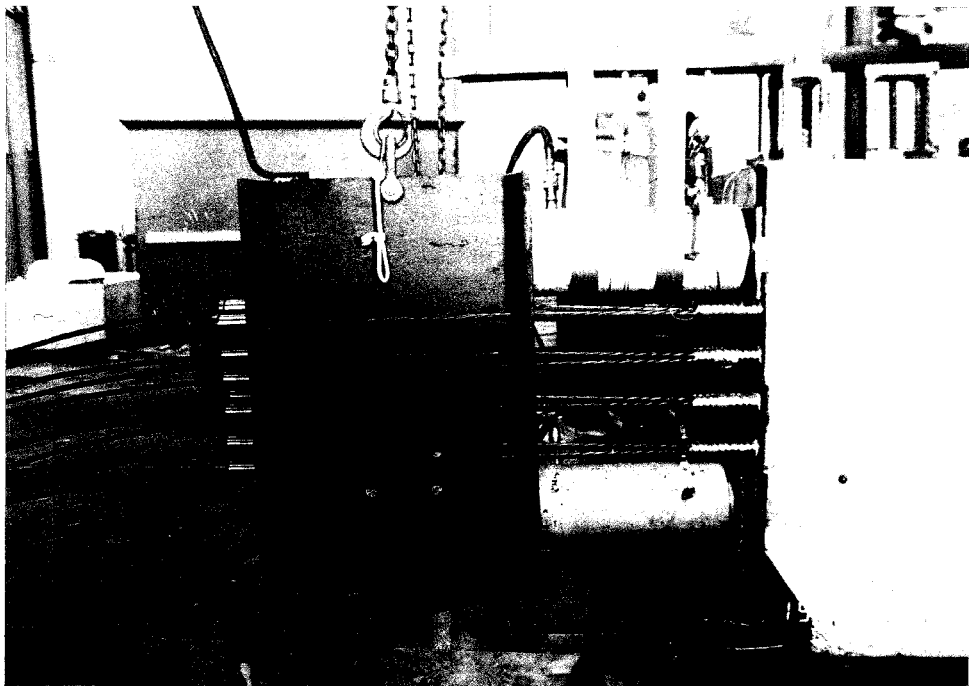


Figure 5.2 Live End Load System.

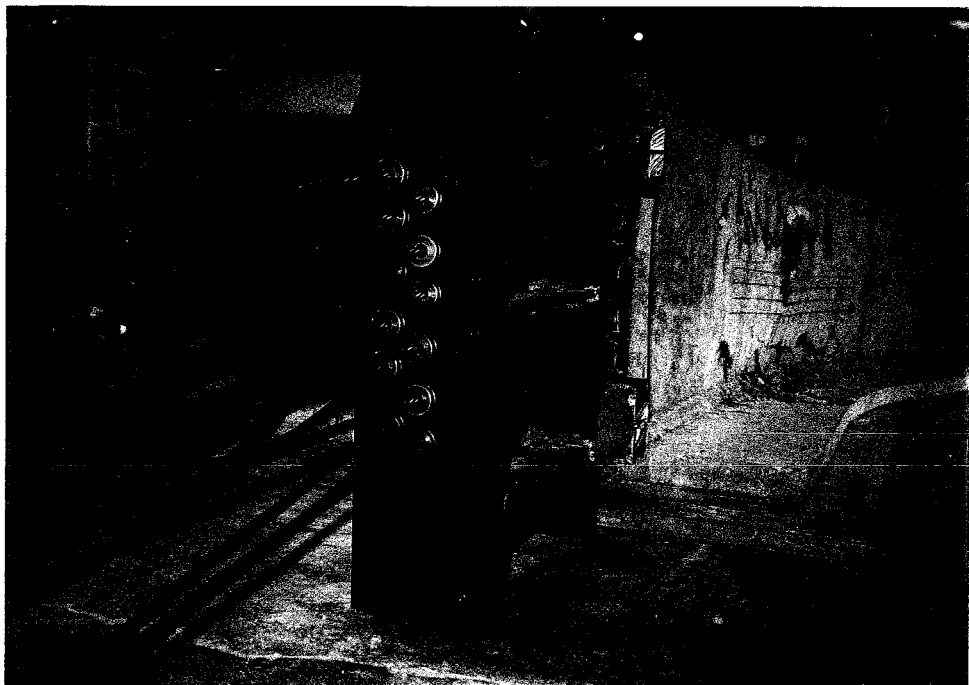


Figure 5.3 Live End Strand Anchorages.

on the other [Figure 5.2]. This pattern alternated for each tendon so that the beam was loaded evenly about the web axis. The edges of all holes were deburred to prevent strands from being cut. A hole size of $\frac{5}{8}$ " was chosen so that 0.6" diameter strand could be used if larger forces were required to fail any of the current or possible future specimens.

A load beam was also used to anchor the strands on the dead end [Figure 5.4]. The flaring of the strands was greater on this beam as threaded screw-chucks were used [Figure 5.5]. Screw-chucks are a lab invention that permitted easy detensioning of strands at the conclusion of a test. Screw-chucks are simply standard chuck bodies machined for external threads. Before stressing, large nuts were barely threaded onto the chucks. At the conclusion of the test when the stress has been removed from the strands, the wedges still firmly gripped the strands and could not be easily removed. Screwing the nuts up the chucks effectively shortened the girder-beam system and allowed the wedges to emerge from the chuck bodies where they could be removed with needle-nose pliers.

To accommodate the flaring strands, large chairs were welded to the dead-end load beam [Figure 5.6]. The overall hole pattern was similar to that used on the live-end beam. Holes were drilled in the flange furthest from the specimen in a symmetrical pattern with a minimum center-to-center distance of $3\frac{1}{2}$ ". This distance was sufficient to give access to two wrenches to remove the nuts. The hole pattern on the flange nearest the specimen was exactly like that for the live-end load beam.

The widely spaced hole pattern caused the dead-end beam to be loaded near the edges of the flange. Calculations showed that the flange flexural stresses were excessive and needed stiffening. Three #9 reinforcing bars were welded between the flanges on each side of the web. Individual

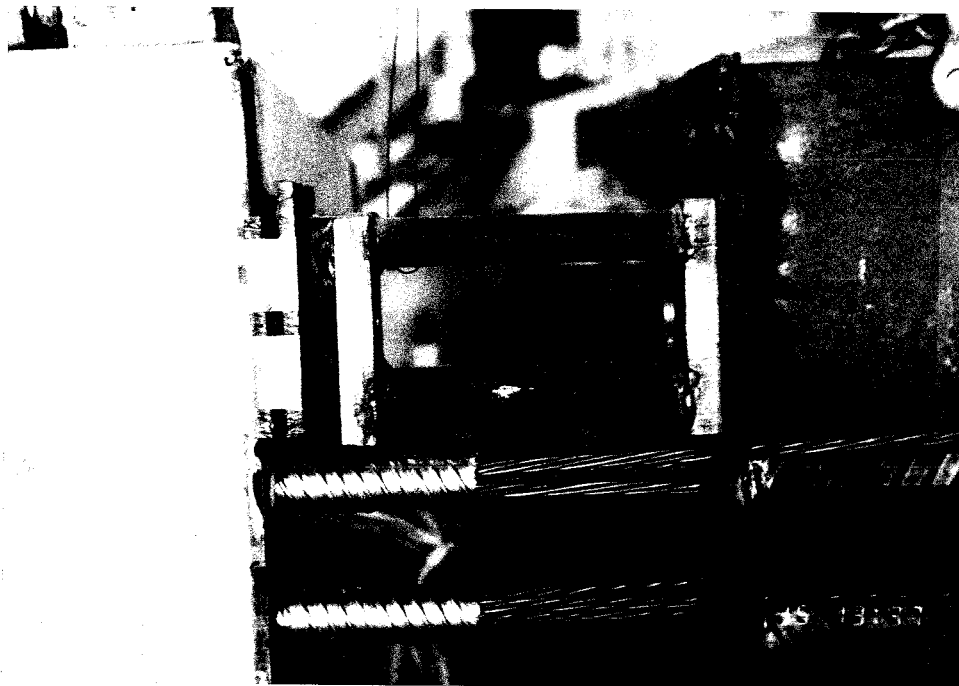


Figure 5.6 Dead End Chairs and Bearing Plates.

bars distributed along the length of the hole pattern were used in lieu of typical plate stiffeners so that access to the strands could be maintained. Their small size allowed one bar on each side to be placed at the middle of the pattern.

A preliminary load beam sizing calculation (AISC eq. K1-8) showed that the web thickness required to prevent compression buckling failure of the unstiffened live end beam web was 0.565" [16]. A design load of 500 kips and clear flange web depth of 16" were assumed. Two 3' long 24" deep beams were located in the laboratory scrap yard and crudely measured with a tape and found to have a web thickness of $\frac{1}{2}$ ". This was deemed acceptable.

The live end beam web buckled during the testing of specimen 1.0DC at a jacking load of 186 kips. Later measurements revealed that the section used was a W24x76 and the actual web thickness was 0.44". The web compression buckling failure load was calculated as 180 kips assuming a web

thickness of 0.44" and a clear flange web depth of 21". The web thickness is cubed in the web compression buckling failure equation. Careless measurements and assumptions made in section selection caused the capacity to be overstated by a factor of 2.77. New calculations were made and the live-end load beam was stiffened with ½" thick stiffeners [Figure 5.3].

5.1.3 Rams

Two 100 ton hydraulic rams were used to stress the tendons [Figure 5.2].

5.1.4 Bearing Plates

Bearing assemblies were placed against the anchorage plates on both the dead and live ends [Figures 5.6 & 5.7]. The assembly consisted of two 8"



Figure 5.7 Live End Bearing Plates.

x 8" x ½" steel plates with a 6" circular, ½" thick neoprene bearing pad sandwiched between. This ensured that the load was distributed uniformly to the girder anchorage zones. Two 8" x 8" x ½" thick spacer plates were added to the lower assembly because the lower ram was 1" shorter than the upper ram.

5.2 LOAD SYSTEM INSTRUMENTATION

Equal pressure was maintained on both rams by connecting them in parallel and activating them by a single pump [Figure 5.8]. A hand pump was used to supply pressure to specimens BC and 1.0DC and an air driven pump was used for specimens 0.2DC and BO.

5.2.1 Pressure Transducers

Two pressure transducers were used to monitor the pressure in the system. They had a 10,000 psi capacity with an accuracy of $\pm 1.5\%$. The output was 10 mv/v.

5.2.2 Switch and Balance

One of the pressure transducers was connected to a strain box indicator (switch and balance unit) so that pre-determined loads could be applied to the girder. Setting the switch and balance unit to known microstrains which corresponded to desired ram forces allowed established load increments to be accurately reached. For each load level, a microstrain value was dialed into the switch and balance unit and the pump was activated until the needle on the unit swung to the zero position.

The relationship between line pressure and load was established prior to testing the specimens. The two rams were individually tested in a 600 kip SATEC universal testing machine. One ram was connected to a pump through a manifold. A pressure transducer and switch and balance unit were also connected to the manifold. The ram was then pumped against the

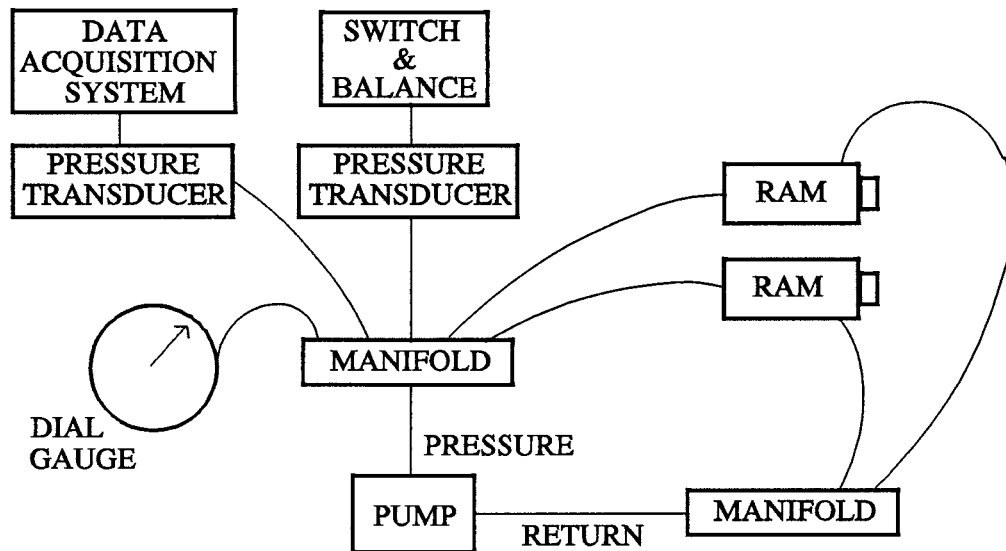


Figure 5.8 Load System Schematic.

loadhead in increments of 20 kips as measured by the test machine until the ram was loaded to 200 kips. The reading on the strain box indicator was recorded at each load stage. The first ram was switched out and the second ram was tested in the same manner.

Calibration curves were developed for each ram [Figure 5.9]. The load reading was divided by the ram area (21.2 in^2) and the pressure was plotted on the vertical axis. The microstrain reading on the strain indicator box was plotted on the horizontal axis. The curves for the two rams were linear and nearly coincident. The fact that the curves were linear meant that the force at any load stage could be attained by simply multiplying the ram areas by the pressure recorded by the transducers. The fact that they were nearly coincident meant that nearly equal forces would be applied by each ram at every pressure.

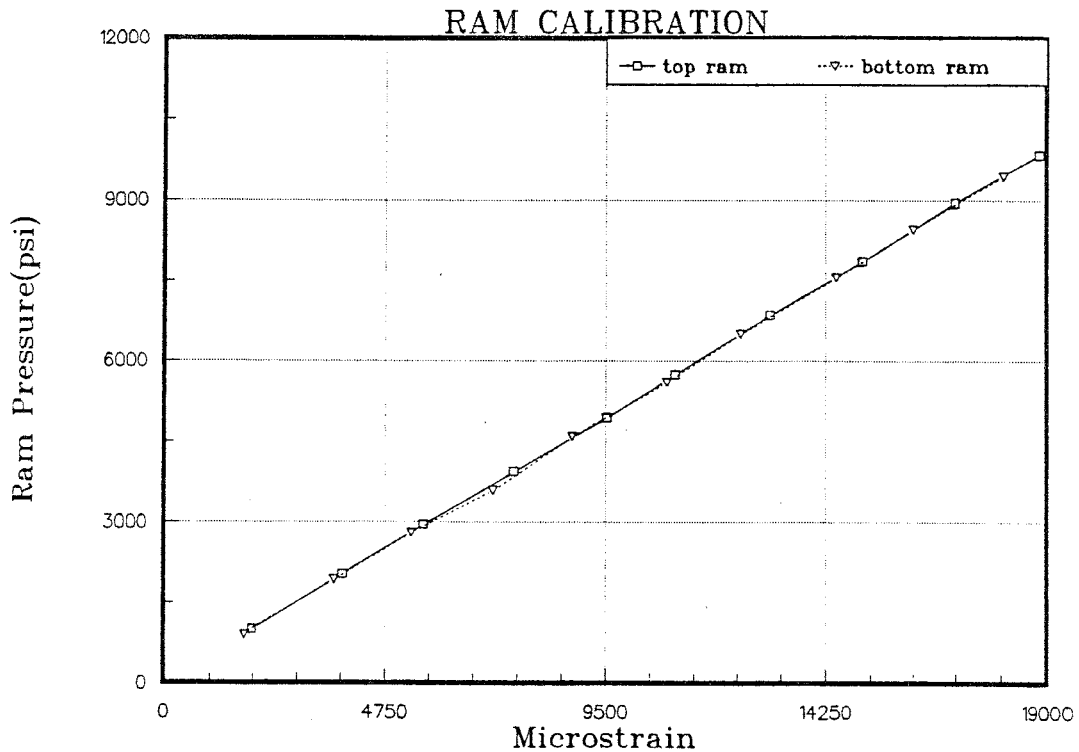


Figure 5.9 Ram Calibration Curve.

5.2.3 Data Acquisition System

All digital instrumentation was connected to a Hewlett-Packard scanner which in turn was connected to an IBM personal computer. A software program developed in the laboratory (HPDAS) controlled the scanning and recorded the data from the instrumentation. To measure and record the force actually applied to the specimen, the scanner applied 10 volts to a full-bridge pressure transducer that was connected to a manifold. A total ram area of 42.4 in² was input into the HPDAS program which used the linear relationship (force = pressure x area) demonstrated by the calibration curves to record the force at every load stage.

5.2.4 Pressure Gauge

An analog pressure gauge was used as a back-up measurement of pressure in the system. A 10,000 psi gauge with a rated accuracy of $\pm 0.25\%$ was used.

5.2.5 Strain Gages

Strain gages were applied to two strands in the live end flaring region for every test. One gage was attached on a strand emerging from the top duct and the other on one of the strands emerging from the bottom duct. The gages were used as a secondary means of measuring jacking force and detecting non-uniformity of strand stresses.

The strain gages used were 5mm type FLA-5-3L-11 manufactured by the Tokyo Sokki Kenkyojo Co. The resistance was 120.3 ± 5 ohms and the gage factor was 2.12.

5.3 SPECIMEN INSTRUMENTATION

The specimen was instrumented to determine the behavior of the girder and the cause of failure. Examinations of the bridge failures summarized in Section 2.3 & 2.4 indicated that local shear in the web or perhaps regional web flexure were the likely causes of failure. Instrumentation was selected primarily to monitor these two failure modes.

All digital instrumentation was connected to the same data acquisition system used for monitoring hydraulic pressure in the loading system. As with loading pressures, specimen instrumentation was scanned and recorded at each load stage using HPDAS. Ten volts were supplied to full-bridge potentiometers and two volts were supplied to quarter-bridge strain gages. Analog measurements (demec gages) were read and recorded manually. The first girder contained more instrumentation than the second.

Instrumentation that was redundant in tests BC and 1.0DC was reduced or eliminated for tests 0.2DC and BO.

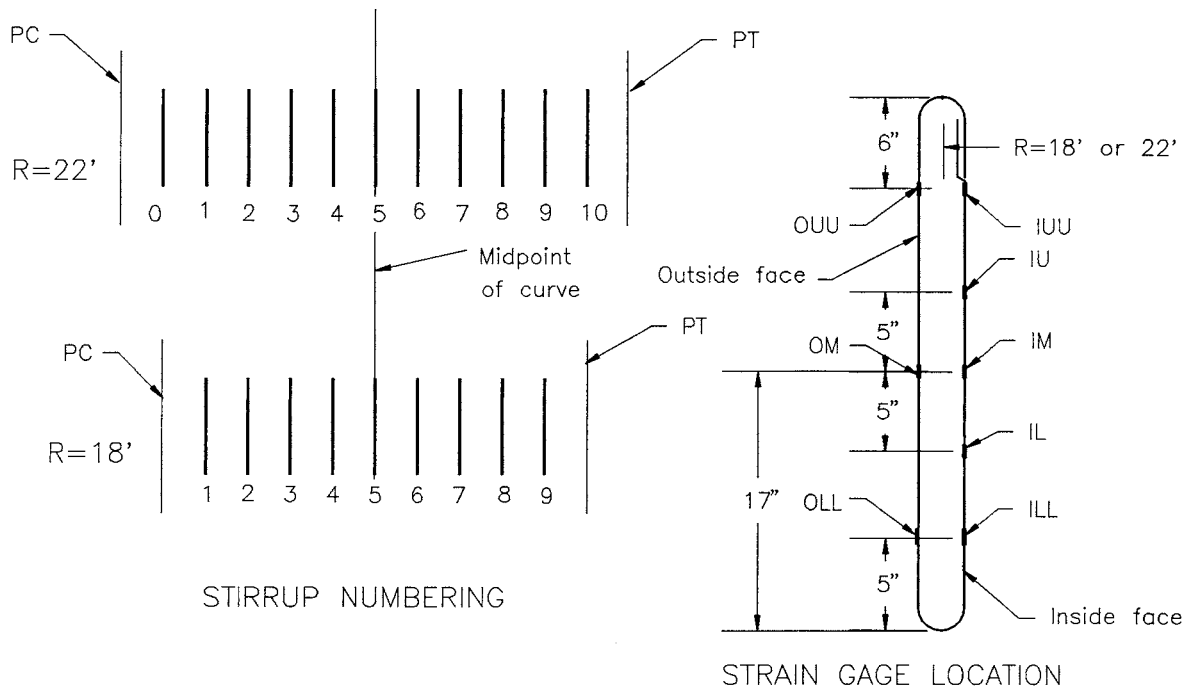
5.3.1 Strain Gages

The same type of resistance strain gages used to monitor strand strains were mounted on the stirrups in the curved region of the webs. These were intended to provide information on regional and local flexural behavior of the webs.

Figure 5.10 describes the location and numbering system for the strain gages. Each stirrup in the curves was given a number between 0 and 10. A series of letters indicates the position of a particular gage on a stirrup. The first letter is either labeled "O" for the leg on the outside of the curve or "I" for the leg on the inside of the curve. The second and third letters (if used) indicate the height of the gage as illustrated. Tables 5.1 and 5.2 show which of all the possible combination of stirrup and strain gage positions actually contained gages. These tables also indicate if a particular gage was actually working at the time of the test. Figures 3.4 and 3.5 show gages positioned relative to other web details and in particular, the duct positions.

5.3.2 Web-Slab Potentiometers

Regional beam behavior was monitored by deflection of the web relative to the top and bottom slabs. U-shaped frames were mounted to the web face on the outside of the curve [Figure 5.11]. The actual attachment points were about 2" below the top slab and 2" above the bottom slab. This permitted the construction of only one type of frame which could be mounted on either web. Ideally, the frame should have been mounted on the slabs. However the deflection anticipated in the first 2" is negligible. A single potentiometer was mounted at the mid-height of the frame (which is also the c.g. of the tendon group). A small mirror glued to the specimen provided a



STRAIN GAGE NOMENCLATURE: XXX

- ↑ ↑ ↑
- UU, U, M, L, LL as illustrated
- Inner face (I) or Outer face (O)
- Stirrup #

Figure 5.10 Strain Gage Nomenclature.

smooth surface on which the potentiometer stem could bear.

Mounting the potentiometers on the outside face of the curve meant that deflections should not be influenced by local beam action; regional beam behavior should be solely responsible for measured deflections. Also potentiometers attached to the back face were protected from exploding concrete.

The web-slab potentiometer nomenclature is given in Figure 5.12. The description begins with the letters WS to signify that deflections of the web

Table 5.1 Girder #1 Strain Gage Inventory.

STRAIN GAGE INVENTORY FOR SPECIMEN 1.0DC								
STIRRUP #	LOCATION OF STRAIN GAGE ON STIRRUP							
	IUU	IU	IM	IL	ILL	OUU	OM	OLL
1			Y					
2			Y				N	
3			Y					
4		Y	Y	Y			N	
5			Y					
6		Y	Y	Y		Y	N	N
7			Y					
8			Y				N	
9			Y					
STRAIN GAGE INVENTORY FOR SPECIMEN BC								
STIRRUP #	LOCATION OF STRAIN GAGE ON STIRRUP							
	IUU	IU	IM	IL	ILL	OUU	OM	OLL
0			Y					
1			Y					
2			Y				N	
3			Y					
4		Y	Y	Y			N	
5			Y					
6		Y	Y	Y		Y	N	N
7			Y					
8			Y				N	
9			Y					
10			Y					
Y - gage installed and worked N - gage installed but did not work								

Table 5.2 Girder #2 Strain Gage Inventory.

STRAIN GAGE INVENTORY FOR SPECIMEN 0.2DC								
STIRRUP #	LOCATION OF STRAIN GAGE ON STIRRUP							
	IUU	IU	IM	IL	ILL	OUU	OM	OLL
1								
2			Y					
3								
4		Y	Y	Y			Y	
5								
6	Y	Y	Y	Y	Y	Y	Y	Y
7								
8			Y					
9								

STRAIN GAGE INVENTORY FOR SPECIMEN BO								
STIRRUP #	LOCATION OF STRAIN GAGE ON STIRRUP							
	IUU	IU	IM	IL	ILL	OUU	OM	OLL
0								
1								
2			Y					
3								
4		Y	Y	Y			Y	
5								
6	Y	Y	Y	Y	Y	Y	Y	Y
7								
8			Y					
9								
10								

Y - gage installed and worked N - gage installed but did not work

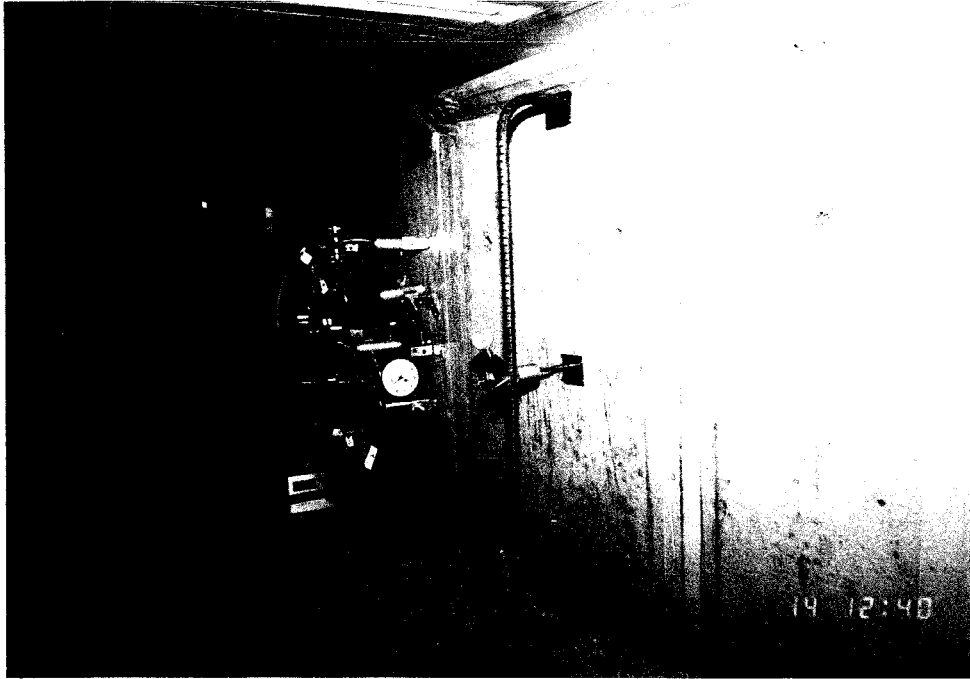
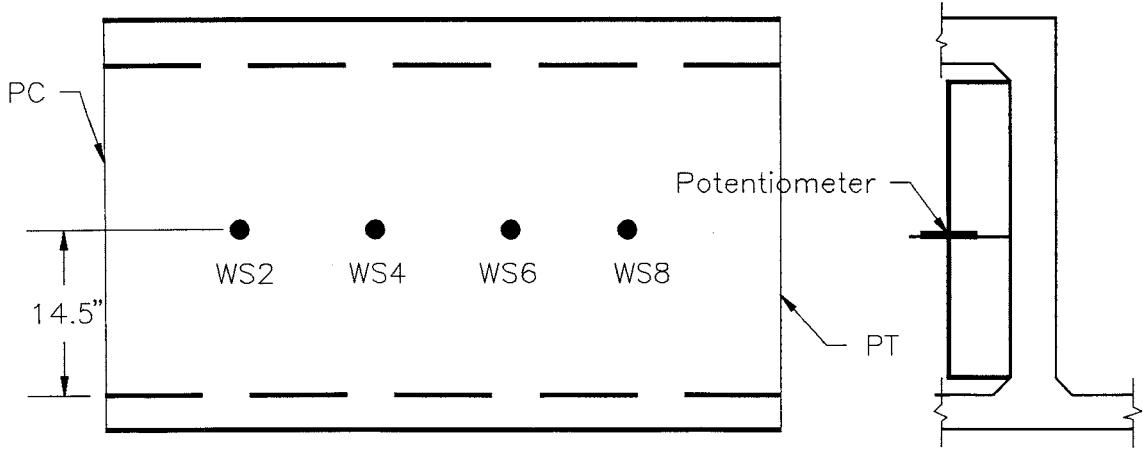


Figure 5.11 Web-Slab Potentiometer.



NOMENCLATURE: WS#
 ↑
 └ Location with respect to stirrup #($\pm 1''$)
 └ Web deflection with respect to slabs

Figure 5.12 Web-Slab Potentiometer Nomenclature.

relative to the slab are being measured. This is followed by the number of the stirrup nearest the potentiometer.

5.3.3 Delamination Gages

Most beam tests done in the laboratory offer the researcher the opportunity to view the profile of the beam. Cracks, both flexural and shear, are visible and their widths can be measured at various load stages. The webs of a girder loaded transversely at mid-height do not allow the researcher the luxury of measuring crack widths using simple, standard measuring devices. The only part of the crack visible is the beginning of the crack on the tension face. This is in effect like watching a standard beam test from underneath the beam. Furthermore, observing cracks from underneath a beam is an unsafe practice as would be close-up inspection of the web from a position on the inside of the curve.

A different method of measuring delamination crack development was required. It was thought that shear failure would involve separation of the front face of the web from the back face. A potentiometer could be connected to both faces to measure this separation [Figure 5.13]. One-eighth inch diameter plastic tubes were cast into the web [Figure 4.13]. These provided voids completely through the web through which a 9" length of thin stove pipe wire could be passed. A ½" square piece of sheet metal was soldered to one end of the wire. The wire was inserted into the hole and the sheet metal was epoxied to the web face on the inside of the curve [Figure 5.14]. The other end of the wire was connected to the stem of a potentiometer with a nylon tie [Figure 5.15]. The length of the wire was adjusted as necessary to precompress the stem spring. The potentiometer was securely fastened to a bracket mounted to the web face on the outside of the curve prior to attaching the wire.

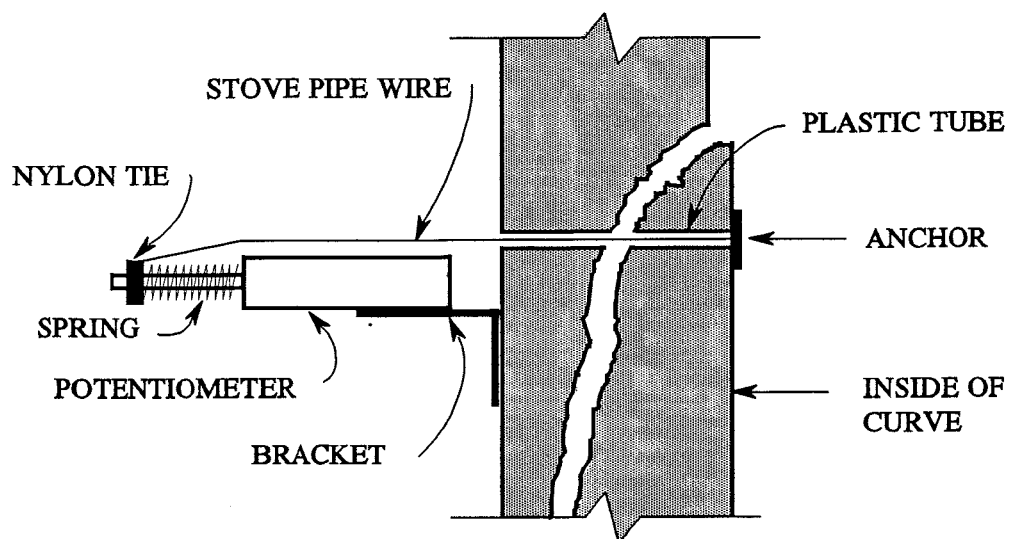


Figure 5.13 Delamination Gage Schematic.

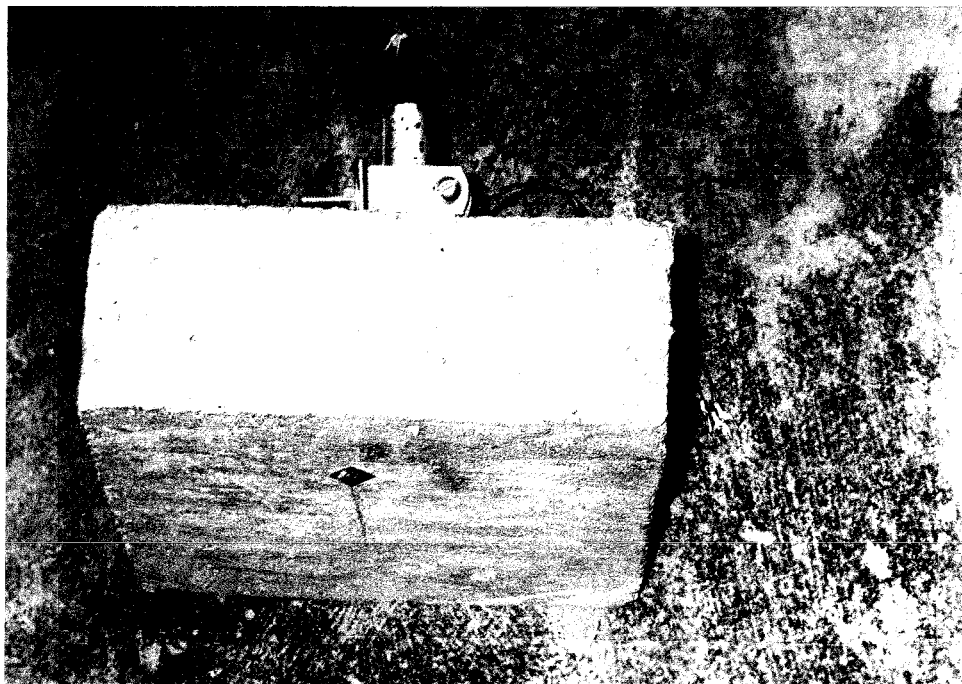


Figure 5.14 Typical Delamination Gage Installation.

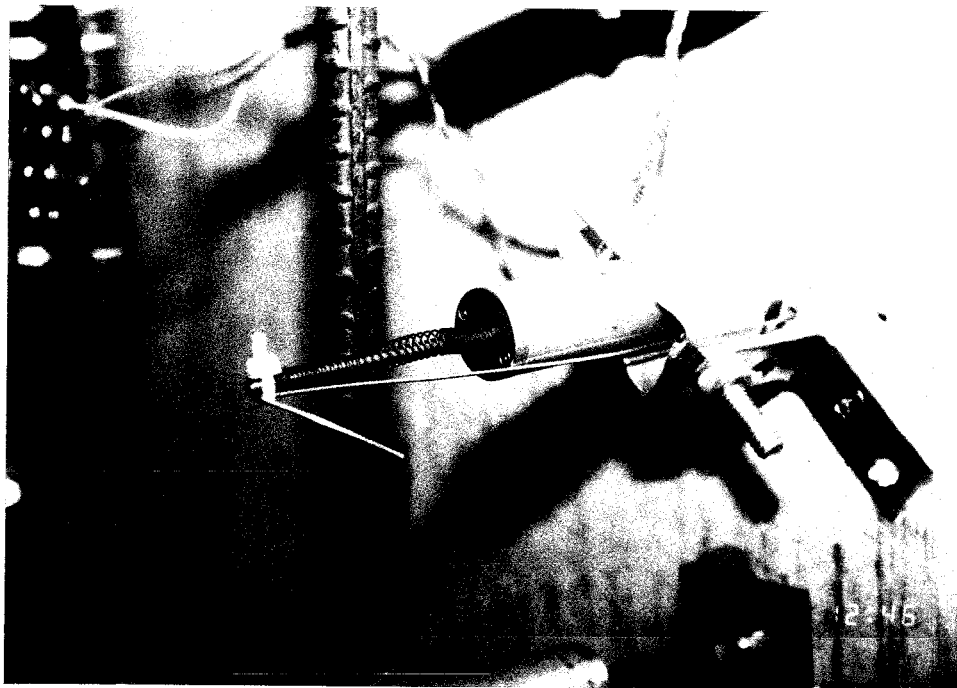


Figure 5.15 Delamination Gage.

The delamination gage nomenclature is shown in Figure 5.16. The letter D indicates that it is a delamination gage. The first number is the number of the nearest stirrup and the second number refers to the duct number immediately below the wire.

5.3.4 Web-Web Potentiometers

As discussed in Section 3.4, the curve length was kept to a minimum because of the complexity of construction. Smaller than anticipated web-slab deflections in test 1.0DC raised concerns that perhaps the curve was too short. It was possible that rather than the entire load being carried vertically through web flexure, a significant portion of the load was being carried transversely through longitudinal web flexure to the PC and PT boundary elements. In other words the model web may have been unintentionally acting as a two-way slab as opposed to a one-way slab.

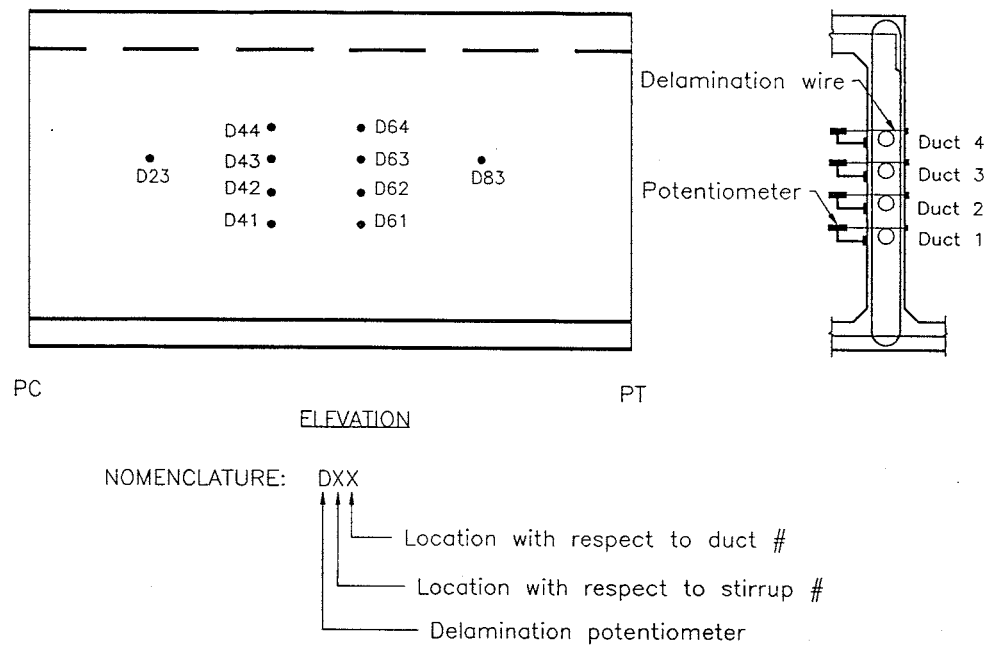


Figure 5.16 Delamination Gage Nomenclature.

To monitor the longitudinal behavior, mid-height deflections relative to the web boundary elements were measured for the second test, specimen BC. A U-shaped frame similar to those used for web-slab deflections was attached to the mid-height of the web at the PC and PT [Figure 5.17]. This frame was also attached to the outside of the curve to eliminate the effects of local beam deflections and prevent destruction of equipment. Potentiometers were placed at approximately the one-quarter points of the curve.

The web-web potentiometer nomenclature is given in Figure 5.18. The letters "WW" indicate that the web deflections are relative to the web at the boundary elements. The number following is the number of the nearest stirrup.

After examining the results from BC, it was considered unnecessary to use this apparatus for further tests. The reduction in use of all types of instrumentation for later tests can be seen in Figures 5.19 & 5.20.

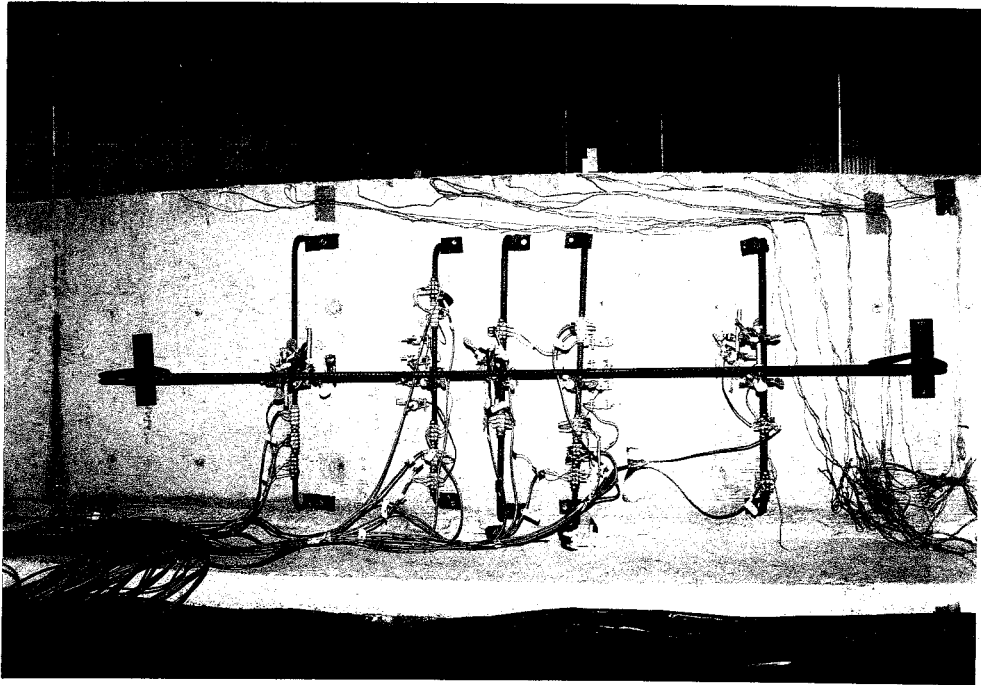
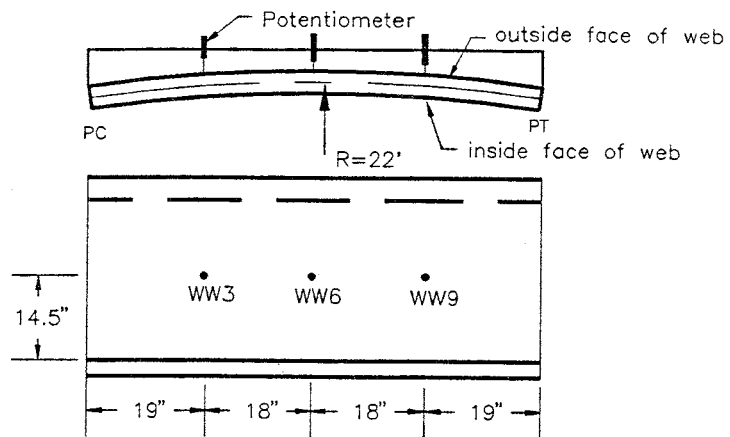


Figure 5.17 Web-Web Potentiometers.



NOMENCLATURE: WW# .

- ↑↑
- ↑ Stirrup closest to potentiometer
- ↑ Web deflection in curve with respect to web at PC & PT

Figure 5.18 Web-Web Potentiometer Nomenclature.

5.3.5 Demec Gages

Another theory for the small web-slab deflections from test 1.0DC was that the distribution of axial forces in the cross-section were preventing larger deflections. A non-uniform distribution of axial force in the cross-section could have resulted in greater compression arch forces in the loaded web and reduced deflections.

Measuring longitudinal strains in the cross-section would provide information on the axial force distribution. Five sets of demec points were glued at the midpoint of the curve (outside face) for specimen BC. One set was attached at each corner of the cross-section, and one at the c.g. of the tendon group of the loaded web. At each load stage, a mechanical gage was used to measure the change in distance between the points that were originally positioned 8.2" apart. Only the 22' radius web could be measured in this manner for reasons of safety. This web provided easy access to the outside face of the curve.

5.4 LOADING PROCEDURE

5.4.1 Friction Test

Prior to testing the first specimen, friction tests were conducted to determine the strand forces at the midpoint of the curve. The pressure transducer described in Section 5.2.3 measures the total strand force between the live end load beam and the girder. However the force critical to understanding lateral breakout is that which is in the curve. Friction tests would allow the force in the curve to be expressed as a percentage of the live end force.

A 25 kip capacity load cell was placed against the anchorage plate on each end of the girder. A single strand was threaded through a duct and the load cells and anchored by a screw-chuck on the dead end. A monostrand

ram bore directly on the load cell on the live end and was used to stress the strand. The load cells directly measured the tensile force in the strand at the live and dead ends.

Each load cell was connected to a strain indicator box and calibrated in a 60 kip Southwark-Emery testing machine so that during the friction tests the force could be read directly from the box. To further check the accuracy of the friction test method, both load cells were placed in line on the dead end of the specimen. Three levels of load (500, 1000 and 1500 lbs.) were applied. The results from the load cells matched one another to within 10 lbs. for all three tests.

Friction tests were run on three ducts: the top duct in specimens BC and 1.0DC and the second duct from the top in specimen BC. Measurements were taken at three load levels for each specimen (500, 1000, and 1500 lbs.). Low load levels were used to ensure that the specimens did not crack prior to the actual tests of the specimens. The strand was not seated at any time during the friction test.

The results of the friction tests are shown in Table 5.3. The live and dead end forces are recorded. The calculated force at the midpoint of the curve is simply the average of the live and dead end forces since the duct layout is symmetrical. The midpoint friction loss is the percent change in strand force between the midpoint of the curve and the live end.

The results show that friction losses were small and were not greatly dependent on web radius or duct positioning. At the 1500 lb. level, friction losses ranged from 1.9% to 2.5%. A friction loss value of 2% was assumed for all test specimens.

Table 5.3 Friction Loss Test Results.

STRAND FRICTION LOSS TO MIDPOINT OF CURVE				
DUCT	P_{live} (lbs.)	P_{dead} (lbs.)	P_{midpoint} (lbs.)	FRICTION LOSS AT MIDPOINT (%)
1.0DC (top)	510	476	493	3.3
	1000	962	981	1.9
	1520	1462	1491	1.9
BC (top)	500	460	480	4.0
	1000	945	972	2.8
	1500	1425	1462	2.5
BC (2nd from top)	502	470	486	3.2
	1002	948	975	2.7
	1500	1428	1464	2.4

5.4.2 Load System Alignment

Steel channels were cantilevered off the girder at the live and dead ends of the girder [Figure 5.2]. The load beams, bearing plates and top ram were suspended from the channels. The bottom ram was temporarily supported by a hand-operated forklift until there was enough load in the ram so that it was self-supporting.

The rams, load beam and bearing plates were positioned so that they were all aligned with the centerline of the web being stressed. The rams were positioned vertically so that the thrust was delivered to the centerline of the double-spiral arrangement located at the top and bottom of the webs. This resulted in approximately 1" of clearance between the rams and the nearest

ducts [Figure 5.6]. The rams were then leveled with a magnetic carpenter's level. The dead end load beam was positioned in a manner similar to the live end load beam; the beam was set at a height so that the centerline of each chair was aligned with the centerline of the double spirals.

5.4.3 Monostrand Stressing

It was necessary to stress and power seat each strand individually before the load beam was pushed by the 100 ton rams [Figure 5.21]. The alternative, allowing the strands to self-seat as the beam was moved, would



Figure 5.21 Monostrand Stressing.

have resulted in large variations in stresses between the individual strands.

The most desirable level of stress in the strands to be achieved through individual stressing was considered to be the smallest one that ensured seating of the wedges. Large monostrand stressing forces might possibly have cracked

the specimen before all of the strands were stressed. Preliminary tests were conducted on a strand threaded through a reaction wall in the laboratory. Using a 25 kip capacity load cell calibrated as described in Section 5.4.1, it was found that consistent seating could be achieved by stressing each strand to a load of 2 kips. This corresponded to a pressure of 500 psi in the pump-ram system. Three tests conducted at this load level showed that seating losses consistently reduced the force in the strand to 1 kip.

When the strands were progressively stressed and seated against the live end load beam, previously seated strands lost some of their stress. This became apparent by simply feeling the strands in the flaring region of the live end. This was not entirely unexpected as axial shortening of the girder (and load system) is a widely recognized phenomenon. Strands that displaced easily when pushed laterally in the flaring region were restressed until uniform deformation was achieved in all 12 strands. During the monostrand stressing of strands in the subsequent three tests, the first strand was stressed to a gauge pressure of 800 psi and each succeeding strand was stressed to a level 25 psi less than the previous strand. This reduced the number of strands requiring restressing.

5.4.4 Loading Procedure

The pistons in the 100 ton rams were extended approximately 1" from their unloaded position prior to the monostrand stressing operation. This allowed the pistons to be retracted after the monostrand operation to unload the girder. Unloading the strands via contraction of the rams did not cause the wedges to lose their grip. This process allowed the instrumentation zero readings to be taken after, rather than before, the monostrand stressing operation. The only advantage to this is that it allowed individual strand stressing to commence prior to completion of final instrumentation checks.

From a CPM point of view, the lengthy monostrand stressing and instrumentation checking tasks could be done in parallel by two teams rather than in series thereby reducing the length of the critical path.

The girders were then loaded in stages so that readings could be taken at the conclusion of each load increment. The value of the tendon force at each load stage was measured by utilizing the switch and balance system described in Section 5.2.2. Initial load increments of approximately 20 kips were applied to the strands. This resulted in a lateral prestress increment of about 1 k/ft. A dial gauge was mounted against the web to measure deflections [Figure 5.11 & 5.19]. A load-deflection plot was maintained throughout the test. When the curve began to flatten (i.e. deflections were getting much larger under constant load increments), the load increments were halved. Stressing continued until the load in the strands dropped off as a result of web explosion or excessive deformation.

There were two unloadings during the course of the test of the first specimen, 1.0DC. The first was a result of the live end load beam failure discussed in Section 5.1.2. The test was stopped and the beam was removed, straightened in the 600 kip loading machine and stiffened with plates. Four days later, the test was restarted. Load increments of approximately 40 kips were used to reach the failure load of the load beam (186 kips). The test was stopped again later that day when it was noticed that the bottom of the load beam was digging into the oversized, bottom slab soffit which extended from underneath the girder. There was concern that a secondary load path was developing and the rams were retracted from a load of 280 kips to 90 kips. This retraction permitted the soffit to be chiseled away and allowed the load beam to clear. The test was resumed the next day. As before, the reloading

was done in approximately 40 kip increments until the previous load of 280 kips was reached.

The test of the second specimen, BC, was also stopped because of interference from the bottom soffit. The soffit was chiseled prior to the start of the test, but it was not done deeply enough to prevent snagging of the load beam. The load was reduced from 130 kips to 60 kips to allow room for further chiseling. The test was resumed that same day. The 130 kip load was re-established in a single load increment.

A grid was drawn on the inside face of all the webs in the curve before loading began [Figure 5.22]. Four horizontal lines were drawn to represent the centerlines of the individual ducts. Vertical lines were drawn to locate the stirrups. This allowed cracks to be located with respect to these important



Figure 5.22 Grid Identifying Stirrups and Duct Centerlines.

elements. A theodolite was used to allow inspection of the cracks from a safe distance.

CHAPTER 6: TEST RESULTS

This discussion of test results is divided into two parts. The first section is a report of the visual observations for each individual test. The remaining sections examine the instrumentation results for all tests. The results for the four specimens are discussed jointly for each type of instrumentation.

The lateral prestress force referred to in all discussions is the lateral force from the strands that was present at the midpoint of the curve. Friction tests revealed a 2% loss between the live end and the midpoint of the curve. For every load level, the hydraulic pressure measured by the pressure transducer was multiplied in the HPDAS data reduction program by the ram area to calculate a live end prestress force. This force was then multiplied by 0.98 and divided by the web radius (18' or 22'). The resulting lateral force per foot of arc is referred to as F_r .

Specimens 1.0DC and BC were both unloaded and reloaded before failure during testing due to equipment problems. The unloadings occurred at load levels which were before serious distress in the specimens and do not appear to have significantly effected the results. For clarity, the unloading and reloading data have been omitted in this chapter. The instrumentation readings for the second loading of specimen 1.0DC did not exactly coincide with those of the first. To smooth the transition, the last load stage prior to

buckling of the load beam ($F_r=7.94$ k/ft) has been omitted as have the reloadings up to $F_r=10.3$ k/ft. Load levels for the second loading resume with $F_r=10.7$ k/ft and continue until $F_r=13.6$ k/ft. Results continue with the third loading at a load of $F_r=14.3$ k/ft. BC was unloaded only once. The first loading ended with $F_r=5.81$ k/ft and all of those results are presented. The graphs resume with a second loading level of $F_r=6.82$ k/ft.

Complete presentations of relevant graphs in this chapter including all loading and unloading readings for specimens 1.0DC and BC are presented in the Appendix.

6.1 VISUAL OBSERVATIONS

The ultimate capacities and first visible cracking load levels for all tests are summarized in Figure 6.1.

6.1.1 Specimen 1.0DC

Specimen 1.0DC had ducts spaced at 1.75" (clear) and located in the center of the web. It was the first detail tested. A theodolite was first utilized for crack detection at a load of $F_r=10.1$ k/ft. A single, thin flexural crack was detected at duct #2 [Figure 6.2]. The crack began a few inches before the PC and extended the same distance past the PT. The crack would have probably been visible had a theodolite been used prior to this load level judging from the behavior of the other tests. Crack inspection was started much earlier on the other specimens. This type of crack was typical of all specimens. In those tests, when the first longitudinal crack appeared, it was only about 1 foot long and located near the midpoint of the curve. It took two or three more load stages for it to extend along the entire curve.

The loading beam failed during the load stage immediately following the detection of the crack. During the second loading four days later, a

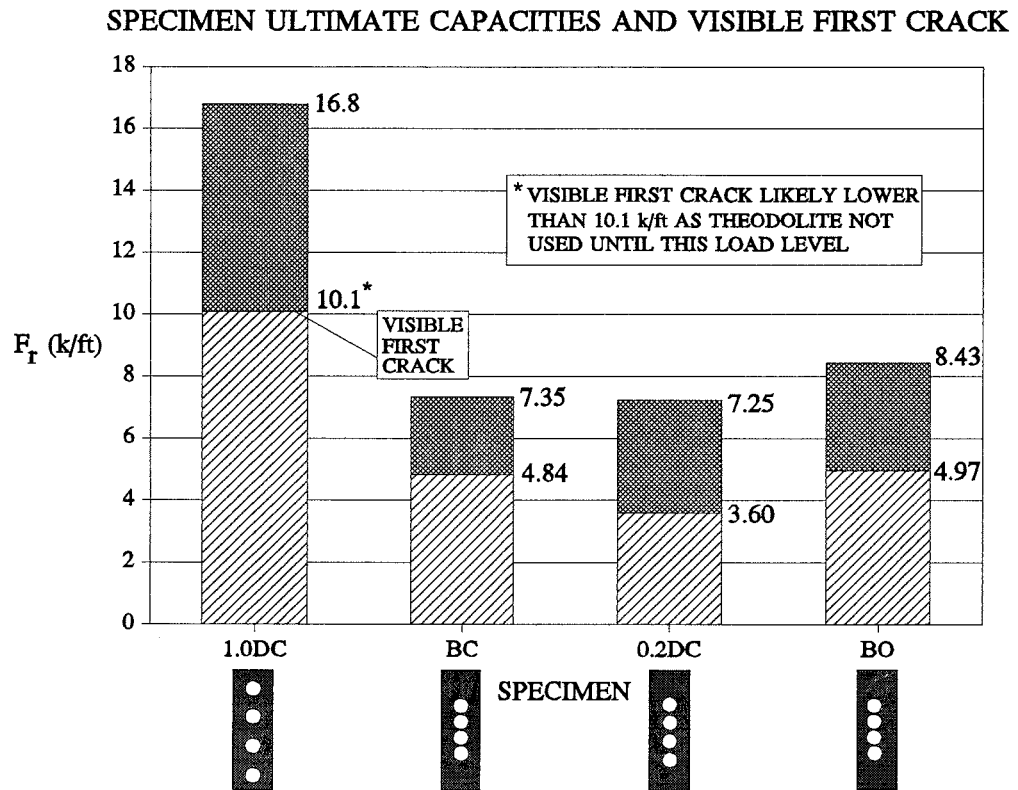


Figure 6.1 Specimen Ultimate Capacities and Visible First Crack.

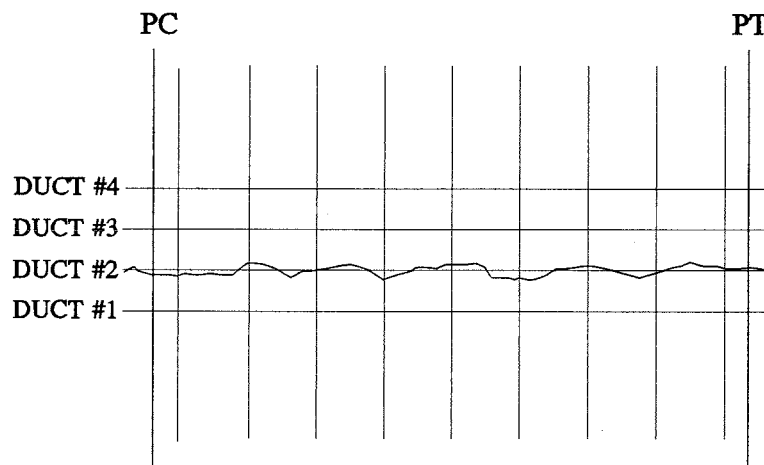


Figure 6.2 Typical First Crack (Flexural) for All Specimens.

second longitudinal crack appeared at duct #3 at a load of $F_r=10.3$ k/ft. Similar longitudinal cracks developed at ducts #1 and #4 at a load of $F_r=12.7$ k/ft.

During the third loading, the web exploded suddenly and without warning [Figure 6.3]. The load had been locked off at $F_r=16.8$ k/ft for about five minutes and readings were being taken when a terrific noise was heard. Concrete fragments flew and landed as far away as 50 feet [Figure 6.4]. The ducts and tendons broke free of the web and formed a chord that extended nearly the whole length of the specimen [Figure 6.5].

Two large panels of concrete that extended from the bottom duct to the top duct remained intact after the explosion [Figure 6.6]. Presumably, they were a single panel when the breakout began but were separated by a crushing failure when snap-through occurred. The panel is thought to have behaved as a longitudinal compression member with a lateral load causing it to buckle. The separation of a single panel into two is not an important observation as failure had already been initiated. Figure 6.6 shows the backside of the panel after it was cut loose and laid on the ground.

The panel had a top-forward tilt [Figure 6.7 & 6.8]. The stirrups pulled free at the lap located at the top, inside face of the web. The stirrups remained well anchored at the bottom of the web. Judging from the pictures, it appears that the tilt may have been the result of the lap pulling free. However the top duct was pulled out further than the bottom duct prior to pullout as delamination gage readings in Section 6.2.2.1 reveal.

The panel was removed by simply cutting the stirrups near the bottom flange so the web could be examined. A void was created in the web where the ducts and surrounding concrete once existed [Figure 6.9]. The hole in the back face of the web in this photograph was made after the test to measure

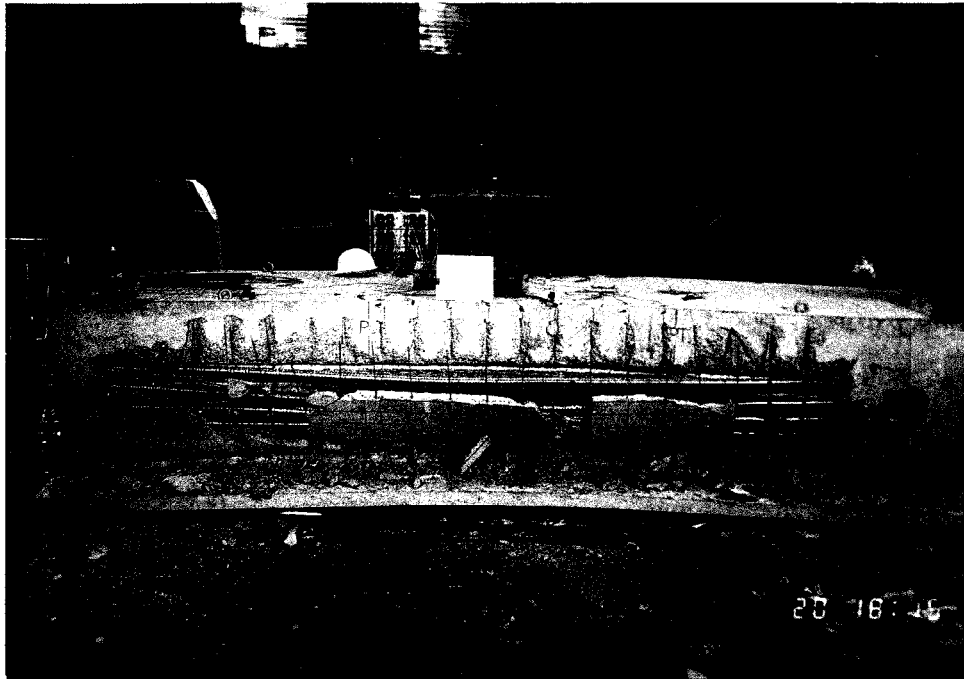


Figure 6.3 1.0DC Elevation View of Failure.

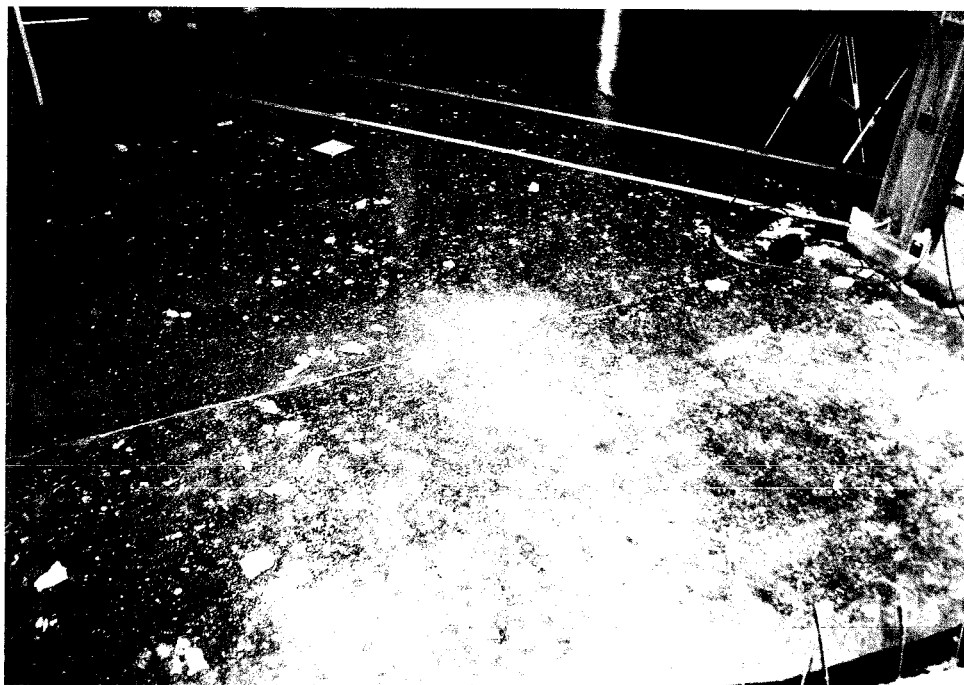


Figure 6.4 1.0DC Concrete Fragments.

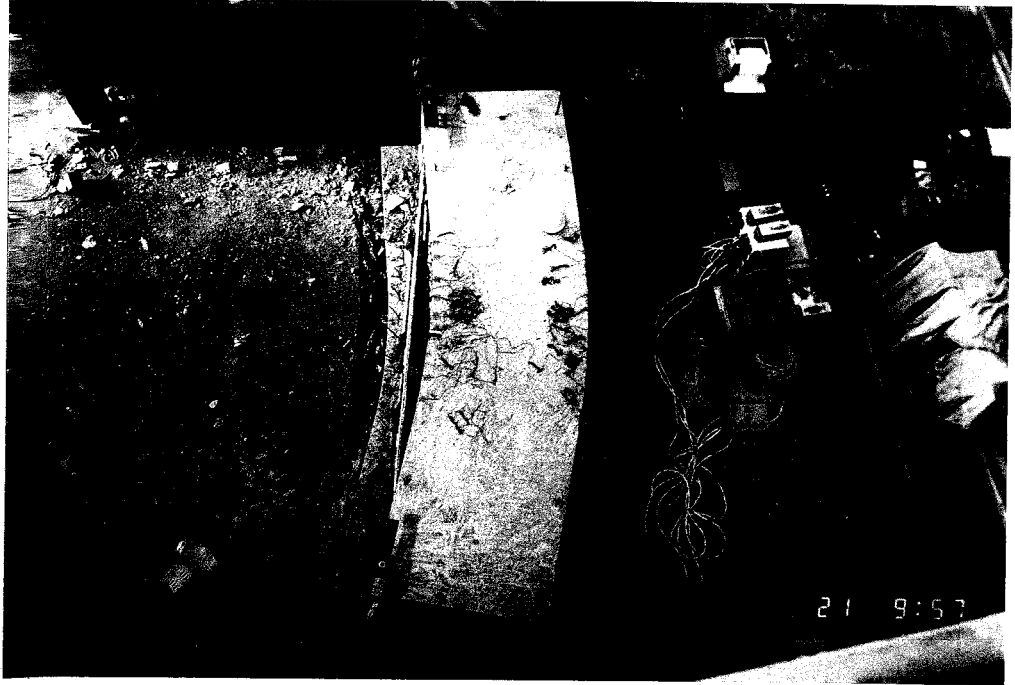


Figure 6.5 1.0DC Plan View of Failure.

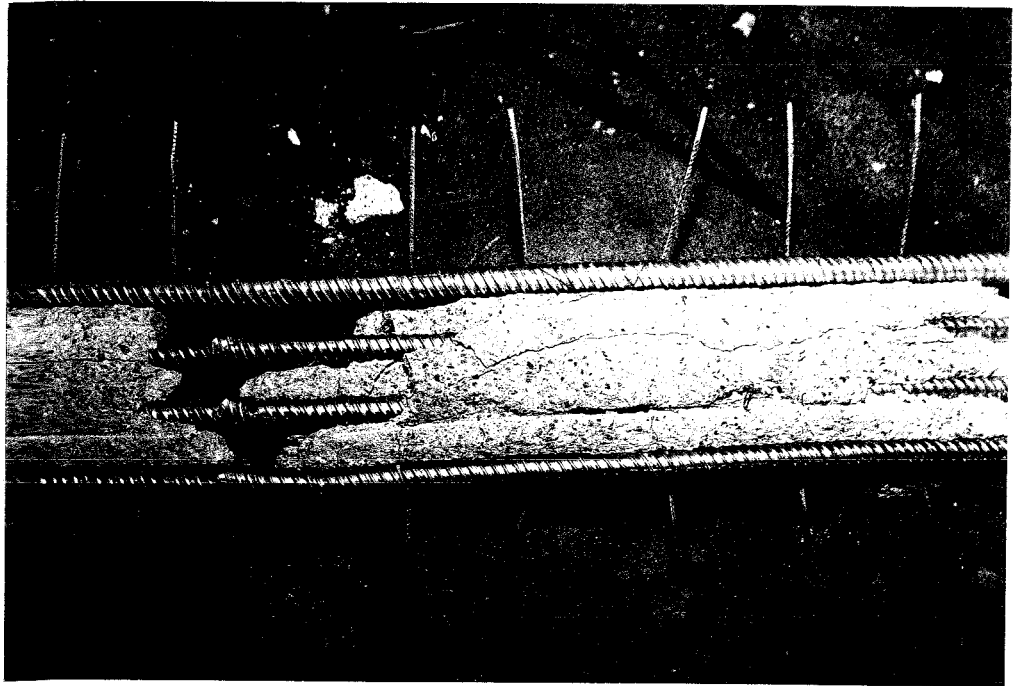


Figure 6.6 1.0DC View of Interior Surface of Concrete Panel.



Figure 6.9 1.0DC Failure Plane After Removing Concrete Panel.

the concrete thickness. The void began between $1\frac{1}{2}$ and 2 inches above the top of the top duct on the inside face of the web [Figure 6.10]. The crack progressed downward and inward at about a 45 degree angle until intercepted by the top duct. The crack continued on the backside of the duct at a steeper angle until it was within approximately $\frac{1}{4}$ " of the outside face of the web at the elevation of duct #3. The crack proceeded down the back face of the web and out through the bottom duct such that it became nearly symmetrical about the horizontal axis of the tendon group. The diagonal crack near the bottom duct was slightly steeper than the top diagonal crack. It ended on the inside face between 2 and 4 inches from the bottom of the bottom duct. The pullout of the inside leg of the stirrups caused the cracks to end further away from the tendon group at regular intervals so that the crack was not horizontal at the web face [Figure 6.8]. In describing the location of cracks on the inside face of the web for all specimens, the level of the crack between stirrups is

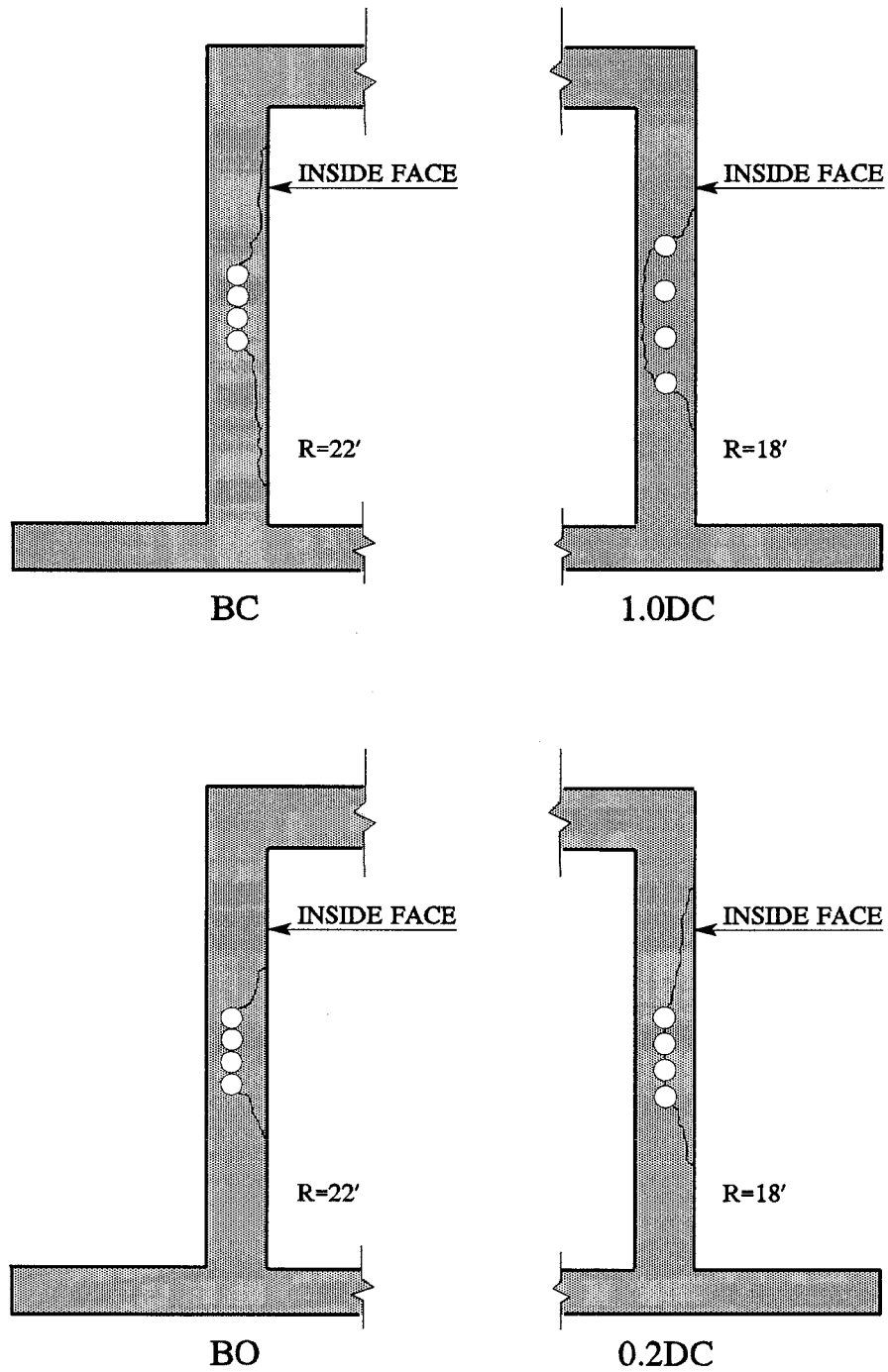


Figure 6.10 Specimen Failure Planes.

assumed as this is where first cracking occurs. Only with excessive delamination did the stirrups peel the concrete far away from the duct group.

The shape of the void and the location of the inclined cracking suggest a type of shear failure. The curving, diagonal cracks that emanated from the inside face of the web at about 45 degrees and turned and became parallel to the compression face of the bending member are indicative of diagonal tension cracks in high flexural regions [17]. Usually this appears as a single S-shaped crack. However the shear reversal combined with voids created by the ducts caused the failure plane to take the shape of two opposing S-shaped cracks. The diagonal cracks occurred at the top and bottom of the duct group. This was a region of maximum shear [Figure 6.11]. Actually,

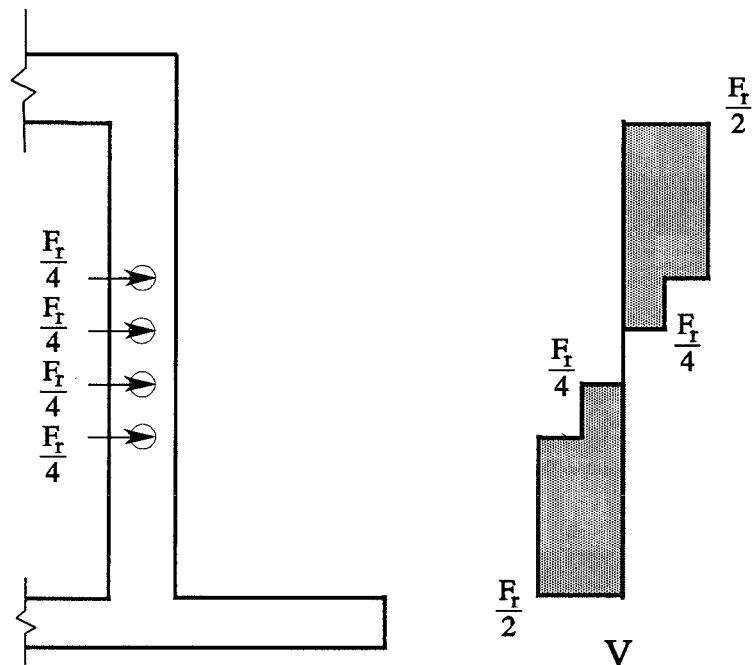


Figure 6.11 Shear Diagram for Specimen 1.0DC.

anywhere on the web outside of the duct group was the maximum shear region but this was the weakest of the high shear regions because of the voids created by the ducts.

Two small cracks were noticed upon inspection of the interior of the box [Figure 6.12]. One crack ran along the top slab near the fillet and the other along the bottom slab. These would seem to indicate that flexural tension in the negative moment areas created by regional beam action caused these cracks. Readings from a strain gage placed near the top slab on the outside leg of stirrup #4 confirm that tension existed in this region. These results are discussed in Section 6.3.3.

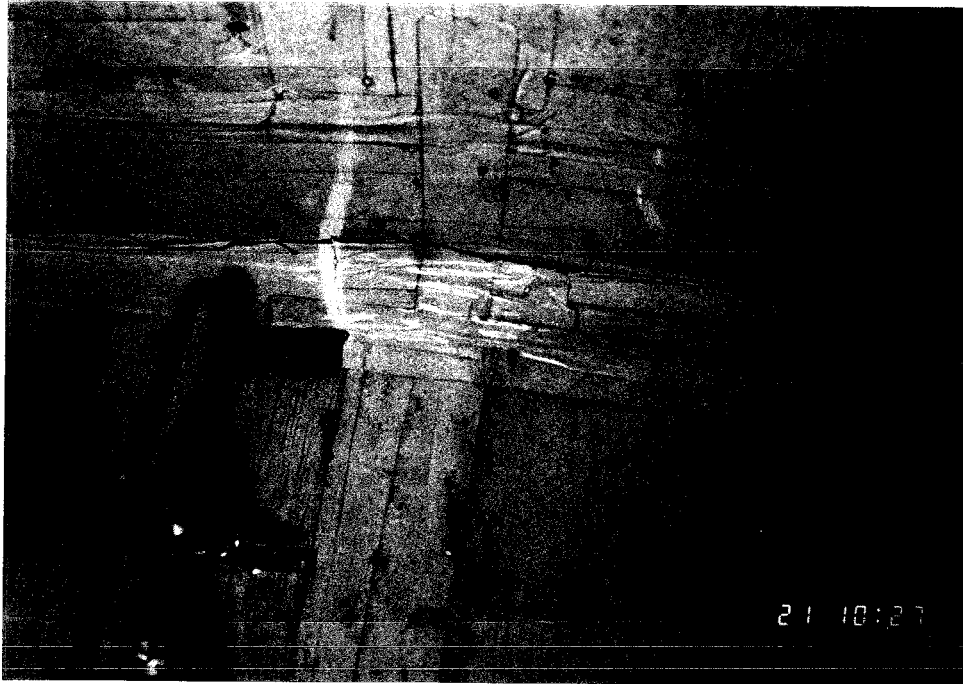


Figure 6.12 1.0DC Top Slab Crack (Enhanced with a Felt-Tip Marker).

6.1.2 Specimen BC

The next test was of specimen BC. The ducts in this specimen were bundled and centered in the web. It was monitored closely for signs of cracking from the beginning of loading using a theodolite positioned at a safe

distance. A longitudinal, flexural crack similar to that observed in specimen 1.0DC first appeared at duct #2 at a load of $F_r=4.84$ k/ft [Figure 6.2]. When the load reached $F_r=5.81$ k/ft, it was noticed that the live end load beam was contacting the plywood soffit. The load was temporarily reduced to $F_r=2.74$ k/ft while the interference was removed. It was then reloaded to $F_r=5.84$ k/ft and regular loading resumed. At a load of $F_r=7.35$, two severe longitudinal cracks occurred [Figure 6.13]. The larger of the two cracks was above the tendon group and had a very erratic path. It varied between 5" and 10" away from the top of the top duct. The second crack had a similar appearance and was located between 5" and 10" below the bottom of the bottom duct. The cracks were the edges of a large panel of concrete that was delaminating from the web.

The lateral prestress force dropped to 6.58 k/ft as a result of the cracking. Apparently, the cracking allowed the tendon path to become slightly shorter and caused the tendons to shed load. Further stressing stages only exacerbated the delamination of the panel and the load remained nearly constant at around $F_r=6.5$ k/ft [Figures 6.14 & 6.15]. At the final load stage ($F_r=6.48$ k/ft), slow crushing of the panel occurred near stirrup #3 due to high snap-through compression forces [Figure 6.16]. The rams were retracted at this stage and the lateral prestress force returned to zero.

Figure 6.17 was taken after loading was completed and shows the flexural cracking in the concrete cover over the ducts. The front panel was removed using a chipping hammer. An acetylene torch was used to cut the rebar and ducts to reveal the back face [Figures 6.18 & 6.19]. As the imprint on the back face reveals, the ducts remained well-bundled during casting. A single, thin vertical crack that is not visible in the photos ran down the depth

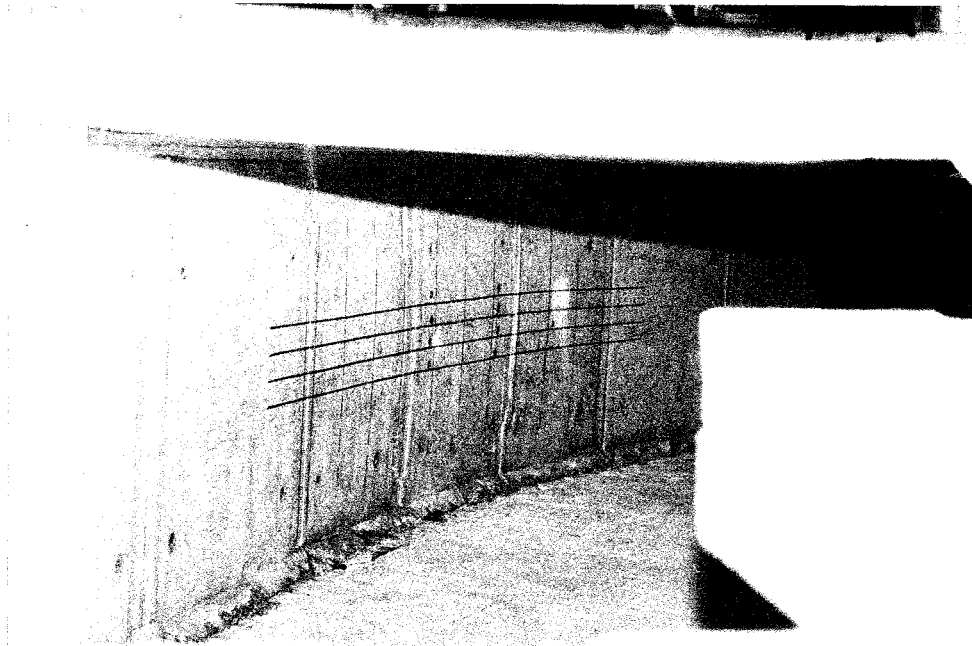


Figure 6.13 BC at Ultimate (Shear Cracks Barely Visible in Shadow).

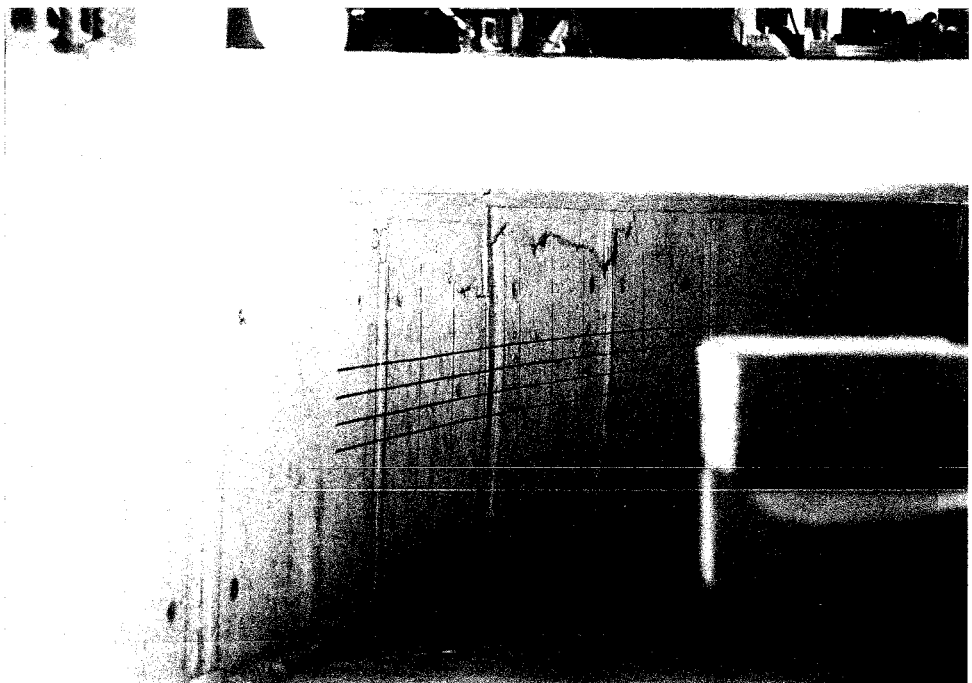


Figure 6.14 BC Cracking at One Stage After Ultimate.

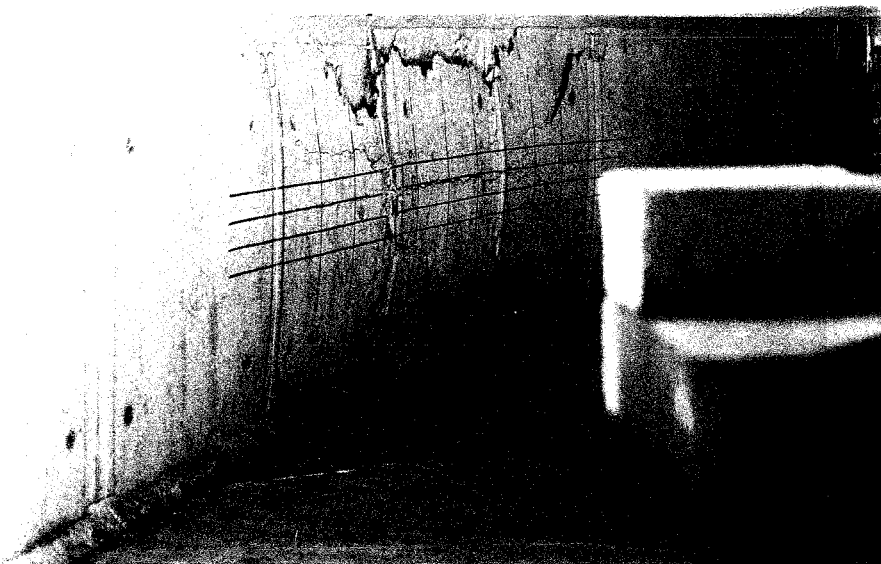


Figure 6.15 BC at Two Load Stages After Ultimate.



Figure 6.16 BC at Snap-Through.



Figure 6.17 BC Flexural Cracking After Completion of Test.

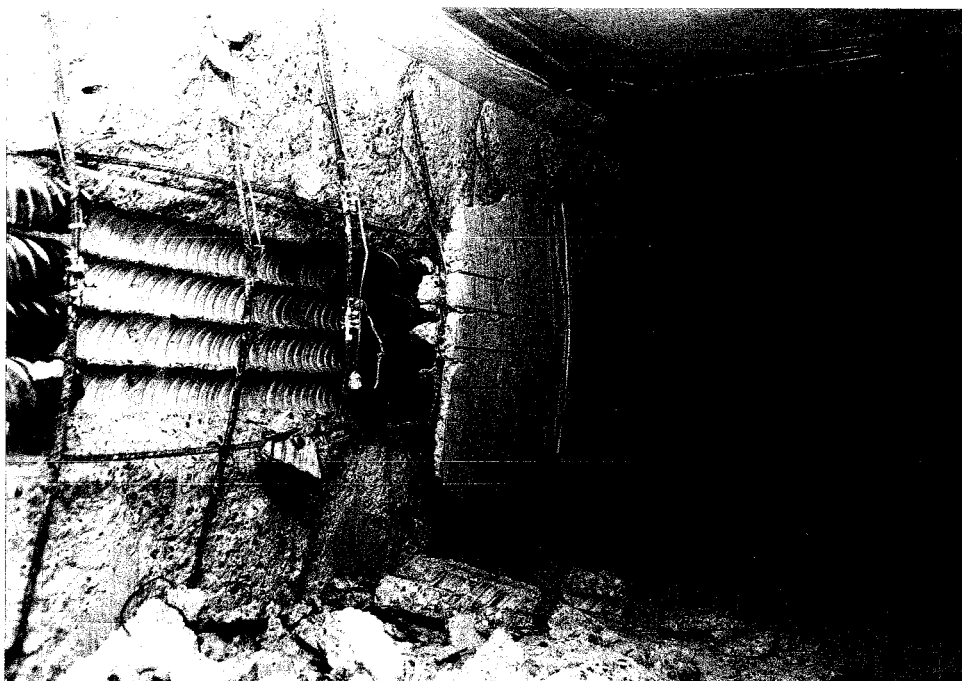


Figure 6.18 BC After Removing Concrete Panel.

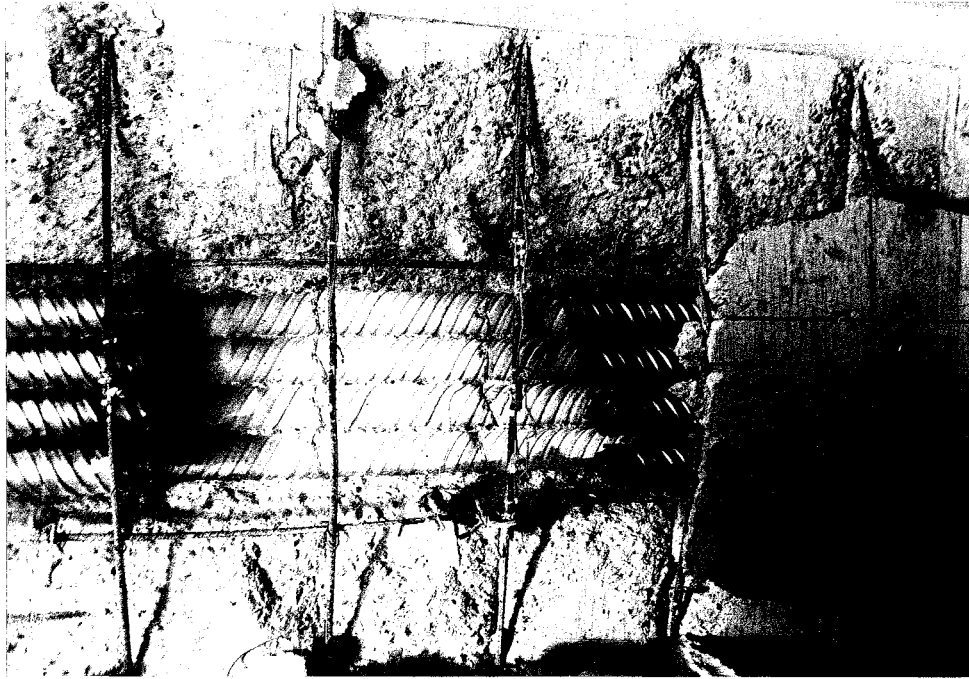


Figure 6.19 BC View of Surface Behind Ducts.

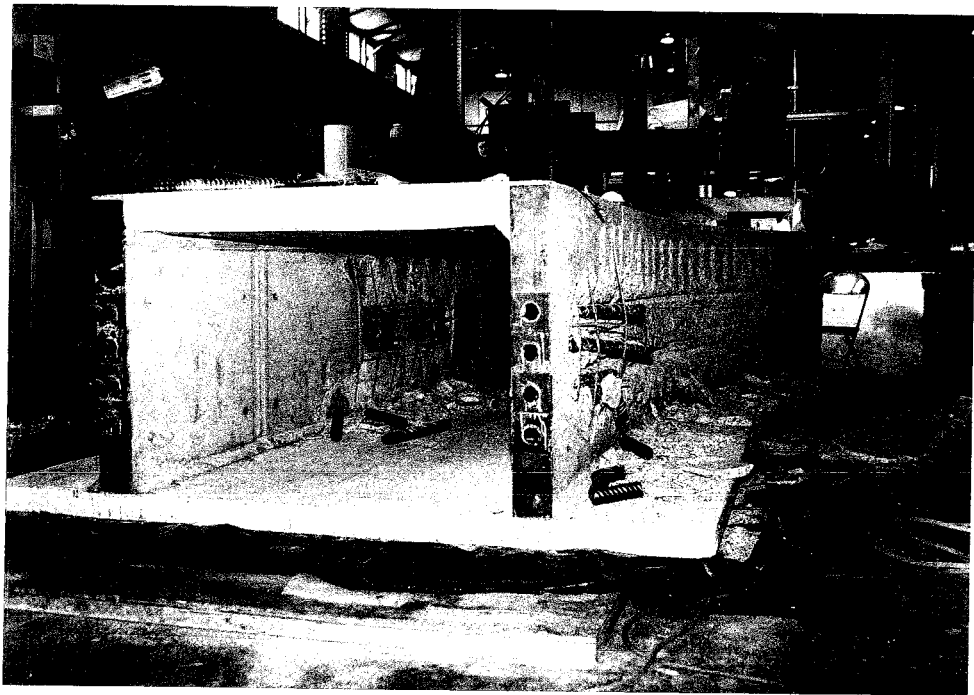


Figure 6.20 Overview of 1.0DC and BC.

of the tendon group between stirrups #3 and #4. This may have been caused by longitudinal bending of the web as it spanned from PC to PT.

The diagonal cracks between the inside face and the top and bottom ducts were similar to, but steeper than, those in 1.0DC [Figure 6.10]. The failure plane did not extend to near the back face as in 1.0DC because of the vertical void presented by the bundled ducts. The stirrups remained anchored at the top and bottom of the web. This was likely due to the fact that the failure load was less than half of that of specimen 1.0DC.

Figure 6.20 shows an overview of girder #1 prior to its removal and the commencement of construction of girder #2.

6.1.3 Specimen 0.2DC

Specimen 0.2DC had ducts spaced at 0.33" (clear) and centered in the web. It was the first web tested in girder #2. This specimen had been patched above the top duct as described in Sections 4.2.6 and 4.2.7. The overall behavior was very similar to specimen BC.

At a load of $F_r=3.60$ k/ft, a longitudinal flexural crack was noticed at duct #2 [Figure 6.2]. No further cracking was noticed until a load of $F_r=7.25$ k/ft when longitudinal cracks appeared above and below the duct group [Figure 6.21]. Their location and shape were similar to those of specimen BC. The top crack was slightly lower than the BC top crack and even dipped down to the level of the patch near stirrups #3 and #4. Further stressing increased the delamination without increasing the load [Figure 6.22]. On the third reapplication of load after the emergence of the panel, the load increased to 7.48 k/ft. However the web was heavily cracked and the capacity was probably enhanced by the longitudinal arching of the panel prior to snap-through. The load decreased to $F_r=6.90$ k/ft after snap-through at stirrup #4 [Figures 6.23 & 6.24]. The ultimate load carrying capacity of the web is

considered to be 7.25 k/ft as the later, higher load was an aberration due to a temporary load path achieved after the web was heavily damaged. The rams were retracted and the test was concluded after no more increase in load carrying capacity was achieved. An overhead photo of the breakout indicates that the failure was not explosive like that of 1.0DC [Figure 6.25].

Removal of the panel revealed that the duct spacing remained intact during casting [Figure 6.26]. The vertical cracking through the thin (0.33") concrete layers between ducts occurred at the vertical centerline of the ducts.

The top diagonal tension failure plane emerged on the front face between 2" and 10" above the top of the top duct. About 8" of the 21" long patch/concrete interface coincided with the failure plane allowing the crack to surface 2" above the top duct. Two dark epoxy patches can be seen on the diagonal failure plane at the top left of Figure 6.26. The failure plane was behind the remaining 13" of the patch length [Figure 6.27]. Two thin cracks above the top duct indicate the top and bottom borders of the patch [Figure 6.28]. The patch was not as large as the discoloration seen in other photos. These were merely stains made by the troweling motion necessary to put the grout in. The bottom diagonal crack was shallower than the BC bottom crack [Figure 6.10]. It was uniformly 5" below the bottom of the bottom duct. Figure 6.27 shows a slight bowing and top-forward tilt of the duct group. No vertical cracking was detected on the back face behind the removed panel.

The patch appears to have affected the behavior of this specimen very little. The failure plane bypassed about two-thirds of the patch. As discussed later in the results of the delamination gages, the 0.33" concrete layers were proven ineffective at load stages before the diagonal tension failure planes developed. Therefore the ultimate load capacity should and does nearly equal that of specimen BC (7.25 k/ft vs. 7.35 k/ft).

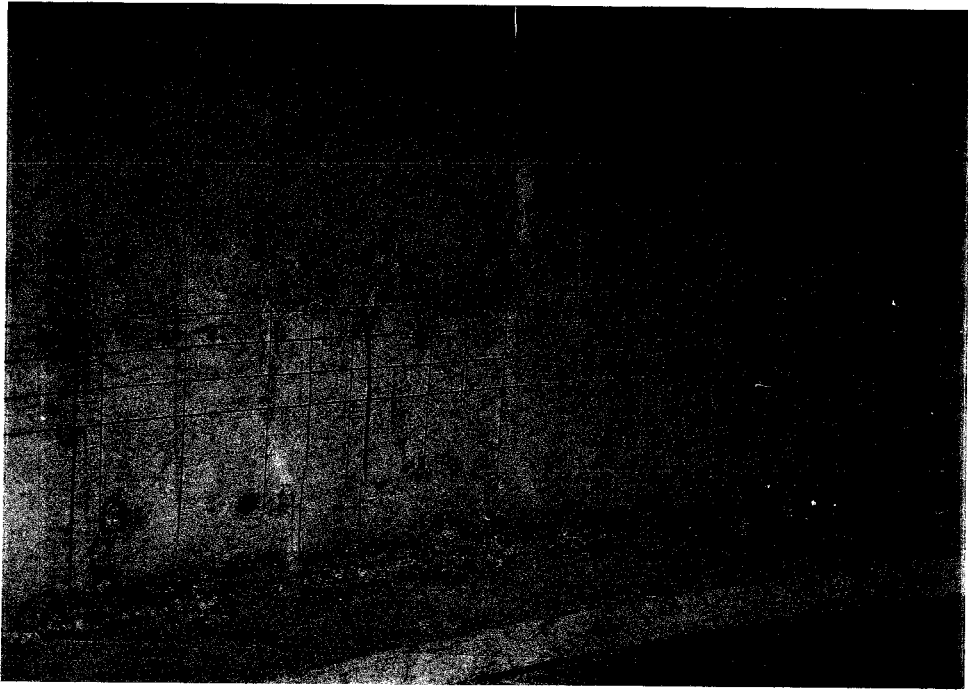


Figure 6.21 0.2DC Start of Visible Delamination Cracks at Ultimate.

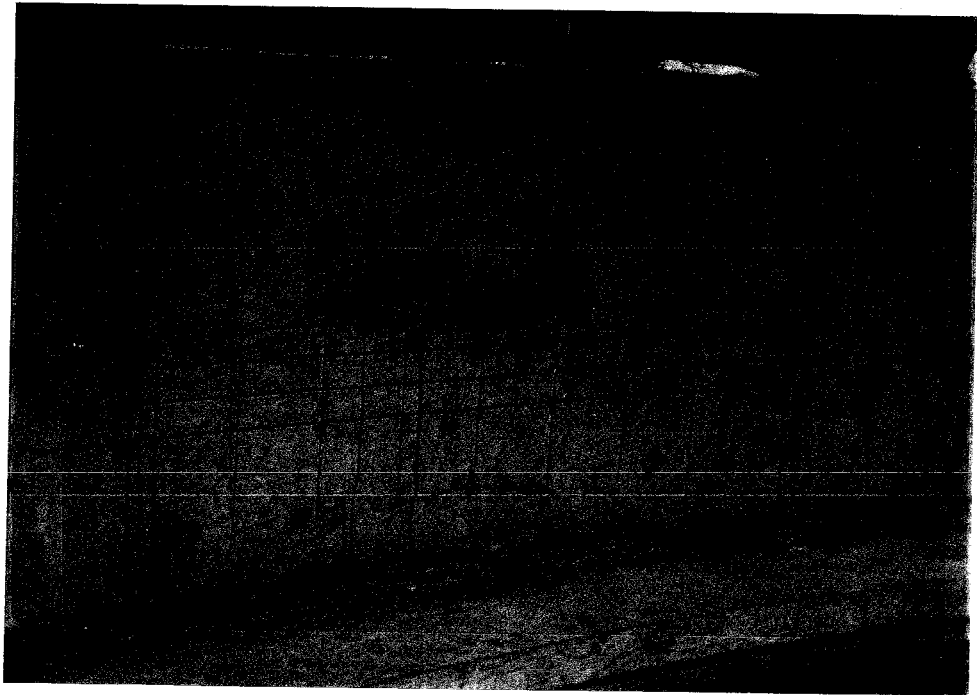


Figure 6.22 0.2DC at Load Stage after Ultimate.

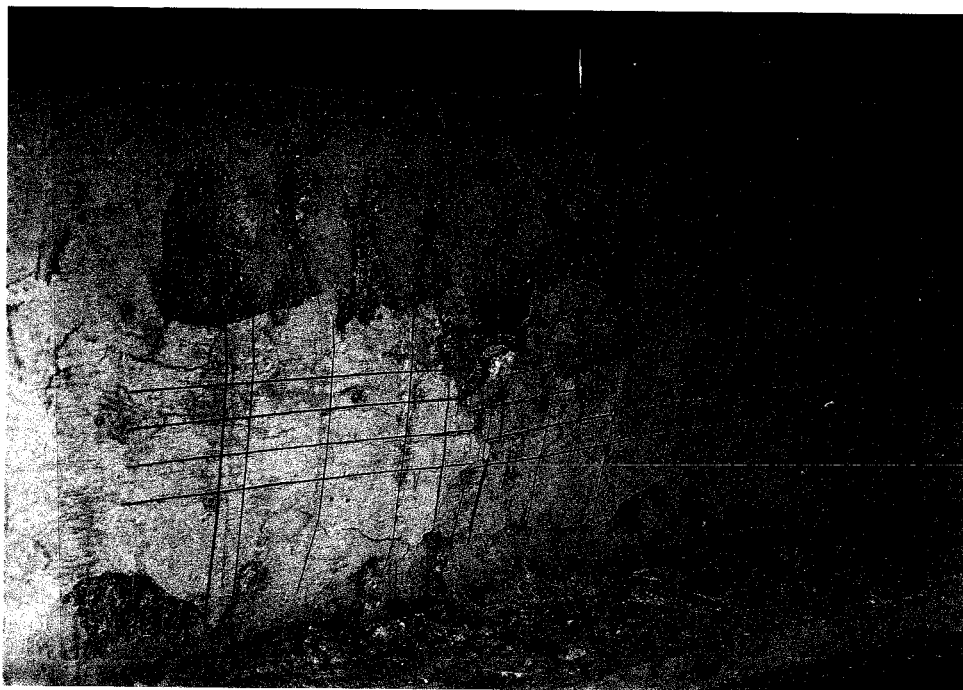


Figure 6.23 0.2DC at Snap-Through.

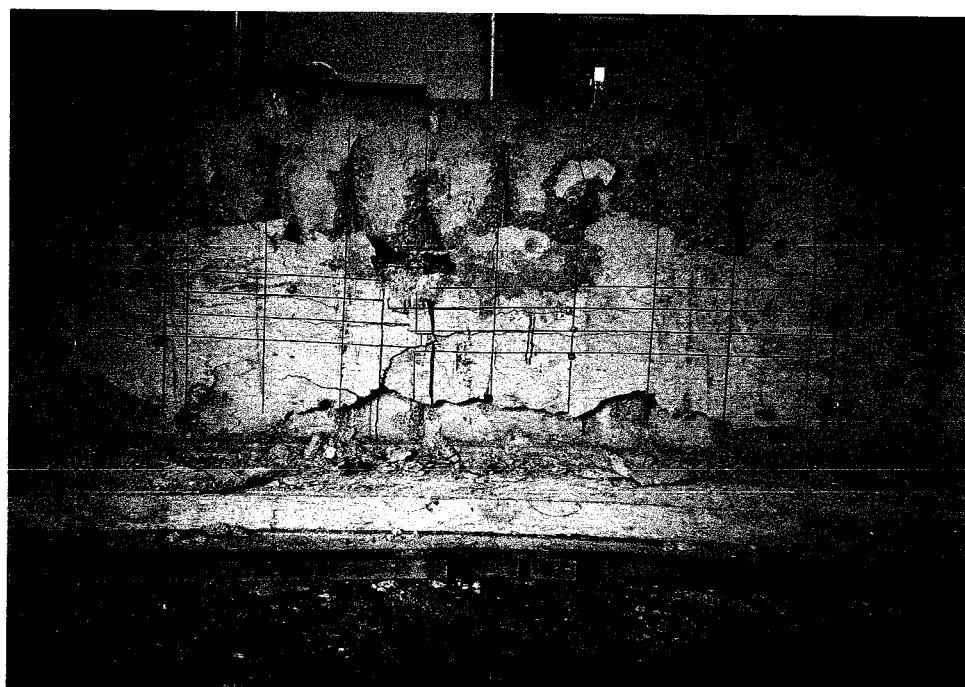


Figure 6.24 0.2DC Elevation View of Failure.

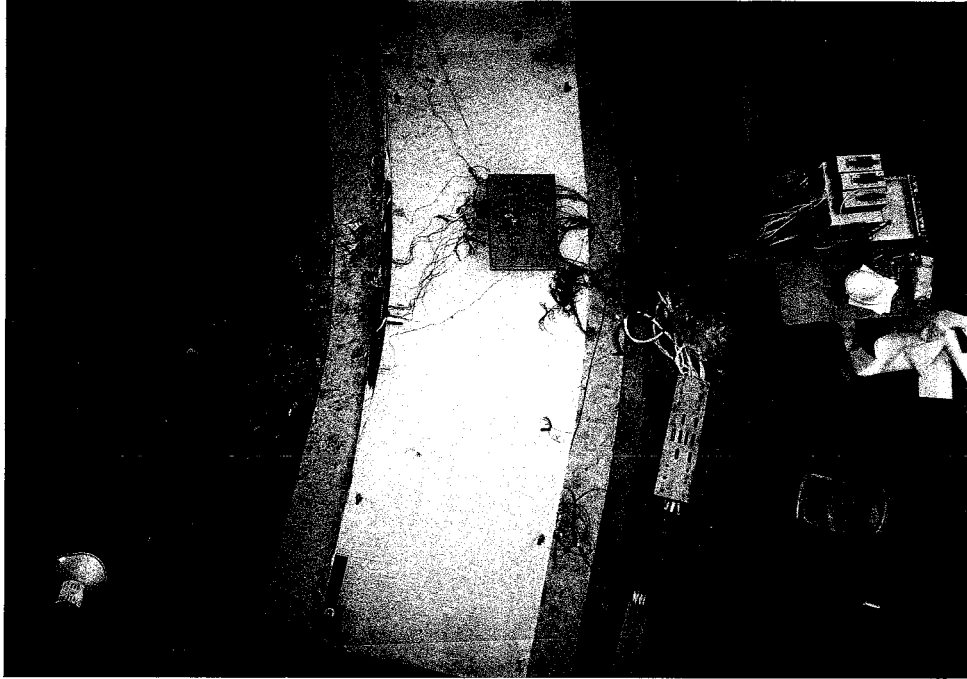


Figure 6.25 0.2DC Plan View of Failure.



Figure 6.26 0.2DC View of Surface Behind Ducts.

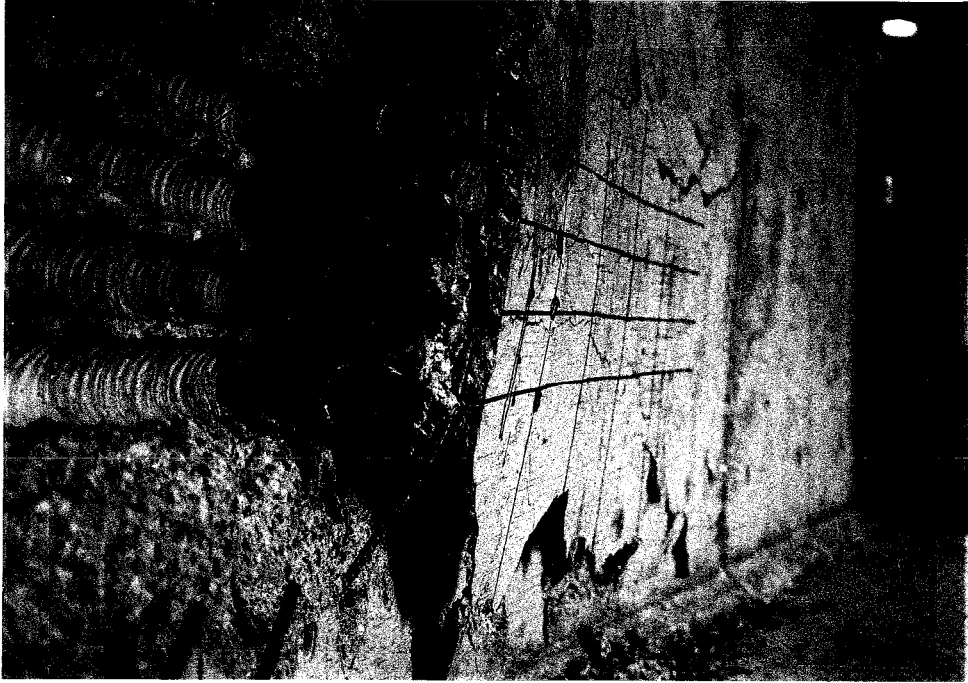


Figure 6.27 0.2DC After Removing Concrete Panel.

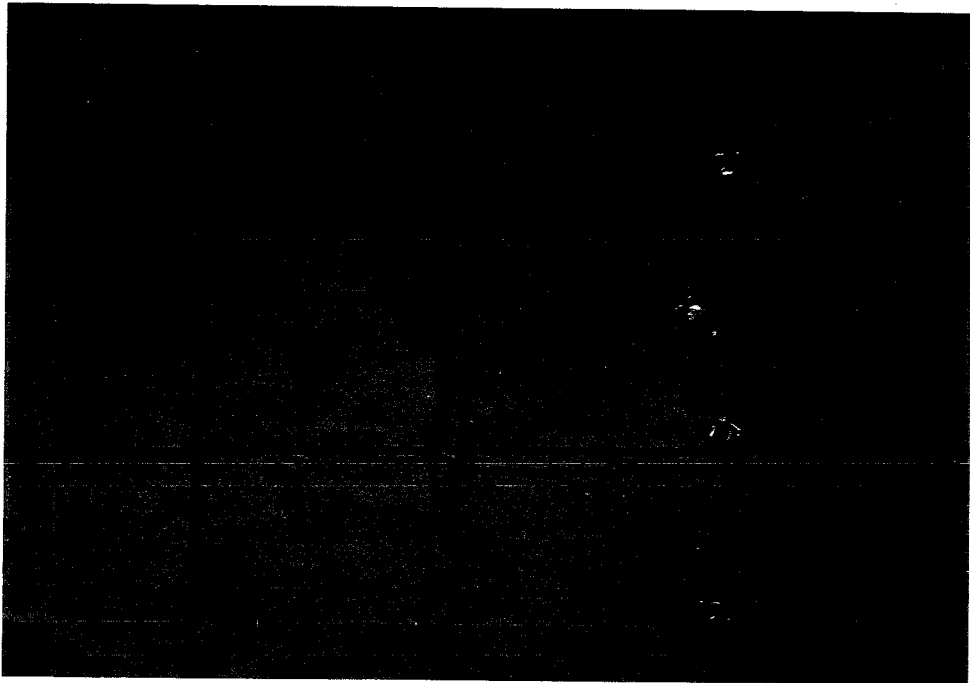


Figure 6.28 0.2DC Flexural Cracking After Completion of Test.

6.1.4 Specimen BO

Specimen BO had bundled ducts positioned against the outside leg of the stirrup. The behavior of specimen BO was similar to that of BC and 0.2DC. A longitudinal flexural crack appeared at duct #2 at a load of $F_r=4.97$ k/ft [Figure 6.2]. This specimen had been patched over the full height of the bundled tendons between stirrups #6 and #7. The crack at this load stage was to the PC side of the crack. At the next load stage, $F_r=5.92$ k/ft, the crack extended through the patch. Longitudinal cracks above and below the duct group were noticed at $F_r=8.43$ k/ft. As was typical of BC and 0.2DC, this was the ultimate capacity of the detail. Further stressing only caused further delamination without an increase in load [Figure 6.29]. The stirrups remained embedded in the top and bottom of the web. Crushing of concrete did not occur at a concentrated point along the curve as happened in the previous three tests. A diagonal crack developed across the panel that allowed the panel to shorten at snap-through.

The delamination cracks were closer to the duct group (3" above the top duct and 3" below the bottom duct) in the middle of the curve than at the ends [Figure 6.29]. Before stirrup #3 and after stirrup #7, the cracks moved away from the duct group and extended nearly to the top and bottom slabs. The top crack went through the patch/concrete interface [Figure 6.30]. The bottom crack went through the patch just above the bottom of the void. The patching probably changed the behavior little. Certainly the 4" length of the patch that was intercepted by the bottom crack had little effect. The top interface was likely a plane of weakness but it was only 7" long. As expected the ultimate capacity of the detail was greater than for BC (8.43 k/ft vs. 7.35 k/ft).



Figure 6.29 BO at Snap-Through.

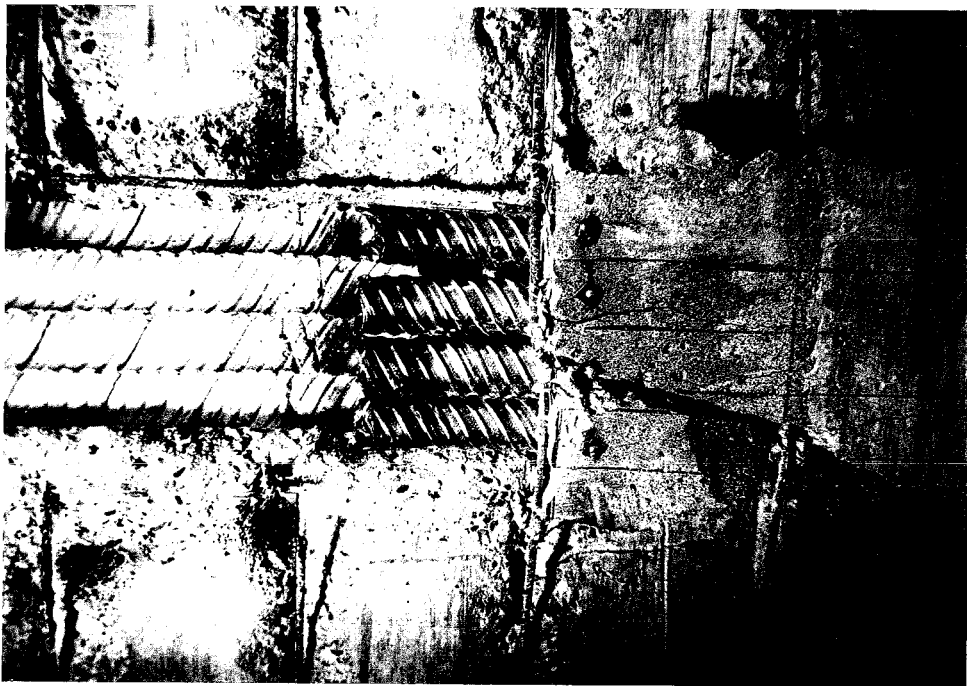


Figure 6.30 BO Cracking at Patch.

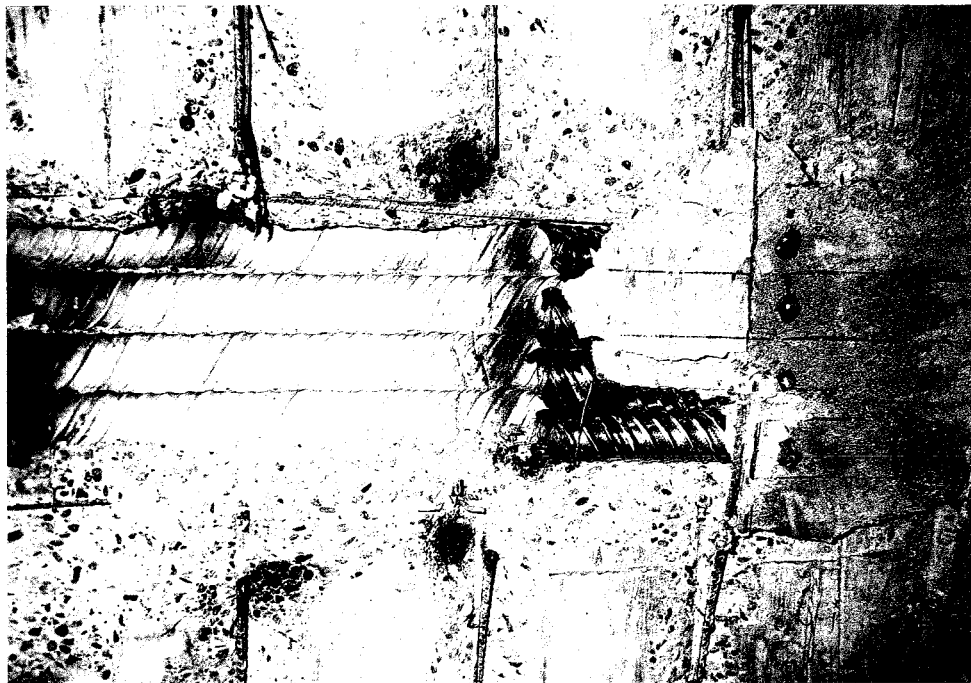


Figure 6.31 BO View of Surface Behind Ducts.



Figure 6.32 BO Top-Forward Tilt.

Figure 6.31 shows that the ducts remained in position during casting. As with the other three specimens, the duct group had a top-forward tilt [Figure 6.32]. A slight bulging of the cover concrete can also be seen. No vertical cracking was observed on the back face behind the removed panel.

6.2 DELAMINATION GAGES

The delamination gage results are very important for understanding the cause and behavior of the breakout phenomenon. They were also used as an indicator during stressing that failure was near. During the 1.0DC test, the web deflection and stirrup strains were closely monitored yet failure was unanticipated. After examining the instrumentation data from this test it became apparent that the delamination gages in the diagonal tension cracking region were dormant until failure was imminent. Gage D64 was monitored for signs of movement during the following three tests.

The philosophy behind placing delamination gages was to use one gage to monitor each duct at a specified stirrup location. The tubes were laid across the top of the ducts prior to casting. The layout proved well-suited for monitoring the deflection of the thin cover and shear cracking within and at the top of the duct group, but it neglected the shear cracking at the bottom of the duct group. It would have been wise to include a delamination gage below the bottom of the bottom duct.

For the girder #1 tests (BC and 1.0DC), four gages were located near stirrup #4 and four gages near stirrup #6. The results were quite similar and therefore the gages near stirrup #4 were omitted in the 0.2DC and BO tests.

The gages were very reliable and gave results consistent with other instrumentation and observed behavior. The only gage to give unexplainable readings was gage D62 in the 0.2DC test. Some plastic tubes cast into 1.0DC

twisted during casting and the wire could not be inserted into positions D42, D44, D62 and D63. Therefore these gages were never installed. Gages D61 and D62 of the BO test stopped working after the ultimate capacity was reached and large displacements began to occur.

6.2.1 Comparisons of Web Delaminations

Comparisons of web delaminations for gages D61 and D64 at stirrup #6 are displayed in Figures 6.33 and 6.34. The graphs for all gage locations show some distinct patterns. The 1.0DC test showed no delamination until just prior to reaching ultimate capacity whereupon the readings ceased due to the rupture of the web. The D61 and D64 gages also showed no movement

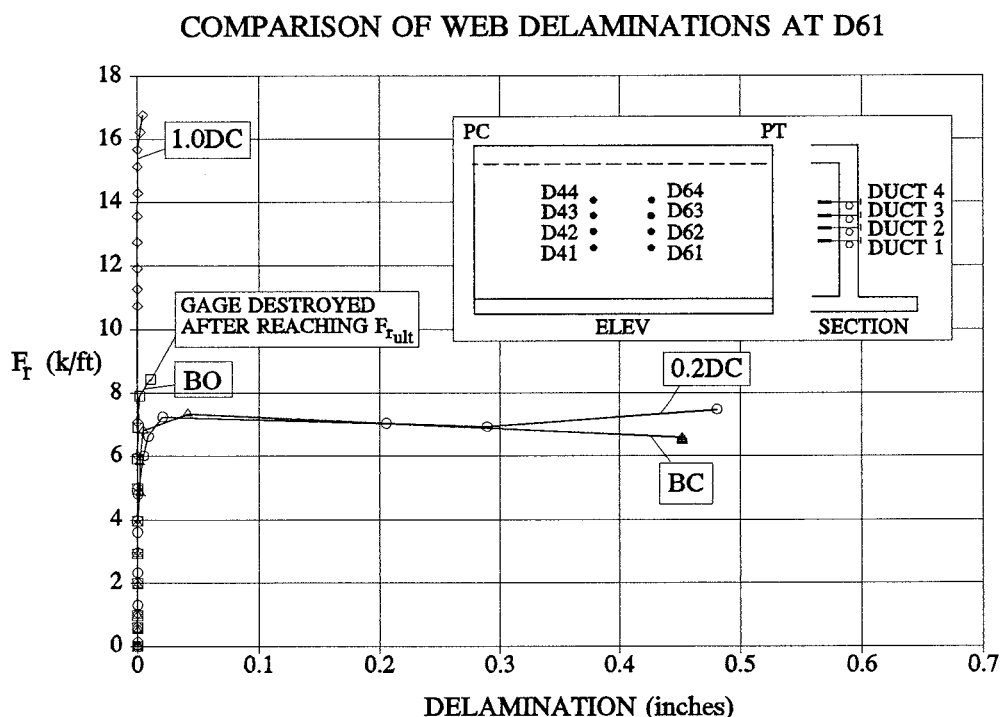


Figure 6.33 Comparison of Web Delaminations at D61.

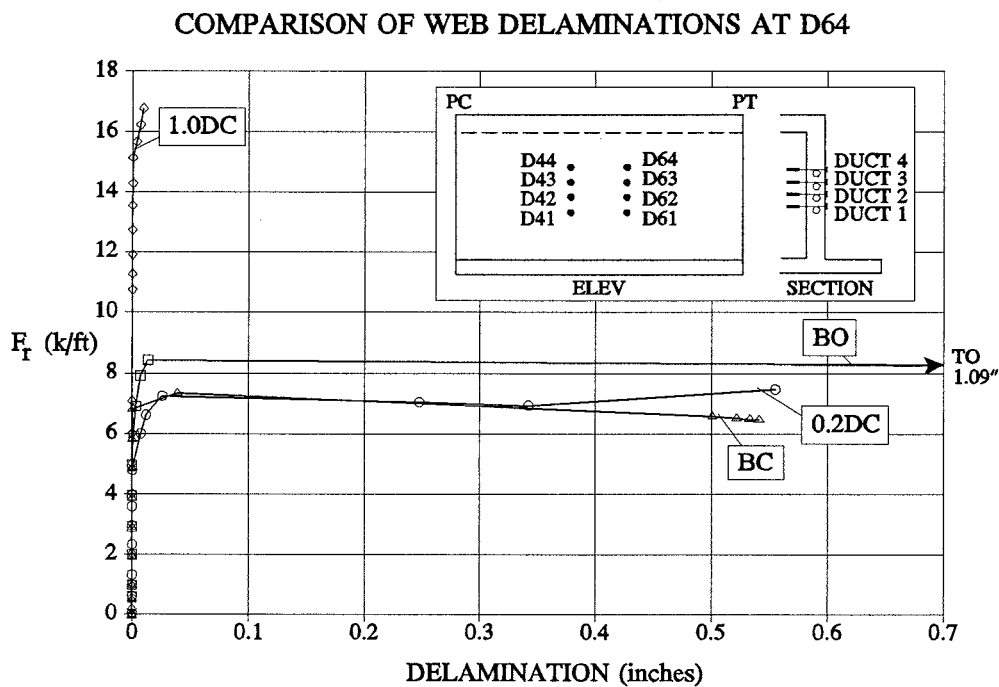


Figure 6.34 Comparison of Web Delaminations at D64.

in the other three tests until just prior to the ultimate capacity. However they continued to give readings past this point as the web delaminations became larger with each stressing operation after the ultimate capacity was reached. The load-delamination curves for gages D62 and D63 are shown in the appendix [Figure A.1 & A.2].

6.2.2 Web Delamination Profiles

Of the four delamination gages aligned vertically at a point on the curve, only the top gage was outside the duct group. The maximum shear in the web was also greatest outside of the duct group. The reading of gages D44 and D64 were due only to shear cracking. Since the other gages were inside the duct group, their movements could detect shear cracking and/or deflection in the cover due to bending. If shear cracking had not begun above

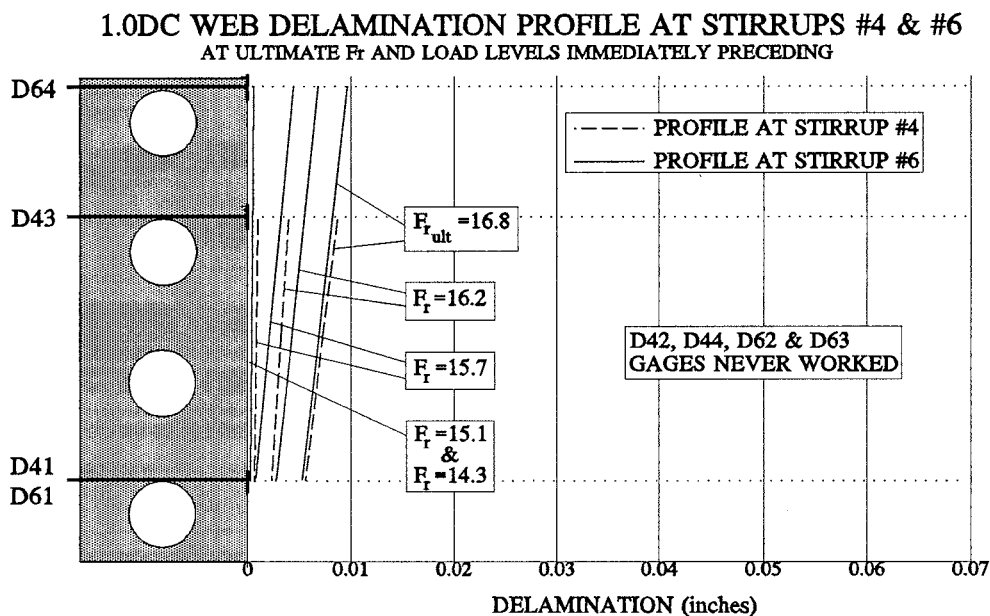


Figure 6.35 1.0 DC Web Delamination Profile at Stirrups #4 & 6.

the duct group, these gages would measure deflection due only to bending. After delamination occurred in the regions outside of the duct group, they measured both bending related deflections and shear cracking displacements.

Web delamination profiles were developed near stirrup #6 for each test so that the deflected shape of the cover and shearing displacement could be determined [Figures 6.35 through 6.38]. Profiles were drawn at the ultimate load and at the load levels immediately preceding so that the progression of the cover deflection can be seen.

6.2.2.1 Specimen 1.0DC

The profiles near stirrup #4 and stirrup #6 were superimposed because gages D42, D44, D62 and D63 never worked [Figure 6.35]. Near stirrup #4, the D43 gage worked properly and gives an indication of the delamination at the middle of the duct group. Gages D41 and D61 measured delaminations

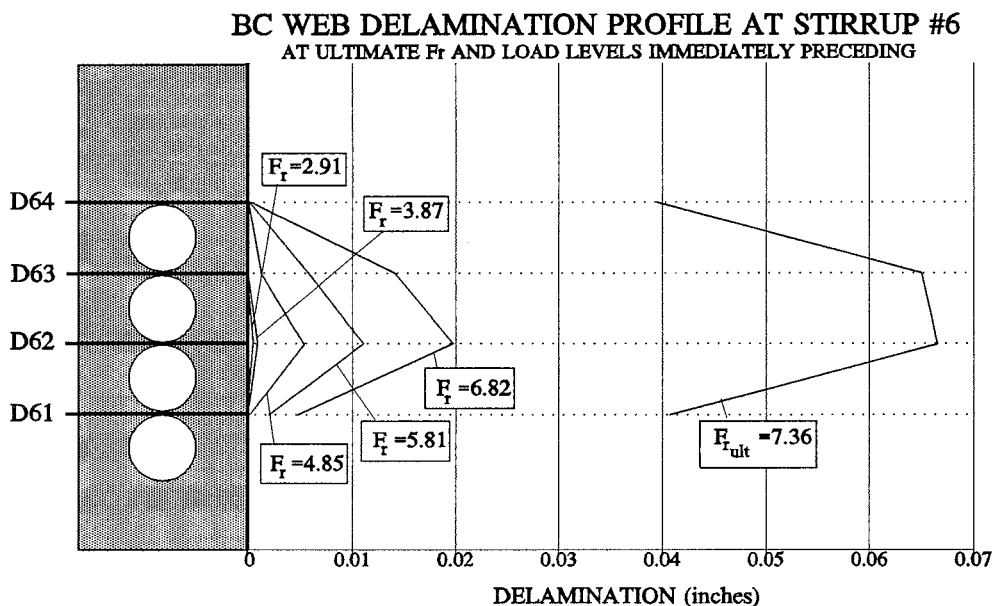


Figure 6.36 BC Web Delamination Profile at Stirrup #6.

near the bottom of the duct group and D64 measured delaminations at the top of the duct group. As can be seen, the profiles near stirrup #4 and #6 were nearly coincident. Since gage D43 does not show delaminations significantly greater than the straight-line interpolation between D61 and D64, it can be concluded that there was no bending of the cover in 1.0DC. Therefore all recorded delaminations were the result of only shear cracking.

6.2.2.2 Specimen BC

Local bending of the cover before and after the advent of shear cracking can be seen in the profile of specimen BC [Figure 6.36]. Deflection was first detected by gage D62 at a load of 2.91 k/ft. Deflection of the thin cover became larger with increasing load. When the load reached the ultimate capacity, 7.25 k/ft, delamination occurred at D64 indicating that

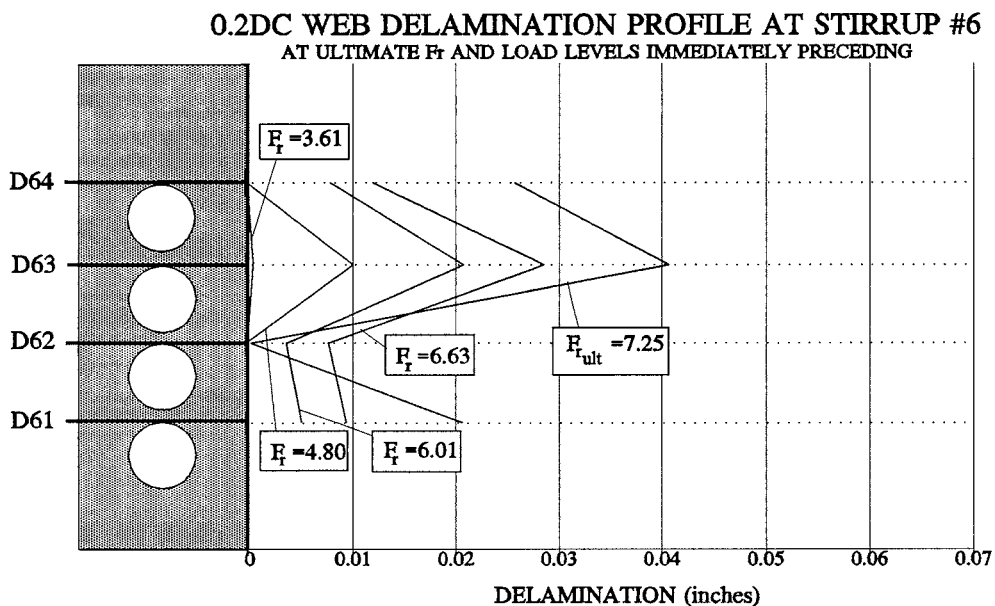


Figure 6.37 0.2DC Web Delamination Profile at Stirrup #6.

shear cracking had begun above the duct group. At this load, the gage reading of D62 became quite large. Results at stirrup #4 were similar and are reported in the appendix [Figure A.3].

6.2.2.3 Specimen 0.2DC

Local bending was also detected in specimen 0.2DC [Figure 6.37]. Deflection began at D63 at a load of 3.61 k/ft. This movement occurred at a load less than that which caused delamination at D64 (6.01 k/ft). This is significant because it demonstrates that the concrete layers were ineffective in carrying tension load at ultimate. Furthermore it appears that at best, they were only effective temporarily as delamination was detected within the duct group only one load stage after it was detected in specimen BC. Delamination at D64 occurred earlier in this test than it did in BC (6.01 k/ft vs. 7.36). Gage D62 gave erratic readings and is not considered reliable.

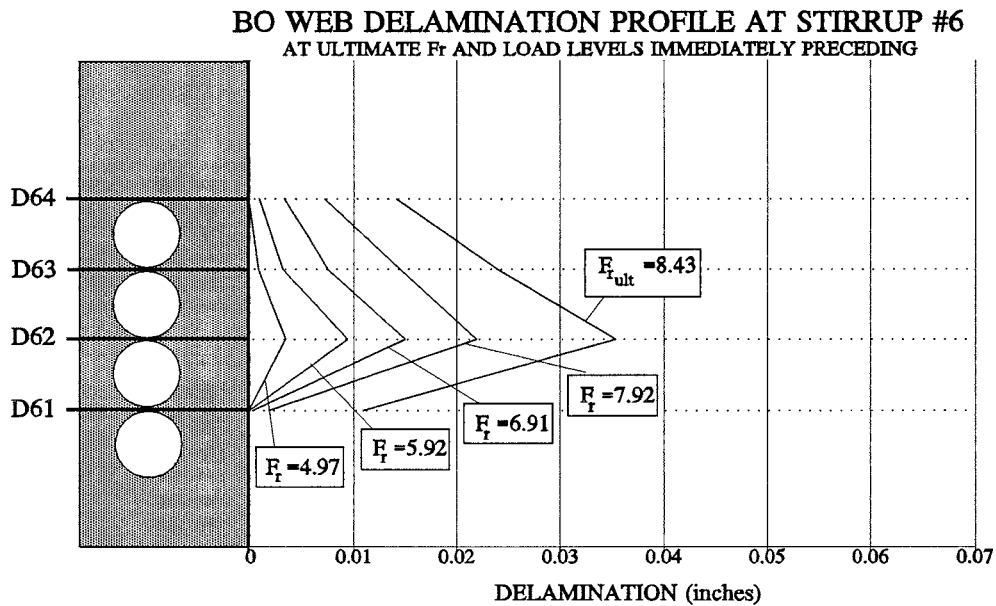


Figure 6.38 BO Web Delamination Profile at Stirrup #6.

6.2.2.4 Specimen BO

Specimen BO had thicker duct cover than BC and 0.2DC and this is reflected in the fact that delamination did not begin until a higher load level [Figure 6.38]. Local cover bending was first detected by Gage D62 at a load of 4.97 k/ft. Gage D64 registered shearing delaminations at the next load stage, 5.92 k/ft. Similar to specimens 1.0DC and 0.2DC, it required a few more load stages after delamination began above the top duct before the ultimate capacity was reached.

6.2.3 Delaminations Outside Duct Groups

A significant relationship exists between ultimate capacity and the delaminations measured outside the duct group. As discussed earlier, delaminations at D64 can be attributed solely to shear cracking.

Unfortunately delamination gages were not installed below the duct group. The delamination here appeared to be a direct precursor to failure.

Since no data exists at this point, the delamination profiles of the previous section were extrapolated. The slope of the delamination between D61 and D62 was used to calculate delaminations at the bottom of the duct group. This method would likely give results that are greater than the actual delamination. The profiles of specimens BC, 0.2DC and BO were typical of simple beam deflected shapes. That is, the slope was greatest near the supports. Only in specimen BO was the slope between D63 and D64 less than the slope between D62 and D63 at ultimate capacity. Even in this instance, it was nearly equal. The extrapolation for specimen 1.0DC was a more straightforward matter. No bending-induced deflection existed, so the slope between D64 and D61 was continued. Gage D62 gave unreliable readings in test 0.2DC so the delamination values at the bottom of the duct group were not calculated. The extrapolated ultimate capacity profiles are shown in Figures 6.39, 6.40 and 6.41. The calculated delamination at the bottom of the duct group at ultimate for 1.0DC was quite small (0.0042") [Figure 6.39]. The profile was extrapolated for the two preceding load levels. This was the only specimen that was able to sustain more load after cracking at the bottom of the duct group appears to have begun. For specimen BC, the delamination was calculated as 0.0163" at ultimate [Figure 6.40]. The profile for the preceding load level was also drawn to determine whether delamination may have occurred prior to reaching the ultimate capacity. It appears as though it did not. In the case of BO, no delamination was calculated at the bottom of the duct group at ultimate [Figure 6.41].

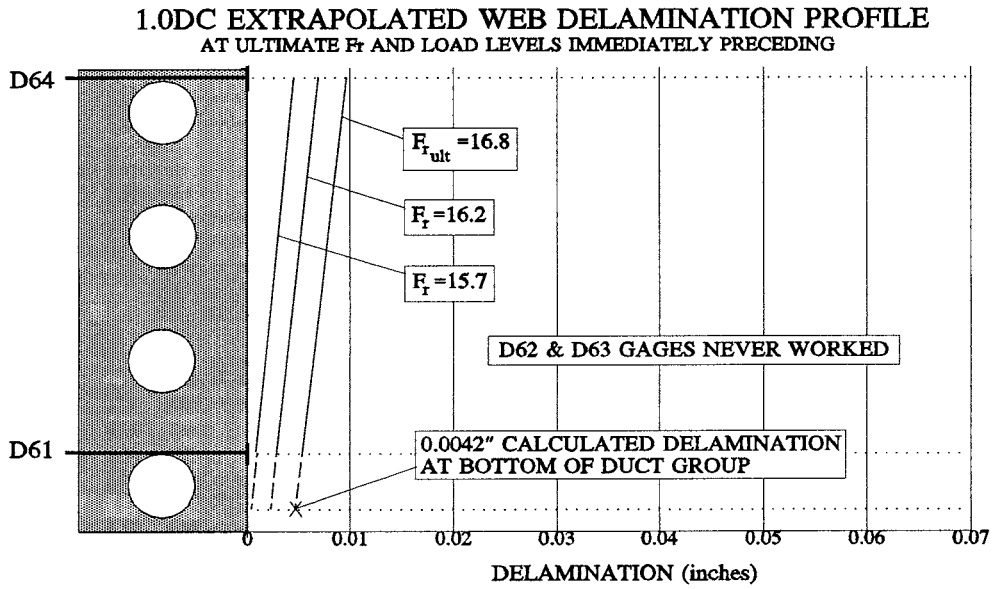


Figure 6.39 1.0DC Extrapolated Web Delamination Profile.

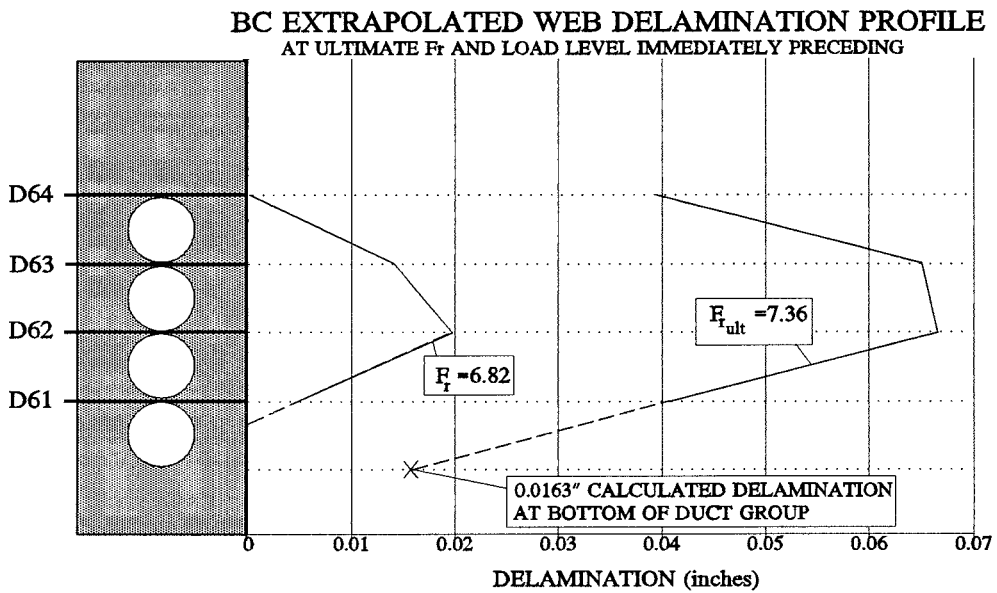


Figure 6.40 BC Extrapolated Web Delamination Profile.

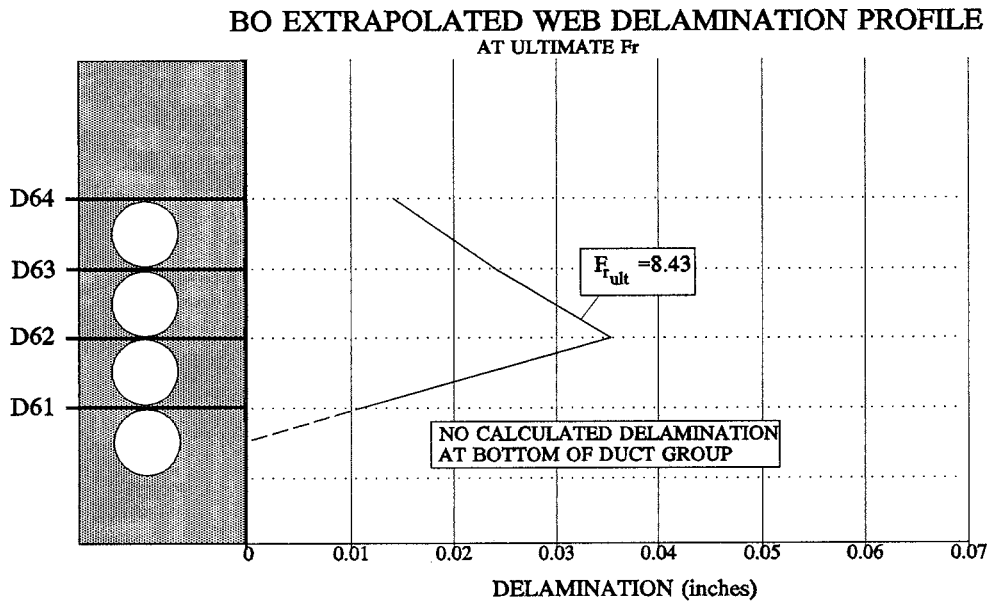


Figure 6.41 BO Extrapolated Web Delamination Profile.

Table 6.1 summarizes the delaminations at the top of the duct group and the extrapolated delaminations at the bottom of the duct group at the ultimate capacity. The delaminations were smallest at the bottom of the duct group. The maximum calculated delamination at ultimate for any of the three specimens was 0.0163" for specimen BC. Since no delaminations were calculated at the bottom of the duct group for specimen 0.2DC, the D61 value was reported. This value was actually lower than the D64 delamination. In fact this is true for all but specimen BC. It is quite likely that if gage D62 was working properly, that the extrapolated 0.2DC results would have been consistent with the other three tests.

These profiles showing the delamination at the top preceding that at the bottom are consistent with the observed behavior of the top-forward tilt of the panels. It is not known why the top duct consistently moved before the

Table 6.1 Delaminations at Ultimate

DELAMINATIONS AT ULTIMATE CAPACITY			
SPECIMEN	TOP OF DUCT GROUP (D64) (in.)	D61 (in.)	BOTTOM OF DUCT GROUP (EXTRAPOLATED) (in.)
1.0DC	0.0095	0.0050	0.0042
BC	0.0392	0.0417	0.0163
0.2DC	0.0261	0.0211	*
BO	0.0136	0.0108	0.0

Minimum delamination for specimen at ultimate capacity

* gage D62 gave unreliable readings

bottom duct. Perhaps it was related to the systematic monostrand stressing operation that always began with the stressing of the bottom strands. This is not a significant observation however. As discussed in Section 5.1, the stressing procedures commonly used in actual construction do not load ducts simultaneously. It is likely that any failure during construction would occur during jacking when tendons may have widely varying levels of stress.

6.3 STRAIN GAGES

The strain gages provided insight into specimen behavior. It is interesting to note that no strain gages indicated that yielding had occurred in a stirrup before the ultimate capacity was reached. Only one gage in one test (specimen 1.0DC) reached the bar yield strain when the specimen was at ultimate. This gage reading was only 5.5% greater than the yield strain. This permitted stirrup behavior to be expressed in terms of stress rather than

strain. Recorded strains were multiplied by the steel modulus of elasticity (28.9 ksi) to generate stresses.

Gages that were working at the start of the test were quite reliable; no gages appear to have malfunctioned during the test. All of the gages on the outside leg of the stirrup except for one were not working at the beginning of the test of specimens 1.0DC and BC. All of the gages on the inside stirrup legs of these specimens and all gages for specimens 0.2DC and B0 were working properly. A complete listing of installed gages and the working status of gages is provided in Tables 5.1 & 5.2.

6.3.1 Comparison of Stresses at IM and IU

Figure 6.42 compares the stirrup stresses on the inside leg adjacent to the c.g. of the duct group (IM gages) versus the lateral prestress force at the midpoint of the curve. This particular gage was chosen for comparison for a number of reasons. This was the most highly stressed region of any of the stirrups through ultimate for specimens BC, 0.2DC and BO. It was the most highly stressed region of 1.0DC until just prior to ultimate. This location was also the first to experience high levels of stress and was indicative of first cracking.

The slope of the stirrup tendon stress-load curves were similar until the load reached about 2.0 k/ft. After a load in specimen BC of 1.93 k/ft and in specimen 0.2DC of 2.32 k/ft, a large increase in stress occurred. The 1.0DC initial slope was maintained until the next load stage, 3.01 k/ft. BO does not show significant stress gains until after a load of 3.97 k/ft. The slopes for BC, 0.2DC and BO were nearly linear and parallel until ultimate. They were also nearly coincident until the gages in BC and 0.2DC ceased at ultimate. The stress-load curve for 1.0DC past the initial slope was not as linear as the others. This is due to the reloadings. 1.0DC had a rate of stress gain about

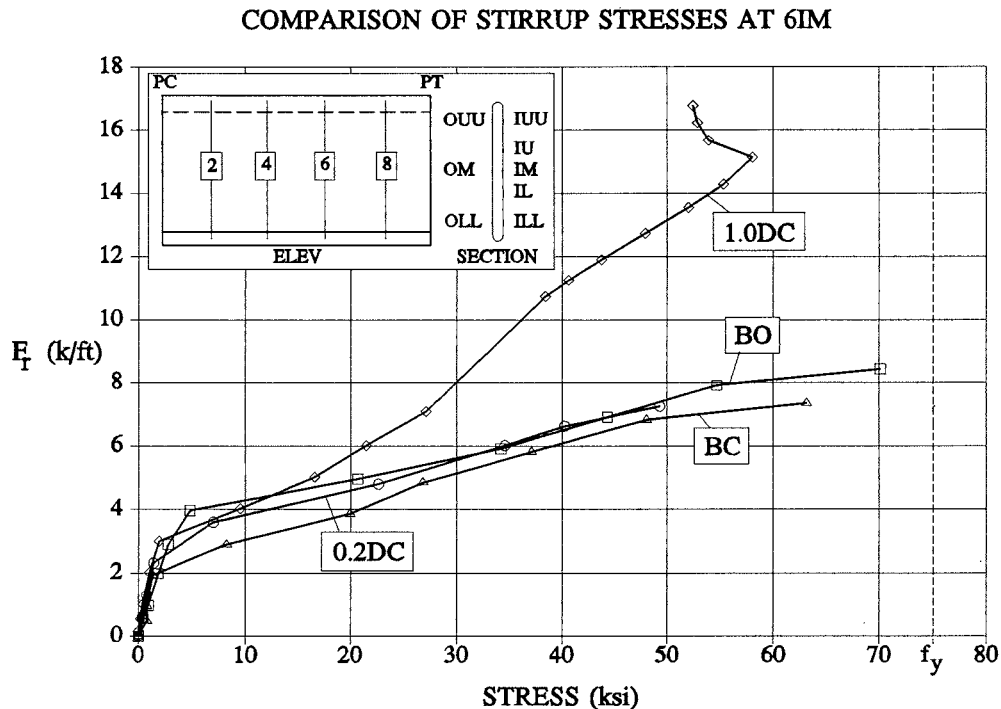


Figure 6.42 Comparison of Stirrup Stresses at 6IM.

half that of the other three specimens. This would be consistent with the TYLI theory that the bundled or closely spaced ducts experience local flexural stresses in addition to the regional beam stresses.

The sudden increase in slope was likely due to the formation of flexural cracks. In all tests, the first cracking as indicated by the strain gages preceded the visual manifestation of cracking. This was not unexpected. Figure 6.43 shows the strain gage-detected first cracking (termed microcracking), the visible first cracking and the ultimate capacities of all specimens. The first cracking loads of the closely spaced details (BC and 0.2DC) appear consistent with the other specimens in so far as they were the lowest of the four specimens. At first glance, it seems as though the first cracking loads of

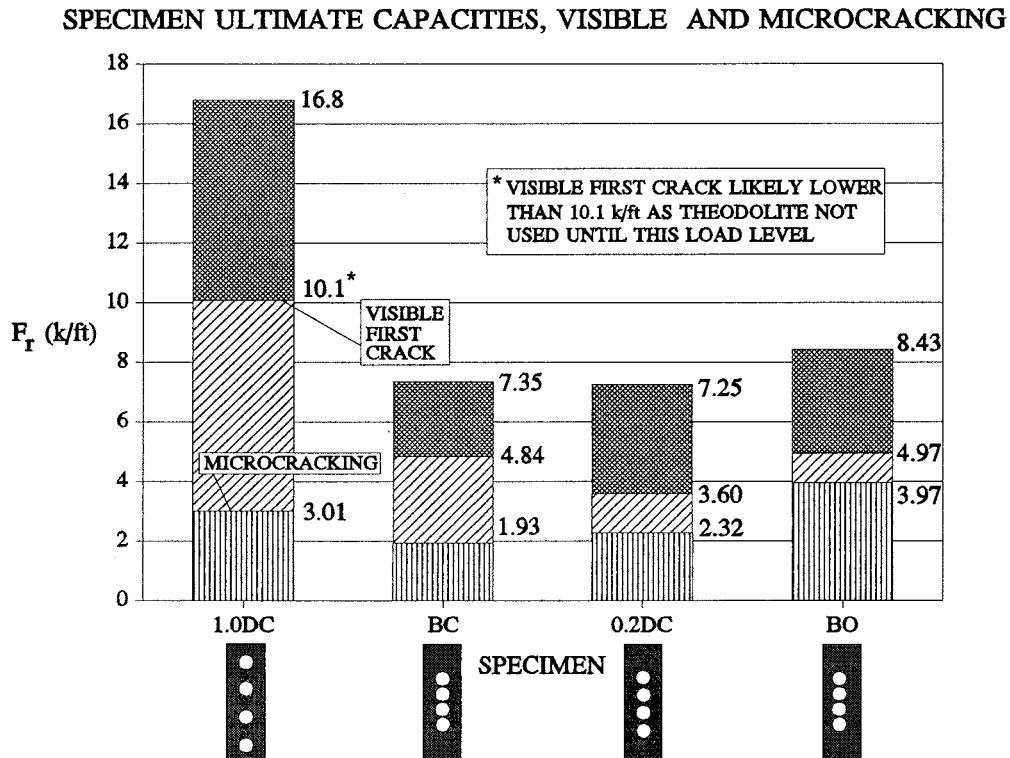


Figure 6.43 Specimen Ultimate Capacities, Visible and Microcracking.

1.0DC and BO should be reversed since 1.0DC was the stronger, stiffer detail. Closer inspection reveals that BO is indeed a superior detail for first cracking because it had thicker cover over the ducts (1.5" vs. 1.125").

However this increased cover thickness did little to slow the stress gain after first cracking as evidenced by the nearly coincident BC, 0.2DC and BO curves [Figure 6.42]. It was expected that the BO slope would be steeper than the BC and 0.2DC slopes because this detail had a greater internal moment arm in the positive moment region (0.875" vs. 0.5").

A comparison of stresses in stirrup #6 is also shown at the IU location [Figure 6.44]. The gage was located 5" above the c.g. of the tendon group on

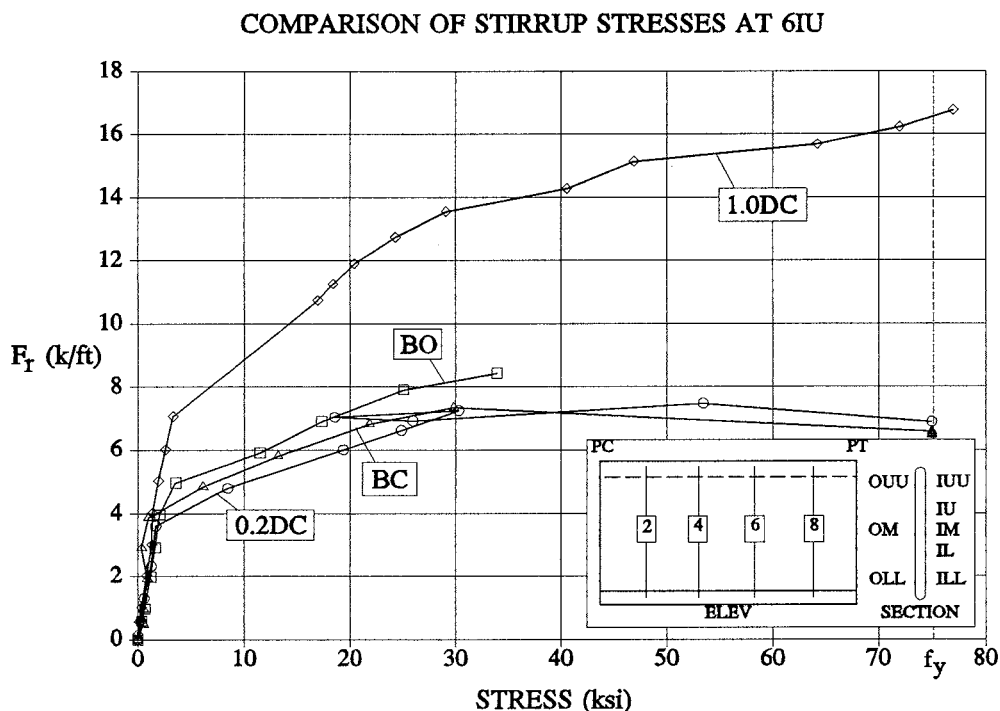


Figure 6.44 Comparison of Stirrup Stresses at 6IU.

the inside leg. This was 1.375" above the top of the top duct for BC and BO, 1" above the top of the top duct for specimen 0.2DC and at the same elevation of the center of the top duct in 1.0DC [Figures 3.4 & 3.5].

This gage gave insight into the flexural behavior of the specimens. The behavior of gage 6IU for specimens BC, 0.2DC and BO was very similar. The 6IU gages for these three specimens show that microcracking began at approximately the same load level (4 k/ft to 5 k/ft). They gained stress rapidly after microcracking. 1.0DC did not crack at this location until a load of 7.94 k/ft. After microcracking, its stress gain was much slower than for the other three specimens. In only one case, 0.2DC did the stress increase after cracking also coincide with inclined shear cracking (which probably began

earlier as a result of the patch). This further supports the TYLI theory that bundled or closely spaced specimens (0.2DC) experience significant local flexural stresses consistent with the fixed-fixed support conditions at the top and bottom of the front face cover.

6.3.2 Stirrup Stresses on the Inside of the Duct Groups (IL, IM, IU)

These three gages were the most highly strained of any of the gages in all specimens. They were located near the duct groups as shown in Figure 3.4 & 3.5 and gave insight into local and regional behavior.

6.3.2.1 Specimen 1.0DC

The 6IL and 6IU gages show increased stress at the start of loading at a rate only slightly less than 6IM [Figure 6.45]. Microcracking began later at these gages than at 6IM which indicates that they experienced less flexural stress. It appears from this figure that first cracking occurred at 6IL and 6IU at a load of 7.08 k/ft. This part of the graph omitted a few load stages to smooth the transition between load stages. The complete stress development of these gages is shown in the appendix. From Figure A.4, it can be seen that actual microcracking for these gages actually began at 7.94 k/ft.

These three gages gained stress at nearly a constant rate after first cracking. At a load of 11.9 k/ft, 6IU began to pick up stress more rapidly. This corresponded to an extremely small movement (4×10^{-5} in.) detected by the D64 delamination gage at the next load stage (12.7 k/ft). 6IL began an increased rate of stress gain after a load of 13.5 k/ft which corresponded to a very small delamination (6×10^{-4} in.) detected in gage D61 at a load of 14.3 k/ft. 6IM remained unaffected by the small delaminations detected at the extremes of the duct group.

At a load level of 15.7 k/ft, all three gages experienced a marked change in behavior. The 6IL gage showed almost no gain in stress while the

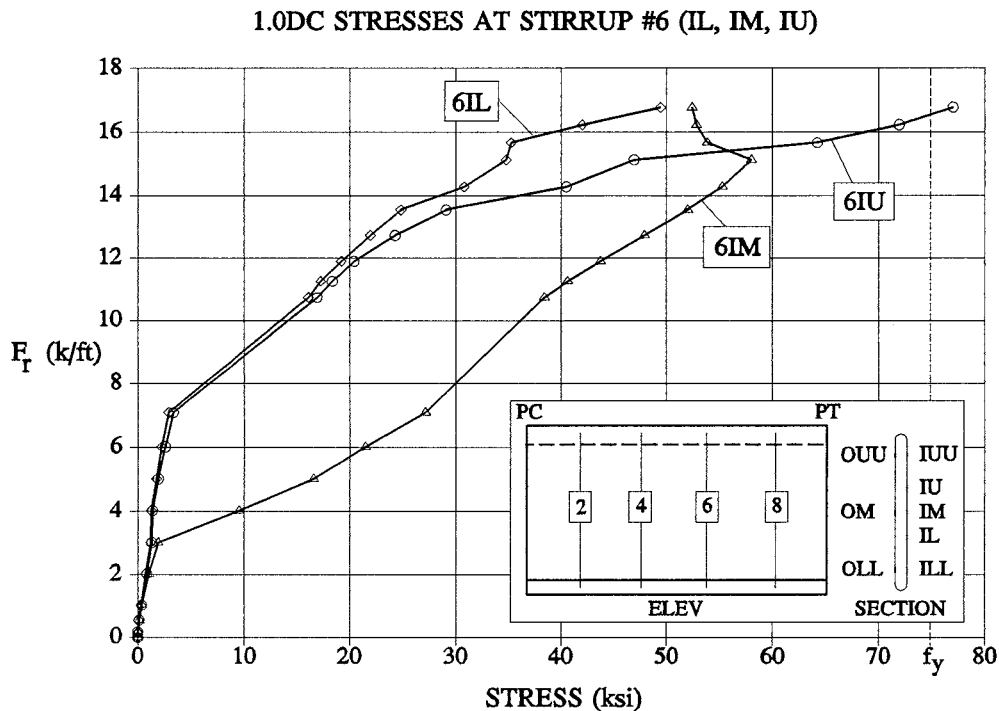


Figure 6.45 1.0DC Stresses at Stirrup #6 (IL, IM, IU)

6IM gage lost stress and the 6IU gage jumped from 45 ksi to 62 ksi. This behavior is explained by superimposing the D64 delamination curve on this graph [Figure 6.46]. The beginning of large delaminations (0.004 in.) caused by the inclined shear crack as detected by D64 clearly was responsible for these abrupt changes. As the top of the concrete cover region began to move out, the 6IU gage became more highly stressed. A new load path was created which caused the 6IM stress to decrease. Perhaps the large shear crack disrupted the integrity of the section and altered the flexural response which was responsible for the stresses in 6IM. The 6IL stress was only stagnant for one load stage (15.7 k/ft) but quickly gained stress over the next two stages (16.2 k/ft and 16.8 k/ft). This gives credence to the profile extrapolation of

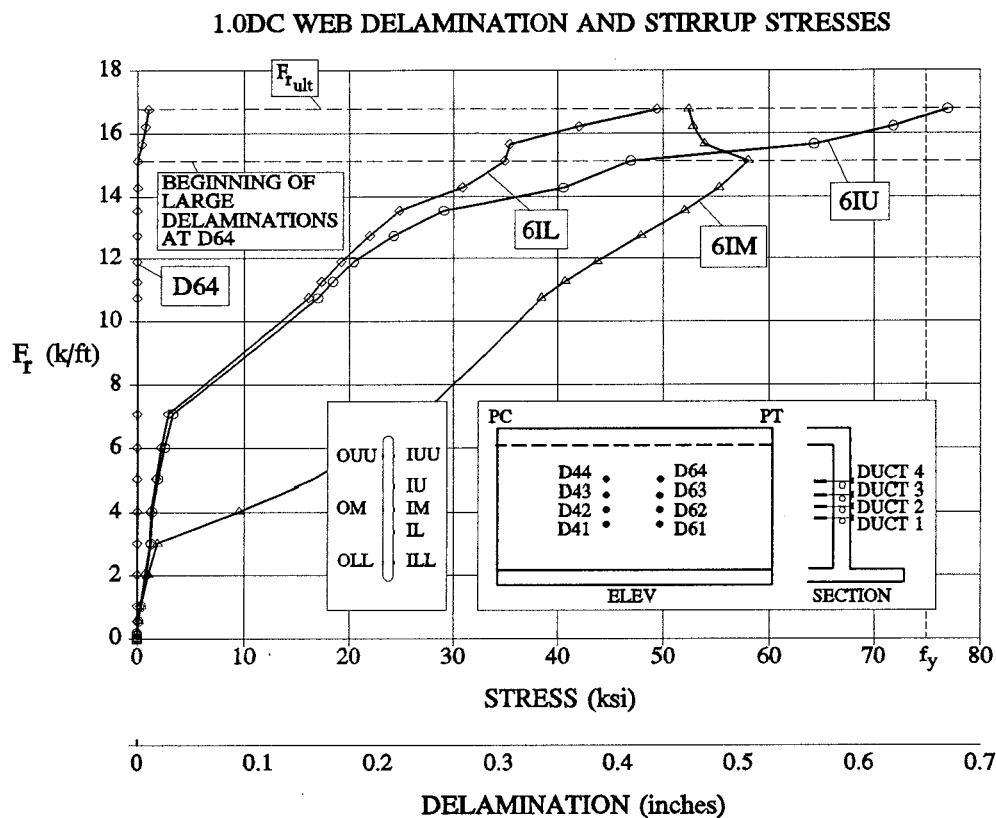


Figure 6.46 1.0DC Web Delamination and Stirrup Stresses.

Figure 6.39 which shows large delaminations first occurring at the bottom of the duct group at a load of 16.2 k/ft.

6.3.2.2 Specimen BC

In specimen BC, the 6IL and 6IU gages did not detect stress increases until a load of 3.87 k/ft [Figure 6.47]. This level was twice the load that caused microcracking at 6IM. The 6IU gage picked up stress more rapidly than the 6IL gage. This is in agreement with the web delamination profile which shows the top of the duct group undergoing more deflection than the bottom (i.e. D63 delaminates more than D61) [Figure 6.36]. The stress in both the gages increased to 30 ksi at the ultimate load capacity. The

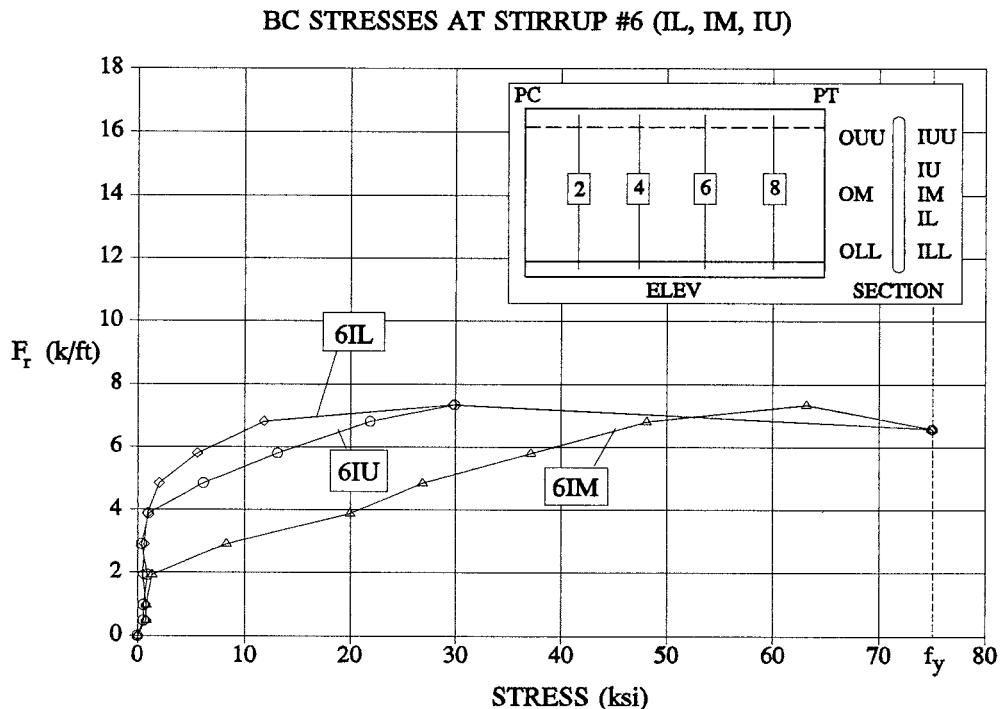


Figure 6.47 BC Stresses at Stirrup #6 (IL, IM, IU).

delamination of gage D64 is superimposed on the graph in Figure 6.48. At the ultimate load (7.35 k/ft), significant delaminations were first detected at D64 (0.0393"). At the advent of large delaminations outside the duct group the rate of stress gain increased for all the gages. This was unlike 1.0DC where only the IU gage significantly increased in stress. At the next stressing operation after the ultimate capacity, all of these gages indicated yielding of the stirrup. All flexural integrity of the section was lost at this load stage and the concrete cover and stirrups acted as a tension membrane. The complete load history for these gages (including the unloading) is shown in the appendix [Figure A.5].

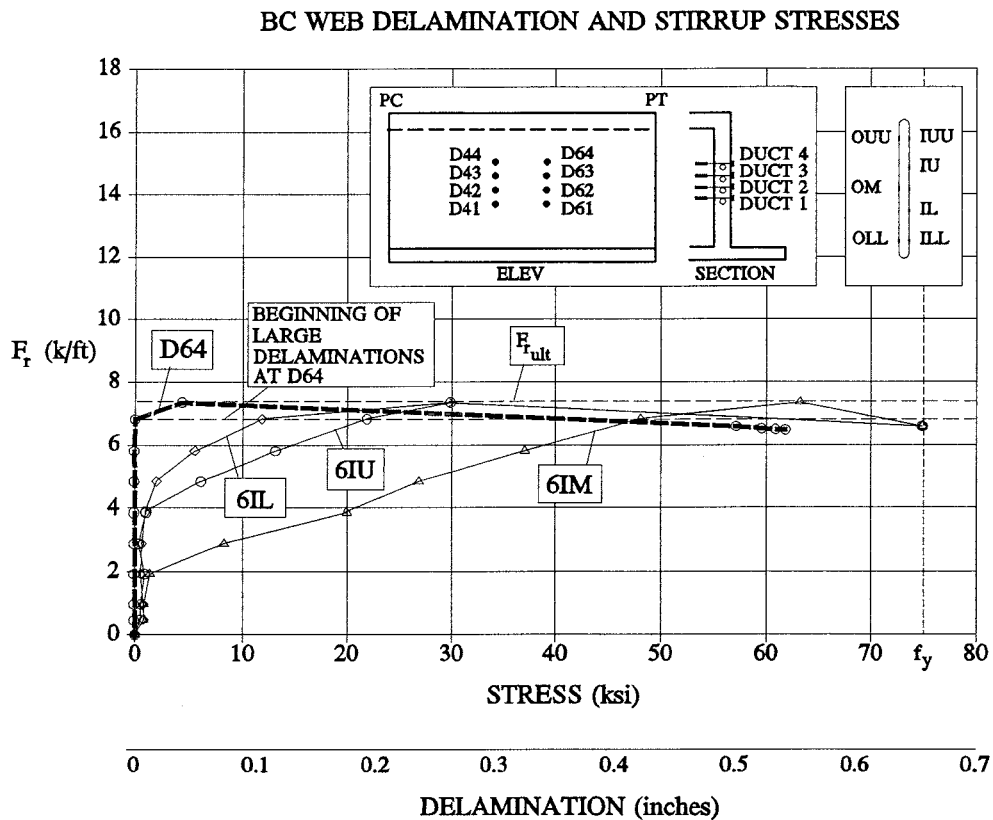


Figure 6.48 Web Delamination and Stirrup Stresses.

6.3.2.3 Specimen 0.2DC

For the test of specimen 0.2DC, the 6IU and 6IL gages behaved almost identically [Figure 6.49]. They both gained stress slowly until microcracking occurred at a load of 3.61 k/ft. This was one load stage after microcracking at 6IM. The rate of stress gain was steady and slightly less than that at IM until the ultimate capacity was reached. From ultimate to the next stressing operation, the stress in the 6IL gage dropped from 27 to 23 ksi. The stress in gage 6IU dropped from 30 ksi to 18 ksi. The stress in these gages increased in the next stressing operation to 39 ksi in 6IL and 25 ksi in 6IU.

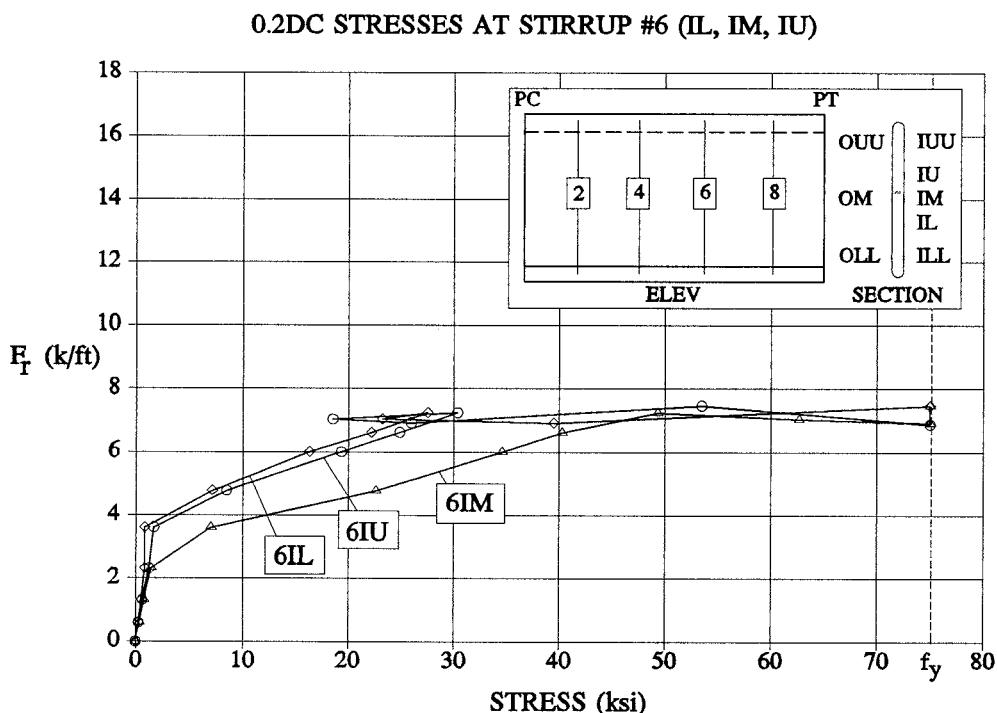


Figure 6.49 0.2DC Stresses at Stirrup #6 (IL, IM, IU).

Continued stressing of the strands brought the stirrups to yield at 6IL and 6IU. The decrease in stress was most likely due to the behavior of the patch at ultimate. The shear cracking may have caused a loss of bond at the 6IU gage which was covered by the patch [Figure 4.24].

The D64 load-delamination curve is superimposed on the load-stress curve for specimen 0.2DC [Figure 6.50]. Delamination began at lower load levels in 0.2DC than BC. No abrupt changes in stress occurred at the start of large delaminations and the 6IU and 6IL curves are only slightly flatter than the corresponding BC gages. At the ultimate load (7.25 k/ft), very large delamination occurred at D64 and both 6IU and 6IL temporarily decreased in stress as described above. Stresses in 6IM increased significantly at this

0.2DC WEB DELAMINATION AND STIRRUP STRESSES

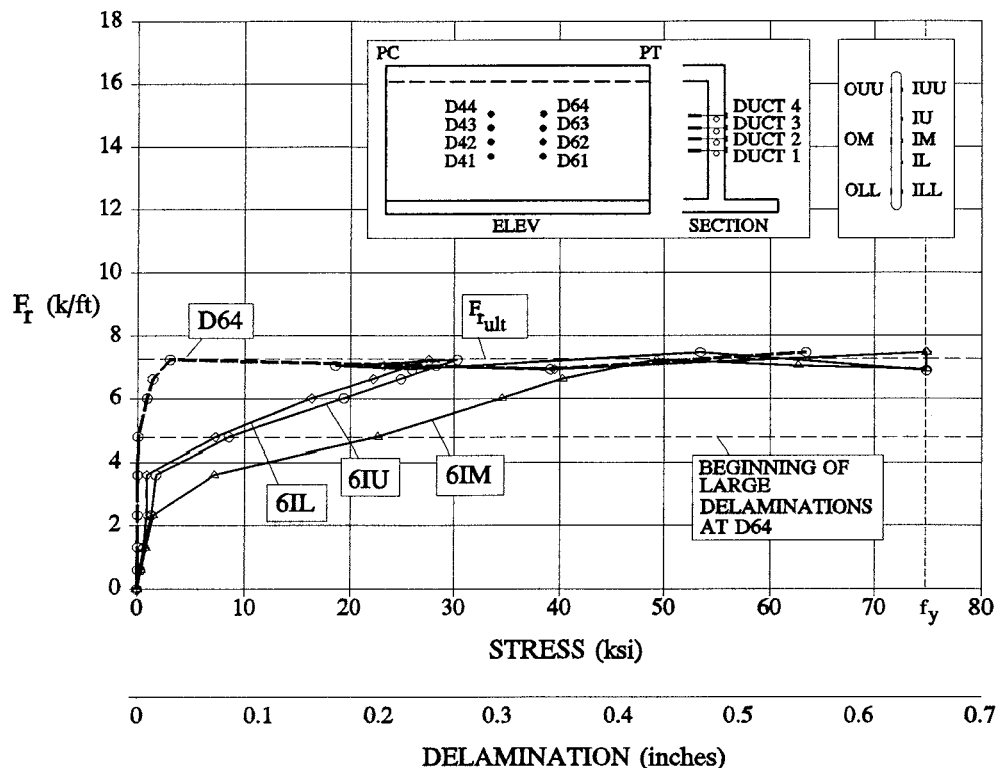


Figure 6.50 0.2DC Web Delamination and Stirrup Stresses.

load level.

6.3.2.4 Specimen BO

In the last specimen tested, BO, the load-stress curves for the #6 stirrup at 6IL, 6IM and 6IU are similar to those for BC [Figure 6.51]. However, the rate of stress gain before microcracking for 6IL and 6IU is noticeably slower than that for IM. Microcracking occurs later at 6IL and 6IU in BO (4.97 k/ft) than BC (3.87 k/ft). These gages show similar but decreased rates of stress gain after microcracking than those in BC. Stresses in 6IU gained faster than 6IL but both were exceeded by 6IM. The gages stopped working after the ultimate capacity was reached.

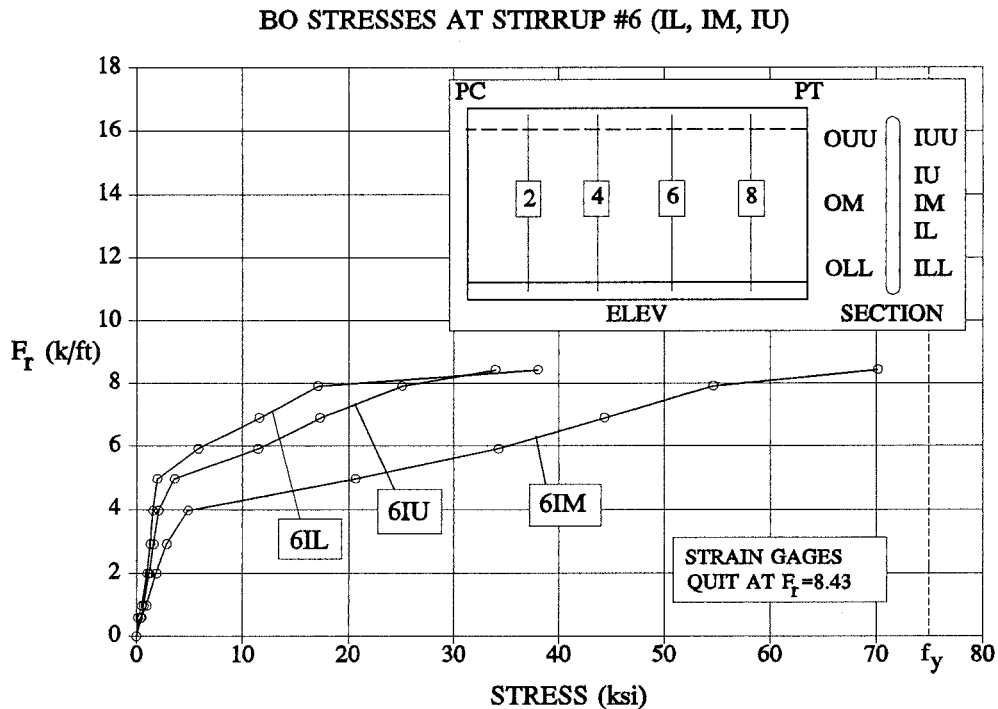


Figure 6.51 BO Stresses at Stirrup #6 (IL, IM, IU).

Figure 6.52 shows the D64 load-delamination curve superimposed on the load-stress curve for specimen BO. No significant changes in stresses occurred at the beginning of delamination. It was not until one load stage before ultimate that the rate of stress gain in the three gages accelerated. At ultimate, the delamination became very large and the 6IL, 6IM and 6IU gages malfunctioned.

6.3.3 Outside Leg Stirrup Stresses

Outside leg gages indicated low stresses (below 15 ksi) in all specimens and all load stages up to and including the ultimate load. They were not directly associated with the failure mechanism but are helpful in understanding regional beam action. As discussed earlier, all the gages

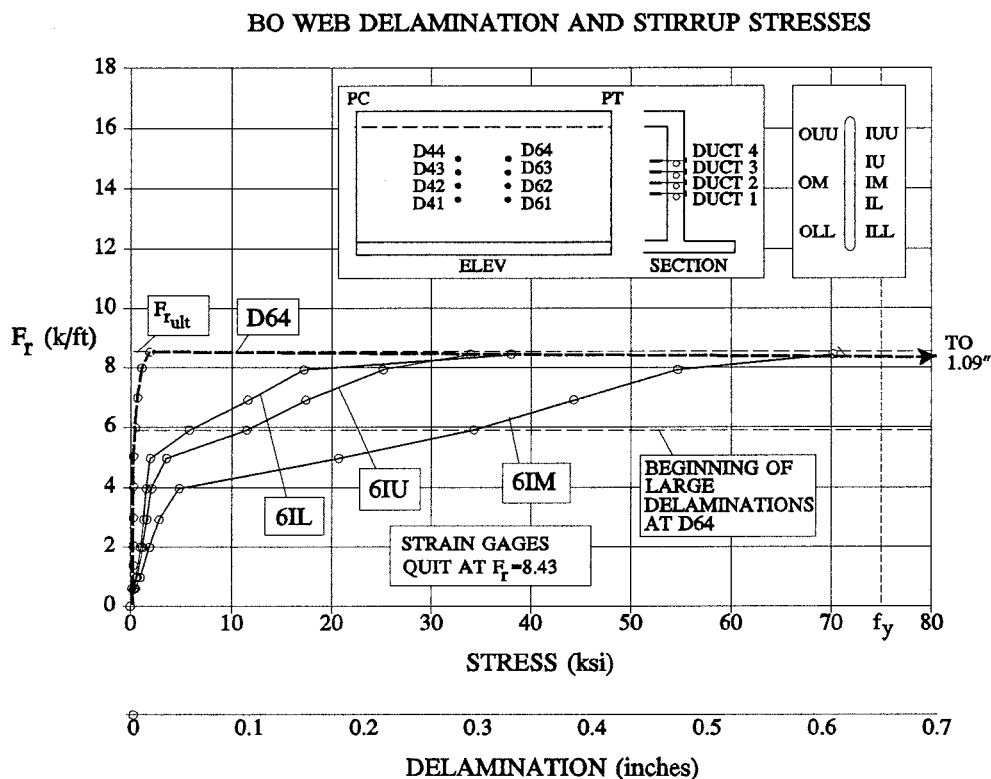


Figure 6.52 BO Web Delamination and Stirrup Stresses.

(except OOU) on the outside legs of specimens 1.0DC and BC did not work.

In specimen 1.0DC, the 4OOU gage indicated that the stirrup at the top outside face was in tension throughout the test [Figure 6.53]. This is consistent with the regional beam, frame action theory which assumes this location to be in flexural tension. Before the onset of microcracking at 4IM in specimen 1.0DC (3.01 k/ft), the stress in OOU was 0.4 ksi tension and the stress in 4IM was 1.5 ksi tension. The stress in 4OOU continued to lag far behind the stress in 4IM throughout the test. Only when large delamination occurred at D64 prior to ultimate did the stress in 4OOU show any significant change.

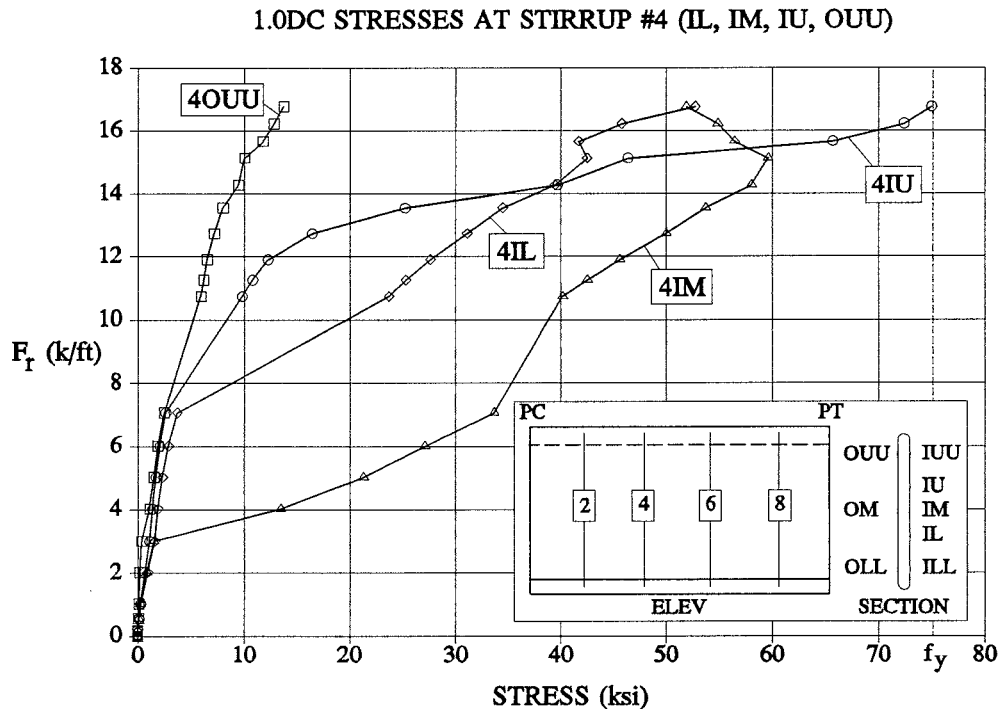


Figure 6.53 1.0DC Stresses at Stirrup #4 (IL, IM, IU, OUU).

Stresses at the top and bottom of stirrup #6 in specimen 0.2DC also point to possible regional beam frame action [Figure 6.54]. The 6OLL and 6OUU gages indicated tension as is consistent with flexural tension zones on the upper and lower outside faces of the web. Furthermore, the opposing inside face gages (6ILL and 6IUU) were in compression albeit only at stresses up to 3 ksi. The 6OM gage remained virtually unstressed until one load stage past microcracking. It then began to slowly develop tensile stresses until large delaminations as detected by D64 began. At the ultimate capacity the tensile stress actually began to significantly reduce.

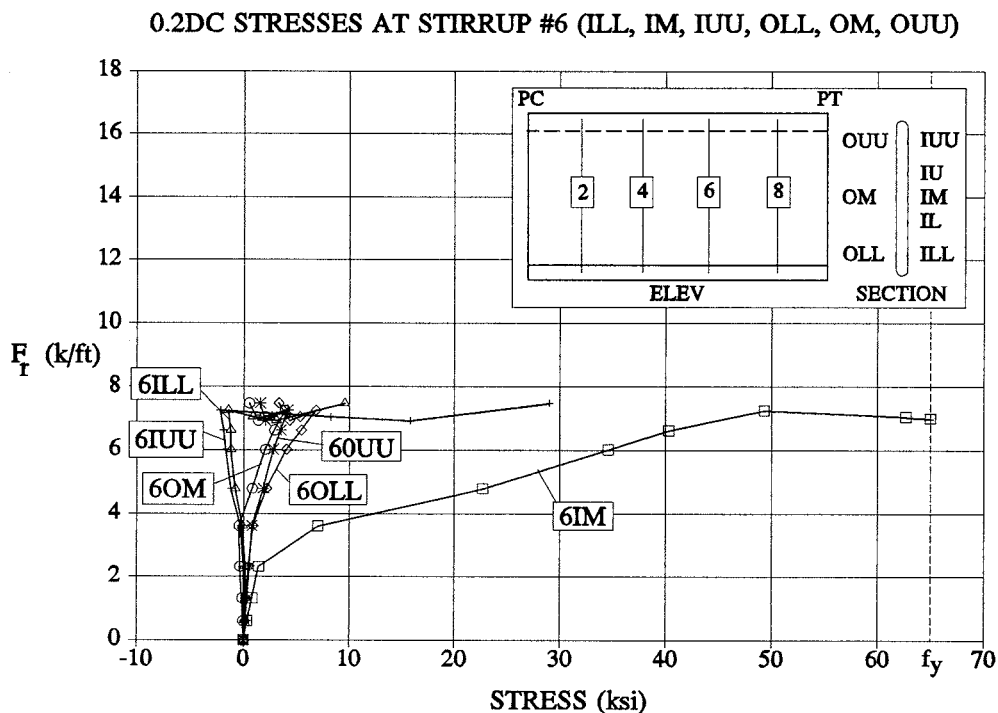


Figure 6.54 0.2DC Stresses at Stirrup #6 (ILL, IM, IUU, OLL, OM, OLL).

6.4 WEB DEFLECTION POTENTIOMETERS

As discussed in Section 5.3, two types of deflection measurements were taken. The web-slab potentiometers measured the outside face mid-height deflection relative to the top and bottom slabs. The web-web potentiometers measured the deflection of the midpoint of the curve at mid-height relative to the PC and PT.

6.4.1 Web-Slab Deflections

The web deflections relative to the slabs near stirrup #6 were measured and plotted for each load stage [Figure 6.55]. All four test specimens deflected nearly the same amount during the early stages of

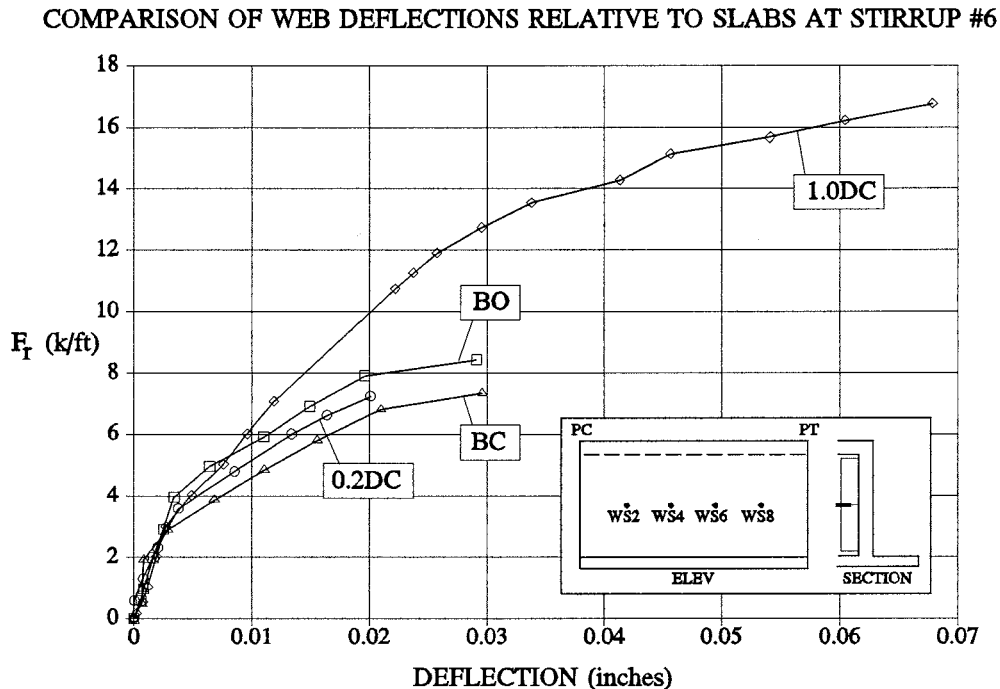


Figure 6.55 Comparison of Web Deflections at Stirrup #6.

loading. At a load of 4 k/ft or less, the rate of deflection increased in all the webs. In specimens 1.0DC, BC, and BO, this distinct change in stiffness corresponded exactly to the beginning of the increased rate of stress gain at the 6IM stirrup. In specimen 0.2DC, a very slight rate of deflection increase occurred at 6IM microcracking ($F_r=2.32$ k/ft) but a large increase occurred at the next load stage (3.61 k/ft). This was when the delamination gages showed that the thin concrete layers were ineffective. The appendix includes a similar graph for a location near stirrup #4 as well as the complete load cycles for specimens 1.0DC and BC near stirrup #6 [Figure A.6 & A.7].

After microcracking, all of the bundled or near bundled arrangements (BC, BO, 0.2DC) had nearly the same stiffness as demonstrated by the rate of deflection gain. Specimen 1.0DC was stiffer in the load range after the

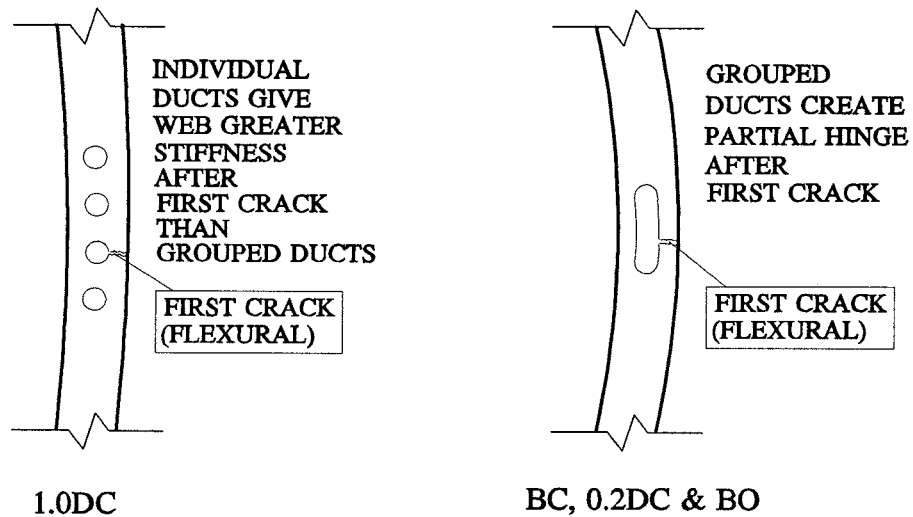


Figure 6.56 Web Deflections After First Crack.

inception of microcracking than the other three specimens. The bundled and near-bundled arrangements presumably had less stiffness because of the essentially continuous void created by the four ducts [Figure 6.56]. Once the flexural crack reached the duct group, what can be called a sideways T-shaped crack existed. The flexural crack only penetrated $1\frac{1}{8}$ " or $1\frac{1}{2}$ " depending on whether the ducts were centered or offset, but the contiguous ducts provided a vertical "crack" that was about 8" long. Once the front cover cracked, the flexural stiffness created by the interaction of the front and back covers was reduced.

By virtue of the difference in stiffnesses between these three specimens and 1.0DC, it appears that a partial hinge formed at microcracking for the grouped duct specimens (or in the case of 0.2DC, at the next load stage). The change in regional beam behavior was detected in 0.2DC stirrup strain gages

6OLL and 6OUU which showed no change in stress gain at microcracking as detected by 6IM ($F_r=2.32$ k/ft) but did once the stiffness reduced sharply at $F_r=3.61$ k/ft [Figure 6.54]. A less pronounced change was detected in the 4OUU gage in specimen 1.0DC, which showed a slight increase in stress coincident with the reduction in stiffness brought about by the flexural crack occurring at a load of 3.01 k/ft. This shows that flexural cracking alone changed the stiffness slightly, but larger loss of stiffness and significant moment redistribution at low loads occurred with cracking of the three grouped-duct specimens. This leads to the conclusion that for the bundled or near bundled arrangements, regional beam flexural stresses were dissipated near the ducts at low load levels by the formation of a partial hinge. The 6IM stirrup stress gains after microcracking in bundled and near-bundled arrangements are likely due mostly to local beam action on the cover.

In three of the specimens, the slope of the load-deflection plot changed again near ultimate to form a trilinear curve [Figure 6.55]. In specimens BC and BO, this occurred in the load stage prior to ultimate. In specimen 1.0DC, the increase in the rate of deflection occurred three load stages before ultimate at a load of 15.7 k/ft. All of these load stages were coincident with the occurrence of large web delaminations. Specimen 1.0DC had a slower rate of deflection increase than BC and BO. The load-deflection curve for specimen 0.2DC was bilinear rather than trilinear.

6.4.2 Web-Web Potentiometers

Three potentiometers were placed at approximately the quarter-points of the longitudinal curve on specimen BC to give an indication of longitudinal moments. Longitudinal moments would have developed if there existed two-way action rather than just vertical regional bending of the web. This would have been a result of the model curve length being too short. The

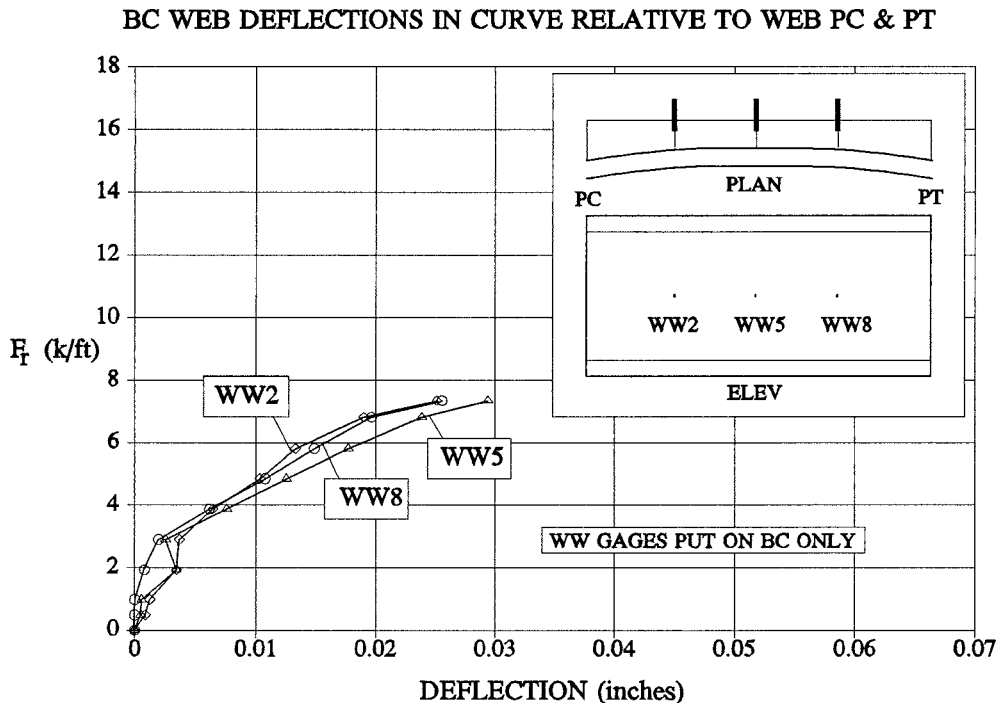


Figure 6.57 BC Web Deflections in Curve Relative to Web PC & PT.

potentiometers were attached to a bar that was connected to the mid-height of the web at the PC and PT.

The load-deflection curves for all three potentiometers were very similar [Figure 6.57]. At a load of 1.93 k/ft, WW5 and WW8 inexplicably showed a large increase in deflection and then decreased deflection at the next load stage (2.91 k/ft). After this load stage, all the curves showed a marked decrease in slope. The curves became trilinear as slopes decreased slightly at the last load stage prior to ultimate.

As expected, the WW5 potentiometer which was positioned at the mid-point of the curve deflected more than the two potentiometers located on either side. However the deflection at WW5 was only slightly greater than the WW2 and WW8 deflections. At the ultimate load, WW5 was only 17%

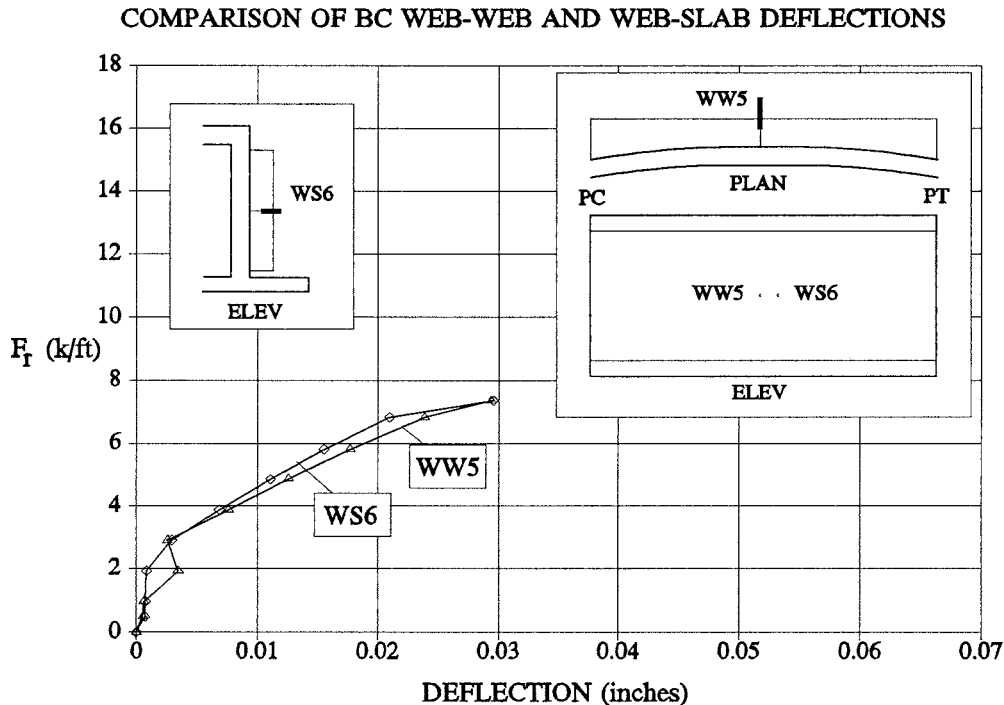


Figure 6.58 Comparison of BC Web-Web and Web-Slab Deflections.

greater than WW2 and 15% greater than WW8. Since the deflection at the midpoint was not significantly greater than at the quarter-points, it appears as though there was not significant flexural action carrying the force to the boundary elements created by the PC and PT.

6.4.3 Comparison of Web-Slab and Web-Web Potentiometers

The specimen BC WS6 and WW5 load-deflection curves are plotted in Figure 6.58. These potentiometers were located approximately 3 inches apart near the midpoint of the curve and at the mid-height of the web. Since they were considered to measure the deflection of the same point, they provided insight into the behavior of the boundary conditions. The curves were nearly identical except for the jump in deflection of the WW5 gage at $F_r = 1.93$ k/ft. The WW5 gage deflected only slightly more than the WS6 gage at the middle

to latter load stages. The fact that the curves were so nearly identical indicates that the web at the PC and PT deflected little relative to the top and bottom slabs at the midpoint of the curve. Hence the PC and PT portions of the web did indeed act as boundary elements.

6.5 DEMEC GAGES

During the test of specimen BC, longitudinal concrete strains were measured at the mid-point of the curve using a demec gage. Each set of points was read twice (each time by a different person) to reduce the chance for incorrect readings. The strains were measured over an approximate 8" length at the corners of the box and at the mid-height of the duct group [Figure 6.59].

The plots show a general trend of linear, increasing strains at the corners. The gages on the loaded web corners (#1 and #3) were in compression and the gages on the opposite web (#4 and #5) were in tension. The loaded web corner readings were very similar and of a magnitude about equal to the opposite web readings. The demec gage adjacent to the ducts (#2) measured very high compressive strains relative to the loaded-web corner readings. The reading in this gage at a load of 0.97 k/ft appears to be in error.

The concrete strain variations across the cross-section indicate that there was not a uniform compression force on the section. This appears reasonable since the section was loaded unsymmetrically about the vertical centerline of the box. However it is interesting to note that the strain was not uniform along the height of the loaded web. The mid-height of the web experienced up to four times as much compression strain as the corners of the box. Since the compressive strains were not uniform on the loaded web, it

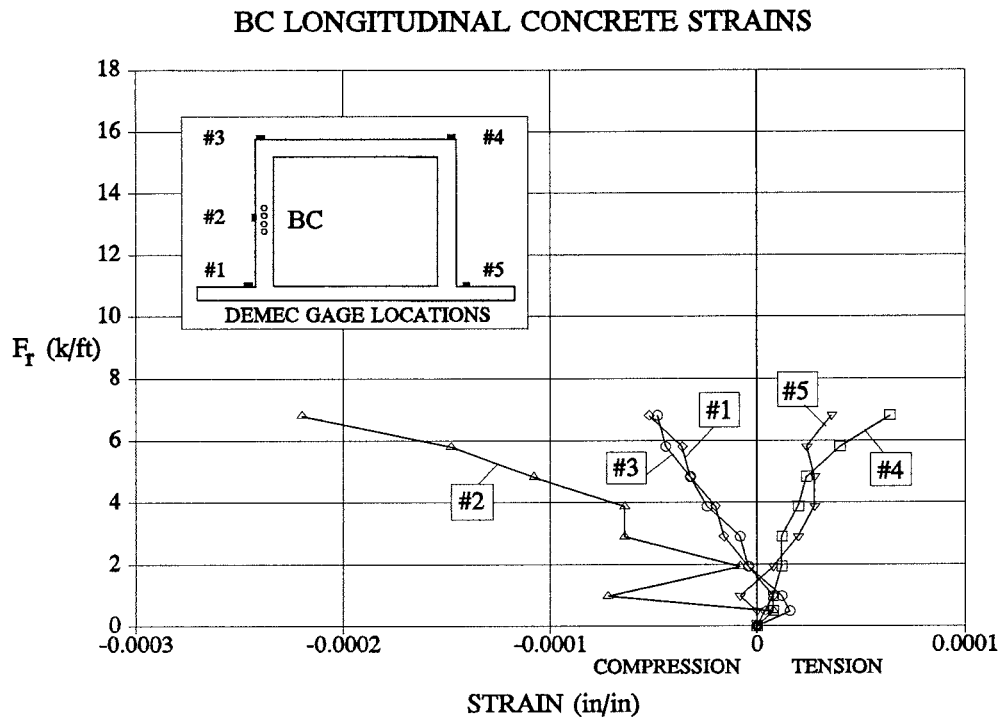


Figure 6.59 BC Longitudinal Concrete Strains.

follows that the compressive arch stresses were also non-uniform. The compressive arch stresses were likely higher at mid-height than at the top and bottom of the web.

CHAPTER 7: FAILURE THEORIES AND DESIGN RECOMMENDATIONS

This chapter compares the failure theories discussed in Chapter 2 to the observed behavior of the test specimens. Based on the observations from the tests and previously published failure analyses and design guidelines, a series of design and detailing recommendations are proposed.

7.1 REGIONAL BEAM ACTION

Regional beam action as discussed in Section 2.2.2 is the phenomenon whereby the lateral loads due to post-tensioning are transferred to the overall girder cross-section by the web acting as a flexural member supported by the top and bottom flanges [Figure 7.1]. The flexural capacity of the web, as a regional beam, was investigated although the shear capacity was not. Any shear failure is assumed to be controlled by the lower capacity of local beam action. Since the local beam has a smaller depth of shear plane than the regional beam, shear failure is more critical in the local beam.

None of the four test specimens failed as a result of regional beam action since:

- 1) The failure planes were not indicative of flexural failure.

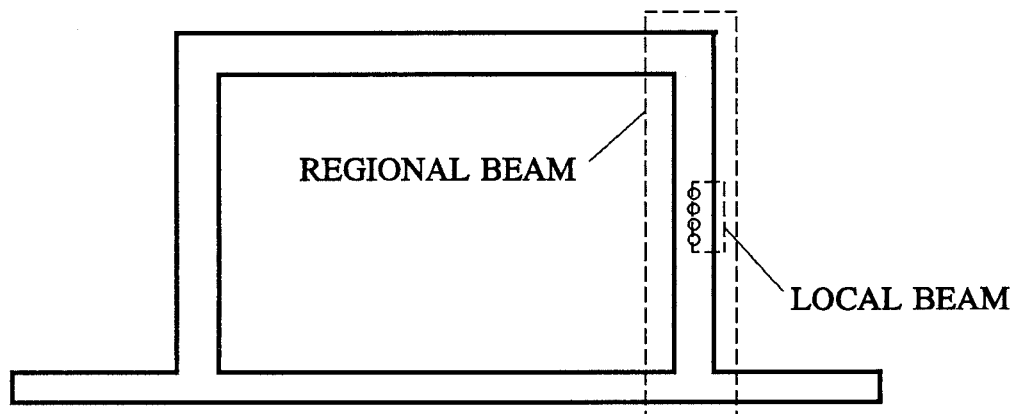


Figure 7.1 Regional Beam and Local Beam Actions.

- 2) Only one stirrup strain gage in one test (1.0DC) reached yield at the ultimate load. This was primarily due to large delaminations which reduced the flexural integrity of the section. Since the sections were greatly underreinforced, flexural failures would have required yielding of the stirrups.

As discussed in Chapter 2, there are two common methods for calculating the bending moments on the web as a result of the lateral post-tensioning force. In the Las Lomas and Kapiolani investigations, TYLI analyzed the cross-section as a frame loaded with the lateral post-tensioning force and the arch compression force. CALTRANS uses as a design equation $M=PL/5$ without consideration of arch compression forces. This discussion compares the results of these methods to the measured moments and deflections of the test specimen 1.0DC.

The web mid-height moment due to post-tensioning was calculated using the TYLI and CALTRANS methods and compared to the observed moment as determined from computations based on the strain gage data. The test data used was from specimen 1.0DC because it had widely separated ducts which allowed for complete horizontal shear transfer between the

compression and tension faces of the web. As a result the flexural integrity of the web was maintained through a large load range. The other three specimens had essentially a single large void which disrupted the horizontal shear transfer and resulted in complex, uncertain member stiffness calculations. Also, these three specimens had local beam stresses affecting the IM strain gage stresses. Specimen 1.0DC had no local beam action occurring as evidenced by the lack of delamination until just prior to failure [Figure 6.35]. Specimen 1.0DC IM strains are assumed to be the result of regional beam flexural strains only.

7.1.1 Frame Analysis

A frame analysis was performed on an uncracked, 1 foot long section of the box. The cross-section was loaded with the largest load sustained by 1.0DC without cracking (3.01 k/ft) so that calculated web deflections for the uncracked section could be compared with measured values. In fact, since the response of the section to loads was linear, the actual load level chosen was not that critical. The response for any other load can be easily determined as a linear proportion.

Since the box was loaded unsymmetrically, it was necessary to take into account the force eccentricity when calculating the arch compressive force [Figure 7.2]. The longitudinal compressive stress due to post-tensioning was calculated at the centerline of the loaded web by summing C_j/A and C_jey/I_{yy} . The lateral component acting as a distributed force on the entire height of the web was calculated by multiplying this stress by the web thickness and dividing by the radius ($C_{arch\ web} = -0.0384$ k/in). Values used for generating the stiffness matrix included a modulus of elasticity based on $f'_c = 5900$ psi ($E = 4400$ ksi), uncracked, non-transformed members ($I_{web} = I_{top\ slab} = 64$ in⁴ and $I_{bottom\ slab} = 27$ in⁴) and member lengths extending to the centroid of connecting members

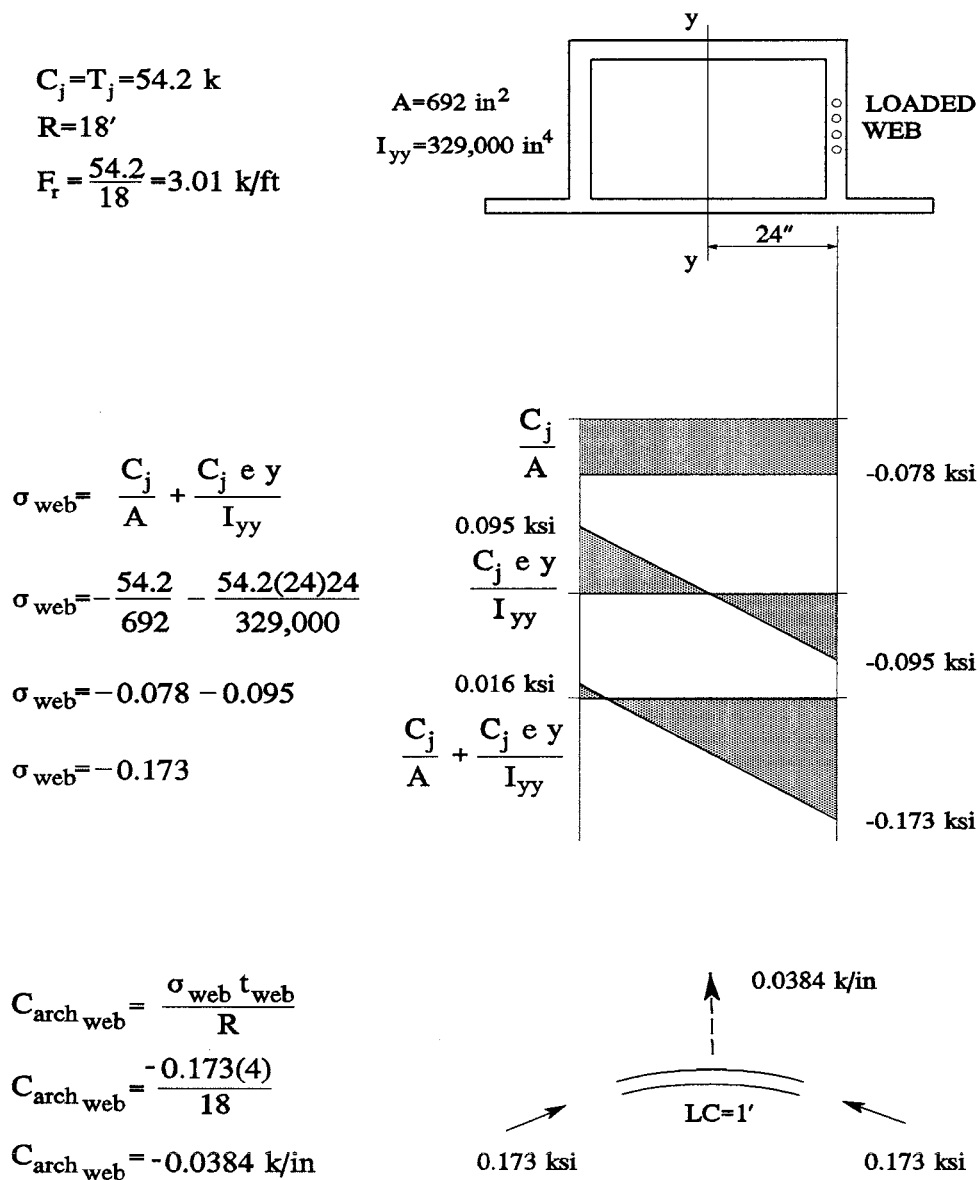
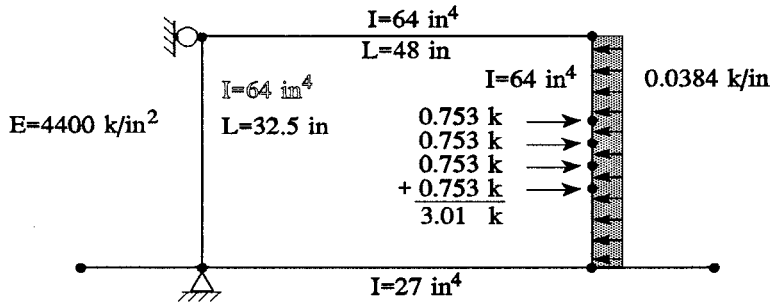
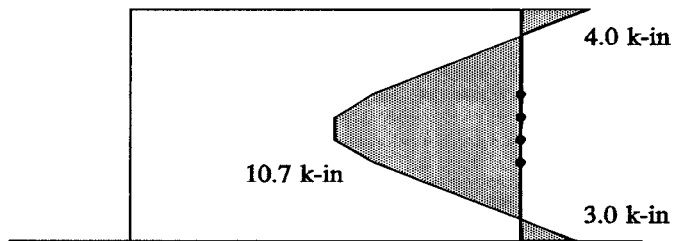


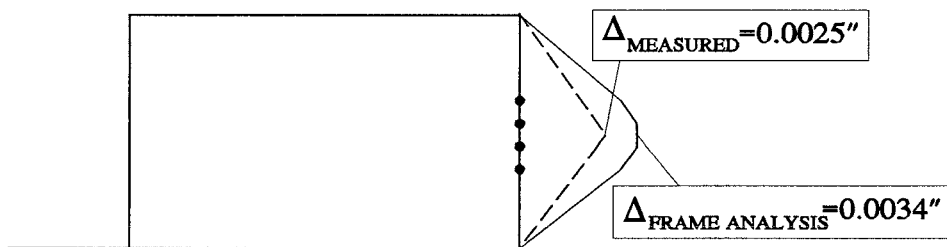
Figure 7.2 1.0DC Compression Arch Forces on Web at Microcracking Load.



FRAME MODEL OF 1' SECTION OF SPECIMEN 1.0DC



CALCULATED MOMENTS ON LOADED WEB



DEFLECTION OF LOADED WEB

Figure 7.3 1.0DC Frame Analysis at Microcracking.

[Figure 7.3].

The computed moment for the largest load sustained without cracking from the frame analysis at the mid-height of the web was 10.7 k-in and deflection was 0.0034". Since uncracked section properties are often assumed to provide correct relative stiffness values for design loads greater than member cracking loads, the analysis results were extrapolated to calculate the moment that corresponded to the ultimate lateral force applied to the specimen ($F_r = 16.8$ k/ft). This moment would be $M_u = 59.7$ k-in [Figure 7.6].

7.1.2 CALTRANS Analysis

The CALTRANS ultimate moment design calculation is much simpler than the frame analysis approach. Using the design equation of $M = PL/5$, the moment at the largest load that sustained moment without cracking, $F_r = 3.01$, ($M_{cr} = 19.6$ k-in) and at the ultimate lateral load ($M_u = 109$ k-in) were easily calculated [Figure 7.6].

7.1.3 Specimen 1.0DC Test Results

The actual moments occurring in the test specimens have to be computed from measured strains assuming an appropriate flexural theory. In this study, moments were calculated for the uncracked section using an average of the strains measured in gages 4IM and 6IM [Figure 7.4]. These gages were on the two stirrups that were on either side of the midpoint of the curve and were located at the mid-height of the web [Figure 5.10]. The uncracked section moments were calculated using a 1 foot wide, transformed section considering both tension and compression steel. At first crack, the indicated moment was 13.1 k-in.

After first cracking, the indicated moments were calculated assuming cracked section theory for a singly reinforced cracked section [Figure 7.5]. Since the web was so lightly reinforced ($\rho = 0.002$), a value of $j = 0.95$ was

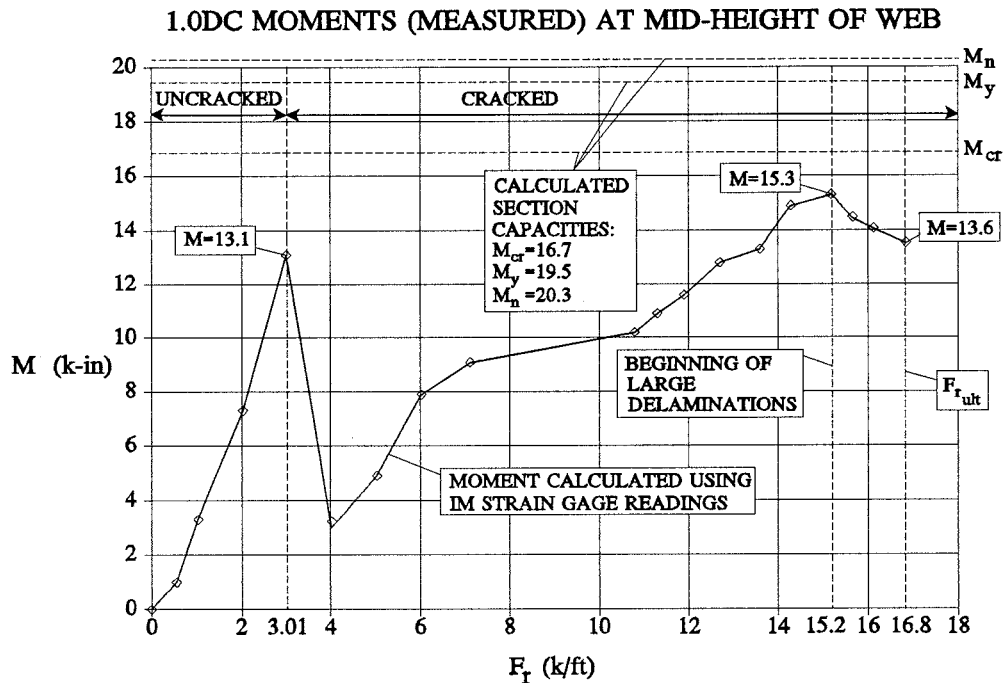


Figure 7.4 1.0DC Moments (Measured) at Mid-Height of Web.

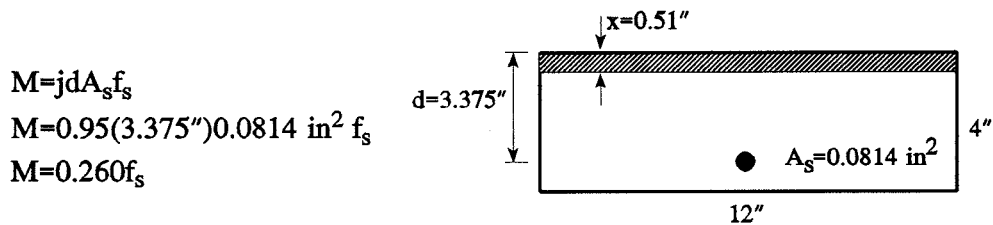


Figure 7.5 Web Cross-Section For Calculating Moments After Cracking.

assumed. Therefore the indicated moment is given by $M = A_s f_s j d = A_s (\epsilon_s E_s) 0.95 d$. The moment at the ultimate load carried by the specimen ($F_r = 16.8 \text{ k/ft}$) was 13.6 k-in [Figure 7.4]. This is not to be confused with the computed ultimate moment capacity of the section; it is merely the moment

indicated by the strain measurements present at the mid-height of the web at the time of the shear failure. The largest indicated moment carried by the web ($M=15.3$ k-in) actually occurred at a load level of $F_r=15.2$ k/ft. This load level was the last before large web delaminations began. After this load level, the flexural integrity of the web was reduced and a partial hinge formed causing a redistribution of moments.

The section capacities of a 1 foot wide strip of the web were also calculated. The cracking moment capacity ($M_{cr}=16.7$ k-in) was calculated based on a cracking stress of $7.5\sqrt{f'_c}$ and an uncracked transformed section moment of inertia. The yield moment ($M_y=19.5$ k-in) was based on a calculated value of $j=0.95$. The nominal moment capacity of the web was 20.3 k-in.

7.1.4 Comparison of Analysis and Test Results

Figure 7.6 shows a comparison of the moments determined from the linear frame analysis and the CALTRANS empirical method with the measured moments from specimen 1.0DC. As can be seen, the frame analysis was fairly accurate as long as the web remained uncracked. The CALTRANS design equation moments substantially exceeded the measured moments before cracking. After cracking, both methods greatly overestimated the measured moments on the web.

The two analysis methods were used before the beginning of testing to predict the failure load due to regional beam action based on a nominal moment capacity of 20.3 k-in [Table 7.1]. The frame analysis method predicts failure at $F_r=5.71$ k/ft. The CALTRANS design method predicts failure at $F_r=3.12$ k/ft. The actual lateral prestress load was $F_r=16.8$ k/ft which greatly exceeded both predictions.

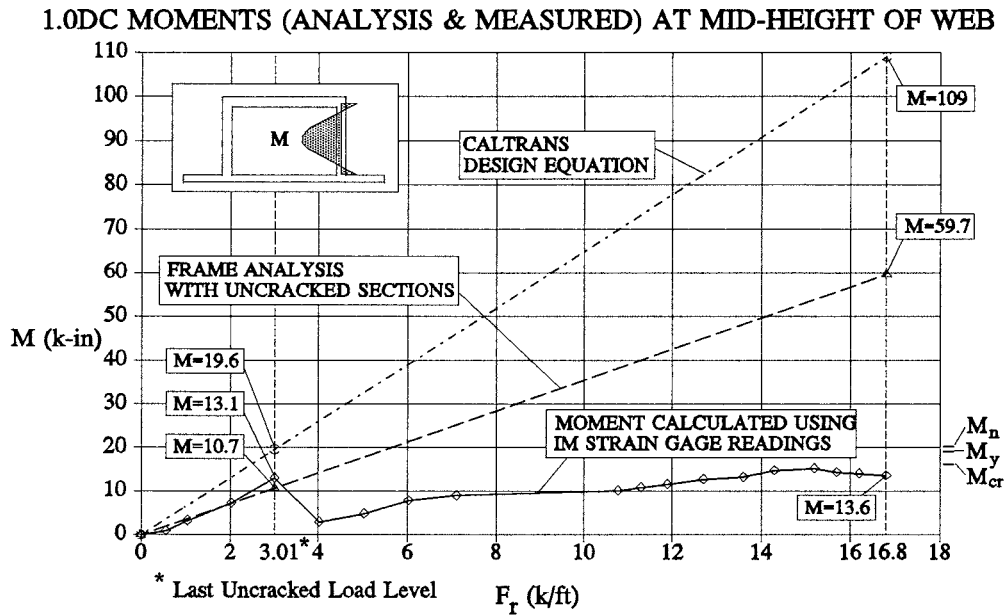


Figure 7.6 1.0DC Moments (Analysis & Measured) at Mid-Height of Web.

Table 7.1 Regional Beam Analysis and Measured Loads.

LATERAL PRESTRESS FORCE		
MAXIMUM DESIGN LOAD FROM CALTRANS EQUATION (k/ft)	FAILURE LOAD FROM FRAME ANALYSIS (k/ft)	MAXIMUM MEASURED LOAD IN 1.0DC (k/ft)
3.12	5.71	16.8

The measured deflection at a lateral load of $F_r=3.01$ k/ft was 0.0025". This was an average of the potentiometer readings at WS4 and WS6 and was somewhat less than the frame analysis calculated deflection of 0.0034" [Figure 7.3].

7.1.5 Longitudinal Arching Action

As shown in Figure 7.6, the web moments behaved consistently with the frame analysis until microcracking began. However once cracked, its behavior was no longer consistent with that of a laterally loaded member in an elastic frame. The moment decreased from 13.1 k-in to 3.0 k-in and then began a slow ascent with increasing lateral load.

A clue to understanding the behavior was found in the Demec longitudinal strain readings of specimen BC. No readings were taken on specimen 1.0DC because this was the first specimen tested and such large regional beam capacity was not anticipated. While precise numerical values of BC strain readings cannot be utilized for 1.0DC, the general behavior is assumed to have existed in both specimens.

Figure 7.7 shows the 6IM strain gage readings juxtaposed on the Demec strain readings. The strain gage measured vertical strains and the Demec points were used to measure longitudinal strains. At a lateral load of $F_r=1.93$ k/ft, the vertical strains at 6IM began to increase sharply. This coincided with large increases in longitudinal strains as measured at Demec point #2 (a large longitudinal strain was measured at a load of $F_r=0.97$ k/ft but this appears to be an aberration). At higher load levels, strains at the mid-height continued to increase faster than the strains at the four corners of the box. At the ultimate lateral load, the strains at points #1, #3, #4 and #5 were significantly less than the strains at point #2.

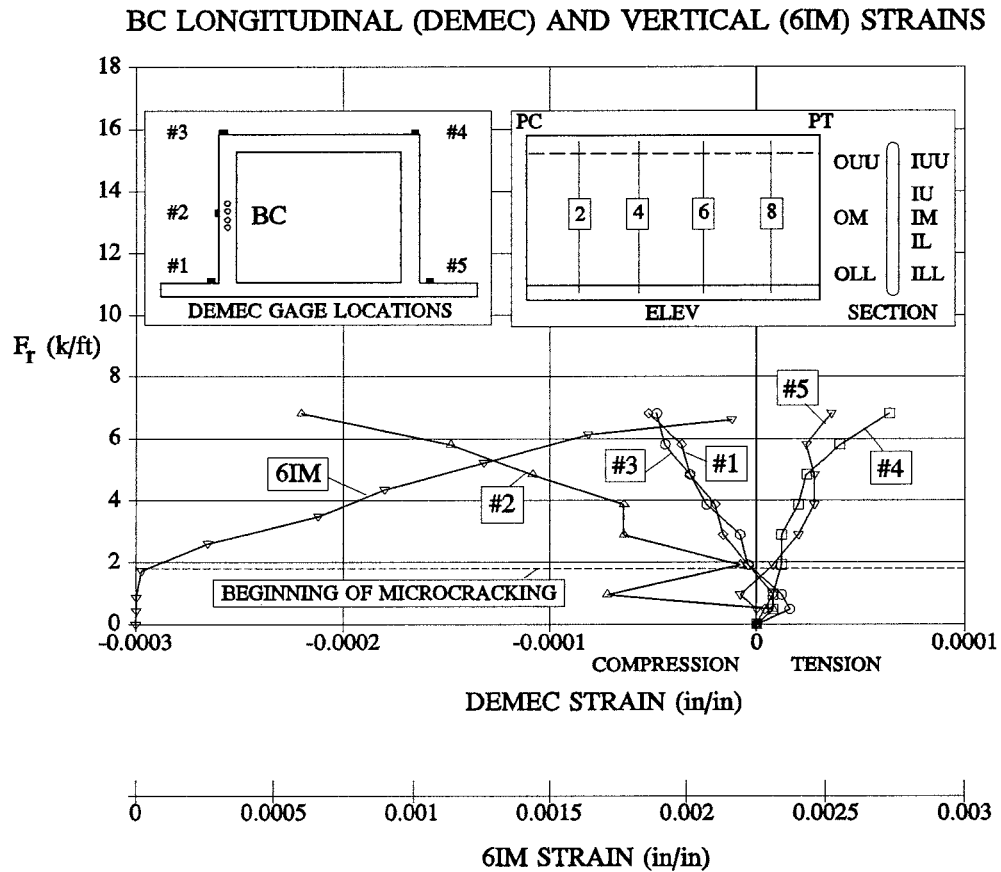


Figure 7.7 Longitudinal and Vertical Strain Relationship at Mid-Height of Web.

The large variation in longitudinal strains on the loaded web after microcracking indicates that the compression stress in the web was not uniform. As a result, the compression arch stress opposing the lateral prestress load was greatest at the mid-height of the web. The exact distribution of this stress is not accurately known but was perhaps similar to that shown in Figure 7.8. The uniform distribution of compression arch stresses is valid for uncracked sections but not for cracked sections.

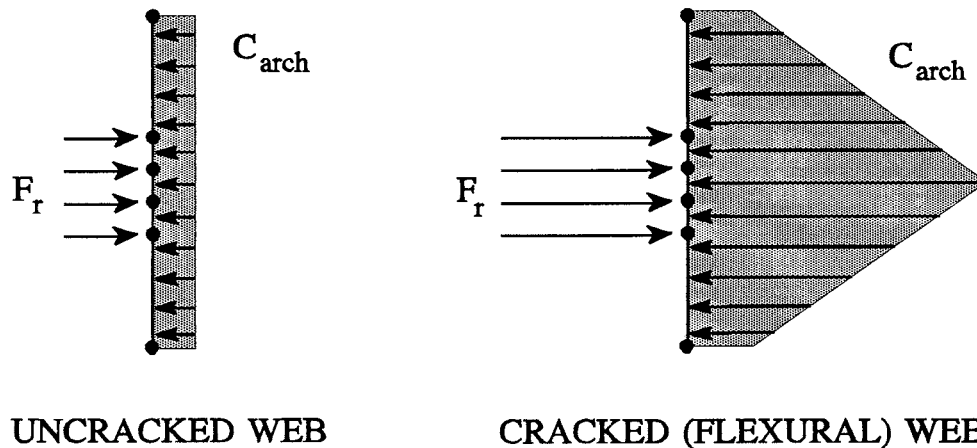


Figure 7.8 Compression Arch Force Distribution on Cracked and Uncracked Web.

As previously shown in Figure 6.55, after microcracking occurred, the stiffness of the web decreased and the deflection began to increase more rapidly. However the indicated moments in Figure 7.6 show that the deflection was not great enough to develop an internal moment on the cracked section that exceeded the nominal moment capacity of the web. Since the web was lightly reinforced, the cracking moment (16.7 k-in) was very nearly equal to the yield moment (19.6 k-in). In a simple beam test of this section where the loading was held constant and the beam was free to deflect, the reinforcement stresses would have immediately increased to more than 50 ksi with the onset of cracking. However in specimen 1.0DC, the measured strains indicated that the stress in the stirrup (6IM) only increased from about 3 ksi to 10 ksi upon cracking. The deflection was restricted by the increased compression arch stresses at mid-height [Figure 6.45].

Perhaps a clearer way of understanding the behavior is to consider the development of a new load path. Before cracking, the flexural stiffness due

to frame action was greater than the stiffness of a so-called longitudinal arch. However once cracking occurred, the longitudinal arch stiffness was greater than the flexural stiffness of the cracked vertical beam. Therefore the load was carried principally by longitudinal arching. Since the out-of-plane load applied to the uniformly curved box was radial, the longitudinal arching caused pure compression. This was a highly efficient means of carrying load for the concrete. For prestressed girder design it is unlikely that a compression failure of this sort could ever occur.

This is not to say that a regional beam flexural failure could not happen. It may be possible to have a very long curve and a thin web that is lightly reinforced. The stiffness of the longitudinal arch is dependent on the length of curve. It could be so long such that moments exceeding the ultimate capacity developed before adequate longitudinal arching occurred. It is difficult to extrapolate the results of these tests to all combinations of curve lengths, web heights, web thicknesses and reinforcement ratios. It should be made clear that the curved length of specimen 1.0DC was only 5 feet long. This scales to a 15 foot curve length in a prototype. However the portion of Las Lomas bridge on the curve was about 100 feet. The test specimen therefore had a very stiff longitudinal arch that prevented large mid-height deflections. It should also be noted that substantially more deflection was required to reach the ultimate moment of the section. The yield moment was not reached at the ultimate load; the web could have withstood additional deflection before reaching the yield stress of the stirrups at mid-height. Significantly more deflection would have been required to yield the stirrups at the top and bottom of the web. Still more deflection would have occurred before reaching the ultimate capacity at mid-height because the section ductility for the web was very large ($\rho_y/\rho_u=22$).

7.2 LOCAL BEAM ACTION

Local beam action is the behavior of the cover adjacent to the duct group on the inside face of the curve when loaded laterally by the tendons. This section extends along the height of the duct group and is subjected to moments and shears as described in Section 2.2.3. By virtue of the soundness of the concrete surrounding the ducts in 1.0DC, no local beam bending occurred in this specimen. However since the failure plane passed through the top and bottom ducts, specimen 1.0DC is addressed in the shear discussion of the local beam.

7.2.1 Bending

Understanding the local beam bending in tests of specimens BC, 0.2DC and BO is very complicated for the following reasons:

- 1) The strain gages placed on the stirrups were very near the neutral axis of the uncracked section. This caused calculated stresses on the extreme fibers to be imprecise.
- 2) The local beam region was very small (for specimen BC: height of duct group=7.25" and minimum cover=1.125") and known behavior of larger beams may not transcend to beams of this size.
- 3) The thickness of the local beam varied from 1.125" to 2". Therefore the uncracked moment of inertia of the local beam varied by a factor of 5.6.
- 4) The strains measured on the stirrups were not the result of local flexural stresses alone. Regional beam stresses, which can be significant, were a maximum at the mid-height of the web.
- 5) Calculating the actual regional beam moments was complicated by the single, large void that is inherent in webs with closely grouped tendons.

- 6) The compressive arch stresses on the inside face may have significantly affected local bending. The compressive arch stresses may have been greater on the inside face than those measured on the outside face due to local beam deflections which in some instances exceeded the regional beam deflections. For reasons of safety, the longitudinal concrete strains were not measured on the inside face of the web.

Because of these factors, a detailed analysis of the structural response by conventional means would have been dubious. However a few general observations on local beam behavior can be made.

Local beam bending does appear to exist and the stresses are significant. Before cracking was initiated, there was little difference in the stresses recorded in the four specimens. However after cracking, larger stirrup stresses were recorded in and near the local beam in specimens BC, 0.2DC and BO than in the same locations in specimen 1.0DC. Recall that specimen 1.0DC had no local bending stresses as indicated by the straight delamination profile [Figure 6.35]. As an example of the effect of local bending, at a lateral prestress force of approximately $F_r = 7$ k/ft, the stirrup stresses at the mid-height of the local beam (6IM) were in the range of 45-55 ksi for specimens BC, 0.2DC and BO but were only about 25 ksi for 1.0DC [Figure 6.42]. The stirrup stresses just outside the local beam region (6IU) varied from 18 to 30 ksi in specimens BC, 0.2DC and BO but were only 3 ksi in 1.0DC at the same load [Figure 6.44]. Furthermore the delamination profiles of BC, 0.2DC and BO show larger deflections in the middle of the duct group than at the ends.

While local bending was clearly present in specimens BC, 0.2DC and BO, it was not believed to be the cause of failure for the same two reasons as discussed in Section 7.1. The failure planes were not indicative of flexural failure and the stirrup stresses did not reach yield in any of the specimens with

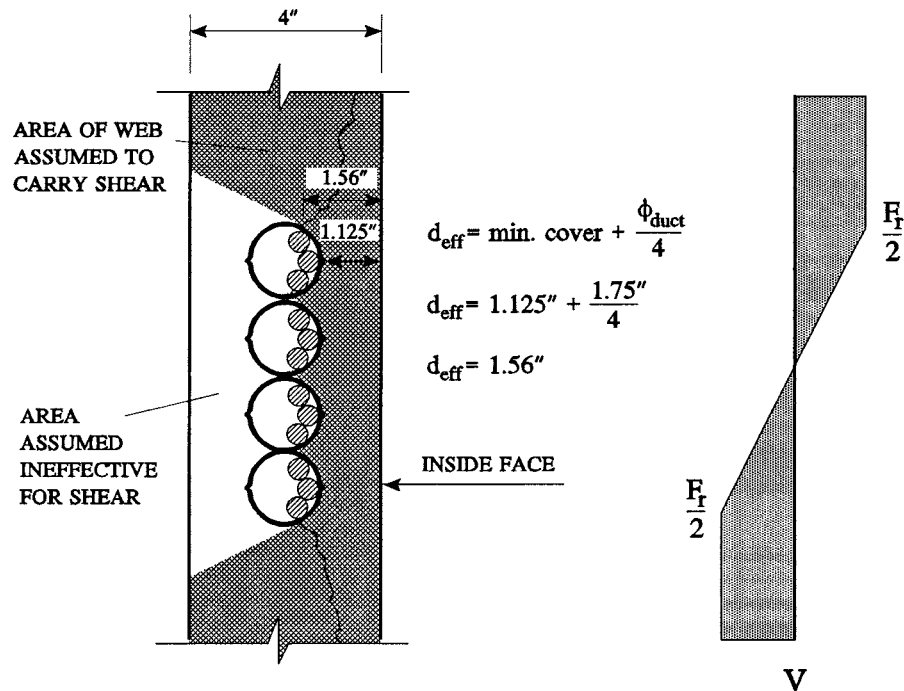


Figure 7.9 BC Effective Shear Plane Depth.

local beam action (BC, 0.2DC and BO) until after the ultimate capacity was reached. Since the section had an area of reinforcement equal to about one-half of the area of reinforcement required for a balanced section, flexural failure could only occur if the reinforcement (stirrups) yielded.

7.2.2 Shear

Shear is considered to be basically a local beam phenomenon because shear stresses were highest in the local beam region. High shear stresses occurred in the local beam because of the presence of the voids created by the ducts and the load location. Since the load was applied from within the web, the outside half of the web behind the local beam was ineffective for carrying shear in specimens BC, 0.2DC and BO [Figure 7.9]. For specimen

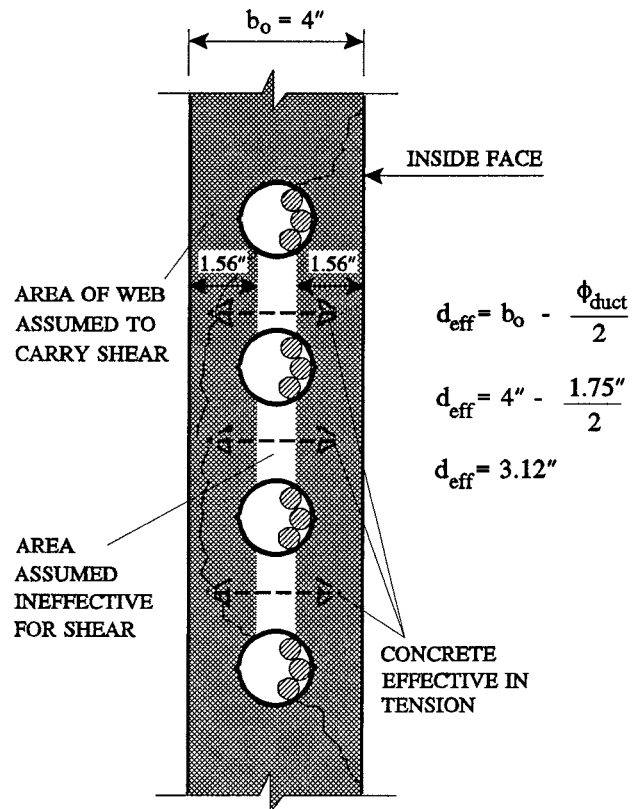


Figure 7.10 1.0DC Effective Shear Plane Depth.

1.0DC with widely spaced ducts, the concrete could have sufficient tensile capacity to transfer load to the outside portion of the web in the duct region [Figure 7.10]. This was evidenced by the single panel of concrete that delaminated from the web [Figure 6.6].

All specimens are considered to have failed in shear for the following reasons:

- 1) The failure planes were characteristic of diagonal tension failure
- 2) The relationship between web delamination and ultimate load was typical of diagonal tension failure.

- 3) The concrete shear stresses at ultimate were close to design recommendations.

7.2.2.1 Diagonal Tension

Shear failures typically begin with a 45 degree inclined crack called a diagonal tension crack [18]. If the beam fails at the load that causes this crack (or at a slightly higher load), diagonal tension failure is said to have occurred. Some beams have the ability to carry more load if the internal forces can redistribute within the uncracked flexural compression zone. A beam that can transmit significantly greater loads into the compression zone may ultimately fail by crushing of the concrete. This is called shear-compression failure. Diagonal tension failure usually occurs in simple beams with a shear span-to-depth ratio (a/d) between 2 and 6. At these ratios, significant moments and therefore tensile stresses are present which combine with the shear stresses to increase the principle diagonal tension stress. Shear-compression failure usually only occurs if the a/d ratio is below 2.5.

The failure planes were indicative of shear failure in all tests. The plane emanated from the top and bottom ducts at about a 45 degree angle [Figure 6.10]. The angle became steeper as the crack neared the inside face of the web. Tests have shown that diagonal tension cracks can have an S-shaped appearance [17]. This S-shaped appearance was more elongated for specimens BC and 0.2DC. It is not known why these two failure planes extended out to near the "supports" at the top and bottom flanges and the other two specimens did not. Perhaps it was related to the fact that they failed at low loads and the tensile steel (stirrups) remained viable. In specimen 1.0DC, the failure was explosive as the stirrups pulled out at the lap.

Every specimen reached ultimate at a load not greater than 10% more than that which initiated delamination in a high shear region. This is shown

by the extrapolated web delamination profiles. There was no delamination at the bottom of the duct group when BO reached ultimate, but large delaminations occurred at the next stressing operation as the actual load decreased slightly [Figure 6.41]. BC reached ultimate at the first load stage after the projected cracking began at the bottom [Figure 6.40]. Specimen 1.0DC showed some ability to redistribute loads as it sustained two and possibly three load stages after apparent cracking below the bottom duct [Figure 6.39]. There is no extrapolated delamination profile for specimen 0.2DC because of aberrant readings from gage D62. However based on the similarity of the delaminations above the top of the bottom duct (D61) in specimens 0.2DC, BC and BO, it appears as though the behavior of 0.2DC at the bottom of the local beam was quite like the others [Figures 6.36, 6.37 and 6.38].

As mentioned in Section 6.2.3, all specimens delaminated at the top of the top duct prior to delaminating at the bottom of the bottom duct. This may have been due to the systematic stressing operation which could have caused the top strands to seat at a higher stress. Nonetheless, failure was not dependent on when the first of the local beam failure planes delaminated but when the second delaminated. In fact all but specimen BC sustained at least three load stages after delamination began at the top (D64). This was likely due to the fact that the web was statically indeterminate and the load was able to distribute to the lower, uncracked end of the local beam.

7.2.2.2 Shear Capacity

Tests on beams without web reinforcement have shown that shear capacity is dependent on $\sqrt{f'_c}$, ρ and $\frac{Vd}{M}$ [18]. $\frac{Vd}{M}$ is a simplified way of representing the magnitude of the flexural tensile stresses relative to the shear stresses. Beams with large reinforcement ratios and small flexural tensile

stresses (large $\frac{Vd}{M}$) can sustain high shear stresses. This is because the tension stress on the concrete is small and therefore the principle diagonal tension stress is low. Only the shear stress greatly affects the diagonal tension stress in this case which allows for a large concrete shear capacity. The relationship of these three parameters is expressed in AASHTO equation 8-48:

$$V_c = (1.9\sqrt{f'_c} + 2500\rho_w \frac{V_u d}{M_u}) b_w d$$

The applicability of this equation for these tests is somewhat uncertain because of the large voids created by the ducts. Further doubts are raised for specimens BC, 0.2DC and BO because of the small size of the local beam section and unknown moments. However it is assumed that the basic relationship between these three parameters still exists and a comparison of the shear capacities can be made without the direct use of equation 8-48. That is to say that specimens with the highest concrete strength and lowest concrete tensile stresses should sustain the greatest shear stresses at failure.

It was not necessary to calculate moments and $\frac{Vd}{M}$ values. Strain gage readings at the IL gage provided a more direct means of measuring concrete tensile stresses. As it so happened, the stresses in the gage nearest the bottom of the bottom duct (6IL) were quite similar for all the tests [Table 7.2]. It was also unnecessary to calculate ρ as the stirrup spacing was the same for all specimens. Therefore the difference in capacities of the four specimens should be principally related to $\sqrt{f'_c}$ and the effective shear plane depth.

Establishing the effective depth of the shear plane was critical to the calculation of the shear stress at failure. This was done by carefully examining

Table 7.2 Calculated Coefficient for $\sqrt{f'_c}$

COMPARISON OF COEFFICIENT FOR $\sqrt{f'_c}$							
SPECIMEN	$F_{r(ult)}$ (k/lf)	V_u (k/lf)	f'_c (psi)	d_{eff} (in)	$\frac{V_u}{bd_{eff}\sqrt{f'_c}}$	ρ	f_t^* (psi)
1.0DC	16.8	8.4	5900	3.12	2.92	0.002	34
BC	7.35	3.67	6000	1.56	2.53	0.002	22
0.2DC	7.25	3.62	5000	1.56	2.73	0.002	28
BO	8.43	4.22	5300	1.94	2.49	0.002	33

b = 12"

* concrete tensile stress as measured by strain gage on stirrup (6IL)

the failure planes of all the specimens. The exact location of these planes varied along the length of the specimen. On all of the inside faces, the failure planes emanated from the surface of the ducts at a point about midway between the center and the edge nearest the inside face [Figure 7.9]. This coincided with the contact point of the outermost strand and the duct. For specimen 1.0DC, the crack also emanated on the back side about midway between the duct vertical centerline and the edge nearest the outside face [Figure 7.10]. Therefore as shown in Figure 7.9, d_{eff} was considered equal to the minimum clear cover of the ducts from the inside face, plus $\frac{1}{4}$ of the duct diameter for specimens BC, 0.2DC and BO. As shown in Figure 7.10, for specimen 1.0DC, this value was increased to also include the minimum clear cover of the ducts on the outside face, plus another $\frac{1}{4}$ of the duct diameter. More simply, it can be taken as the web width less $\frac{1}{2}$ of the duct diameter.

Table 7.2 shows a comparison of $V_u/bd_{\text{eff}}\sqrt{f'_c}$ for each of the specimens where V_u is one-half of the ultimate lateral prestress force. The values were remarkably similar for all the tests. They were also conservative and consistent with the coefficient used for the simplified concrete capacity equation (AASHTO eq. 4-49).

$$V_c = 2\sqrt{f'_c}b_wd$$

The value for specimen 1.0DC ($V_u/bd_{\text{eff}}\sqrt{f'_c} = 2.92$) was the largest as expected. Part of the failure plane crossed the flexural compression region (outside face of web). As mentioned previously, tests have shown that beams can carry loads beyond that which initiates diagonal tension cracking if internal forces can distribute into the flexural compression zone. The failure planes of the other specimens were located exclusively on the inside face of the web which was likely to be completely in flexural tension.

7.3 DESIGN RECOMMENDATIONS

There are many variables that contribute to the capacity of a web to resist lateral post-tensioning forces. These include length of curve, web height, web thickness, reinforcement ratio, concrete strength, the number and arrangement of ducts and special tie-back reinforcement. Unfortunately, the breadth of the problem is great and the scope of the research small. Due to limited resources only four pilot tests could be conducted to examine this multifaceted problem. None of the specimens had tie back reinforcement. The recommendations presented herein must be regarded as tentative but useful in the interim until further tests can be conducted. The author recognizes that there is still much to learn on this topic and has purposefully

kept many of the recommendations general. Hopefully further research will be conducted so that more specific design guidelines can be developed.

7.3.1 Regional Beam Failure

TYLI [6] has suggested that one possible mode of failure is for the web to fail in flexure as a laterally loaded member in a frame. A frame analysis was performed on an uncracked, one foot width of the test model cross-section (specimen 1.0DC). The web was loaded with the lateral post-tensioning force and an opposing arching force created by the effect of axial compression on a curved member [Figure 7.3].

This model was accurate until flexural cracking developed. However the test of specimen 1.0DC showed that after cracking, much of the load was no longer carried transversely by the flexural action of the web, but longitudinally by arching. The specimen carried a load 2.94 times greater than the maximum predicted by the regional flexural beam analysis when it failed in shear. The CALTRANS approach was even more conservative. The specimen carried a load 5.38 times greater than the design load calculated using the CALTRANS approach ($M=PL/5$)

It would be imprudent to offer a universal recommendation that relied on arching action to alleviate regional beam failure especially since the specimens had very short curve lengths. The relationship between the flexural bending stiffness of the web after cracking and the arch stiffness of the web is paramount in assessing the web flexural capacity. Since there are so many variables affecting these stiffnesses, each web must be examined on an individual basis.

In lieu of a complex, post-cracking analysis, an uncracked frame analysis similar to that shown in Section 7.1.1 is recommended. A load factor of 1.0 can be used because the beneficial effect of increased longitudinal

arching after cracking is neglected. The CALTRANS method appears overly conservative.

7.3.2 Local Beam Failure

7.3.2.1 Bending

Due to the complex nature of this failure mode as explained in Section 7.2.1, no conclusive design recommendations can be made. However detailing recommendations given in Section 7.3.3 may improve local beam behavior.

7.3.2.2 Shear

The AASHTO Guide Specification for Segmental Prestressed Concrete Bridges [9] and NCHRP 12-33 Development of a Comprehensive Bridge Specification and Commentary [10] both recommend that the factored load shear stress of the cover concrete be limited to $2\sqrt{f'_c}$. The results of these tests verify this value. Reference [9] implies that the minimum duct cover shall be used as the depth of the shear plane. Reference [10] allows the use of the minimum duct cover plus one half of the duct diameter. These tests showed that the shear planes actually intersected the ducts at a location approximately one-quarter of the diameter of the duct beyond the minimum cover. Effective shear plane depths are shown for various arrangements in Figure 7.11. When the clear spacing is less than one duct diameter, the effective depth shall be taken as the minimum clear cover towards the inside face of the curve as specified over the top or bottom duct plus one fourth of the duct diameter. Offsetting the ducts from the web centerline towards the outside face increases the effective depth as d_{\min} is increased.

For a minimum duct spacing equal to or greater than one duct diameter, two different shear planes can possibly develop. In the test of specimen 1.0DC, the shear plane at the top of the duct group began at the inside face and continued through the duct at about a 45 degree angle until

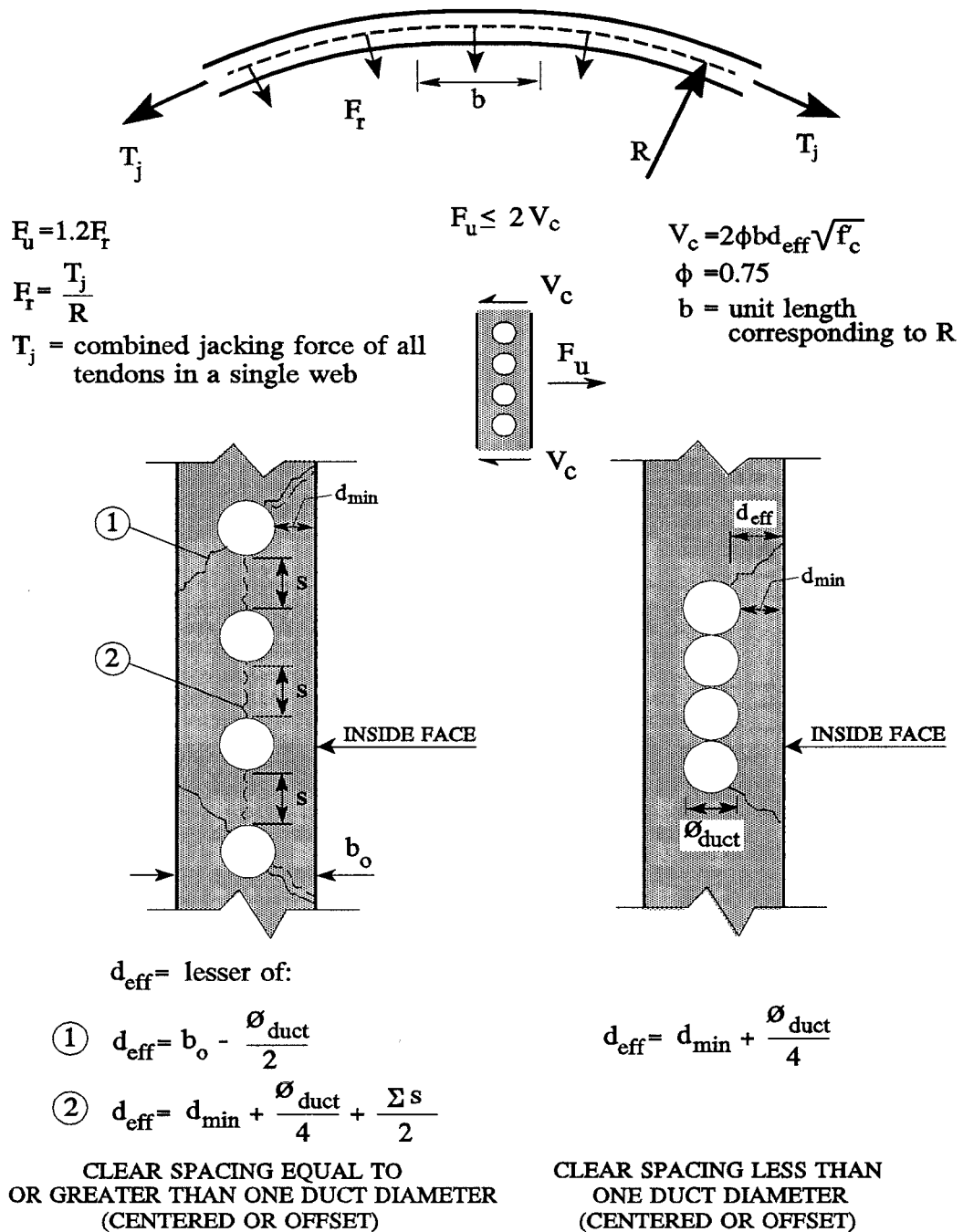
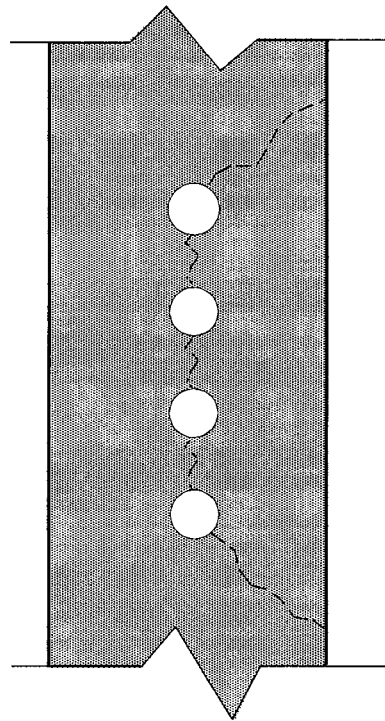
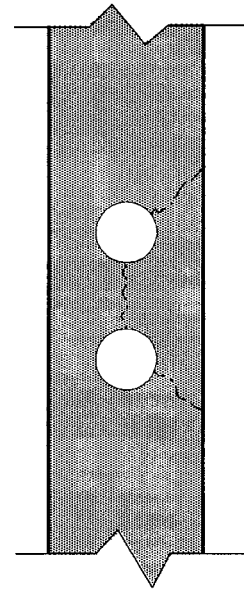


Figure 7.11 Shear Design Recommendation.



DUCTS ARE SMALL RELATIVE TO
WEB WIDTH



TWO DUCT ARRANGEMENT

Figure 7.12 Possible Failure Planes When Vertical Clear Spacing is Greater Than or Equal to One Duct Diameter.

it nearly reached the outside face. This is shown as Failure Plane #1 in Figure 7.11. For this case, the effective depth is the web width less one half of the duct diameter. Although there was only one test of a specimen with duct clear spacing greater than or equal to one duct diameter, the possibility that another type of failure plane could develop must be considered. Such a failure plane would involve shearing planes on the inside face and vertical tensile planes between ducts. This is shown as Failure Plane #2 in Figure 7.11. This type of failure plane might occur in a detail where the diameter of the ducts is small relative to the web width [Figure 7.12]. Here, the resistance

to failure along the vertical planes between the ducts might be less than that of two shear planes on the outside face. The same phenomenon might also occur in the case of a two or three duct arrangement. While the capacity along the vertical planes is not known with certainty, a conservative design stress of $2\sqrt{f'_c}$ appears appropriate. The effective depth of shear plane for this case is the minimum clear cover of the top or bottom duct plus one fourth of the duct diameter plus one half of the summation of vertical clear spacing between ducts (s). As a design recommendation, the effective depth of both planes should be calculated and the lesser value used in calculating V_c . This design recommendation is applicable for both centered and offset ducts.

For specimen 1.0DC, the effective shear plane depth for Failure Plane #1 is 3.12 inches. The effective shear plane depth for Failure Plane #2 is 4.19 inches. This procedure is in agreement with the test results as the actual failure occurred along the shorter failure plane (i.e. #1).

Table 7.3 shows that using the load factor (1.2) for post-tensioning and strength reduction factor for shear (0.75) proposed in Ref. [10] yields a factor of safety between 1.99 and 2.34 for these tests. The load and strength reduction factors seem quite reasonable. The tendon force is usually known and controlled with reasonable certainty. Therefore a low load factor is appropriate. A strength reduction factor below that normally used for shear is advisable since the small dimensions of the local beam region could be significantly reduced by movement of the ducts during casting. Furthermore, the quality of the concrete in a congested area could be reduced as demonstrated in the honeycomb that appeared in two of the specimens in this test.

Figure 7.11 summarizes the recommended design procedure for shear. The total factored lateral prestress force (F_u) must be less than or equal to

Table 7.3 Factor of Safety Provided by Shear Design Equation.

FACTOR OF SAFETY PROVIDED BY SHEAR DESIGN EQUATION						
SPECIMEN	$F_{r(ult)}$ (k/lf)	V_u (k/lf)	f'_c (psi)	d_{eff} (in)	$\frac{\phi}{1.2} V_c$ (k/lf)	$F.S. = \frac{V_u}{\frac{\phi}{1.2} V_c}$
1.0DC	16.8	8.4	5900	3.12	3.59	2.34
BC	7.35	3.67	6000	1.56	1.81	2.02
0.2DC	7.25	3.62	5000	1.56	1.65	2.18
BO	8.43	4.22	5300	1.94	2.12	1.99

$$V_c = 2bd_{eff}\sqrt{f'_c}$$

$$\phi = 0.75$$

$$b = 12''$$

the strength resistance factor times the sum of the nominal concrete shear strength above and below the duct group. The factored lateral prestress force is 1.2 times the jacking force in all the tendons (T_j) divided by the radius of the curve of the web in question. For most structures, the maximum force in the tendons occurs during jacking. If larger forces are anticipated, they should certainly be used in lieu of T_j . The equilibrium relationship assumes that the nominal concrete resistance of the top and bottom is the same, hence the coefficient 2. If the effective depth above and below are indeed different, the nominal shear strengths should be summed and the multiplier neglected. The longitudinal unit length (b), which must be given in inches, corresponds to the unit length of the radius used in calculating F_r (e.g. if R is in feet, then b is 12 inches).

For vertical clear spacings greater than zero but less than the duct diameter, this design recommendation provides for no increase in capacity over that of a bundled arrangement. This particularly applies to the common

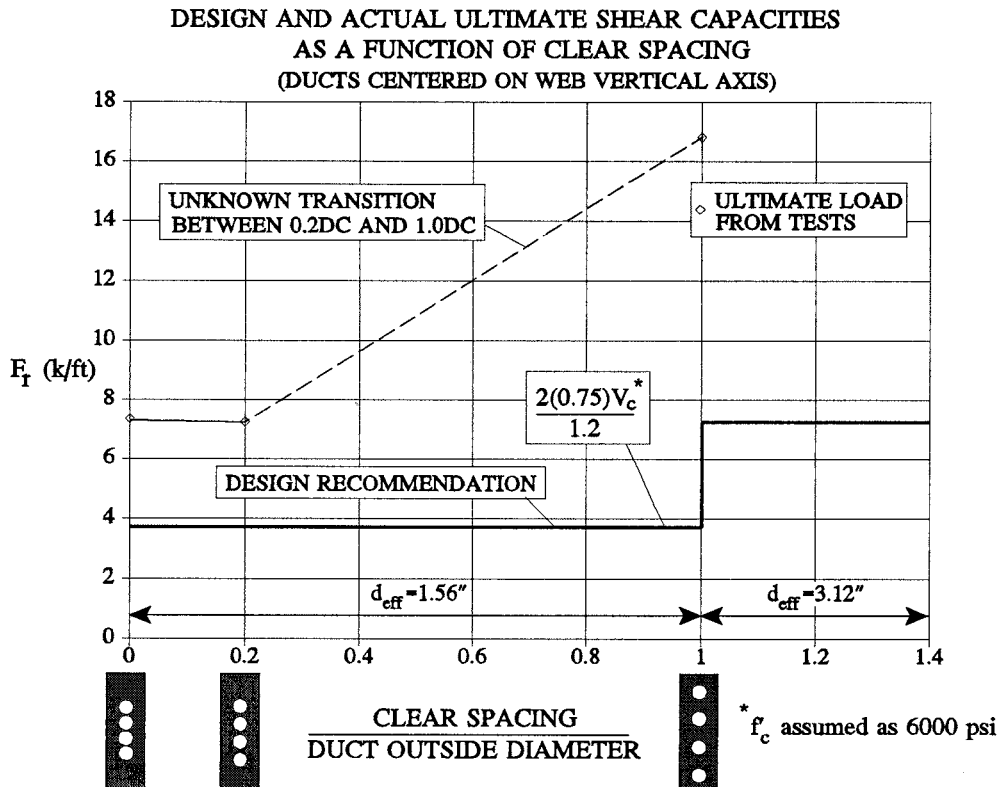


Figure 7.13 Design and Actual Ultimate Shear Capacities as a Function of Vertical Clear Spacing.

practice of spacing the ducts 1 inch apart. It is felt that shrinkage cracks could develop between closely spaced ducts and render the concrete unreliable in transferring forces to the back face of the web. Further research of duct spacings between 0.2DC and 1.0DC may show that the procedure for calculating the effective depth of shear plane for vertical clear spacings greater than or equal to one full duct diameter might be applicable for lesser spacings. It appears that the presence of shrinkage cracks limits this method to some as yet unknown vertical clear spacing.

Figure 7.13 shows the actual test ultimate lateral prestress load for specimens BC, 0.2DC and 1.0DC. The transition in ultimate load between

0.2DC and 1.0DC is shown as a straight, dashed line. However there is no basis in fact for the shape of this line due to a lack of data. Therefore the nominal concrete shear strength for an arrangement centered about the web vertical axis at a clear spacing less than one duct diameter is taken as half that for spacing of one duct diameter. V_c was calculated assuming that the concrete strength was 6000 psi. V_c has been reduced by the load and strength factors so that the factor of safety is evident.

7.3.3 Detailing

Attention to detailing the stirrups will likely improve the ductility of the web when resisting lateral prestress forces. The following are some suggestions:

1. Do not locate the stirrup lap on the inside face of the web.

The straight laps in these tests were placed on the inside face at the top of the stirrup. This was done to locate the lap in the regional beam compression zone at the top of the web instead of the tension zone. However this may have contributed to the explosive failure of specimen 1.0DC. It appears that once the shear failure began, the stirrup was pried out at the lap. It is believed that the best detail would be to use overlapping 180 degree hooks at the top or bottom of the stirrup. If straight laps are used, they should be located on the stirrup leg on the outside face of the curve.

2. Do not use double U-shaped stirrups to complete a hoop.

This may cause a splice to be located in the local beam region. Specimen BC closely represented a scaled model of Las Lomas. Las Lomas had proportionately less reinforcing and apparently some splices were indeed located in the local beam region. All of the splices in all specimens were located at the top of the stirrup. Las Lomas failed in a brittle manner and BC failed in a more ductile fashion.

3. Provide minimum flexural reinforcement. The web as a regional beam should contain enough reinforcement (e.g. stirrups) so that a brittle flexural failure is prevented once the

cracking moment is reached. This will also ensure that the local beam is adequately reinforced against a brittle failure.

4. Provide tie back reinforcement. The quantity and details of such reinforcement needs experimental verification, but application of strut-and-tie methodology indicates that tie back reinforcement should increase ultimate capacity. Tie back reinforcement would surround bundled ducts and anchor them into the full regional beam by intercepting the diagonal shear crack above and below the duct group.

5. Limit the number of bundled or closely spaced ducts. While bending of the cover concrete (i.e. local beam flexure) did not cause failure in these tests, it was clearly present and did create high stresses in the stirrups. In some details, local bending may preclude shear failure. Local bending is complex and no design methodology or specific details can be give at this time. However the problem appears greatly influenced by the number of ducts and limiting them to a reasonable number should improve the behavior of the cover concrete.

CHAPTER 8: SUMMARY AND CONCLUSIONS

8.1 SUMMARY

Lateral tendon forces can cause severe distress in the webs of curved, concrete box girders. Two known horizontally curved bridges in the United States (Las Lomas and Kapiolani) have required major rehabilitation costing millions of dollars. Both bridges were characterized by sharp horizontal curves, large internal tendon post-tensioning forces and bundled tendons. Bundled tendons are preferred for longitudinal flexural design because they allow for greater tendon eccentricity than can be achieved with tendons that are spaced vertically.

Failure theories have been proposed and some design recommendations made to better understand and prevent the lateral tendon breakout problem. These theories and recommendations had never been verified with physical tests. T.Y. Lin International (TYLI) investigated both failures and theorized that the concrete cover adjacent to the ducts acts as a local, vertical beam spanning the height of the bundle [6, 8]. TYLI indicates that this local beam was overstressed in bending and shear in both bridges. A secondary failure mechanism involving the web acting as a laterally loaded member in a frame supported at the top and bottom by the slabs was also investigated by TYLI. Using a frame analysis, TYLI showed that the stirrups

at Las Lomas and Kapiolani were overstressed as flexural reinforcement for the web acting as a regional beam. For design CALTRANS uses a simplified beam analysis to determine the regional beam moment on the web [7].

A test program summarized in this report was undertaken to investigate the effect of duct arrangement on lateral tendon breakout. The arrangement of ducts was investigated because it was considered the most easily changed of the three variables that were considered contributory to the breakout problem. The objectives of the test program were to determine the ultimate capacity of various duct arrangements, verify the existing failure theories or develop new ones and propose design recommendations.

Two $\frac{1}{3}$ scale box girders were constructed for testing. Each girder had two webs, so that the following four duct arrangements could be tested:

1.0DC - vertical clear spacing of ducts equaled one duct diameter

BC - bundled ducts

0.2DC - vertical clear spacing of ducts equaled 20% of one duct diameter

BO - bundled ducts offset to the outside of the curve

Each arrangement contained four ducts. The Texas Department of Transportation prefers the 1.0DC arrangement for all internal tendons. CALTRANS uses a combination of 0.2DC and 1.0DC along with tie back reinforcement to prevent a local failure.

Three $\frac{1}{2}$ " diameter prestressing strands were positioned in each duct and stressed simultaneously until failure.

8.2 CONCLUSIONS

The arrangement with ducts spaced with a vertical clear spacing of one full duct diameter (1.0DC) provided more than twice the ultimate capacity of the bundled and centered arrangement (BC). Spacing the ducts at 20% of a duct diameter (0.2DC) did not result in an ultimate capacity greater than that for specimen BC. Offsetting a bundled arrangement to the outside of the web (BO) increased the ultimate capacity over that for BC in proportion to the increase in concrete cover over the ducts.

All four specimens failed locally in shear at the location of the ducts. Evidence for the shear failure includes the location and shape of the failure plane, the detection of delamination in the web just prior to failure and the unyielded flexural reinforcement (stirrups) which would have yielded in the event of a flexural failure. Bending of the concrete cover adjacent to the ducts occurred during the testing of BC, BO and 0.2DC but was not the cause of failure.

The webs also experienced bending in a regional view as the webs acted as members in a frame loaded laterally and supported at the top and bottom by the slabs. However this bending was much less than that predicted by either an elastic frame analysis or the simplified CALTRANS approach. The frame analysis was accurate over a small load range (uncracked section) but predicted much higher moments than were actually measured on the cracked section. Longitudinal strain measurements on specimen BC indicated that the primary load path became longitudinal rather than transverse once cracking was initiated. It appears that the cracked stiffness of the web in the transverse direction is much less than the longitudinal axial stiffness of the web. As a result much of the load is transmitted directly to the supports (end of horizontal curve) by longitudinal arching.

8.3 DESIGN RECOMMENDATIONS

8.3.1 Shear

Shear should be checked in the immediate vicinity of the duct group. The capacity of the concrete along the shearing planes should meet or exceed the factored lateral prestress force with a load factor of 1.2 applied. One diagonal shearing plane intersects the top duct and one intersects the bottom duct. The shearing planes are confined to the concrete between the plane of the ducts and the plane of the curved inside face whenever the vertical clear spacing between the ducts is less than one duct diameter. The depth of shear plane can be taken as equal to the minimum cover over the ducts plus $\frac{1}{4}$ of the duct diameter. Offsetting the ducts towards the outside of the curve will increase the minimum cover and hence the ultimate capacity.

Whenever the clear spacing between ducts is equal to or greater than one duct diameter, the diagonal shearing planes may extend through the ducts and into the concrete between the ducts and the plane of the outside curved face of the web. In this case, the depth of the shear planes can be taken as equal to the web width less $\frac{1}{2}$ of the duct diameter. In some instances, the capacity may be further limited by a failure plane that passes vertically through the duct group rather than diagonally to the outside face. This case should also be checked. The relationship between the number of ducts, duct diameter and web width will determine which of these two failure planes will occur for any given specimen.

8.3.2 Flexure

Flexural bending of the relatively thin concrete cover is not a well understood phenomenon. Therefore no specific design methodology is proposed. However limiting the number of closely spaced or bundled ducts will likely improve the capacity.

Bending of the web on a regional scale can be conservatively checked using an elastic frame analysis. A load factor of 1.0 can be used because the beneficial effect of increased longitudinal arching after cracking is neglected.

8.3.3 Detailing

Careful attention to reinforcement details will likely improve the behavior of the web. Overlapping 180 degree hooks located in either the top or bottom slab should be used for the stirrups. Straight laps should be avoided or at least located on the outside of the curve. The stirrups (acting as flexural reinforcement) should be spaced to meet minimum flexural reinforcement requirements. Tie-back reinforcement which intercepts the diagonal shearing planes may increase the ultimate capacity.

8.4 FUTURE RESEARCH

This report summarizes the first known physical testing of the lateral breakout phenomenon. The only variable investigated was the duct arrangement. More testing is needed to fill in the lack of data for vertical clear spacings between 20% and 100% of a duct diameter. Other geometric variables also need study. In particular the relationship between the number of ducts, duct diameter and web width as they affect the shape of the actual failure plane needs investigation. The local bending effect appears to be dependent on the number of bundled ducts. Safe limits could be established by testing bundled arrangements with varying number of ducts.

Tie-back reinforcing that intercepts the diagonal shearing planes appears very promising. Optimum tie dimensions and spacing need to be verified through physical tests. Decreased stirrup spacing may prove useful for local and regional bending. Combinations of duct arrangement and

reinforcing details may show behavior not anticipated by investigating details separately and should be verified experimentally.

As a recommendation to future researchers, it is suggested that longitudinal bars in the web be monitored with strain gages to determine longitudinal load carrying characteristics of the web. Also the curve length should be increased to diminish any effect of short curve lengths on longitudinal arching.

APPENDIX A: ADDITIONAL GRAPHS

COMPARISON OF WEB DELAMINATIONS AT D62

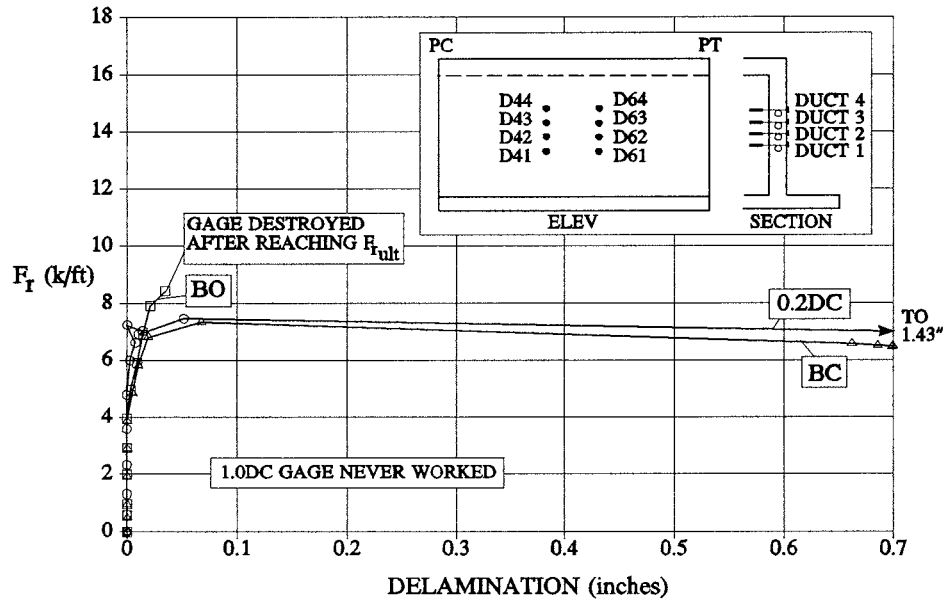


Figure A.1 Comparison of Web Delaminations at D62.

COMPARISON OF WEB DELAMINATIONS AT D63

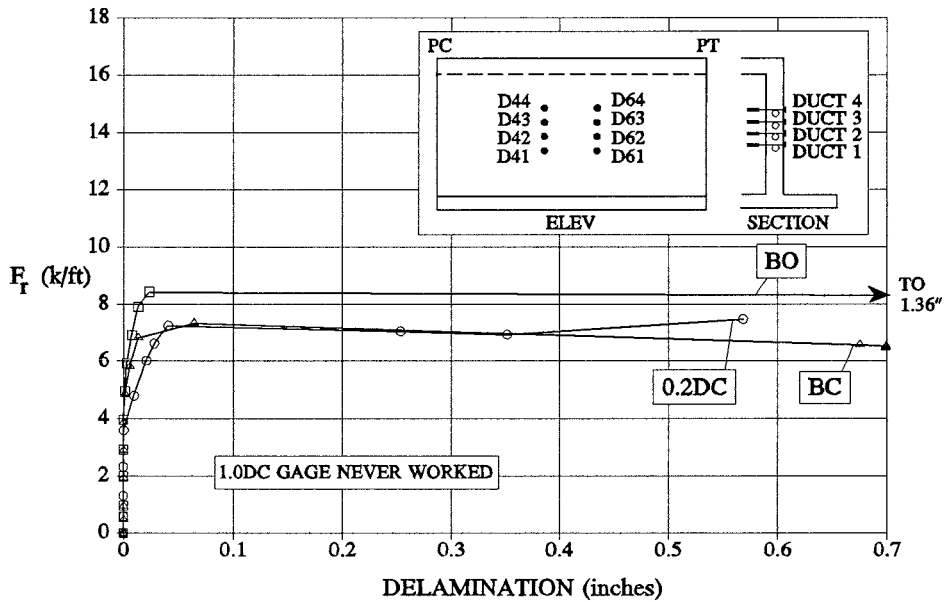


Figure A.2 Comparison of Delaminations at D63.

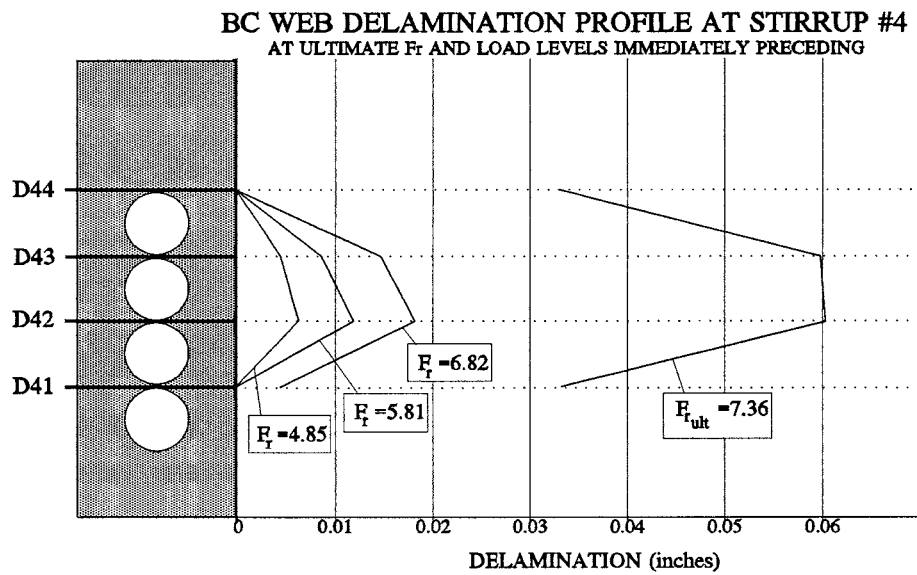


Figure A.3 BC Web Delamination Profile at Stirrup #4.

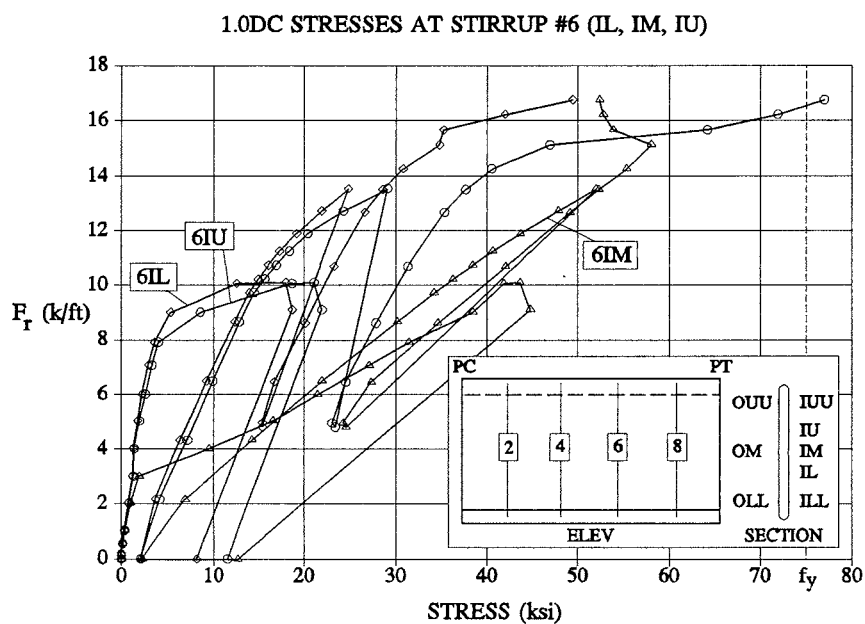


Figure A.4 1.0DC Stresses at Stirrup #6 (IL, IM, IU)-Complete Load History

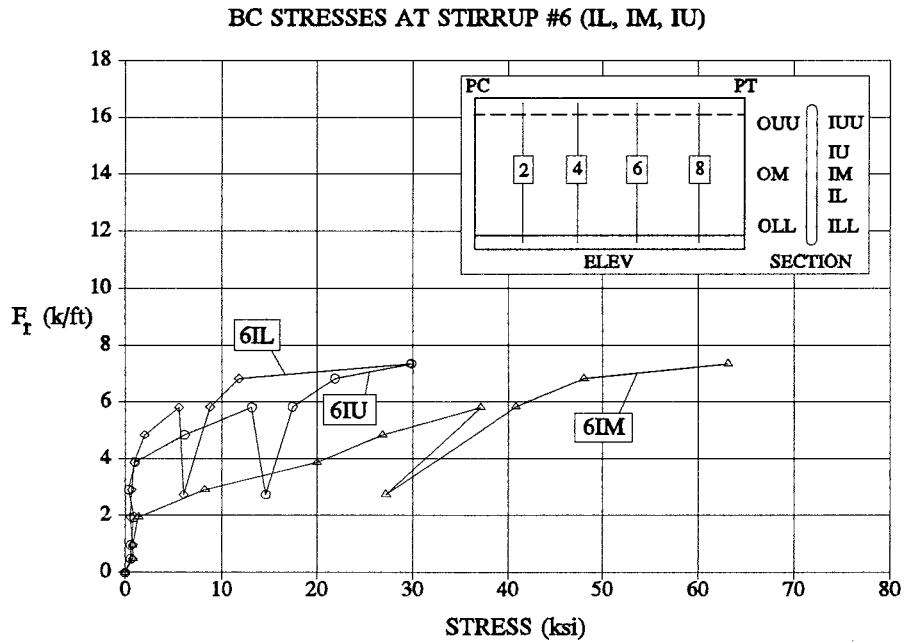


Figure A.5 BC Stresses at Stirrup #6 (IL, IM, IU)-Complete Load History.

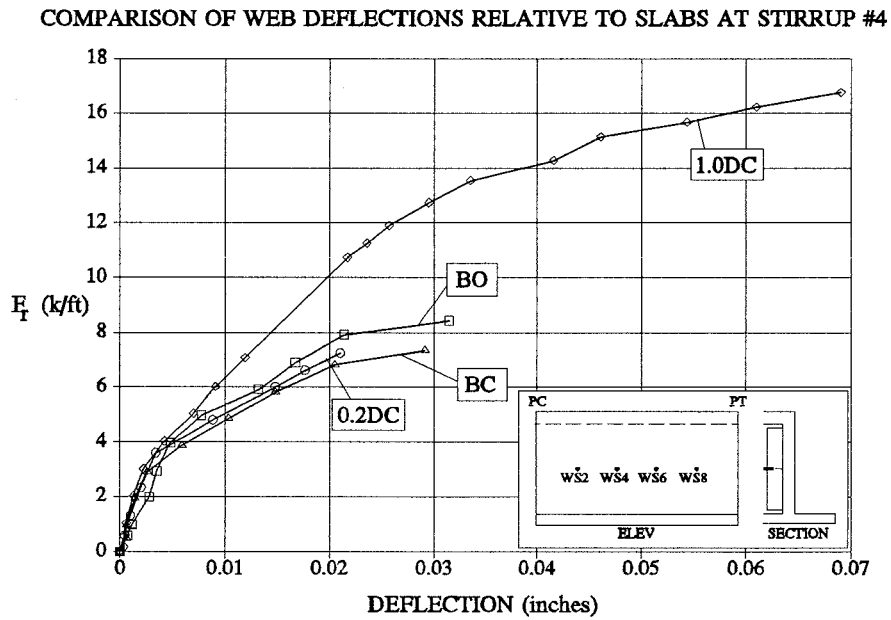


Figure A.6 Comparison of Web Deflections Relative to Slabs at Stirrup #4.

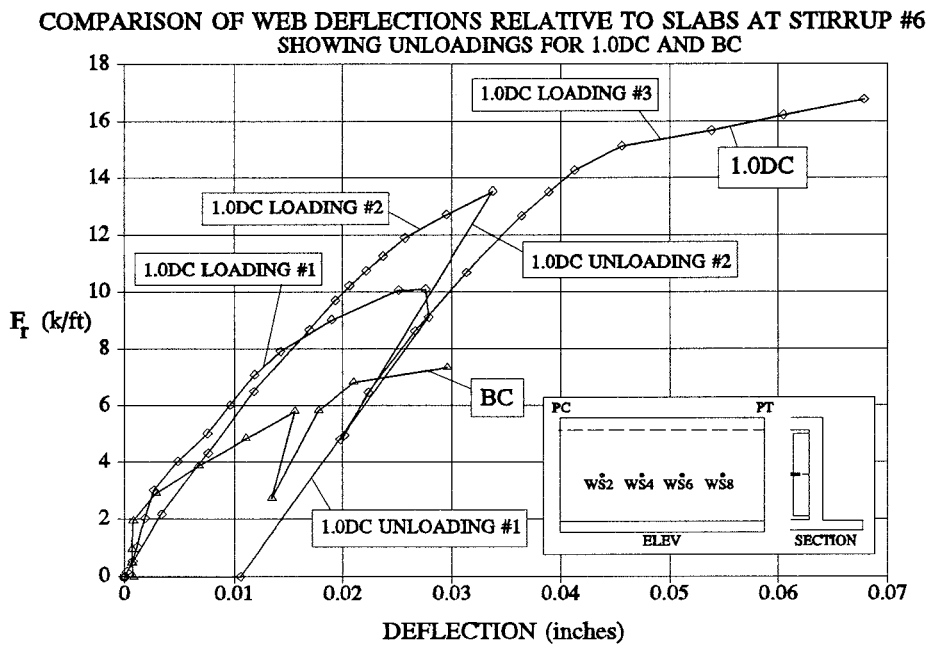


Figure A.7 Comparison of Web Deflections Relative to Slabs at Stirrup #4- Complete Load History.

REFERENCES

1. Lin, T.Y. and Burns, N.H., Design of Prestressed Concrete Structures, Third Ed., John Wiley and Sons, Inc., New York, 1981.
2. Hindi, A., "Enhancing the Strength and Ductility of Post-tensioned Segmental Concrete Box-Girder Bridges," Ph.D. Dissertation, The University of Texas at Austin, 1990.
3. Standard Specification for Highway Bridges, Fourteenth Ed., American Association of State Highway and Transportation Officials (AASHTO), 1989.
4. Svensson, H.S., "The Application of Prestressing of Bridges in Germany," External Prestressing in Bridges, Special Publication SP-120, American Concrete Institute, 1990.
5. Carter, L.L., "Deviator Behavior In Externally Post-Tensioned Bridges," Master's Thesis, The University of Texas at Austin, 1987.
6. T.Y. Lin International, "Las Lomas Bridge-Causes of Structural Failure," Report to Department of Army, San Francisco District Corp. of Engineers, 1979 (unpublished).
7. Podolny, W., "The Cause of Cracking in Post-Tensioned Concrete Box Girder Bridges and Retrofit Procedures," Journal of Prestressed Concrete Institute, vol. 30, no. 2, March/April 1985.
8. T.Y. Lin International, "Interim Report-Kapiolani Interchange On-Ramp Project No. I-H1-1(159):24," Hawaii DOT, 1982 (unpublished).

9. Guide Specification for Design and Construction of Segmental Concrete Bridges, American Association of State Highway and Transportation Officials (AASHTO), 1989.
10. National Cooperative Highway Research Program Report 12-33B, "Comprehensive Bridge Specification and Commentary- Concrete Structures," Draft copy, 1991 (unpublished).
11. Anonymous, "Niederösterreichs, 'Europabrücke': Mensch und Technik im Schlagzeilenhagel," *Baumaschine-Baugerät-Baustelle*, October, 1989.
12. Moe, J., Shearing Strength of Reinforced Concrete Slabs and Footings Under Concentrated Loads, Portland Cement Association Research & Development Laboratories, Development Department Bulletin D47, 1961.
13. Taylor, A.W., "Behavior of Thin Walled Hollow Concrete Bridge Piers & Pylons," Ph.D. Dissertation, The University of Texas at Austin, 1990.
14. Ahuja, D., "Effect of Duct Spacing on Breakout of Post-Tensioning Tendons in Horizontally Curved Concrete Box Girders," Master's Report, University of Texas at Austin, 1991.
15. Texas State Department of Highways and Public Transportation, "Standard Specifications for Construction of Highways, Streets and Bridges," 1982.
16. American Institute of Steel Construction, Inc., Manual of Steel Construction-Load & Resistance Factor Design, Chicago, IL, 1986.
17. Ferguson, P., Reinforced Concrete Fundamentals, Fourth Ed., John Wiley & Sons, Inc., New York, 1979.
18. Report of ACI-ASCE Committee 326, "Shear and Diagonal Tension," Journal of the American Concrete Institute, Proceedings V. 59, January & February, 1962.

19. California Department of Transportation, "Memo to Designers," 11-31 Curved Post-Tensioned Bridges, September, 1985.

VITA

Dean William Van Landuyt was born in Joliet, Illinois in 1959 to Raymond Edmund and Grace Rose Van Landuyt. He graduated from the University of Texas at Austin with a Bachelor of Science in Civil Engineering in 1982. After graduation, he began work as a Engineering Assistant in the Bridge Division of the Texas Highway Department. Some of his designs include the San Antonio "Y" segmental box girder project, rehabilitation of the Corpus Christi Harbor Bridge and numerous other bridges. He led the project that developed the first federally approved concrete bannister railing. He has been a registered professional engineer in Texas since 1986. In January, 1990 he was accepted into the Department's graduate program and began full-time studies at the University. He returned to the Bridge Division in September, 1991 and is currently involved in the development of new, aesthetically pleasing bridges.

Permanent Address: TxDOT
11th & Brazos
Austin, TX 78701

This thesis was typed by the author.

